ANALYTICA CHIMICA ACTA

International monthly devoted to all branches of analytical chemistry
Revue mensuelle internationale consacrée à tous les domaines de la chimie analytique
Internationale Monatsschrift für alle Gebiete der analytischen Chemie

Editors

PHILIP W. WEST (Baton Rouge, La., U.S.A.)
A.M.G. MACDONALD (Birmingham, Great Britain)

Associate Editor

D.M.W. ANDERSON (Edinburgh, Great Britain)

Editorial Advisers

R. Belcher, Birmingham
G. Charlot, Paris
E.A.M.F. Dahmen, Enschede
G. den Boef, Amsterdam
G. Duykaerts, Liège
D. Dyrssen, Göteborg
H. Flaschka, Atlanta, Ga.
T. Fujinaga, Kyoto
G.G. Guilbault, New Orleans, La.
J. Hoste, Ghent
H.M.N.H. Irving, Leeds
O.G. Koch, Neunkirchen/Saar
H. Malissa, Vienna
J. Mitchell, Jr., Wilmington, Del.
G.H. Morrison, Ithaca, N.Y.
E. Pungor, Budapest
J.P. Riley, Liverpool
J.W. Robinson, Baton Rouge, La.
Y. Rusconi, Geneva
J. Růžička, Copenhagen
D.E. Ryan, Halifax, N.S.
S. Siggia, Amherst, Mass.
R.K. Skogerboe, Fort Collins, Colo.
W.I. Stephen, Birmingham
G. Tölg, Schwäbisch Gmünd, B.R.D.
A. Walsh, Melbourne
H. Weisz, Freiburg i. Br.
T.S. West, Aberdeen
Yu.A. Zolotov, Moscow

ELSEVIER SCIENTIFIC PUBLISHING COMPANY

AMSTERDAM

Anal. Chim. Acta, Vol. 82, No. 2, 231–450, April 1976

Published monthly

Completing Volume 82

ANALYTICA CHIMICA ACTA

Publication Schedule for 1976

Vol. 81, No. 1	January 1976	
Vol. 81, No. 2	February 1976	(completing Vol. 81)
Vol. 82, No. 1	March 1976	
Vol. 82, No. 2	April 1976	(completing Vol. 82)
Vol. 83	May 1976	(complete in one issue)
Vol. 84, No. 1	June 1976	
Vol. 84, No. 2	July 1976	(completing Vol. 84)
Vol. 85, No. 1	August 1976	
Vol. 85, No. 2	September 1976	(completing Vol. 85)
Vol. 86	October 1976	(complete in one issue)
Vol. 87, No. 1	November 1976	
Vol. 87, No. 2	December 1976	(completing Vol. 87)

Subscription price for 1976 (covering November '75/December '76, Vols. 80–87): Dfl. 840.00 plus Dfl. 96.00 postage. Subscribers in the U.S.A. and Canada receive their copies by airmail. Additional charges for airmail to other countries are available on request. For advertising rates apply to the publishers.

Subscriptions should be sent to:
Elsevier Scientific Publishing Company, P.O. Box 211, Amsterdam, The Netherlands.

GENERAL INFORMATION

Languages

Papers will be published in English, French or German.

Detailed information

Authors should consult Vol. 73, p. 435 for detailed instructions. Reprints of this information are obtainable from Dr. Macdonald or from: Elsevier Editorial Series Ltd., Mayfield House, 256 Banbury Road, Oxford (Great Britain).

Submission of papers

Papers should be sent to:

Prof. Philip W, West,
Coates Chemical Laboratories,
College of Chemistry and Physics,
Louisiana State University,
Baton Rouge 3,
La. 70803 (U.S.A.)

or to:

Dr. A.M.G. Macdonald,
Department of Chemistry,
The University,
P.O. Box 363
Birmingham B15 2TT (Great Britain)

Reprints

Fifty reprints will be supplied free of charge. Additional reprints (minimum 100) can be ordered at quoted prices. They must be ordered on order forms which are sent together with the proofs.

For your copy of the latest EASTMAN Organic Chemicals Catalog

or to order any of the 6,000 chemicals it contains,

contact one of these laboratory supply houses.

AUSTRALIA
H. B. Selby and Co., Pty., Ltd.
Adelaide
Brisbane
Hobart
Oakleigh
Perth
Sydney
Ramsay Surgical Limited
Victoria

BELGIUM
s.a. Belgolabo N.V.
Overijse

BRAZIL
Atlantida Representaçoes e Importaçoes, Ltda.
Rio de Janeiro
Tennant Quimica S.A.
São Paulo

CANADA
Fisher Scientific Co., Ltd.
Edmonton
Montreal
Ottawa
Don Mills
Vancouver
Dartmouth
Sargent-Welch Scientific of Canada, Ltd.
Weston

CHINA, REPUBLIC OF
San Ho Instrument Co.
Taipei, Taiwan
Teh Ying Co., Ltd.
Taipei, Taiwan

DENMARK
Struers K/S
Copenhagen K

ECUADOR
Rafael Valdez
Guayaquil

FINLAND
Havulinna Oy
Helsinki

FRANCE
Touzart & Matignon
Paris

WEST GERMANY
Serva International
Chemie-Handels GmbH & Co.
Heidelberg

GREECE
P. Bacacos S.A.
Athens

GUATEMALA
F. Krafka and Co., Ltd.
Guatemala City

INDIA
Kodak Limited
Bombay

ISRAEL
Landseas (Israel) Ltd.
Tel Aviv
Yaron Chemicals Ltd.
Tel Aviv

ITALY
Prodotti Gianni, s.r.l.
Milan

JAPAN
Nagase and Co., Ltd.
Tokyo

KOREA
The Sang Chung Commercial Co., Ltd.
Seoul

MEXICO
Alfonso Marhx, S.A.
Mexico 1, D.F.
Hoffman-Pinther and Bosworth, S.A.
Naucalpan de Juarez

MOZAMBIQUE
Baird & Tatlock (S.A.) Pty. Ltd.
Lourenco Marques

NETHERLANDS
N.V. Holland-Indie
Argenturen Mij, HIAM
Amstelveen

NEW ZEALAND
Kempthorne, Prosser & Co. Ltd.
Wellington
Dunedin
Geo. W. Wilton and Co. Ltd.
Wellington

NORWAY
Norliens Kemisk Tekniske Aktieselskap
Oslo

PORTUGAL
Soquimica, Sociedad de Representaçoes de Quimica
Lisbon

PUERTO RICO
Fisher Scientific Co.
Santurce
Puerto Nuevo

RHODESIA
Baird & Tatlock International Ltd.
Salisbury
Bulawayo

SOUTH AFRICA, REPUBLIC OF
Baird and Tatlock S.A. Pty.
Johannesburg
Durban
Port Elizabeth
Paarden
Eiland
Chemlab (Pty) Ltd.
Transvaal

SOUTHWEST AFRICA
S.W.A. Scientific Services (Pty) Ltd.
Windhoek

SPAIN
Quimigranel S.A.
Barcelona

SWEDEN
KEBO AB
Stockholm 6

SWITZERLAND
Dr. Bender and Dr. Hobein AG
Zurich 6

THAILAND
White & Co., Ltd.
Bangkok

UNITED KINGDOM
Kodak Limited
Kirkby, Liverpool

VENEZUELA
Equipos Cientificos y Educativos, S.A.
Caracas
Reactivos, S.A.
Caracas

ZAMBIA, REPUBLIC OF
Baird and Tatlock (London) Ltd.
Ndola
Lusaka

EASTMAN Organic Chemicals are stocked locally in the continental U.S.A. by:

AMERICAN SCIENTIFIC & CHEMICAL, BECKMAN SCIENCE ESSENTIALS, CURTIN MATHESON SCIENTIFIC, FISHER SCIENTIFIC, GAC LABORATORIES, LABPRODUCTS, INC., NORTH-STRONG, PREISER SCIENTIFIC, SARGENT-WELCH SCIENTIFIC, SCICHEMCO, SCIENTIFIC & INDUSTRIAL SALES & SERVICE, VWR SCIENTIFIC, WARD'S NATURAL SCIENCE ESTABLISHMENT

The catalog may also be obtained from:
Eastman Kodak Company
Dept. 412L
Rochester, N.Y. 14650, U.S.A.

Kodak

THE STRUCTURAL CHEMISTRY OF PHOSPHORUS

by **D. E. C. CORBRIDGE,** University of Leeds, Great Britain.

1974. 556 pages. US$104.25/Dfl. 250.00 ISBN 0-444-41073-2

The growing importance of phosphorus chemistry has been evident for some years. The greatly increased academic interest in phosphorus compounds during the last two decades has been matched by their increasingly widespread use. The many fields of application now include food manufacture, water treatment, detergents, oil additives, electrical materials, refractories, fireproofing agents, plasticisers, metal treatment, fertilisers, insecticides, nerve gases and medicine.
Compounds of phosphorus play a vital role in living processes and the number of current organic and biochemical investigations involving them is considerable.

Phosphorus rivals carbon both in structural versatility and capacity for covalent bond formation, and newly synthesised compounds are being reported at an astronomically increasing rate. A knowledge of the molecular and crystal structures of these compounds forms an essential background to the complete understanding of their properties and behaviour.

In view of the role of phosphorus compounds in widely differing and important fields of investigation, available structural information has been collected together to form what is hoped will serve as a useful reference work. The book outlines the structural principles of phosphorus chemistry, and presents a comprehensive and up-to-date survey of existing knowledge of crystal and molecular structure.

CONTENTS:

Elsevier
P.O. BOX 211
AMSTERDAM, THE NETHERLANDS

BOOKS IN CHROMATOGRAPHY

Journal of Chromatography Library

■ Volume 1: **Chromatography of Antibiotics**
by G.H. Wagman and M.J. Weinstein
1973. 247 pages. US $ 26.95/Dfl. 65.00.
ISBN 0-444-41106-2

■ Volume 2: **Extraction Chromatography**
edited by T. Braun and G. Ghersini
1975. 584 pages. US $ 54.25/Dfl. 130.00.
ISBN 0-444-99878-0

■ Volume 3: **Liquid Column Chromatography**
A Survey of Modern Techniques and Applications
edited by Z. Deyl, K. Macek and J. Janák
1975. 1198 pages. US $ 120.95/Dfl. 290.00.
ISBN 0-444-41156-9

■ Volume 4: **Detectors in Gas Chromatography**
by J. Ševčík
1975. about 280 pages. Price to be announced.
ISBN 0-444-99857-8

Chromatography of Environmental Hazards

by Lawrence Fishbein

■ Volume I: Carcinogens, Mutagens and **Teratogens**
1972. 506 pages. US $ 56.25/Dfl. 135.00.
ISBN 0-444-40948-3

■ Volume II: **Metals, Gaseous and Industrial Pollutants**
1973. 649 pages. US $ 62.50/Dfl. 150.00.
ISBN 0-444-41059-7

■ Volume III: **Pesticides**
1975. 838 pages. US $ 108.50/Dfl. 260.00.
ISBN 0-444-41158-5

■ Volume IV: **Drugs**
1976. In preparation

Bibliography of Electrophoresis 1968-1972. And Survey of Applications

edited by Z. Deyl, J. Kopecký, J. Davídek, M. Juřicová and R. Helm.
Supplementary Volume No. 4. Published in conjunction with the Journal of Chromatography
1975. about 850 pages. Price to be announced.
ISBN 0-444-41225-5

Bibliography of Paper and Thin-Layer Chromatography 1970-1973. And Survey of Applications

edited by K. Macek, I.M. Hais, J. Kopecký, V. Schwarz, J. Gasparič and J. Churáček.
Supplementary Volume No. 5. Published in conjunction with the Journal of Chromatography
1976. about 430 pages. Price to be announced.
ISBN 0-444-41299-9

Advances in Chromatography 1974

edited by A. Zlatkis and L.S. Ettre
1974. 788 pages. US $ 66.75/Dfl. 160.00.
ISBN 0-444-41267-0

Pharmaceutical Applications of Thin-Layer and Paper Chromatography

edited by K. Macek
1972. 759 pages. US $ 104.25/Dfl. 250.00.
ISBN 0-444-40923-8

Practical Manual of Gas Chromatography

edited by J. Tranchant
1969. 407 pages. US $ 41.75/Dfl. 100.00.
ISBN 0-444-40677-8

AN EXTENSIVE BROCHURE GIVING FULL DETAILS OF ALL THESE TITLES IS AVAILABLE FROM THE PUBLISHER

ELSEVIER SCIENTIFIC PUBLISHING COMPANY

P.O. Box 211, Amsterdam, The Netherlands.

Distributed in the U.S.A. and Canada by:
AMERICAN ELSEVIER PUBLISHING COMPANY, INC.,
52 Vanderbilt Ave., New York, N.Y. 10017

Prices are subject to change without prior notice.

577 E

Reagents

MERCK

The right way to optimal separations

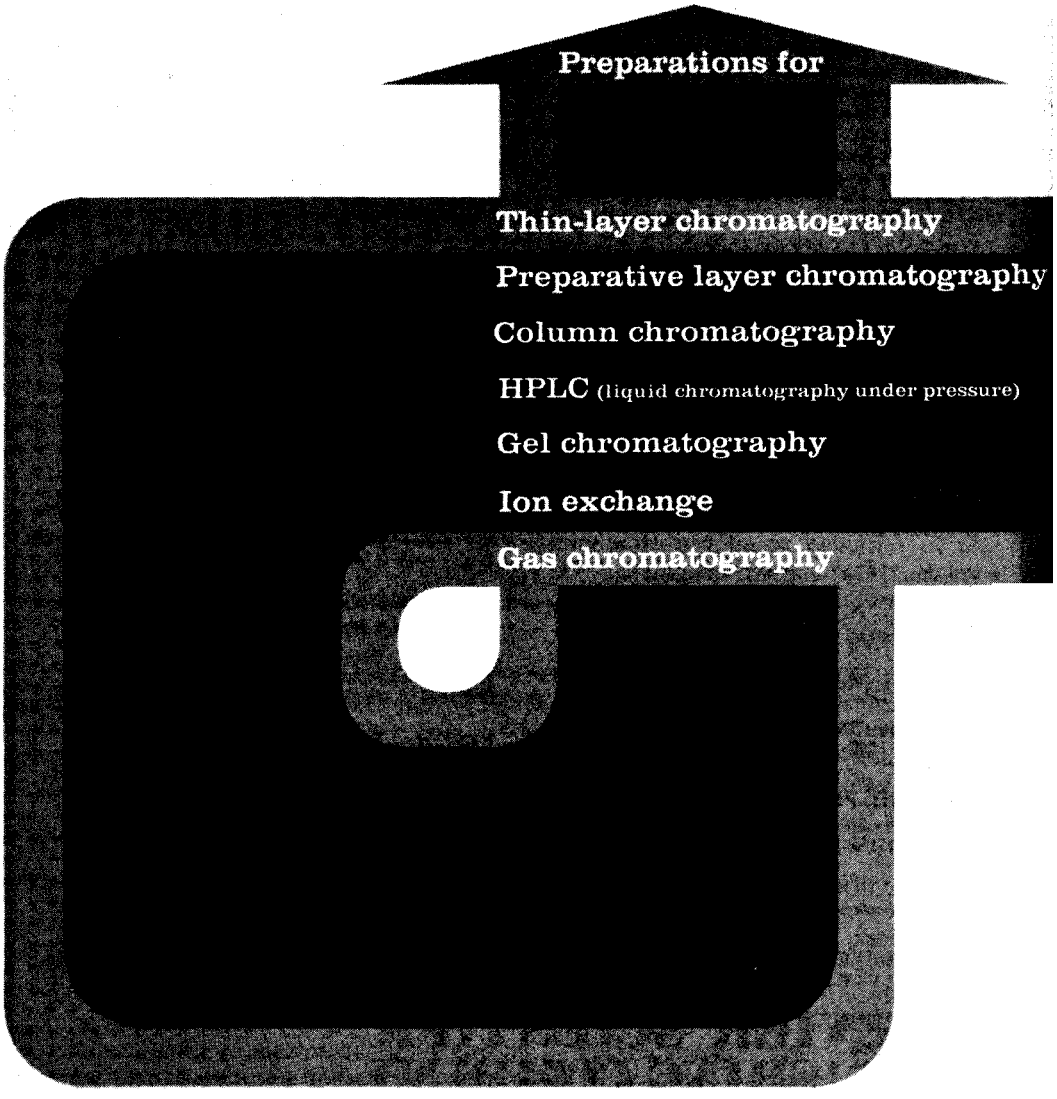

Silica gels 40, 60, 100 (Å pore diameter)
Merckogel® SI (max. 25000 Å)
Silanised Silica gel (hydrophobic)
Kieselguhr

Aluminium oxides 60 (type E), 90, 150 (type T)
Cellulose · Cellulose ion exchangers
LiChrosorb® (Merckosorb®) · Perisorb®
Merckogel® PVA, Merckogel® PGM

Please ask for our special brochures

375-EÜ a

E. Merck, Darmstadt Germany

Analytica Chimica Acta, 82 (1976) 231—243
©Elsevier Scientific Publishing Company, Amsterdam — Printed in The Netherlands

THE CURRENT—POTENTIAL RELATIONSHIP IN DIFFERENTIAL PULSE POLAROGRAPHY

G. J. M. HELJNE and W. E. VAN DER LINDEN

Laboratory for Analytical Chemistry, University of Amsterdam, Nieuwe Achtergracht 166, Amsterdam (The Netherlands)

(Received 6th September, 1975)

SUMMARY

A new derivation of the current—potential relationship in differential pulse polarography is presented, based on the evaluation of the concentration profile which exists at the moment of pulse application. Agreement between theory and experiment seems acceptable when allowance is made for some instrumental artefacts.

During the last decade differential pulse polarography (d.p.p.) has proved to be a valuable tool for the determination of very small concentrations of electroactive species. In this technique a linearly increasing voltage ramp is imposed on a dropping mercury electrode, as in ordinary d.c. polarography, but near the end of the life of each drop, at a fixed time t_0, a potential step ΔE is superimposed on the ramp potential E. The current is sampled just before t_0 and at a time δ after the application of the pulse. The difference between these two currents is recorded as a function of the ramp potential E [1].

To allow for the optimum adjustment of the instrumental parameters, it is desirable to have available an equation which correctly describes the current—potential relationship. The literature seems to contain only one paper in which an equation is given which can be ascribed unambiguously to d.p.p. [2]:

$$i_{dpp} = \frac{nFkm^{2/3}(t_0 + \delta)^{2/3} D^{1/2} C^0}{(\pi\delta)^{1/2}} \left\{ \frac{(1 - \sigma^2)\epsilon_1}{(1 + \epsilon_1)(1 + \sigma^2\epsilon_1)} \right\} \quad (1)$$

where $\sigma^2 = \exp[(nF/RT)\Delta E]$; $\epsilon_1 = \exp[(nF/RT)(E_1 - E_{1/2})]$; $km^{2/3}(t_0 + \delta)^{2/3} = A(t_0 + \delta)$, the area of the electrode at time $t_0 + \delta$; and C° is the bulk concentration.

The authors state that this equation is obtained by making the usual assumptions: the electrode reaction is uncomplicated and reversible; the DME can be treated as a planar electrode in its response to the potential step and as an expanding sphere towards d.c. processes. For the derivation of eqn. (1) reference is made to a paper by Parry and Osteryoung [3]. They

obtained an equation for the differential pulse current (the authors use the term "derivative pulse mode" but actually describe the differential pulse technique) by subtracting $i(E_1, t_0)$ from $i(E_1 + \Delta E, t_0 + \delta)$ and substituting:

$$i(E_1, t_0) = (i_d)_{E_1} \frac{1}{(1 + \exp[(nF/RT)(E_1 - E_{1/2})])};$$

$$i(E_1 + \Delta E, t_0 + \delta) = (i_d)_{E_2} \frac{1}{(1 + \exp[(nF/RT)(E_2 - E_{1/2})])}$$

where $E_2 = E_1 + \Delta E$. Apparently for both $(i_d)_{E_1}$ and $(i_d)_{E_2}$ the Cottrell expression $nFA(D/(\pi t))^{\frac{1}{2}}$ was substituted. This is permissible, however, only if the lapse of time between application of the potential step and sampling of the current is the same as the lapse of time during which the potential E_1 was applied to the electrode; moreover, at the instant of application of the potential step the initial condition $C(x,o) = C^0$ must hold true, x being the distance from the electrode surface. This last condition is essential in the derivation of the Cottrell equation, but is not fulfilled in d.p.p., as a concentration profile will generally exist at time t_0 because of the electrode reaction at the ramp potential E_1. All the prerequisites mentioned above can be fulfilled only by applying the potentials E_1 and E_2 to subsequent drops, which would mean a fundamental difference in comparison with the differential pulse technique as described above.

In this paper a current—potential relationship is derived based on assumptions which are the same as used for the derivation of eqn. (1), but the derivation takes into account a concentration profile according to the discussion presented by MacGillavry and Rideal [4]. The response to the potential step is evaluated for the case where both the electroactive species OX and its reduction product R are present, following a treatment given by Delahay [5].

CURRENT—POTENTIAL RELATIONSHIP

The general equation for diffusion towards a stationary spherical electrode.

$$\frac{\partial C(r, t)}{\partial t} = D\left[\frac{\partial^2 C(r, t)}{\partial r^2} + \frac{2}{r}\frac{\partial C(r, t)}{\partial r}\right] \tag{2}$$

has to be modified in the case of a dropping electrode in order to take account of the surface expansion. For this purpose, r is replaced by a moving coordinate ρ defined by $\rho^3 = r^3 - r_0^3$, where r_0 is the radius of the drop. This replacement leads to

$$\frac{\partial C(\rho, t)}{\partial t} = D\frac{(\rho^3 + \gamma t)^{4/3}}{\rho^5}\left[\rho\frac{\partial^2 C(\rho, t)}{\partial \rho^2} + 2\left(\frac{\rho^3 - \gamma t}{\rho^3 + \gamma t}\right)\frac{\partial C(\rho, t)}{\partial \rho}\right] \tag{3}$$

where $\gamma t = r_0^3$ and $\gamma = 3m/(4\pi d)$ (m = weight of mercury delivered per unit time and d = density of mercury). Although it is not completely correct [6],

we will neglect ρ^3 in respect of γt. Introduction of the new variables $x = \rho^3$ and $y = t^{7/3}$ allows the transformation of eqn. (3) to

$$\frac{\partial C(x, y)}{\partial y} = m \frac{\partial^2 C(x, y)}{\partial x^2} \tag{4}$$

where $m = (27/7)\gamma^{4/3}D$.

In order to take account of the presence of both OX and R, eqn. (4) has to be solved for both species. For this solution the following initial and boundary conditions will be used:

Initial conditions: $C_{OX}(r, 0) = C^0; C_R(r, 0) = 0$

Boundary conditions: $$D_{OX}\left(\frac{\partial C_{OX}(r, t)}{\partial r}\right)_{r=r_0} + D_R\left(\frac{\partial C_R(r, t)}{\partial r}\right)_{r=r_0} = 0 \tag{5}$$

$$\frac{C_{OX}(r_0, t)}{C_R(r_0, t)} = \theta_1 = \frac{f_R}{f_{OX}} \exp[(nF/RT)(E_1 - E^0)] \tag{6}$$

(f_{OX} and f_R are the activity coefficients of species OX and R respectively).

The results are (see Appendix 1):

$$C_{OX}(r, t) = C^0 - \frac{C^0}{(1 + \theta_1\xi)} \operatorname{erfc}\left[\frac{1}{6(D_{OX}t)^{\frac{1}{2}}}\left(\frac{7}{3}\right)^{\frac{1}{2}}\left(\frac{r^3 - r_0^3}{r_0^2}\right)\right] \tag{7}$$

$$C_R(r, t) = \frac{C^0\xi}{(1 + \theta_1\xi)} \operatorname{erfc}\left[\frac{1}{6(D_R t)^{\frac{1}{2}}}\left(\frac{7}{3}\right)^{\frac{1}{2}}\left(\frac{r^3 - r_0^3}{r_0^2}\right)\right] \tag{8}$$

where $\xi = (D_{OX}/D_R)^{\frac{1}{2}}$.

The current at time t_0 is given by:

$$i(t_0) = nFA(t_0)D_{OX}\left(\frac{\partial C_{OX}(r, t)}{\partial r}\right)_{r=r_0} = nFA(t_0)\left(\frac{D_{OX}}{\pi t_0}\right)^{\frac{1}{2}}\left(\frac{7}{3}\right)^{\frac{1}{2}}\frac{C^0}{(1 + \theta_1\xi)} \tag{9}$$

To evaluate the concentration profile and so the current at a time δ after the application of the potential step at time t_0, the linear diffusion equation must be solved for a planar electrode for both species OX and R:

$$D\left(\frac{\partial^2 C(r_x, t^*)}{\partial r_x^2}\right) = \frac{\partial C(r_x, t^*)}{\partial t^*} \tag{10}$$

where $r_x = r - r_0$ and $t^* = t - t_0$.

The boundary conditions (5) and (6) change to:

$$D_{OX}\left(\frac{\partial C_{OX}(r_x, t^*)}{\partial r_x}\right)_{r_x = 0} + D_R\left(\frac{\partial C_R(r_x, t^*)}{\partial r_x}\right)_{r_x = 0} = 0 \tag{11}$$

and

$$\frac{C_{OX}(r_x = 0, t^*)}{C_R(r_x = 0, t^*)} = \frac{C_{OX}(r_0, t^*)}{C_R(r_0, t^*)} = \theta_2 = \frac{f_R}{f_{OX}} \exp\left[\frac{nF}{RT}(E_2 - E^0)\right] \tag{12}$$

The new initial conditions can be obtained from eqns. (7) and (8):

$$C_{OX}(r_x, 0) \equiv C_{OX}(r,t_0)_{E_1} = C_{OX}(r_x + r_0, t_0)_{E_1} = C^0 - \frac{C^0}{(1 + \theta_1\xi)}$$

$$\times \text{erfc}\left[\frac{1}{6(D_{OX}t_0)^{\frac{1}{2}}}\left(\frac{7}{3}\right)^{\frac{1}{2}}\left(\frac{(r_x + r_0)^3 - r_0^3}{r_0^2}\right)_{t = t_0}\right] \tag{13}$$

$$C_R(r_x, 0) \equiv C_R(r, t_0)_{E_1} = C_R(r_x + r_0, t_0)_{E_1} = \frac{C^0\xi}{(1 + \theta_1\xi)}$$

$$\times \text{erfc}\left[\frac{1}{6(D_R t_0)^{\frac{1}{2}}}\left(\frac{7}{3}\right)^{\frac{1}{2}}\left(\frac{(r_x + r_0)^3 - r_0^3}{r_0^2}\right)_{t = t_0}\right] \tag{14}$$

Since the duration of the potential pulse is short, the perturbation of the existing concentration profile will be limited to the region near the electrode surface; so r_x is small, and the radius-dependent part of eqns. (13) and (14) can be replaced by:

$$\frac{(r_x + r_0)^3 - r_0^3}{r_0^2} = \frac{r_x^3 + 3r_x^2 r_0 + 3r_x r_0^2}{r_0^2} \cong 3r_x.$$

For small values of the argument z the error function can be replaced by

$$\text{erf}[z] \cong (2/\pi^{\frac{1}{2}})z$$

so that eqns. (13) and (14) can be written:

$$C_{OX}(r_x, 0) = \frac{C^0\theta_1\xi}{(1 + \theta_1\xi)} + \frac{C^0}{(1 + \theta_1\xi)}\left(\frac{7}{3}\right)^{\frac{1}{2}}\frac{r_x}{(\pi D_{OX}t_0)^{\frac{1}{2}}} = a + br_x \tag{15}$$

$$C_R(r_x, 0) = \frac{C^0\xi}{(1 + \theta_1\xi)} - \frac{C^0\xi}{(1 + \theta_1\xi)}\left(\frac{7}{3}\right)^{\frac{1}{2}}\frac{r_x}{(\pi D_R t_0)^{\frac{1}{2}}} = c + dr_x. \tag{16}$$

By means of Laplace transformation (see Appendix 2), the following solutions of eqn. (10) are obtained:

$$C_{OX}(r_x, t^*) = \frac{C^0\xi(\theta_2 - \theta_1)}{(1 + \theta_1\xi)(1 + \theta_2\xi)}\text{erfc}\left[\frac{r_x}{2(D_{OX}t^*)^{\frac{1}{2}}}\right] + \frac{C^0\theta_1\xi}{(1 + \theta_1\xi)} + \frac{C^0}{(1 + \theta_1\xi)}\left(\frac{7}{3}\right)^{\frac{1}{2}}\frac{r_x}{(\pi D_{OX}t_0)^{\frac{1}{2}}} \tag{17}$$

$$C_R(r_x, t^*) = \frac{C^0(\theta_1 - \theta_2)(\xi^2)}{(1 + \theta_1\xi)(1 + \theta_2\xi)}\text{erfc}\left[\frac{r_x}{2(D_R t^*)^{\frac{1}{2}}}\right] + \frac{C^0\xi}{(1 + \theta_1\xi)} - \frac{C^0}{(1 + \theta_1\xi)}\left(\frac{7}{3}\right)^{\frac{1}{2}}\frac{r_x}{(\pi D_R t_0)^{\frac{1}{2}}}. \tag{18}$$

At time δ after application of the potential step, the current is

$$i(t_0 + \delta) = nFA(t_0 + \delta)D_{OX}\left(\frac{\partial C_{OX}(r_x, t^*)}{\partial r_x}\right)_{r_x = 0,\, t^* = \delta}$$

$$= nFA(t_0 + \delta)C^0\left(\frac{D_{ox}}{\pi\delta}\right)^{\frac{1}{2}} \frac{\xi(\theta_1 - \theta_2)}{(1 + \theta_1\xi)(1 + \theta_2\xi)} +$$

$$nFA(t_0 + \delta)C^0\left(\frac{7}{3}\right)^{\frac{1}{2}}\left(\frac{D_{ox}}{\pi t_0}\right)^{\frac{1}{2}}\left(\frac{1}{1 + \theta_1\xi}\right). \qquad (19)$$

Subtracting eqn. (9) from eqn. (19), and using ϵ_1 and σ^2, we find for the differential pulse polarographic current:

$$i_{dpp} = i(t_0 + \delta) - i(t_0) = nFA(t_0 + \delta)C^0\left(\frac{D_{ox}}{\pi\delta}\right)^{\frac{1}{2}} \frac{\epsilon_1(1 - \sigma^2)}{(1 + \epsilon_1)(1 + \sigma^2\epsilon_1)} +$$

$$\left\{\frac{(t_0 + \delta)^{2/3} - t_0^{2/3}}{t_0^{2/3}}\right\} nFA(t_0)C^0\left(\frac{7}{3}\right)^{\frac{1}{2}}\left(\frac{D_{ox}}{\pi t_0}\right)^{\frac{1}{2}}\left(\frac{1}{1 + \epsilon_1}\right). \qquad (20)$$

The first term on the right-hand side of eqn. (20) is equal to the solution proposed by Christie and Osteryoung (see eqn. 1). The second term can be considered as a correction term which causes an upward shift of the base-line at the cathodic side of the peak in the case of a scan in cathodic direction. This effect results from a straightforward treatment via the evaluation of the concentration profile, which is more correct, in our opinion, than the rather artificial separation of the faradaic current into a d.c.-contribution and a contribution because of the pulse[2]. A justification for this separation was given only recently by Klein and Yarnitzky [7], based on an equation for the pulse response of an electrode reaction derived by Oldham [8].

When the approximate relationship given by the first term of eqn. (20) is considered a few parameters of the differential pulse peak can be derived [3]. When $d(i_{dpp})/dE$ is put equal to zero, the maximum current is found:

$$i_{peak} = i_{dpp}^{max} = nFA(t_0 + \delta)C^0\left(\frac{D_{ox}}{\pi\delta}\right)^{\frac{1}{2}}\left(\frac{1 - \sigma}{1 + \sigma}\right) \qquad (21)$$

while

$$E \text{ peak} = E_{1/2} - \Delta E/2. \qquad (22)$$

The width of the peak at $i_{dpp} = (1/2)i_{peak}$ is given by:

$$W_{1/2} = (RT/nF)\ln(\epsilon_1''/\epsilon_1')$$

where ϵ'' and ϵ' are the roots of the quadratic equation

$$\sigma^2\epsilon_1^2 - (\sigma^2 + 4\sigma + 1)\epsilon_1 + 1 = 0$$

which is obtained by taking i_{dpp} equal to $i_{peak}/2$.

More complicated parameters are obtained by starting from the correct eqn. (20), but since the corrections are not very large, eqns. (21)—(23) will suffice.

RESULTS AND DISCUSSION

To verify eqns (20)–(23), the PAR 174 (Princeton Applied Research) was used in connection with drop timer PAR 172; it has a pulse duration of 57 ms just before the drop is dislodged. The current is sampled during a period of 16.7 ms just before the pulse is applied and 40 ms thereafter. The memory time constant is 17 ms in current-sampled d.c. (s.d.c.) and normal pulse polarography (n.p.p.), but 85 ms in the d.p.p. mode [1].

S.d.c., n.p.p. and d.p.p. curves were recorded for 5.10^{-4} M solutions of thallium(I) and cadmium(II), both 0.1 M in potassium nitrate at 25 °C (mercury flow rate m = 2.90 mg s^{-1}, height of mercury reservoir 50 cm, droptime τ = 1 s and scan rate 1 mV s^{-1}). Potentials were measured vs. SCE.

Equation (20) can be rearranged to:

$$i_{dpp} = nFkm^{2/3}\left(\frac{D_{OX}}{\pi}\right)^{\frac{1}{2}} C^0\left[\left\{\frac{(t_0+\delta)^{2/3}}{\delta^{1/2}}\left(\frac{\epsilon_1(1-\sigma^2)}{(1+\epsilon_1)(1+\sigma^2\epsilon_1)}\right)\right\} + \left(\frac{7}{3}\right)^{\frac{1}{2}}\left(\frac{(t_0+\delta)^{2/3}-(t_0)^{2/3}}{(t_0)^{1/2}}\right)\left(\frac{1}{1+\epsilon_1}\right)\right] =$$

$$nFkm^{2/3}\left(\frac{D_{OX}}{\pi}\right)^{\frac{1}{2}} C^0\left[X\left(\frac{\epsilon_1(1-\sigma^2)}{(1+\epsilon_1)(1+\sigma^2\epsilon_1)}\right) + Y\left(\frac{1}{1+\epsilon_1}\right)\right] \qquad (24)$$

where X and Y depend only on the droptime τ (τ is taken equal to $t_0 + \delta$). Because the current is sampled over a period of time, the average must be taken. For the PAR 174, values of X and Y are calculated by numerical integration (Table 1).

For the verification of eqn. (24), reliable values of the factor $nFkm^{2/3}(D_{OX}/\pi)^{\frac{1}{2}}$ are necessary. These values were calculated from the experimental s.d.c. and n.p.p. curves, by means of different formulae [10, 11]. The results are presented in Table 2 and compared with those calculated from values of the diffusion coefficients taken from the literature [9]. Since the experiment was in good agreement with theory, the theoretical values were used in further calculations.

Figure 1 shows the experimental and theoretical differential pulse polarogram calculated from eqn. (24) in the case of a pulse ΔE = 5 mV and a droptime τ = 1 s. The agreement is rather good, except for the magnitude of the base-line shift ($\Delta i_{\text{base-line}}$) caused by the correction term. Since this discrepancy was found in all experiments (see Table 3), there are probably

TABLE 1

Values of X and Y from eqn. (24) for PAR 174

τ(s)	0.5	1.0	2.0
X	2.843	4.541	7.230
Y	0.101	0.053	0.031

TABLE 2

Values of $nFkm^{2/3}(D_{OX}/\pi)^{\frac{1}{2}}$ at 25 °C (resulting current in mA)

	Literature		Sampled d.c. pol.		Normal pulse pol.	
	D_{OX}[a]	Theor. value	Ilkovič	Lingane and Loveridge [10][b]	Brinkman and Los [11][c] (1)	(2)
Thallium(I)	18	4.00	4.45	3.95	4.13	4.04
Cadmium(II)	6.9	4.95	5.38	4.97	5.07	5.00

[a]Expressed as 10^{-6} cm^2 s^{-1}.
[b]When other extended equations were used, the deviations from the values given were less than 2 %.
[c]1) refers to eqn. (15) of ref. 11.
2) refers to eqn. (20) of ref. 11.

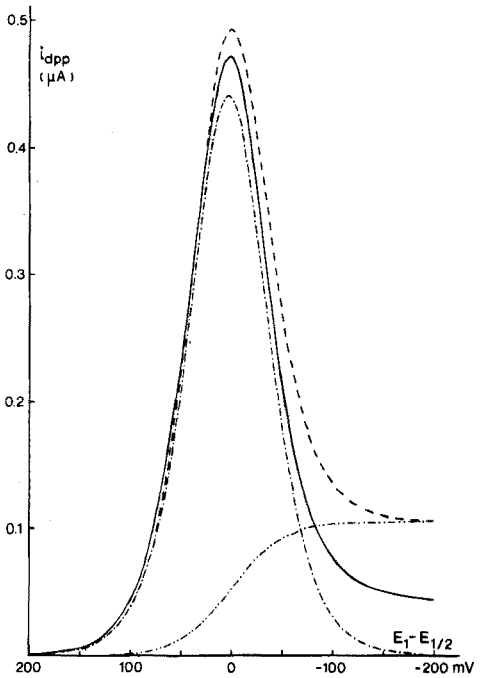

Fig. 1. Differential pulse polarogram of 5.10^{-4} M Tl(I) in 0.1 M KNO_3. Pulse amplitude ΔE = 5 mV, droptime τ = 1 s. Theoretical curves: —·— first term of the right-hand side of eqn. (24); —··— second term; — — — total current. Experimental curve———.

some minor effects which have not been taken into consideration. For instance, there is a systematic deviation caused by the large memory time constant, which results in a slightly lower peak current depending on the scan rate, as Christie et al. [12] showed. (Wetsema [13] recently reported

TABLE 3

Values of $\Delta i_{\text{base-line}} / i_{\text{peak}}$ for PAR 174

	Theoretical			Experimental	
	droptime τ (s)			τ = 1 s	
$n\Delta E$	0.5	1.0	2.0	Tl	Cd
5	0.543	0.215	0.085	0.095	
10	0.315	0.114	0.043	0.050	0.049
15	0.222	0.078	0.029		
20	0.172	0.059	0.022		0.025
25	0.141	0.048	0.018	0.019	
30	0.120	0.041	0.015		
50	0.077	0.026	0.009	0.009	0.010
75	0.056	0.019	0.007		
100	0.047	0.016	0.006	0.000	0.004
150	0.039	0.013	0.005		
200	0.037	0.012	0.004		0.000
300	0.036	0.012	0.004		

problems of the same character in absolute measurements of pulse-polarographic currents with the PAR 170 Electrochemistry System.) Furthermore, the continuous change of the potential during the pulse and sampling periods is not accounted for. Also noteworthy is the fact that, in our experience, this shift of the base-line disappears if no maximum suppressor is added to the solution. A few drops of 0.2 % Triton X-100 solution were used in the present experiments for verification of the theoretical relationship.

Because the influence of the correction term in eqns. (20) and (24) is most pronounced for small values of $n\Delta E$ and for short drop times, it is obvious that in these regions eqns. (21)—(23) will show some small deviations, which were indeed found in these experiments. Apart from these deviations, the influence of the memory time constant was found to result in a cathodic shift of the peak potential, in accordance with the results of Christie et al. [12]. The shift was 8 mV for cadmium and 11 mV for thallium in comparison with s.d.c. and eqn. (22).

Finally, some attention was given to the possibilities of d.p.p. as a technique suitable for the determination of stability constants. In a system containing 10^{-4} M cadmium(II) and 10^{-2} M glycine in 0.1 M potassium nitrate, the concentration of ligand $[L^-]$ was varied by addition of potassium hydroxide. The method of DeFord and Hume [14] was used, $E_{1/2}$ being replaced by E_{peak}, and two constants were obtained graphically:

$\log \beta_{ML} = 4.6$ and $\log \beta_{ML_2} = 8.0$

which are in agreement with the values in the literature [15, 16]. This technique seems to offer a means of determining the complexing properties of systems at low concentration levels.

APPENDIX 1

The equation for diffusion towards an expanding sphere can be written [4] as

$$\frac{\partial C(x, y)}{\partial y} = m \frac{\partial^2 C(x, y)}{\partial x^2} \tag{1.1}$$

where $m = (27/7)\gamma^{4/3}D$, $y = t^{7/3}$ and $x = \rho^3 = r^3 - r_0^3$.
The initial conditions are:

$$C_{OX}(r, 0) = C^0 \rightarrow C_{OX}(x, 0) = C^0 \tag{1.2}$$

$$C_R(r, 0) = 0 \rightarrow C_R(x, 0) = 0\,. \tag{1.3}$$

By defining the new quantity $U(x, y) = C^0 - C_{OX}(x, y)$ the initial condition (1.2) can be replaced by

$$U(x, 0) = 0 \tag{1.4}$$

Laplace transformation of eqn. (1.1) with respect to y for both OX and R yields:

$$m_{OX} \frac{\partial^2 C_{OX}(x, y)}{\partial x^2} = \frac{\partial C_{OX}(x, y)}{\partial y} \rightarrow m_{OX} \frac{d^2 \bar{C}_{OX}(x, s)}{dx^2} = s\bar{C}_{OX}(x, s) - C_{OX}(x, 0)$$

or

$$m_{OX} \frac{\partial^2 U(x, y)}{\partial x^2} = \frac{\partial U(x, y)}{\partial y} \rightarrow m_{OX} \frac{d^2 \bar{U}(x, s)}{dx^2} = s\bar{U}(x, s) - U(x, 0) \tag{1.5}$$

and

$$m_R \frac{\partial^2 C_R(x, y)}{\partial x^2} = \frac{\partial C_R(x, y)}{\partial y} \rightarrow m_R \frac{d^2 \bar{C}_R(x, s)}{dx^2} = s\bar{C}_R(x, s) - C_R(x, 0). \tag{1.6}$$

Both $U(x, 0)$ and $C_R(x, 0)$ are equal to zero, so

$$\frac{d^2 \bar{U}(x, s)}{dx^2} - \frac{s}{m_{OX}} \bar{U}(x, s) = 0 \tag{1.7}$$

and

$$\frac{d^2 \bar{C}_R(x, s)}{dx^2} - \frac{s}{m_R} \bar{C}_R(x, s) = 0\,. \tag{1.8}$$

General solutions of these second-order differential equations are

$$\bar{U}(x, s) = C_1 \cdot e^{\left(\frac{s}{m_{OX}}\right)^{\frac{1}{2}} x} + C_2 \cdot e^{-\left(\frac{s}{m_{OX}}\right)^{\frac{1}{2}} x} \text{ and } \bar{C}_R(x, s) = C_3 \cdot e^{\left(\frac{s}{m_R}\right)^{\frac{1}{2}} x} + C_4 \cdot e^{-\left(\frac{s}{m_R}\right)^{\frac{1}{2}} x}$$

As the values for $\bar{U}(x, s)$ and $\bar{C}_R(x, s)$ should remain finite for $x \rightarrow \infty$, C_1 and C_3 must be zero, leaving

$$\bar{U}(x, s) = C_2 \cdot e^{-\left(\frac{s}{m_{OX}}\right)^{\frac{1}{2}} x} \tag{1.9}$$

$$\bar{C}_R(x, s) = C_4 \cdot e^{-\left(\frac{s}{m_R}\right)^{\frac{1}{2}} x}. \tag{1.10}$$

The constants C_2 and C_4 can be found by using the boundary conditions (5) and (6). Transformation of these equations into the new coordinate system leads to:

$$D_{OX}\left(\frac{\partial C_{OX}(x, y)}{\partial x}\right)_{x=0} + D_R\left(\frac{\partial C_R(x, y)}{\partial x}\right)_{x=0} = 0$$

or

$$-D_{OX}\left(\frac{\partial u(x, y)}{\partial x}\right)_{x=0} + D_R\left(\frac{\partial C_R(x, y)}{\partial x}\right)_{x=0} = 0 \tag{1.11}$$

and

$$\frac{C_{OX}(0, y)}{C_R(0, y)} = \theta_1 \text{ or } \frac{C^0 - U(0, y)}{C_R(0, y)} = \theta_1. \tag{1.12}$$

Laplace transformation gives:

$$-D_{OX}\left(\frac{d\bar{U}(x, s)}{dx}\right)_{x=0} + D_R\left(\frac{d\bar{C}_R(x, s)}{dx}\right)_{x=0} = 0 \tag{1.13}$$

and

$$\frac{C^0}{s} - \bar{U}(0, s) = \theta_1 \cdot \bar{C}_R(0, s) \tag{1.14}$$

Substitution of eqns. (1.9) and (1.10) leads to:

$$C_4 = C_2\left(\frac{D_{OX}}{D_R}\right)^{\frac{1}{2}} = C_2\xi \text{ and } \frac{C^0}{s} - C_2 = \theta_1 C_4$$

After some algebra it is found that:

$$C_2 = \frac{C^0}{s}\,\frac{1}{(1 + \theta_1\xi)} \text{ and } C_4 = \frac{C^0}{s}\,\frac{\xi}{(1 + \theta_1\xi)}.$$

So

$$\bar{U}(x, s) = \frac{C^0}{s}\,\frac{1}{(1 + \theta_1\xi)}\, e^{-\left(\frac{s}{m_{OX}}\right)^{\frac{1}{2}} x}$$

and

$$c_r(x, s) = \frac{C^0}{s}\,\frac{\xi}{(1 + \theta_1\xi)}\, e^{-\left(\frac{s}{m_R}\right)^{\frac{1}{2}} x}.$$

Inversed transformation yields:

$$U(x, y) = \frac{C^0}{(1 + \theta_1 \xi)} \operatorname{erfc}\left[\frac{x}{2(m_{OX} y)^{\frac{1}{2}}}\right]$$

or

$$C_{OX}(r, t) = C^0 - \frac{C^0}{(1 + \theta_1 \xi)} \operatorname{erfc}\left[\frac{1}{6(D_{OX} t)^{\frac{1}{2}}} \left(\frac{7}{3}\right)^{\frac{1}{2}} \left(\frac{r^3 - r_0^3}{r_0^2}\right)\right] \tag{1.15}$$

and

$$C_R(x, y) = C^0 \frac{\xi}{(1 + \theta_1 \xi)} \operatorname{erfc}\left[\frac{x}{2(m_R y)^{\frac{1}{2}}}\right]$$

or

$$C_R(r, t) = C^0 \frac{\xi}{(1 + \theta_1 \xi)} \operatorname{erfc}\left[\frac{1}{6(D_R t)^{\frac{1}{2}}} \left(\frac{7}{3}\right)^{\frac{1}{2}} \left(\frac{r^3 - r_0^3}{r_0^2}\right)\right]. \tag{1.16}$$

APPENDIX 2

It should be borne in mind that in the evaluation of the concentration profile in response to the application of the potential step, the counting of time is started again from the instant t_0, where $t^* = 0$. Since we assume the electrode to behave now as a planar and non-expanding one, we must also define a linear coordinate $r_x = r - r_0$, and express the initial and boundary conditions in this coordinate (eqns. 11, 12, 15 and 16).

Laplace transformation of the diffusion eqn. (10) for both OX and R yields:

$$D_{OX}\left(\frac{d^2 \bar{C}_{OX}(r_x, s)}{dr_x^2}\right) = s\, \bar{C}_{OX}(r_x, s) - C_{OX}(r_x, 0) \tag{2.1}$$

and

$$D_R\left(\frac{d^2 \bar{C}_R(r_x, s)}{dr_x^2}\right) = s\, \bar{C}_R(r_x, s) - C_R(r_x, 0). \tag{2.2}$$

Introduction of eqns. (15) and (16) gives:

$$\frac{d^2 \bar{C}_{OX}(r_x, s)}{dr_x^2} = \frac{s}{D_{OX}} \bar{C}_{OX}(r_x, s) - \frac{a + br_x}{D_{OX}} \tag{2.3}$$

and

$$\frac{d^2 \bar{C}_R(r_x, s)}{dr_x^2} = \frac{s}{D_R} \bar{C}_R(r_x, s) - \frac{c + dr_x}{D_R} \tag{2.4}$$

The general solutions of these differential equations are:

หอสมุด กรมวิทยาศาสตร์

$$\bar{C}_{OX}(r_x, s) = C_5 e^{\left(\frac{s}{D_{OX}}\right)^{\frac{1}{2}} r_x} + C_6 e^{-\left(\frac{s}{D_{OX}}\right)^{\frac{1}{2}} r_x} + (a + br_x)/s \tag{2.5}$$

$$\bar{C}_R(r_x, s) = C_7 e^{\left(\frac{s}{D_R}\right)^{\frac{1}{2}} r_x} + C_8 e^{-\left(\frac{s}{D_R}\right)^{\frac{1}{2}} r_x} + (c + dr_x)/s. \tag{2.6}$$

The constants C_5 and C_7 must be zero in order to obtain finite values of $\bar{C}_{OX}(r_x, s)$ and $\bar{C}_R(r_x, s)$ when $r_x \to \infty$. Laplace transformation of the boundary conditions (11) and (12) yields:

$$\bar{C}_{OX}(0, s) = \theta_2 \bar{C}_R(0, s) \tag{2.7}$$

$$D_{OX}\left(\frac{d\bar{C}_{OX}(r, s)}{dr_x}\right)_{r_x = 0} + D_R\left(\frac{d\bar{C}_R(r_x, s)}{dr_x}\right)_{r_x = 0} = 0 \tag{2.8}$$

Introduction of eqns. (2.5) and (2.6) into eqn. (2.8), gives:

$$D_{OX}\left[-C_6\left(\frac{s}{D_{OX}}\right)^{\frac{1}{2}} e^{-\left(\frac{s}{D_{OX}}\right)^{\frac{1}{2}} r_x} + \frac{b}{s}\right]_{r_x = 0} + D_R\left[-C_8\left(\frac{s}{D_R}\right)^{\frac{1}{2}} e^{-\left(\frac{s}{D_R}\right) r_x} + \frac{d}{s}\right]_{r_x = 0}$$

$$= D_{OX}\left(-C_6\left(\frac{s}{D_{OX}}\right)^{\frac{1}{2}} + \frac{b}{s}\right) + D_R\left(-C_8\left(\frac{s}{D_R}\right)^{\frac{1}{2}} + \frac{d}{s}\right) = -\left\{C_6(sD_{OX})^{\frac{1}{2}} + \right.$$

$$\left. + C_8(sD_R)^{\frac{1}{2}}\right\} = 0$$

since

$$\frac{bD_{OX}}{s} + \frac{dD_R}{s} = \frac{C^0 D_{OX}}{(1 + \theta_1 \xi)}\left(\frac{7}{3}\right)^{\frac{1}{2}} \frac{1}{(D_{OX} t_0)^{\frac{1}{2}}} - \frac{C^0 \xi}{(1 + \theta_1 \xi)}\left(\frac{7}{3}\right)^{\frac{1}{2}} \frac{D_R}{(D_R t_0)^{\frac{1}{2}}} = 0.$$

From eqns. (2.5), (2.6) and (2.7) it follows that:

$$\bar{C}_{OX}(0, s) = \theta_2 \bar{C}_R(0, s) \to C_6 + \frac{a}{s} = \theta_2\left(C_8 + \frac{c}{s}\right)$$

thus

$$C_6 = -\frac{1}{s}(D_R)^{\frac{1}{2}}\left(\frac{a - c\theta_2}{\theta_2(D_{OX})^{\frac{1}{2}} + (D_R)^{\frac{1}{2}}}\right)$$

and

$$C_8 = \frac{1}{s}(D_{OX})^{\frac{1}{2}}\left(\frac{a - c\theta_2}{\theta_2(D_{OX})^{\frac{1}{2}} + (D_R)^{\frac{1}{2}}}\right).$$

If eqn. (2.5) is rewritten as:

$$\bar{C}_{OX}(r_x, s) = -\frac{1}{s}(D_R)^{\frac{1}{2}}\left(\frac{a - c\theta_2}{\theta_2(D_{OX})^{\frac{1}{2}} + (D_R)^{\frac{1}{2}}}\right) e^{-\left(\frac{s}{D_{OX}}\right)^{\frac{1}{2}} r_x} + \frac{a + br_x}{s}$$

then inverse transformation gives:

$$C_{OX}(r_x, t^*) = -\left(\frac{a - c\theta_2}{\theta_2(D_{OX})^{\frac{1}{2}} + (D_R)^{\frac{1}{2}}}\right)(D_R)^{\frac{1}{2}} \operatorname{erfc}\left[\frac{r_x}{2(D_{OX} t^*)^{\frac{1}{2}}}\right] + a + br_x \tag{2.9}$$

Substitution of the correct values of a, b and c gives:

$$C_{OX}(r_x, t^*) = \frac{C^0\xi(\theta_2 - \theta_1)}{(1 + \theta_1\xi)(1 + \theta_2\xi)} \operatorname{erfc}\left[\frac{r_x}{2(D_{OX}t^*)^{\frac{1}{2}}}\right] + \frac{C^0\theta_1\xi}{(1 + \theta_1\xi)} + \\ + \frac{C^0}{(1 + \theta_1\xi)}\left(\frac{7}{3}\right)^{\frac{1}{2}} \frac{r_x}{(\pi D_{OX}t_0)^{\frac{1}{2}}}. \quad (2.10)$$

The same can be done for eqn (2.6), giving $C_R(r_x, t^*)$.

REFERENCES

1 Instruction Manual, Polarographic Analyzer, Model 174, Princeton Applied Research, Princeton, N.J., 1974.
2 J. H. Christie and R. A. Osteryoung, J. Electroanal. Chem. Interfacial Electrochem., 49 (1974) 301.
3 E. P. Parry and R. A. Osteryoung, Anal. Chem., 37 (1965) 1634.
4 D. MacGillavry and E. K. Rideal, Rec. Trav. Chim. Pays-Bas, 56 (1937) 1013; see also I. M. Kolthoff and J. J. Lingane, Polarography, Interscience, New York, 2nd ed., 1952, pp. 35—40.
5 P. Delahay, New instrumental methods in electrochemistry, Interscience, New York, 1954, pp. 52—55.
6 H. Strehlow and M. von Stackelberg, Z. Elektrochem. 54 (1950) 51.
7 N. Klein and Ch. Yarnitzky, J. Electroanal. Chem. Interfacial Electrochem., 61 (1975) 1.
8 K. B. Oldham, Anal. Chem., 40 (1968) 1024.
9 J. Heyrovsky and J. Kůta, Grundlagen der Polarographie, Akademie-Verlag, Berlin, 1965.
10 J. J. Lingane and B. A. Loveridge, J. Amer. Chem. Soc., 72 (1950) 438.
11 A. A. A. M. Brinkman and J. M. Los, J. Electroanal. Chem. Interfacial Electrochem., 7 (1964) 171.
12 J. H. Christie, J. Osteryoung and R. A. Osteryoung, Anal. Chem., 45 (1973) 210.
13 B. J. C. Wetsema, Thesis, Free University, Amsterdam, 1975.
14 D. D. DeFord and D. N. Hume, J. Amer. Chem. Soc., 73 (1951) 5321.
15 L. G. Sillén and A. E. Martell, Stability Constants, Spec. Publ. no. 17, The Chemical Society, London, 1964; Supplement no. 1, Spec. Publ. no. 25, 1971.
16 G. J. M. Heijne and W. E. van der Linden, Talanta, 22 (1975) 923.

Analytica Chimica Acta, 82 (1976) 245—254
© Elsevier Scientific Publishing Company, Amsterdam — Printed in The Netherlands

AUTOMATED POLAROGRAPHIC ANALYSIS
PART II. RESPONSE TIME AND PRECISION STUDIES

WALTER LUND and LISE-NETTE OPHEIM
Department of Chemistry, University of Oslo, Oslo 3 (Norway)
(Received 24th September 1975)

SUMMARY

A systematic study of various experimental parameters which may influence the response time and precision of an automated polarographic system is described. The effects of segmented streams, flow rate, pump stop during sample shifts, debubbler position, current damping, scale expansion, sampling rate and type of deaerating gas are discussed. Low response times are favoured by the use of segmented streams, a high aspiration rate, a short distance between the debubbler and the working electrode and a low current damping, while the best precision is obtained by using scale expansion, pump stop during sample shifts, a low sampling rate and argon gas for deaeration. Under optimized conditions a standard deviation of 0.3 % was obtained.

In a previous paper [1] the design of the flow-through cells and deaeration procedures used in automated polarographic analysis were discussed. One of the interesting parameters of an automated system is the optimal sampling rate, which depends on the response time of the system. Usually there will also be a relationship between the sampling rate and the analytical precision, the best precision being obtained at low sampling rates. The response time and precision of an automated polarographic system may be influenced by many experimental parameters, the effects of which are described in this paper.

EXPERIMENTAL

Apparatus

The automated system is based on the AutoAnalyzer principle (Technicon), with a gas-segmented flow stream which is moved by a peristaltic pump from the sampler to the detector unit. Details of the automated system have been given in Part I [1], in which particular attention is given to the design of detectors and the construction of a sampler—deaeration unit. For the work described here, each of the peristaltic pumps (Ismatec Mini-Micro-2) was equipped with a ten-step Multur-M 120 J gearbox (Erwin Halstrup, West Germany), so that the rotation speed of the pumps could be varied. An external d.c.-offset was connected in series with the recorder (Radiometer

Servograph REC 51), which was equipped with an event marker. Unless otherwise stated, argon gas was used for deaerating the sample solutions and for segmenting the flowing streams.

RESPONSE TIME STUDIES

Measurement of the response time

The response time studies were carried out by analyzing solutions containing alternately 100 p.p.m. chlordiazepoxide and a wash solution; both solutions contained 0.01 M sulphuric acid. A fixed potential of —0.49 V vs. Ag/AgCl (sat.KCl) was maintained for all analyses. A typical current—time curve is shown in Fig. 1, in which the sequence of events is as follows: A, the sample shift takes place; B, the sample containing chlordiazepoxide arrives at the detector; C, the steady-state current of the sample is reached; D, a new sample shift takes place; E, the wash solution reaches the detector; F, the steady-state current for the wash solution is attained. The distance A—B is defined here as the "dead time" of the system, whereas the distance B—C is defined as the response time (Technicon calls B—C the "wash-out time"). Owing to the difficulties in locating the points B and particularly C, the uncertainty in the measured response times was estimated to be ±5 s. The response times referred to in this paper usually represent the mean of at least 2—3 separate measurements.

Effect of segmenting the flowing stream

In systems of the AutoAnalyzer type, where the samples are carried through various modules before entering the detector, there will be a certain

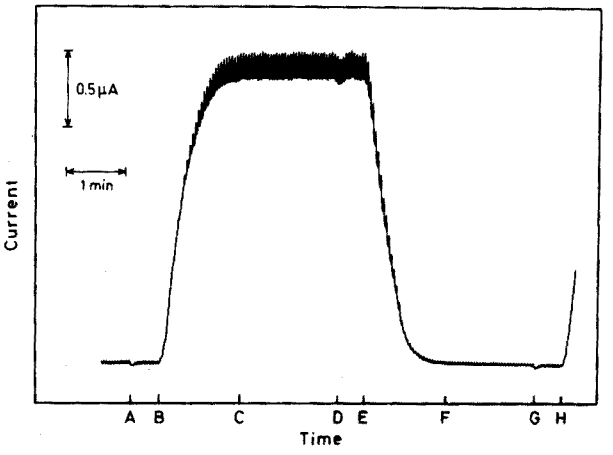

Fig. 1. Current—time curve for samples containing alternately 100 p.p.m. chlordiazepoxide and supporting electrolyte. The letters A—H are explained in the text.

degree of mixing of consecutive solutions. The response time of the system will depend on the extent of this mixing, and also on the design of the detector system. When the term "response time" is used in this paper, it is the sum of these effects which is implied. In an AutoAnalyzer system the mixing of consecutive solutions is prevented by segmenting the flow streams by means of gas bubbles. Air is normally used for this purpose, but for polarographic analysis an inert gas is necessary to prevent oxygen from entering the solutions [1]. It is usually convenient to use the same gas both for deaeration of the sample solutions and for segmenting the flow streams.

For a given aspiration rate the number of gas segments, as well as the total gas volume, depends on the gas flow rate which is used. The response time was measured at different gas flow rates, while the aspiration rate was kept constant at 1.20 ml min^{-1}. It was found that the response time was independent of the argon flow rate in the region 0.03—3 ml min^{-1}. A response time of 2.5 min was observed in these experiments; in the absence of gas segments the response time was found to be 4 min, indicating that the segmentation has, after all, a favourable effect on the response time. A gas rate of 0.3 ml min^{-1} was used throughout this work.

Effect of flow rate

It was expected that the response time would be a function of the flow rate of the system. The response time was therefore measured at various rates of aspiration, by varying the speed of the peristaltic pump and the inner diameter of the pump tubing; measurements were made both with and without pump stop during sample shifts, the effect of pump stop being

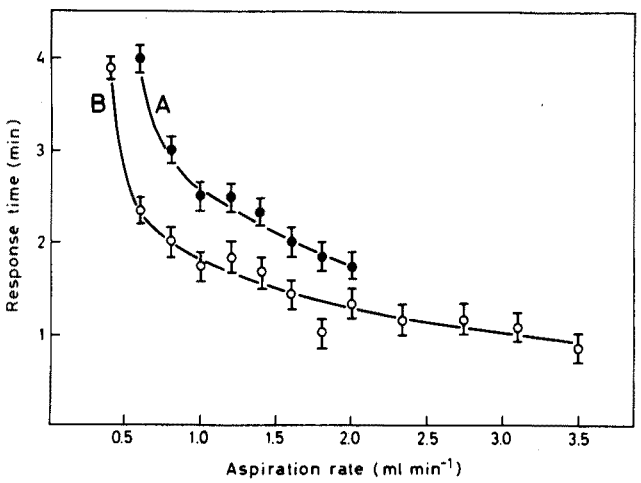

Fig. 2. Effect of aspiration rate on the response time. A, pump stop is used during sample shifts; B, without pump stop.

discussed in the next paragraph. "Response volumes" were calculated by multiplying the response time by the aspiration rate. As can be seen from Fig. 2 and Table 1, the response time decreases with increasing aspiration rate, the decrease being particularly marked for the low aspiration rates. However, the response volume increases with increasing aspiration rate, and thus for most practical purposes a medium aspiration rate is to be preferred. Unless otherwise stated, an aspiration rate of 1.20 ml min^{-1} was used in this work.

TABLE 1

Effect of aspiration rate on response time and response volume

Aspiration rate (ml min^{-1})	Without pump stop		With pump stop	
	Response time (s)	Response volume (ml)	Response time (s)	Response volume (ml)
0.40	235	1.6		
0.60	140	1.4	240	2.4
0.80	120	1.6	180	2.4
1.00	105	1.8	150	2.5
1.20	110	2.2	150	3.0
1.40	100	2.3	140	3.3
1.60	85	2.3	120	3.2
1.80	60	1.8	110	3.4
2.00	80	2.7	105	3.4
2.35	70	2.7		
2.75	70	3.2		
3.10	65	3.3		
3.50	50	2.9		

In discussing the effect of flow rate, the linear velocity of the solution must also be considered. While the flow rate (in ml min^{-1}) will be the same in all parts of the system (and equal to the aspiration rate), the linear velocity (in cm s^{-1}) will vary with the diameter of the tubing in the different parts of the system. However, no variation in response time was found when tubings with inner diameters ranging from 0.03 to 0.05 in. were used, indicating that the linear velocity of the solution was of minor importance in the present case. The aspiration rate was 0.60 ml min^{-1} in these experiments.

Effect of pump stop during sample shifts

When the sampling probe shifts from one sample cup to the next, air is normally drawn into the system. This air segment prevents mixing of consecutive samples and has therefore a favourable effect on the response time. However, when a polarographic detector is used, the introduction of air causes an increase in the background current, owing to the polarographic reduction of oxygen. This may have an adverse effect on the precision of the

analytical method [1]. For this reason a separate time delay circuit was built into the timer unit, effecting a 2-s halt of the peristaltic pumps during the sample shifts. The effect of this pump stop on the response time is illustrated in Table 1 and Fig. 2. Obviously, the pump stop increases significantly the response time of the system for all the aspiration rates used, owing to the absence of a gas segment between consecutive samples.

Effect of debubbler position

In a system of the AutoAnalyzer type, the gas bubbles used for segmenting the flow streams are removed by a debubbler before the solutions enter the detector. The distance between the debubbler and working electrode should be kept as short as possible, in order to minimize cross-mixing of samples in this region. The response time was decreased by ca. 30 % when the distance between the debubbler and working electrode was decreased from 6.5 to 4.5 cm. For this reason the debubbler was always positioned as close as possible to the working electrode.

Effect of damping of the current

In d.c. polarography the current oscillations, which are caused by the growth and fall of the mercury drops, are damped before being recorded. This damping may result in an increase in the response time of the system. For ordinary values of the time constant (ca. 20 s), the effect of damping on the response time was negligible, but for high time constants, long response times were observed. For example, the response time increased from 100 to 180 s when the time constant of the damping was increased from 25 to 100 s. A high time constant was used in connection with the expanded-scale procedure for high-precision analyses, which are described below.

PRECISION STUDIES

The relationship between current and concentration was investigated by analyzing solutions containing 60—140 p.p.m. chlordiazepoxide, at a constant potential of —0.49 V vs. Ag/AgCl (sat.KCl). As expected, the relationship was linear; regression analysis gave an F value of 0.031, compared to the value 2.87 for the F-distribution with 4 and 20 degrees of freedom, respectively, at the 95 % level.

A particular test programme was used for the precision studies. Five test solutions, containing 96, 98, 100, 102 and 104 p.p.m. chlordiazepoxide in 0.01 M sulphuric acid were used, and five replicates were analyzed for each concentration. Each series therefore comprised 25 samples, which were analyzed in a fixed, randomized order. The sequence of samples was such that each of the five test solutions in turn was preceded by samples representing the four other concentrations. This was done to eliminate any

systematic errors arising from memory effects, in cases where the washing step between the samples was omitted. For each series the pooled standard deviation was calculated from the equation

$$s_r(\%) = \frac{100}{\bar{x}} \sqrt{\frac{1}{20} \sum_{j=1}^{5} \sum_{i=1}^{5} (x_{ij} - \bar{x}_j)^2}$$

where the j values indicate the five test solutions, and the i values the five replicates for each of these solutions; $\bar{x}$ represents the mean concentration of the 25 samples. In automated analyses there may sometimes be a drift or systematic variation in the results as a function of time. In the present work no such drift was observed, when 60 samples were analyzed in the course of 90 min (sampling time 1.5 min).

The use of expanded scale

Usually a wash solution is introduced between each sample in a system of the AutoAnalyzer type, but there are various reasons for omitting this step. For example, the sampling time can be increased without decreasing the sampling rate, and when samples of similar concentrations are analyzed, the recorder sensitivity can be increased markedly, resulting in better precision, if the instrument is equipped with a sufficient d.c. offset capability. The principle of the scale-expansion procedure is illustrated in Fig. 3. Figure 3(a) shows a current–time curve for solutions containing 96, 98, and 100 p.p.m. chlordiazepoxide, respectively; 0.01 M sulphuric acid was used as wash solution between each sample. Figure 3(b) shows the analysis of the same three solutions with a ten times scale expansion; no wash solution was used in this case.

The scale expansion produces a significant improvement in the current measurements, and thus in the precision of the analysis. Typically, the standard deviation was decreased from 2.4 % to 0.7 % when 25 samples were analyzed without and with scale expansion, respectively, at a sampling rate of 15 samples h^{-1}.

When scale expansion is used, the increase in recorder sensitivity must usually be accompanied by an increase in the d.c.-offset of the recorder. For many recorders, like the one used in the present investigation, the built-in d.c.-offset has an insufficient range for this purpose, and an external d.c.-offset must be connected in series with the recorder.

When the recorder sensitivity is set to a high value, a high damping of the current oscillations must also be used, in order to obtain useful current–time curves. This in turn results in an increase in the response time of the system, as discussed above. Nevertheless, it was found that scale expansion gave improved precision even for relatively short sampling times, i.e. 2 min, although the effect is more marked for sampling times of 4 min, as shown in Table 2.

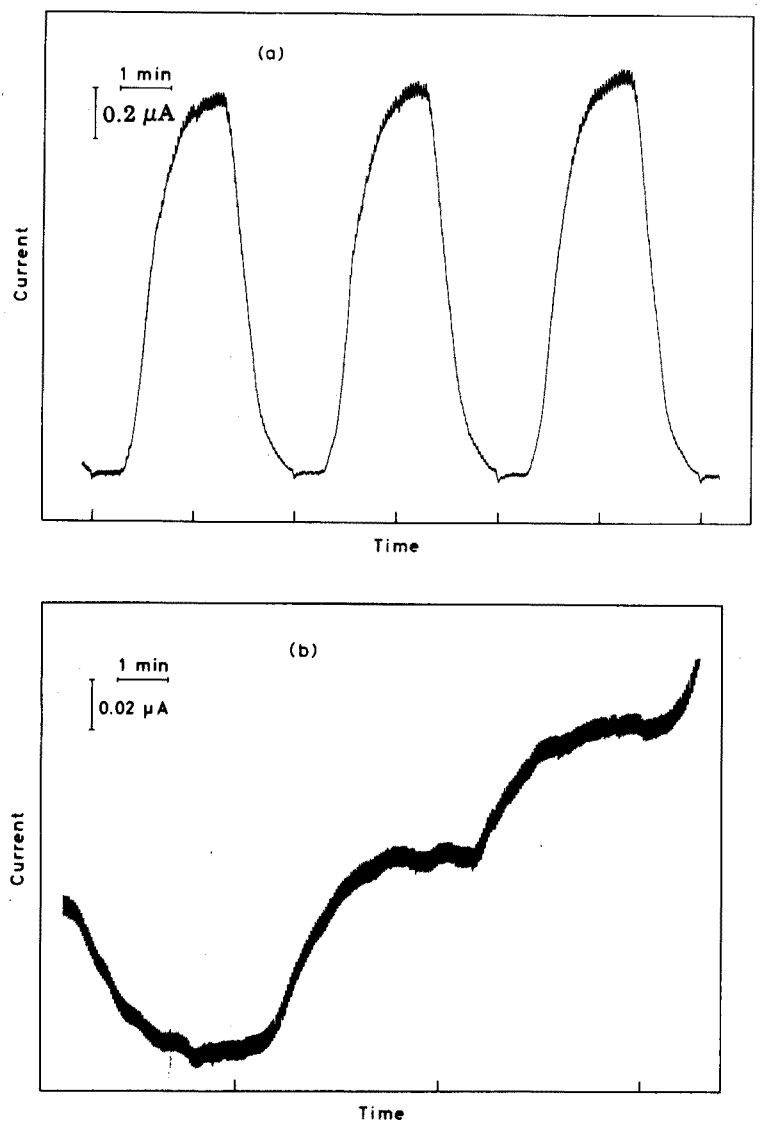

Fig. 3. Current—time curves for samples containing 96, 98 and 100 p.p.m. chlordiazepoxide. (a) Normal recording. Sampling time 2 min, wash time 2 min. (b) With the expanded scale procedure. Sampling time 4 min. The sample shifts are indicated on the time axis.

Effect of pump stop

As discussed above, the use of the pump stop during sample shifts causes a significant increase in the response time of the system. However, the pump stop procedure has a favourable effect on the precision of the system, owing to the lower background current obtained in this case [1]. The results given

in Table 2 show that the precision is improved markedly by the use of pump stop during sample shifts, for all the three procedures investigated. The best precision is obtained when the pump stop procedure is combined with scale expansion and a sampling time of 4 min; the standard deviation was then as low as 0.3 %.

TABLE 2

Effect of scale expansion and pump stop on precision

Sampling time (min)	Wash time (min)	Sensitivity (μA cm^{-1})	Damping, time const. (s)	s_r(%) without pump stop	s_r(%) with pump stop
Scale expansion					
4	0	0.01	75	0.7	0.3
2	0	0.01	75	1.2	0.8
No scale expansion					
2	2	0.1	25	2.4	1.2

Effect of sampling rate

Table 2 also shows that a significant improvement in precision can be obtained when the sampling time is increased from 2 to 4 min. Only in the latter case does the current reach a constant (steady state) value for each sample, before a new sample arrives at the detector. The effect of sampling time on precision is shown in Table 3; these results were obtained by analyzing series of 25 samples at sampling times varying from 1 to 4 min, corresponding to sampling rates from 60 to 15 samples per hour. The analyses were carried out by the expanded scale procedure with a pump stop during sample shifts, and with ordinary welding argon for deaeration. It can be seen that the standard deviation decreases as the sampling time is increased from 1 to 3 min. Above 3 min the precision is constant, indicating that the steady-state current for each sample is reached at these sampling times, and that the response time is ca. 3 min in these experiments. For a sampling time of 60 s no correlation was found between the current and concentration.

When scale expansion is used at short sampling times, the current measurements may represent a problem; frequently no well-defined peaks or shoulders can be distinguished on the current—time curves. Typically, a current—time curve like that shown in Fig. 4 is obtained; here ten samples are analyzed by using scale expansion, with a sampling time of 75 s. In such cases, it is recommended that the recorder be equipped with an event marker, which indicates at which points on the time axis the sample shifts take place. The current readings are made at a fixed time, equal to the "dead time" (AB in Fig. 1), after each sample shift. The dead time is most easily determined by analyzing a few standards with markedly different concentrations. In the present investigation the currents were measured in this way whenever a sampling time below 2 min was used.

TABLE 3

Effect of sampling time and type of deaerating gas on precision

Sampling time (s)	s_r(%)		
	Argon ordinary	Argon purified	Nitrogen purified
75	1.1		1.1
90	0.8	0.9	1.0
120	0.7	0.5	0.8
150	0.4	0.5	0.7
180	0.3	0.4	0.5
210	0.3		0.7
240	0.3		

Effect of deaerating gas

Three types of inert gas were tested for deaeration: highly purified nitrogen, spectroscopically pure argon and ordinary welding argon. The results are shown in Table 3. Clearly, the best precision is obtained when argon is used for deaeration. This can be explained by the higher density of argon being more effective in preventing diffusion of air into the open sample cups. There appears to be no significant difference in the precision obtained for the two qualities of argon. As welding argon is inexpensive, this gas was preferred.

DISCUSSION

For routine analysis it is usually of interest to find a system which is capable of giving both a high sampling rate and a good precision. A high

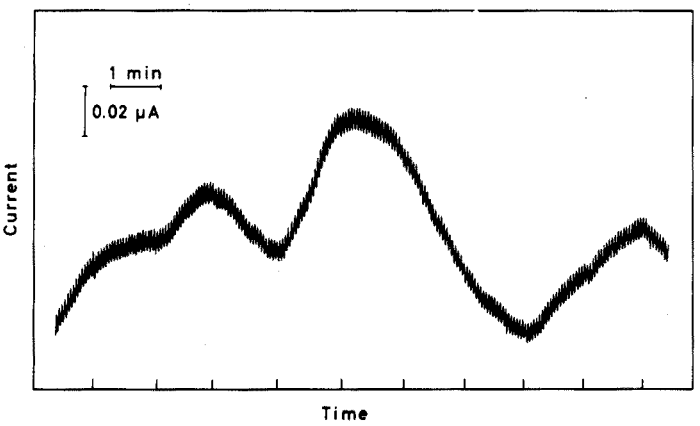

Fig. 4. Current—time curve for the analysis of ten samples, with scale expansion and a high sampling rate (sampling time 75 s). The sample shifts are indicated on the time axis.

sampling rate means that the response time of the system must be low. However, with the present system, it was found that experimental parameters which have a favourable effect on the precision, frequently have an adverse effect on the response time of the system. Thus, the use of pump stop during sample shifts gives rise to a low background current and thus to improved precision, but the response time is also increased, owing to the absence of an air segment between different samples, which results in cross-mixing of samples. The scale expansion procedure gives improved precision, but the high damping of the current, which has to be used in this case, has an adverse effect on the response time of the system. Furthermore, the scale expansion procedure complicates the current measurements, particularly at high sampling rates. The response time can be decreased by increasing the aspiration rate, but this results in an increase in the corresponding response volume, which would be a disadvantage for the analysis of small sample volumes.

In spite of these rather conflicting effects of different experimental parameters, the following points are significant. The use of scale expansion, no wash solution between samples and pump stop during sample shifts appears to be advantageous, as this system gives the best precision for low, as well as for high sampling rates. Under optimized conditions a standard deviation of 0.3 % was obtained. A medium aspiration rate is recommended, as is the use of segmented streams. The distance between the debubbler and the working electrode should be as short as possible, and the deaeration should be carried out with argon gas. The sampling time cannot be decreased below the response time of the system without a sacrifice in precision. At high sampling rates particular attention must be paid to the manner in which the current readings are measured, when the expanded scale procedure is used.

Finally it should be pointed out that the expanded scale procedure is not restricted to polarographic systems; it should be generally applicable for automated analysis, irrespective of the type of detector system which is used.

REFERENCES

1 W. Lund and L. N. Opheim, Anal. Chim. Acta, 79 (1975) 35.

Analytica Chimica Acta, 82 (1976) 255—264
©Elsevier Scientific Publishing Company, Amsterdam — Printed in The Netherlands

LEAD(II) TRANSPORT PROCESSES IN ANODIC STRIPPING VOLTAMMETRIC ANALYSIS

LLOYD M. PETRIE and RODGER W. BAIER

Department of Chemistry, Duke University Marine Laboratory, Beaufort, North Carolina 28516 (U.S.A.)

(Received 14th August 1975)

SUMMARY

The principal lead(II) transport processes occurring in anodic stripping voltammetric analysis of sea water have been studied by liquid scintillation spectrometry of ^{210}Pb. From an initial lead(II) concentration of $6.3 \cdot 10^{-9}$ M (ca. 1.3 p.p.b.), the concentration after 95 min is reduced by: (1) 84 % at pH 8.2, (2) 78 % at pH 4.6, and (3) 39 % at pH 3.0. Primary losses are due to adsorption onto cell and electrode materials. Significant chemisorption of lead(II) associated with chloride occurs at the platinum wire counter electrode. The data support a diffusion-limited adsorption mechanism as the primary transport for lead(II) from solution.

With improvements to polarographic analyzing equipment and thin-layer mercury electrodes [1], anodic stripping voltammetry (a.s.v.) has been routinely applied to determinations of Cd, Cu, Pb, and Zn in sea-water [2]. Metal speciation and stability constants for some reactions have also been investigated [3—9].

Under conditions of partial deposition, trace metal concentrations and speciation in the sample solution are not altered by the a.s.v. analysis itself. Fitzgerald demonstrated that only a few percent of the total amount of metals in solution need undergo reversible redox reactions at the working electrode [10]. However, several irreversible and undesirable processes can occur which change the concentration and speciation of the trace metals. First, input of trace metals during reagent additions can contaminate the sample. Secondly, metals can be removed from solution by adsorption to cell materials. Thirdly, apparent rapid increases in the mercury layer activity result in higher stripping peak currents with consecutive analyses of a given sample. Several workers have qualitatively described those factors that may influence the mercury layer activity [11—13]. It was the purpose of this work to identify and quantify the principal transport processes for low concentrations of lead during a.s.v. analysis of sea-water.

Radioactive ^{210}Pb was selected as a suitable indicator of lead(II) transport and accumulation at the part-per-billion level, with measurements by liquid scintillation spectrometry [14]. Before the technique could be applied to

^{210}Pb, the effects of radioactive decay products needed to be considered. The decomposition mechanism is given by:

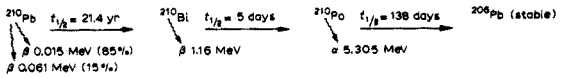

At secular equilibrium $N_{Pb}/N_{Bi} = 1560$ and $N_{Pb}/N_{Po} = 57$, and these ratios represent the greatest amounts of ^{210}Bi and ^{210}Po present relative to ^{210}Pb. Since the counter can distinguish beta radiations greatly differing in energy, ^{210}Bi interference is small, but photon emission from high-energy α-particles released during ^{210}Po decay would interfere.

EXPERIMENTAL

The sea-water used was collected from 1000 m by a plastic balloon at position 32° 25'N and 75° 59'W. The water was transferred to 20-l polyethylene bottles and stored in darkness at 2 °C. This sea-water was used without filtering, and is referred to as "deep sea-water."

Anodic stripping voltammetry

All experiments were performed with the apparatus shown in Fig. 1. Initially, the cell and electrodes were washed with 10 % HNO_3 and stored in deep sea-water for 6—12 h. Then the wax-impregnated graphite electrode (WIGE) was polished with 0.05-μm alumina on felt, rinsed, and plated at −1.0 V in a $4 \cdot 10^{-4}$ M $Hg(NO_3)_2$ sea-water solution for 90 min. Trace metal impurities that accumulated in the mercury layer were then removed by maintaining an electrode potential of −0.1 V for 10—15 min.

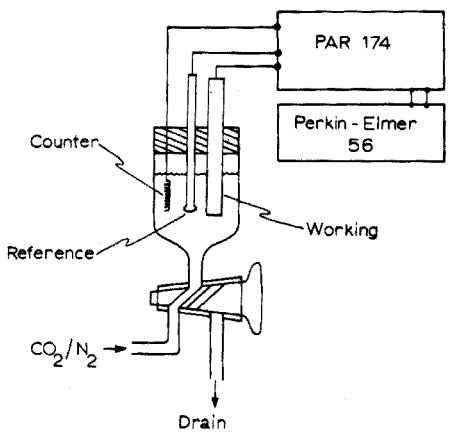

Fig. 1. Anodic stripping voltammetry cell. The cell is fitted with a 6-mm wax-impregnated graphite electrode, Ag/AgCl reference electrode and unprotected Pt wire counter electrode. A Princeton Applied Research PAR 174 polarographic analyzer and a Perkin—Elmer 56 chart recorder were used for current measurement and recording.

A.s.v. runs were performed by plating for 2 min at −0.8 V and scanning at 10 mV s^{-1}. After introduction of a new sample, nitrogen was bubbled through the cell to remove dissolved oxygen, and bubbling was maintained during the plating step to exclude oxygen and to provide mixing. The resulting pH of the solution was typically 8.2 with nitrogen, 4.6 with carbon dioxide, and 3.0 with the addition of a few drops of 5 % reagent-grade hydrochloric acid. No detectable change in the lead peak at its minimum level occurred when the same quantity of acid was added to a buffered sample.

Liquid scintillation spectrometry

A Picker Liquimat soft-β liquid scintillation counter was used to determine interference from ^{210}Po. The counter was equipped with a variable discriminator to permit precise adjustment of the energy window. The scintillation liquid consisted of 5 g of 2,5-diphenyloxazole (PPO), 500 ml of octylphenoxypolyethoxyethanol (Triton X-100), and 1000 ml of toluene (scintillation grade). A 1-ml aqueous sample containing 0.93 μCi ^{210}Po and another containing 1.0 μCi ^{210}Pb were each mixed with 20 ml of scintillation liquid in glass scintillation vials. The activity of each vial was counted for each 50 unit increment of the logarithmic β-energy window scale of the counter (0—1000 units = 0—1.72 MeV). Figure 2 summarizes the activity vs. β-energy scans for ^{210}Po and ^{210}Pb. The high-energy α-radiation from ^{210}Po interfered with the measured activity of the 0.061-MeV β-radiation but not with the 0.015-MeV radiation of ^{210}Pb. Therefore, by setting the variable energy window discriminator to measure β-activity between 0 and 0.055 MeV, only the

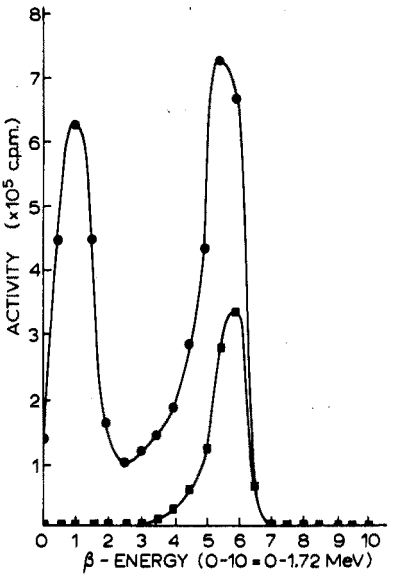

Fig. 2. Activity vs. β-energy — ^{210}Pb (•) and ^{210}Po (▪).

activity of 0.015-MeV ^{210}Pb β-radiation was measured. This provided an activity measurement proportional to ^{210}Pb and free from interference.

For all subsequent ^{210}Pb activity measurements a 0—0.055 MeV energy window was used and the Liquimat was replaced by an equivalent soft-β liquid scintillation counter (Beckman LS-133). As expected for measurement of low-energy β-particles, the counting efficiency of ^{210}Pb on the Beckman LS-133 was only 20 %.

Loss of lead(II) from sea-water

With plating. To investigate the decrease in the bulk solution concentration of lead(II) during both long-term (95-min) and short-term (20-min) a.s.v. studies, radio-lead experiments were performed. Sufficient stock ^{210}Pb with carrier was added to the cell to provide an initial lead concentration of $6.3 \cdot 10^{-9}$ M and an activity of $1.31 \cdot 10^{6}$ d.p.m.

Experiments of 95-min duration consisted of plating and stripping cycles performed at 10—15-min intervals, each followed by removal of a 1-ml sample for activity measurements. After 95 min the cell and electrodes were rinsed, soaked in 10 % nitric acid for 10 min, and again rinsed before reassembly. The acid washings were neutralized with ammonia solution to pH 7 ± 0.5 to prevent scintillator degradation, combined with 15 ml of scintillation cocktail, and measured for activity to determine the lead associated with cell materials. Three runs were performed at pH 8.2, two runs at pH 4.6, and one run at pH 3.0.

During the 20-min experiments, the same procedure was followed except that three consecutive plating-stripping cycles were performed at pH 8.2 during the 20-min period. Equipment was acid-washed and rinsed as before. Experiments were performed to determine if lead(II) transport differed between differential pulse and direct current scan modes for two differential Signal Processing Boards used with the PAR 174 polarographic analyzer. Two boards were tested to insure that no instrument malfunction was affecting lead(II) transport.

Without plating. Experiments were conducted to determine the relative lead(II) adsorption onto several types of materials during 20 min. Samples of Teflon, polyethylene, Pyrex, quartz, bare graphite rod, WIGE, and coiled platinum wire were placed into a stirred polyethylene beaker containing sea-water with an initial lead concentration of $6.3 \cdot 10^{-9}$ M and a radio-lead activity of $1.31 \cdot 10^{6}$ d.p.m. After 20 min at 21—23 °C, the materials were rinsed, and acid washings were evaluated by the previously described techniques.

RESULTS AND DISCUSSION

Loss of lead(II) from sea-water

Figure 3 shows the reduction in solution activity of ^{210}Pb during 95 min at pH 8.2, 4.6, and 3.0. The data points represent means of multiple experiments in which plating-stripping cycles preceded each activity measurement. Table 1 shows the partitioning of lead(II) during the 95-min period. As expected, glass adsorption was considerable at high pH, decreasing to nearly zero at pH 3.0 [15, 16]; $Pb(OH)_n$ species have been postulated to be the predominant complexes participating in glass adsorption [17]. At all pH values 4—6 % of the total lead(II) accumulated on the WIGE.

Unexpectedly, a considerable quantity of lead(II) collected on the unprotected platinum counter electrode. This electrode was not protected in the usual way from the sample solution by a fritted glass tube for two reasons [4]: first, any gas evolved at the counter electrode during plating would be immediately swept from solution by the bubbling N_2 or CO_2, preventing gas interference with the analytical current measurement; secondly glass protectors pose a potential metal contamination problem, since they are difficult to rinse thoroughly between samples. Some evidence related to the mechanism of lead(II) accumulation at the counter electrode is available.

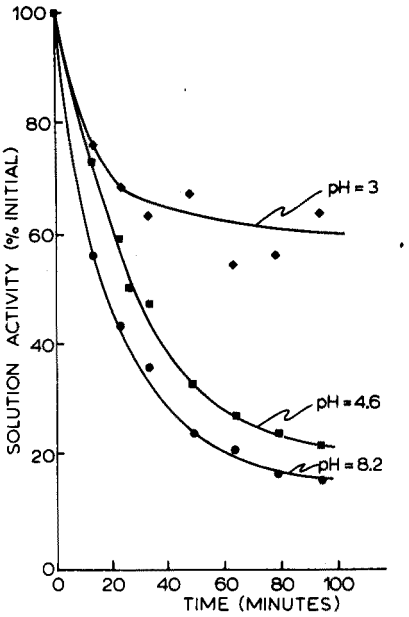

Fig. 3. ^{210}Pb solution loss. The losses of ^{210}Pb solution activity during 95-min sample exposures to the a.s.v. cell are given for solution pH values of 3.0, 4.6 and 8.2.

TABLE 1

^{210}Pb loss from a.s.v. cell solution at various pH values
(Initial activity of ^{210}Pb = $1.3 \cdot 10^6$ d.p.m. with 20 % efficiency. Time of ^{210}Pb exposure to cell = 95 min. Average values ± standard deviations are given.)

% of initial activity	pH		
	8.2	4.6	3.0
In solution	16 ± 4	22 ± 5	62
Wall adsorption	29 ± 15	23	2
Reference electrode	15	4	1
Graphite electrode	4	4 ± 1	5
Counter electrode	30	41	24
Difference	10	6	6

Radioactive ^{36}Cl equilibrated with deep sea-water and then placed in the a.s.v. cell, demonstrated that 18 % of the total chloride in sea-water collected on to the platinum wire in 60 min, representing $1 \cdot 10^{-3}$ mol of chloride. Since platinum reacts readily with chloride ions [18], two mechanisms seem possible. In one, chloride initially chemisorbs on to platinum to form a negative monolayer around the positive platinum wire to which positively charged lead(II) complexes, e.g. $Pb(OH_2)_n^{2+}$, $PbCl^+$, $Pb(OH)^+$, could be associated; alternatively, $Pb(Cl)_n$ complexes chemisorb on to the platinum directly.

Table 2 summarizes the lead(II) losses to cell materials during a 20-min exposure. No significant differences in lead(II) transport exist between differential pulse and direct current potential scan modes with old and new Signal Processing Boards in the PAR 174. The graphite electrode collection was higher, possibly because of wax erosion; loss of wax was detected visually by accumulation of some mercury on to the WIGE during mercury plating, and its removal exposed more adsorption sites for lead(II)

TABLE 2

^{210}Pb loss from a.s.v. cell solution with various electronic modes
(Initial activity of ^{210}Pb = $1.3 \cdot 10^6$ d.p.m. with 20 % efficiency. Time of ^{210}Pb exposure to cell = 20 min.)

% Initial activity	Diff. pulse		Direct current	
	New SPB	Old SPB	New SPB	Old SPB
In solution	58	39	47	54
Wall adsorption	17	23	14	12
Reference electrode	11	6	8	4
Graphite electrode	10	17	17	15
Counter electrode	6	16	9	10
Difference	1	2	5	5

complexes. The extent of adsorption on the cell wall, reference electrode, and counter electrode was less than in the 95-min experiments, implying that these adsorption rates are relatively low. The total 20-min loss (50 %) compares favorably with measurements given in Fig. 3.

Diffusion-limited adsorption model

If it is assumed that the adsorption reactions of lead(II) complexes occur more rapidly than the rate at which lead complexes can diffuse to the adsorption sites, the overall adsorptive loss of lead(II) from solution may be represented by a diffusion-limited model:

$$\frac{dC_s}{dt} = \frac{k_1 A}{D} (C - C_f) C_0 \qquad (1)$$

Since

$$\frac{dC_s}{dt} \propto \frac{-dC}{dt},$$

then

$$\frac{-dC}{dt} = k(C - C_f) \qquad (2)$$

where A = surface area of adsorbing material, cm^2,
C = Pb(II) sea-water concentration, % initial concentration,
C_f = equilibrium Pb(II) sea-water concentration, % initial concentration,
C_0 = initial Pb(II) sea-water concentration, mol cm^{-3},
C_s = Pb loading on adsorbing material, mol g^{-1} of adsorbent,
D = distribution ratio, of Pb in solid to Pb in liquid phase,
k = overall transfer coefficient, min^{-1},
k_1 = mass-transfer coefficient, cm (g adsorbent)$^{-1}$ min^{-1},
t = time, min.

Integration of eqn. (2) gives:

$$\ln(C - C_f) = -kt + \text{constant} \qquad (3)$$

The data for the 95-min loss experiments were fitted to a least-squares regression of eqn. (3). Table 3 and Fig. 4 give the results. In general, this diffusion-limited model represents the overall solution losses of lead(II) from sea-water. Wai and Rodriguez [19] successfully represented the adsorptive loss of cadmium(II) from distilled water to container walls by the same relationship.

TABLE 3

Linear regression data fit

pH	C_f	$\ln(C-C_f) = -kt + b$	Fraction total var. remain.
8.2	15	$\ln(C-15) = -0.088t + 4.508$	$3.26 \cdot 10^{-4}$
4.6	21	$\ln(C-21) = -0.078t + 4.552$	$5.96 \cdot 10^{-5}$
3.0	61	$\ln(C-61) = -0.050t + 2.927$	$7.75 \cdot 10^{-3}$

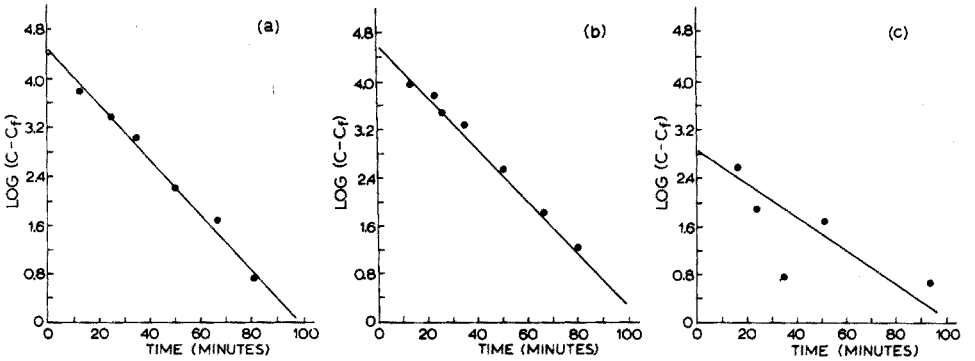

Fig. 4. Lead(II) losses from solution. The data from Fig. 3 were fitted to the diffusion-limited adsorption model represented by $\ln(C-C_f) = -kt + b$, where b is the integration constant. Compare Table 3. (a) pH = 8.2, $C_f = 15$; (b) pH = 4.6, $C_f = 21$; (c) pH = 3.0, $C_f = 61$.

Lead(II) adsorption on to cell materials

Table 4 shows the relative adsorption of lead(II) on to several materials at pH 8.2 during 20-min exposures in deep sea-water initially containing lead(II) and ^{210}Pb at the same concentrations used in the previous experiments.

Adsorption on to cell materials was estimated by multiplying the wetted areas of the a.s.v. cell component by the relative adsorption values from Table 4. These values were compared to the measured ^{210}Pb adsorption from previous experiments as shown in Table 5. Lead collection on the wall and platinum wire can be explained adequately by adsorption alone, but collection at both the reference and working electrodes may occur by other mechanisms as well.

ACKNOWLEDGEMENTS

This research was supported by the Oceanography Section, National Science Foundation, NSF Grant DES74-12831. The authors express their thanks to Dr. David Hastings and the entire research group of Dr. John Gutknecht for their invaluable assistance with liquid scintillation spectrometry.

TABLE 4

Relative lead(II) adsorption on to different materials

Cell material	Relative adsorptivity[a] (d.p.m./cm^2)
Teflon	21,200 ± 1 %
Polyethylene	28,500 ± 11 %
Pyrex	12,000 ± 13 %
Quartz	17,400 ± 27 %
WIGE	40,500 ± 24 %
Bare graphite	125,000 ± 4 %
Pt wire	357,000 ± 11 %

[a]Average values ± standard deviation for triplicate experiments.

TABLE 5

Estimated vs. measured adsorption on to a.s.v. cell materials

Cell material	Estimated d.p.m.	Measured d.p.m.
Cell walls (Pyrex)	473,000 ± 61,000	360,000 ± 55,000
Counter electrode (Pt wire)	357,000 ± 39,000	200,000 ± 90,000
Reference electrode (Pyrex)	34,000 ± 5,000	146,000 ∓ 55,000
Working electrode (WIGE)	32,000 ± 8,000	146,000 ± 55,000

REFERENCES

1 T. Copeland, Anal. Chem., 46 (1974) 1257.
2 A. Zirino, S. Lieberman and M. Healy, in G. Whitnack (Ed.), Marine Electrochemistry, The Electrochemical Society, New Jersey, 1973, p. 319.
3 A Piro, Proc. Symp. Interaction of Radioactive Contaminants with Const. of Marine Environment, IAEA, Seattle, 1972, p. 3.
4 R. Baier, Lead Distribution in Coastal Waters, University of Washington, Ph.D. dissertation, 1971.
5 A. Zirino and S. Yamamoto, Limnol. Oceanogr., 17 (1972) 661.
6 H. Allen, W. Matson and K. Mancy, Journal WPCF, 42 (1970) 573.
7 W. Bradford, Limnol. Oceanogr., 18 (1973) 757.
8 M. Shuman and G. Woodward, Anal. Chem., 45 (1973) 2032.
9 Y. Chau, R. Gächter and K. Lum-Shue-Chan, J. Fish. Res. Bd. Can., 31 (1974) 1515.
10 W. Fitzgerald, Study of Certain Trace Metals in Sea-Water Using ASV, Mass. Inst. Technol., Ph.D. dissertation, 1970.
11 T. Florence, Electroanal. Chem. Interface Electrochem., 27 (1970) 273.
12 R. Gilbert, Electrochemical Studies of Environment Trace Metals, Mass. Inst. Technol., Ph.D. dissertation, 1971.
13 D. Hume and J. Carter, Chem. Anal., 17 (1972) 747.
14 Y. Koboyashi and D. Maudsley, Biological applications of Liquid Scintillation Counting, Academic Press, New York, 1974.

15 O. Høgdahl, Semi-Annual Progress Report, No. 7, Central Inst. for Indus. Res., Oslo, Oct. 30, 1965.
16 D. Robertson, Anal. Chim. Acta, 42 (1968) 533.
17 M. Fuerstenau, D. Elgillani and J. Miller, AIME Transactions, 274 (1970) 11.
18 F. Cotton and G. Wilkinson, Advanced Inorganic Chemistry Wiley-Interscience, New York, 1966.
19 C. Wai and J. Rodriguez, Anal. Chem., 46 (1974) 771.

Analytica Chimica Acta, 82 (1976) 265—272
©Elsevier Scientific Publishing Company, Amsterdam — Printed in The Netherlands

AMPEROMETRIC MEASUREMENT OF HEXACYANOFERRATE(III)-COUPLED DEHYDROGENASE REACTIONS*

LAWRENCE C. THOMAS and GARY D. CHRISTIAN

Department of Chemistry, University of Washington, Seattle, Washington 98195 (U.S.A.)

(Received 30th July 1975)

SUMMARY

The electrochemical oxidations of hexacyanoferrate II ion and reduced nicotinamide adenine dinucleotide at carbon electrodes are described. Amperometric methods for nicotinamide adenine dinucleotide oxidoreductase analyses by amperometric monitoring of hexacyanoferrate II are reported for lactic dehydrogenase in serum.

Nicotinamide adenine dinucleotide (NAD) oxidoreductase assays are important biochemical analyses and are generally performed by spectrophotometric techniques. Few amperometric methods for these assays have been developed. Methods utilizing direct amperometry of NADH [1], amperometry of reduced oxidation—reduction dyes [2], and amperometric monitoring of hexacyanoferrate(II) in the enzyme-catalyzed reduction of hexacyanoferrate(III) with lactate [3] have been investigated. Electroanalytical methods offer a great potential to clinical analyses because they are inexpensive and simple, easily interfaced to other equipment, and unaffected by turbidity [4—7].

Hexacyanoferrate(II and III) reactions have been used in the assay of glucose [3, 8, 9], reducing sugars [10], urate [11], and monoamine oxidase [12] either by direct reaction or by peroxidase coupling with hydrogen peroxide. Hexacyanoferrate(III) has been used in potentiometric oxidation—reduction titrations of reduced NAD (NADH) [13]; the rate of this direct oxidation is pH-independent and has a reaction half-time of about 5 min for sub-millimolar concentrations [14]. Hexacyanoferrate(III) has also been treated with lactate and succinate in the presence of dehydrogenase enzymes [3, 6, 15—18], for the production of carbon dioxide for manometry [19], and with NADH by diaphorase coupling for potentiometric [8] and spectrophotometric [20] measurements. This iron(III)—cyanide complex reacts directly with many enzymes and natural electron-transport species, including NADH and reduced nicotinamide adenine dinucleotide phosphate (NADPH) [6].

*Presented in part at the Symposium on Electroanalytical Techniques in Bioanalytical Chemistry, 166th National Meeting of the American Chemical Society, Chicago, August 26—31, 1973.

The hexacyanoferrate(II and III) system is an attractive oxidation–reduction couple. Both NAD(P)H and hexacyanoferrate(III) are stable in the presence of oxygen [6, 17], and the electrochemistry of the iron(III)–cyanide complex ion in biological media has been established [21]. The voltammetric half-wave potential of the $Fe(CN)_6^{3-}/Fe(CN)_6^{4-}$ system is only moderately positive, where amperometric residual currents in the presence of serum are low [1, 2]. The system is electrochemically reversible and thus conducive to continuous biamperometric measurements [7, 22].

In this study the voltammetry of NADH, hexacyanoferrate(II), and hexacyanoferrate(III) in the same solution is described; a three-electrode cell is used. In addition, the application of this system to amperometric (three-electrode and biamperometric) assays of lactate dehydrogenase (L-lactate: NAD oxidoreductase, LDH) in serum is described.

EXPERIMENTAL

Reagents

Diaphorase (DIL IJB, 23 I.U. mg^{-1}), NAD (DPNR 2HA), and NADH (DPNH 2KA) were obtained from Worthington Biochemical Corporation. LDH (lot 220068) was obtained from Calbiochem. Other chemicals were reagent-grade quality, and deionized distilled water was used for preparation of all solutions. All solutions were made in 0.1 M Na_2HPO_4, adjusted to pH 7.4 with NaOH, unless stated otherwise.

Apparatus

A Princeton Applied Research (PAR) Model 174 polarograph, with its output monitored by a millivolt recorder, was used for scanning voltammetry. An integrator/potentiostat [23] was used to supply potentials for continuous amperometric measurements. An instrumental configuration described previously [23], consisting of a Beckman Glucose Analyzer interfaced to the integrator/potentiostat and a millivolt recorder was used to generate signals proportional to both the amperometric current and the rate of current change. A carbon paste electrode (0.07 cm^2) [23], a pair of glassy carbon electrodes (0.38 cm^2 each; Chemtrix, Inc.), a Coleman C-712 saturated calomel electrode (SCE), and a platinum gauze electrode were employed. They were used for twin glassy carbon electrode biamperometry or in three-electrode combinations, with the platinum gauze electrode as the auxiliary electrode, in configurations similar to those described previously [1, 23].

Procedure

Solutions of NADH and potassium hexacyanoferrate(III) in 0.1 M tris-(hydroxymethyl)aminomethane (Tris), pH 8.0, were allowed to react for 15

min. Then current—voltage curves of the solutions (now containing NADH, hexacyanoferrate (II), hexacyanoferrate (III), and NAD) were recorded, for the three-electrode cell with a carbon paste working electrode. All current–voltage curves were recorded by scanning toward more positive potentials in quiet solutions at a scan rate of 5 m V s^{-1}. A similar procedure, with phosphate buffers, was used to record voltammograms at a glassy carbon electrode. Carbon paste and glassy carbon electrodes were rinsed with distilled water between each voltammetric scan.

Assays of LDH in serum were performed by three-electrode amperometry with a glassy carbon working electrode at +0.45 V vs. SCE. An aliquot (100 μl) of pooled serum, diluted (1 + 9) by additions of LDH solution and phosphate buffer, was added to 6 ml of a solution containing 0.105 M D,L-lactate, $4.7 \cdot 10^{-3}$ M potassium hexacyanoferrate(III) and diaphorase ($3.4 \cdot 10^{-2}$ mg ml^{-1}). This solution was contained in a 10-ml beaker and stirred by a 2 × 8 mm magnetic stirring bar. After stabilization of the amperometric residual current (at ca. 230 nA), 250 μl of $1.4 \cdot 10^{-2}$ M NAD was added to the solution. This resulted in a concentration of NAD similar to that considered optimal in other studies [1, 2, 8]. The change in current, which was proportional to the change in hexacyanoferrate(II) concentration, was recorded for a fixed-time interval of 5 min after the addition of NAD.

Biamperometric measurements were made with the above cell with glassy carbon electrodes. Reagent concentrations were optimized by recording the Glucose Analyzer output, proportional to the rate of biamperometric current change, upon additions of 0.023 I.U. of LDH to various reaction solutions.

Biamperometric assays of LDH in serum were done by addition of 100 μl of pooled serum diluted (1 + 9) with LDH in phosphate buffer, to 5 ml of reaction solution ($5.3 \cdot 10^{-2}$ mg ml^{-1} diaphorase, $4.2 \cdot 10^{-3}$ M potassium hexacyanoferrate(III), and $5.7 \cdot 10^{-2}$ M D,L-lactate). After stabilization of the current, 50 μl of $2.7 \cdot 10^{-2}$ M NAD was added and the slope of the recorded current—time line was determined. In all enzyme assays, the glassy carbon electrodes were rinsed briefly with distilled water and wiped lightly with tissue paper between each assay.

RESULTS AND DISCUSSION

Three-electrode voltammetry of NADH and hexacyanoferrate(II) at a carbon paste electrode shows that the NADH oxidation wave is at higher potential and is well separated from the hexacyanoferrate(II) wave, and that both waves are well defined (Fig. 1). The anodic current at slow scan rates, from each species, can be measured in the presence of the other over a wide range of hexacyanoferrate(II) concentrations (Fig. 2). For a fixed initial concentration of NADH, the total current at +0.75 V vs. SCE, after equilibration of the added hexacyanoferrate(III) to form hexacyanoferrate(II)

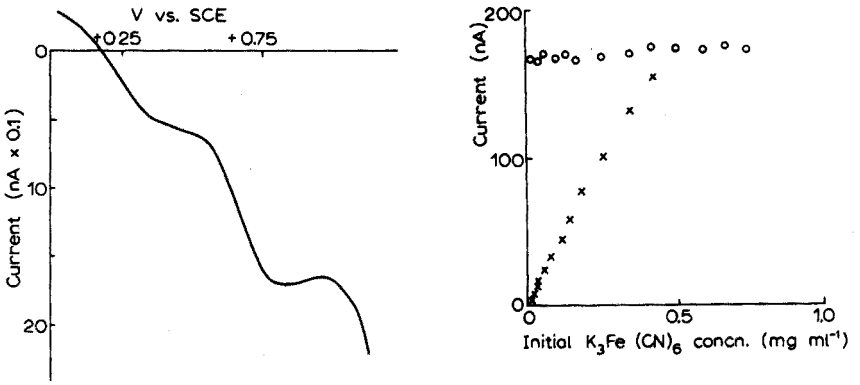

Fig. 1. Current—voltage curve of hexacyanoferrate(II) and NADH on carbon paste electrode in 0.1 M Tris, pH 8.0, at a scan rate of 5 mV s^{-1}. First wave hexacyanoferrate(II), second wave NADH oxidation.

Fig. 2. Current—concentration curves after reaction of a solution of hexacyanoferrate(III) with NADH to form hexacyanoferrate(II). Initial [NADH] = $4 \cdot 10^{-4}$ M in 0.1 M Tris, pH 8.0. ○, current at +0.75 V vs. SCE. ×, current at + 0.50 vs. SCE, on a carbon paste electrode at a scan rate of 5 mV s^{-1}.

is constant. The current at +0.45 V vs. SCE, arising from hexacyanoferrate(II), increases proportionately with the addition of hexacyanoferrate(III).

At a glassy carbon electrode, a less well separated set of waves is generated (Figs. 3 and 4). The hexacyanoferrate(II) half-peak potential remains relatively constant at about +0.15 V vs. SCE, but the NADH wave has half-peak potentials of +0.65 V and +0.38 V vs. SCE at carbon paste and glassy carbon electrodes, respectively [1]. These data indicate that a titration of

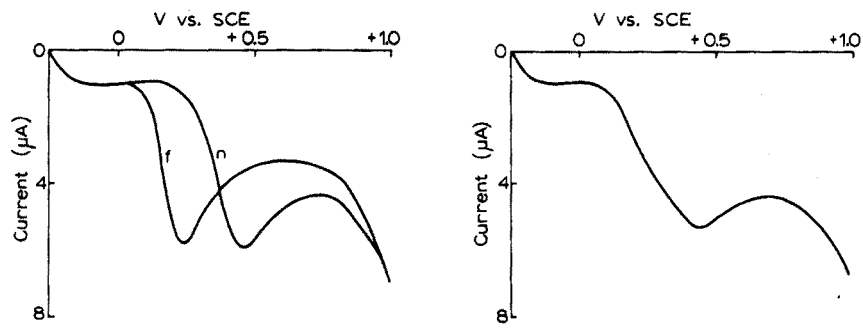

Fig. 3. Current—voltage curves on glassy carbon electrode at a scan rate of 20 mV s^{-1} in 0.1 M Na_2HPO_4, pH 7.3. f, [$Fe(CN_6^{4-}$] = $6.8 \cdot 10^{-4}$ M n, [NADH] = $8.4 \cdot 10^{-4}$ M.

Fig. 4. Current—voltage curve on glassy carbon at a scan rate of 20 mV s^{-1} in 0.1 M Na_2HPO_4, pH 7.3, for a solution containing $3.4 \cdot 10^{-4}$ M $Fe(CN)_6^{4-}$ and $4.2 \cdot 10^{-4}$ M NADH.

hexacyanoferrate(III) with NADH can be followed amperometrically, and therefore that an enzymatic NAD reduction can be monitored by measuring the formation of hexacyanoferrate(II). This would allow amperometric measurements at potentials less positive than those used in direct NADH measurements [1]. In addition, biamperometry could be used to follow the change in concentration of hexacyanoferrate(II) in the electrochemically reversible $Fe(CN)_6^{3-}/Fe(CN)_6^{4-}$ couple.

The feasibility of the above enzyme measurements was demonstrated with LDH reactions. A fixed-time change in the three-electrode current on a glassy carbon electrode at +0.45 V vs. SCE was related to the activity of LDH in diluted serum (Fig. 5). The LDH activities spanned the range of physiological LDH activities in serum samples. The variation about the calibration line approximated the noise level of the instrumental configuration used for these measurements, which was about ± 5 nA. The major contribution to the noise was the high residual currents observed in the reaction solution with serum present.

The rate of biamperometric current change caused by hexacyanoferrate(II) production in the presence of LDH was measured with a pair of glassy carbon electrodes. An applied potential difference of 100 mV was shown to be sufficient to monitor accurately the current, which was proportional to the concentration of hexacyanoferrate(II) in the presence of a large excess of hexacyanoferrate(III); this proportionality, using small applied potentials, is consistent with previous studies (7, 22, 24). A linear relationship between the rate of current change (hexacyanoferrate(II) production) and initial hexacyanoferrate(III) concentration was established (Fig. 6). However, the residual current for the reaction solution showed a geometric increase with increased hexacyanoferrate(III) concentration (Fig. 7). Because noise levels in amperometric currents are directly proportional to the current, optimization must consider the signal-to-noise ratio with changing hexacyanoferrate(III) concentration. Concentrations approximating $4 \cdot 10^{-3}$ M hexacyanoferrate(III) were used in subsequent measurements. Concentrations of $7 \cdot 10^{-2}$ M D,L-lactate, $3 \cdot 10^{-4}$ M NAD, and $4 \cdot 10^{-2}$ mg ml^{-1} diaphorase were chosen in a similar fashion (Figs. 8—10), with an added constraint of reagent expense.

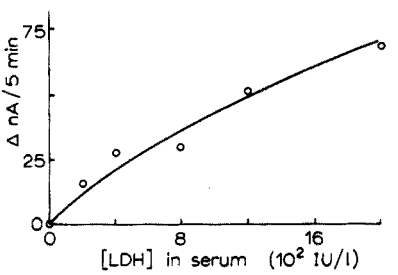

Fig. 5. Rate of three-electrode current change vs. activity of lactic dehydrogenase in serum.

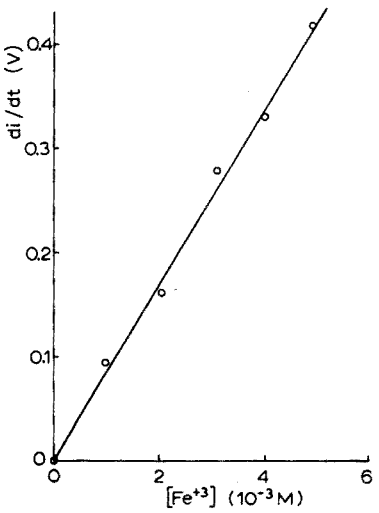

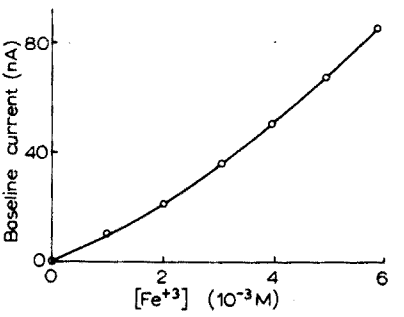

Fig. 6. Rate of current change versus initial hexacyanoferrate(III) concentration for additions of LDH to a reaction solution containing 0.008 mg ml^{-1} diaphorase, $2.8 \cdot 10^{-4}$ M NAD, $4.6 \cdot 10^{-2}$ M D,L-lactate and hexacyanoferrate(III) in 0.1 M Na_2HPO_4, pH 7.3.

Fig. 7. Biamperometric residual current vs. hexacyanoferrate(III) concentration on twin glassy carbon electrodes. ΔE = 100 mV, in a reaction solution of the same composition as that for Fig. 6.

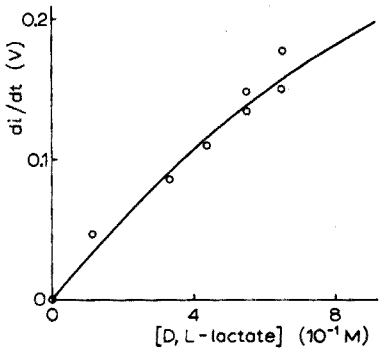

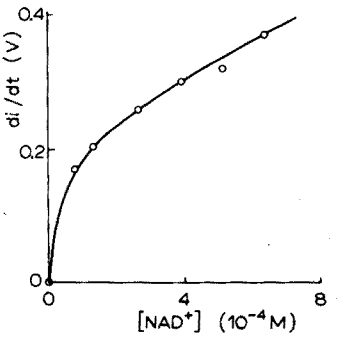

Fig. 8. Rate of biamperometric current change versus lactate concentration for additions of LDH to a reaction solution containing $8 \cdot 10^{-3}$ mg ml^{-1} diaphorase, $2.8 \cdot 10^{-4}$ M NAD, $4.14 \cdot 10^{-3}$ M $Fe(CN)_6^{3-}$, and lactate in 0.1 M Na_2PO_4, pH 7.3.

Fig. 9. Rate of biamperometric current change vs. NAD concentration for additions of LDH to a reaction solution containing $8 \cdot 10^{-2}$ mg ml^{-1} diaphorase, $5.7 \cdot 10^{-2}$ M D,L-lactate, $4.14 \cdot 10^{-3}$ M $Fe(CN)_6^{3-}$, and NAD in 0.1 M Na_2HPO_4, pH 7.3.

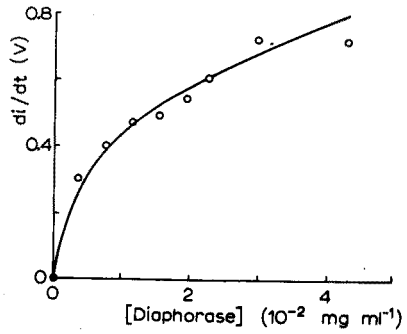

Fig. 10. Rate of biamperometric current change vs. diaphorase concentration for additions of LDH to a reaction solution containing $6.8 \cdot 10^{-2}$ M D,L-lactate, $2.8 \cdot 10^{-4}$ M NAD, $4.14 \cdot 10^{-3}$ M $Fe(CN)_6^{3-}$, and diaphorase in 0.1 M Na_2HPO_4, pH 7.3.

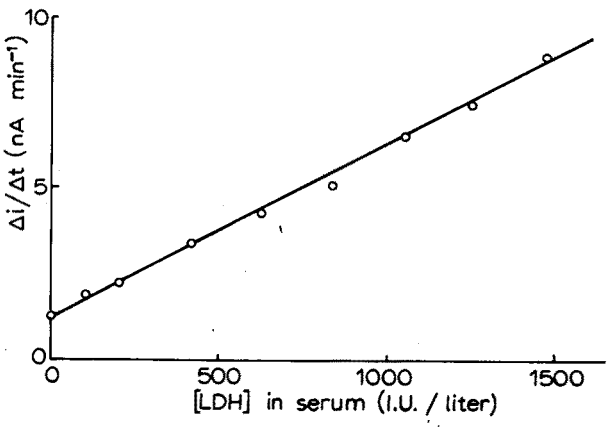

Fig. 11. Rate of biamperometric current change versus activity of lactic dehydrogenase in serum for 100 μl of serum in 5 ml of reaction solution containing $6.4 \cdot 10^{-2}$ mg ml^{-1} diaphorase, $5.6 \cdot 10^{-2}$ M D,L-lactate, $2.1 \cdot 10^{-3}$ M $Fe(CN)_6^{3-}$, and $3.1 \cdot 10^{-4}$ M NAD.

Hexacyanoferrate(III)-coupled biamperometric assays of LDH in serum were performed. Figure 11 illustrates the relationship between the rate of hexacyanoferrate(II) production and the activity of LDH in serum. The non-zero intercept is due to non-enzymatic reactions in the serum reaction solution which produce changes in current at a constant rate in absence of the coenzyme. This rate is the same from sample to sample, and may be due to direct reactions of hexacyanoferrate(III) with products of enzymatic reactions not requiring the introduced NAD. The LDH activities again encompass the physiological range of LDH activities found in human sera. An average deviation of ca. ± 44% for replicate samples was obtained, the primary deviations originating from stirring fluctuations. Improvements in the cell design would undoubtedly result in improved precision and sensitivity.

These results indicate the applicability of amperometry to analyses of enzymes in serum. The simplicity of the biamperometric system makes it attractive as an electrometric method of measuring rates of product formation in hexacyanoferrate(III)-coupled dehydrogenase reactions.

REFERENCES

1 L. C. Thomas and G. D. Christian, Anal. Chim. Acta., 77 (1975) 153.
2 M. D. Smith and C. L. Olsen, Anal. Chem., 46 (1974) 1544; 47 (1975) 1074.
3 D. L. Williams, A. R. Doig and A. Korosi, Anal. Chem., 42 (1970) 118.
4 H. B. Mark, Talanta, 19 (1972) 733.
5 P. M. G. Broughton and J. B. Dawson, in O. Bodansky and A. L. Latner (Eds.), Advances in Clinical Chemistry, Vol. 15, Academic Press, New York, 1972.
6 J. L. Peel, in J. R. Norris and D. W. Ribbons (Eds.), Methods in Microbiology, Academic Press, New York, 1972.
7 G. D. Christian, Advances in Biochemical Engineering and Medical Physics, 4 (1971) 95.
8 R. I. Porterfield, Thesis, Ohio State University, 1972.
9 W. J. Blaedel and C. L. Olsen, Anal. Chem., 36 (1964) 343.
10 D. K. Kidby and D. J. Davidson, Anal. Biochem., 55 (1973) 321.
11 L. G. Morin, Clin. Chem., 20 (1974) 51.
12 W. D. Mason and C. L. Olsen, Anal. Chem., 42 (1970) 488.
13 S. J. Leach, J. H. Borendale and M. G. Evans, Aust. J. Chem., 6 (1953) 395.
14 K. A. Schellenberg and L. Hellerman, J. Biol. Chem., 231 (1958) 547.
15 M. Kjeld, Scand. J. Clin. Lab. Invest., 29 (1972) 421.
16 E. B. Kearney and T. P. Singer, J. Biol. Chem., 219 (1956) 499.
17 H. Bergmeyer (Ed.), Methods of Enzymatic Analysis, Academic Press, New York, 1963.
18 T. P. Singer, E. B. Kearney and P. Berath, J. Biol. Chem., 223 (1956) 599.
19 J. H. Quastel and A. H. M. Wheatley, Biochem. J., 32 (1938) 936.
20 Worthington Enzyme Manual, Worthington Biochemical Corporation, Freehold, New Jersey, 1972.
21 W. C. Purdy, Electroanalytical Methods in Biochemistry, McGraw-Hill Book Company, New York, 1965.
22 L. B. Anderson and C. N. Reilly, J. Electroanal. Chem., 10 (1965) 295.
23 L. C. Thomas, G. D. Christian and J. D. S. Danielson, Anal. Chim. Acta, 77 (1975) 163.
24 F. Vydra and P. Peták, J. Electroanal. Chem., 24 (1970) 379.

Analytica Chimica Acta, 82 (1976) 273—284
©Elsevier Scientific Publishing Company, Amsterdam — Printed in The Netherlands

RELATION ENTRE OXOACIDITÉ (ÉCHANGES DE O^{2-}) ET ACIDITÉ DANS DES SELS FONDUS. APPLICATION A LA SOLUBILISATION DES OXYDES MÉTALLIQUES

BERNARD TRÉMILLON et GÉRARD PICARD

Laboratoire d'Électrochimie Analytique et Appliquée (L. A. au CNRS, no. 216), École Nationale Supérieure de Chimie de Paris, Université Pierre et Marie Curie, 75231-Paris-Cedex 05 (France)

(Reçu le 22 septembre 1975)

RÉSUMÉ

Un traitement quantitatif des réactions d'oxoacidité, notamment de la solubilisation des oxydes métalliques, dans deux sels ioniques fondant à température relativement basse — le chlorure d'éthylammonium et le bromure d'éthylpyridinium — est décrit à l'aide de résultats expérimentaux précédemment obtenus. Une "fonction d'oxoacidité", Ω, est définie, permettant le classement quantitatif des forces des oxoacides et oxobases dans ces milieux fondus. Il est ensuite montré comment influent sur les phénomènes d'oxoacidité les propriétés d'acidité (de Brønsted), caractérisées par le pH des sels fondus considérés; une relation Ω/pH est établie, qui fait intervenir la pression partielle de vapeur d'eau. De la sorte, des prévisions quantitatives de réactions d'oxoacidité causées par l'action d'acides ou de bases deviennent réalisables, impliquant le contrôle de l'humidité des sels fondus. L'influence de ces phénomènes sur les propriétés d'oxydoréduction est également envisagée, au moyen de diagrammes potentiel d'équilibre/Ω. Leur exploitation pratique est évoquée en conclusion.

SUMMARY

A quantitative treatment of oxo-acidity reactions, particularly the solubilization of metal oxides in two low-melting salts — ethylammonium chloride and ethylpyridinium bromide — is described, with the aid of experimental results obtained previously. An "oxo-acidity function", Ω, is defined, allowing the quantitative classification of oxo-acid/oxo-base strengths in these molten media. The influence of the Brønsted acidity properties (characterized by pH in the fused salts) on the oxo-acidity phenomena is then discussed. A Ω/pH relation is established, the partial pressure of water vapor being introduced. In this way, quantitative estimates of oxo-acidity reactions caused by the action of acids or bases become possible when the moisture content of the fused salts is controlled. The influence of these phenomena on oxidation—reduction properties is also considered, by means of equilibrium potential/Ω diagrams. Their practical exploitation is discussed.

Il est devenu classique, en chimie des sels fondus, de substituer à la notion d'acidité de Brønsted—Lowry le concept d'acidité selon Lux—Flood, correspondant à la mise en jeu de l'ion oxyde O^{2-} et désigné plus précisément

par "oxoacidité" pour éviter la confusion avec l'autre concept. Les réactions acide—base classiques n'ayant — pratiquement du moins — plus cours à haute température, les réactions entre "oxoacides" et "oxobases" deviennent en revanche d'importance primordiale.

Dans deux sels ioniques fondant à température relativement basse, nous avons trouvé la possibilité d'étudier expérimentalement (par méthodes électroanalytiques) à la fois des équilibres acide—base (échange de H^+) et des équilibres oxoacide—oxobase (échange de O^{2-}): il s'agit du bromure d'éthylpyridinium (BEP; T_F = 114 °C) et du chlorure d'éthylammonium (CEA; T_F = 108 °C). En ce qui concerne le premier type d'équilibres, les résultats ont pu être interprêtés et présentés selon les raisonnements habituels, en définissant des échelles de pH [1]: X^- désignant l'ion halogénure (Br^- ou Cl^-), le proton solvaté correspond ici à la molécule HX dissoute (HBr ou HCl) et pH = —log [HX] (mol kg^{-1}). Les valeurs de pK_a de plusieurs couples acide—base (HA/A):

$$K_A = \frac{[HX][A]}{[HA]}$$

(en admettant que l'activité de X^- est invariable) ont pu être déterminées au moyen d'une électrode à hydrogène (cf. Tableau 1).

En ce qui concerne les équilibres d'échange de O^{2-}, une difficulté est apparue pour présenter les résultats selon le même modèle que pour les équilibres acide—base, en faisant appel à la grandeur $pO^{2-} = -\log [O^{2-}]$, car l'ion oxyde libre (solvaté) ne peut subsister dans les deux sels considérés. En effet, O^{2-} provoque la décomposition (irréversible) du cation éthylpyridinium et la dissociation quantitative du cation éthylammonium [2, 3].

Pour tourner cette difficulté, nous avons défini une nouvelle grandeur, jouant le rôle de pO^{2-} et permettant le classement quantitatif de la force des oxoacides et oxobases susceptibles d'exister et de réagir dans les deux sels fondus; nous l'avons appelée "fonction d'oxoacidité" et désignée par Ω.

Cette fonction présente en outre l'avantage de faire apparaître une relation fondamentale entre oxoacidité et acidité, c'est-à-dire une correspondance entre l'échelle Ω (ou l'échelle de pO^{2-} lorsque celle-ci peut être définie) et l'échelle de pH.

Une conséquence importante sur le plan pratique est la prévision de la mise en solution d'oxydes insolubles (ou leur insolubilisation) par action d'acides ou de bases, dans ces sels fondus ou des sels analogues (le chlorure de pyridinium par exemple). De même, des variations de propriétes d'oxydo-réduction peuvent être interprêtées selon ces principes.

L'étude qui suit a pour objet de faire la démonstration des raisonnements mis en oeuvre, dans le cas du BEP et du CEA à la température commune de 127 °C (400 K) à laquelle les résultats expérimentaux précédemment décrits ont été obtenus.

TABLEAU 1

Constantes d'acidité $pK_A = -\log K_A$ (mol kg^{-1}) à 0,2—0,3 près) de systèmes acide—base dans le bromure d'éthylpyridinium (BEP) et dans le chlorure d'éthylammonium (CEA) fondus, à 127 °C; d'après réf. 1.

Système acide—base	BEP	CEA[a]
Acide perchlorique—perchlorate	Acide fort	Acide fort
Acide bromhydrique—bromure	Acide fort	Acide fort
Acide chlorhydrique—chlorure	Acide fort	Acide fort
Acridinium—acridine	3,3	
α-Picolinium—picoline	5,2	4,1
Pyridinium—pyridine	5,3	4,3
Acide citrique—dihydrogénocitrate	6,1	4,3
Dihydrogénocitrate—monohydrogénocitrate	7,4	—
Acide salicylique—salicylate	7,6	4,5
Hydrazinium—hydrazine	7,8	—
Acide phosphorique—dihydrogénophosphate	7,8	4,3
Acide succinique—succinate	8,45	5,3
Acide benzoïque—benzoate	8,7	6,1
Acide formique—formiate	9,2	5,4
Ammonium—ammoniac	10,2	
Acide acétique—acétate	10,2	Base forte
Pipéridinium—pipéridine	Base détruisant le cation éthylpyridinium	Base forte
Acide fluorhydrique—fluorure	Base détruisant le cation éthylpyridinium	Base forte
Ethanolammonium—éthanolamine	Base détruisant le cation éthylpyridinium	Base forte

[a]Constante d'autoprotolyse du chlorure d'éthylammonium fondu à 127 °C: $pK_s = -\log[HCl][EtNH_2]$ ($mol^2\ kg^{-2}$) = 8,1.

PRINCIPES THÉORIQUES

Fonction d'oxoacidité Ω

La non-existence de O^{2-} libre interdit de caractériser, comme on le fait dans les halogénures alcalins fondus par exemple, les couples oxoacide—oxobase (M/MO) par une constante de dissociation par solvolyse: $K_B = [M]\ [O^{2-}]/[MO]$ d'où $pO^{2-} = pK_B + \log [M]/[MO]$ si MO est soluble, ou $K_S = [M]\ [O^{2-}]$ d'où $pO^{2-} = pK_S + \log[M]$ si MO est insoluble. Mais on peut atteindre les constantes d'échange de O^{2-} entre deux couples distincts. Dès lors, choisissant un couple de référence, la comparaison quantitative des forces relatives des oxoacides et des oxobases devient possible.

Le couple de référence choisi est celui dont l'eau est l'oxobase, l'oxoacide conjugué étant par conséquent H^+, c'est-à-dire HX dans le cas présent [$2\ HX + O^{2-} = H_2O\ (+\ 2\ X^-)$]. Les équilibres d'échange dont les constantes sont utilisées sont donc:

$$M + H_2O\ (+\ 2\ X^-) \leftrightarrows MO + 2\ HX \qquad (1)$$

L'eau comme l'halogénure d'hydrogène sont volatils et il existe des équilibres entre leur forme dissoute et leur forme gazeuse dans l'atmosphère au contact du sel fondu. Ceci entraîne que, dans les conditions d'idéalité de la phase gazeuse, on peut exprimer les activités de ces deux constituants par leurs pressions partielles respectives, P_{H_2O} et P_{HX}. Il vient alors, pour les équilibres (1):

$$K = \frac{[MO]}{[M]} \cdot \frac{P_{HX}^2}{P_{H_2O}} \left(\text{ou } K = \frac{1}{[M]} \cdot \frac{P_{HX}^2}{P_{H_2O}}, \text{ si MO}\downarrow \right)$$

Nous posons, par définition:

$$\log \frac{P_{HX}^2}{P_{H_2O}} = \Omega$$

De la sorte, un système M/MO dans le sel fondu peut être caractérisé, en raison de l'établissement de l'équilibre (1), par des valeurs de la fonction Ω répondant à la formule:

$$\Omega = \log K + \log \frac{[M]}{[MO]} \text{ (ou } \log K + \log[M] \text{ si MO}\downarrow)$$

Cette formule est analogue à celle exprimant pO^{2-} quand celui-ci peut être défini (dans ce cas, en appelant K_B^0 la constante de dissociation de $H_2O(g)$ $(+\ 2\ X^-) \leftrightarrows 2\ HX(g) + O^{2-}$, on a la relation: $\Omega = pO^{2-} - pK_B^0$, avec $\log K = pK_B - pK_B^0$). L'échelle Ω permet donc, grâce aux valeurs de $\log K (= \Omega^0)$, le classement quantitatif des forces relatives des oxoacides (M) et oxobases (MO).

Relation entre Ω et pH

Dans les conditions d'idéalité des solutions d'halogénure d'hydrogène, le pH dans chaque sel fondu est relié à la pression de vapeur P_{HX}, en application de la loi de Henry, par:

$$pH = -\log P_{HX} + \text{cte.}$$

De ce fait, sous pression de vapeur d'eau imposée, la fonction Ω et le pH sont reliés entre eux par:

$$\Omega = \text{cte.} - 2\ pH$$

Cette relation signifie qu'en présence d'eau dans des conditions d'activité constante on peut faire se correspondre l'échelle de classement des forces des acides et des bases avec celle des forces des oxoacides et oxobases. On en déduit les possibilités de réaliser des réactions entre systèmes oxoacide—oxobase et systèmes acide—base, par exemple la destruction d'une oxobase (comme un oxyde métallique insoluble) par action d'un acide HA:

$$MO\downarrow + 2\ HA \leftrightarrows M + H_2O + A$$

RÉSULTATS EXPÉRIMENTAUX ET EXPLOITATION

Les valeurs Ω^0 permettant le classement des forces de divers systèmes oxoacide—oxobase dans le BEP et le CEA, calculées d'après les valeurs expérimentales de constantes d'équilibre précédemment déterminées [2, 3], sont rassemblées dans le Tableau 2. Il s'agit des systèmes correspondant à un certain nombre de cations métalliques usuels dont les oxydes sont insolubles (mais solubilisables par des actions chimiques).

La discussion sur l'ordre des forces relatives a été présentée précédemment [3].

TABLEAU 2

Classement, sur l'échelle $\Omega_{2-} = \log P_{HX}^2/P_{H_2O}$, de systèmes cation—oxyde métallique (accepteur—donneur de O^{2-} ou oxoacide—oxobase) dans le bromure d'éthylpyridinium BEP(HX = HBr) et dans le chlorure d'éthylammonium CEA(HX = HCl) fondus, à 127 °C. Pouvoir oxoacide de M^{n+}. D'après réfs. 2—5.
(Ω^0: valeur de Ω pour concentration des constituants solubles = 1 mol kg^{-1})

Système oxoacide—oxobase	Ω^0	
	Dans BEP	Dans CEA
M$^+$		
$Ag^+/Ag_2O\downarrow$	−47,4	−29,8
$Cu^+/Cu_2O\downarrow$	−34,3	−18,7
M^{2+}		
$Cu^{2+}/CuO\downarrow$	—	−11,7
$Hg^{2+}/HgO\downarrow$	−40,7	−23,0
$Ni^{2+}/NiO\downarrow$	−33,7	−15,6
$Sn^{2+}/SnO\downarrow$	−22,8	−10,7
M^{3+}		
Al^{3+}/AlO^+	−23,9	—
$AlO^+/Al_2O_3\downarrow$	−25,7	—
Cr^{3+}/CrO^+	−25,0	—
$CrO^+/Cr_2O_3\downarrow$	−20,2	—
Fe^{3+}/FeO^+	−25,8	—
$FeO^+/Fe_2O_3\downarrow$	−16,7	—
$Fe^{3+}/Fe_2O_3\downarrow$		−6,5
M^{4+}		
$Sn^{4+}/SnO_2\downarrow$	−11,2	−4,7
Ti^{4+}/TiO^{2+}	−21,4	−3,9
$TiO^{2+}/TiO_2\downarrow$	−21,8	−5,1
U^{4+}/UO^{2+}	−4,9	—
$UO^{2+}/UO_2\downarrow$	−4,3	—
Zr^{4+}/ZrO^{2+}	−23,7	—
$ZrO^{2+}/ZrO_2\downarrow$	0,1	—
$Zr^{4+}/ZrO_2\downarrow$	−11,8	−0,8

Solubilité apparente des oxydes métalliques. Influence de l'acidité

Des diagrammes d'équilibre de solubilité apparente des oxydes métalliques en fonction de Ω ont été déduits des valeurs du Tableau 2; ils sont représentés Fig. 1. Pour un oxyde du type MO, la solubilité calculée est $S = [M^{2+}]$; pour M_2O_3, elle est exprimée par $S = [M^{3+}] + [MO^+]$; et pour MO_2 par $S = [M^{4+}] + [MO^{2+}]$, en supposant que les oxyhalogénures (MO^+, MO^{2+}) sont solubles, que des espèces condensées ne se forment pas et que l'on se limite au cas des solutions pratiquement idéales ($S < 1$—2 mol kg^{-1}). Toutes les concentrations ont été exprimées en mol kg^{-1}.

L'échelle de pH est placée en correspondance de l'échelle Ω grâce aux graphes de la Fig. 1 situés au-dessus des diagrammes de solubilité apparente. Les correspondances entre pH et log P_{HX} sont données expérimentalement, à 127 °C, par [4]:

dans le CEA: $pH = -\log P_{HCl}\,(atm) - 0{,}3$

dans le BEP: $pH = -\log P_{HBr}\,(atm) - 3{,}0$

Sur les échelles de pH, les couples acide—base figurent à leurs valeurs respectives de pK_A. On peut remarquer que:
(a) le CEA étant un solvant amphiprotonique, son équilibre d'autoprotolyse impose une limitation de l'échelle de pH; les valeurs maximales sont atteintes dans les solutions les plus concentrées d'éthylamine, la base forte dans le milieu (analogue à OH^- dans l'eau); ces valeurs sont de l'ordre de 8;
(b) le BEP n'est pas un solvant amphiprotonique et ne donne pas lieu à un équilibre d'autoprotolyse; l'échelle de pH s'y trouve néanmoins limitée pratiquement, à un maximum de pH ~ 12, par la stabilité du sel fondu dont les bases trop fortes provoquent la décomposition (comme l'ion oxyde).

L'exploitation des graphes s'effectue de la manière suivante. À un milieu de pH donné (fixé par exemple par un système tampon) correspond, par projection orthogonale, une valeur sur l'échelle log P_{HX}. L'intersection de la droite de pente —2 partant de cette valeur avec la droite correspondant à la valeur de log P_{H_2O} choisie (par exemple, log $P_{H_2O} = -3$), puis la projection orthogonale du point d'intersection obtenu sur l'échelle Ω située en-dessous, fournissent la valeur de Ω correspondant à celle du pH pour la pression de vapeur d'eau considérée. Par exemple, dans le CEA fondu à 127 °C, le mélange tampon chlorure de pyridinium—pyridine à concentrations égales, pH = 4,3, et la pression de vapeur d'eau 10^{-3} atm correspondent à Ω = —6,2; sous la pression de vapeur d'eau 0,1 atm, le même mélange tampon de pH correspond à Ω = —8,2. On en déduit immédiatement que, dans le premier cas (atmosphère "sèche"), l'oxyde Fe_2O_3 est solubilisé, attaqué par le cation acide pyridinium, tandis que cette solubilisation n'a pas lieu en atmosphère "humide"; en revanche, NiO, CuO, SnO sont solubilisés dans les deux cas. Pour TiO_2, SnO_2, ZrO_2, l'acidité du cation pyridinium est insuffisante; celle de HCl est nécessaire, avec une atmosphère sèche en ce qui concerne les

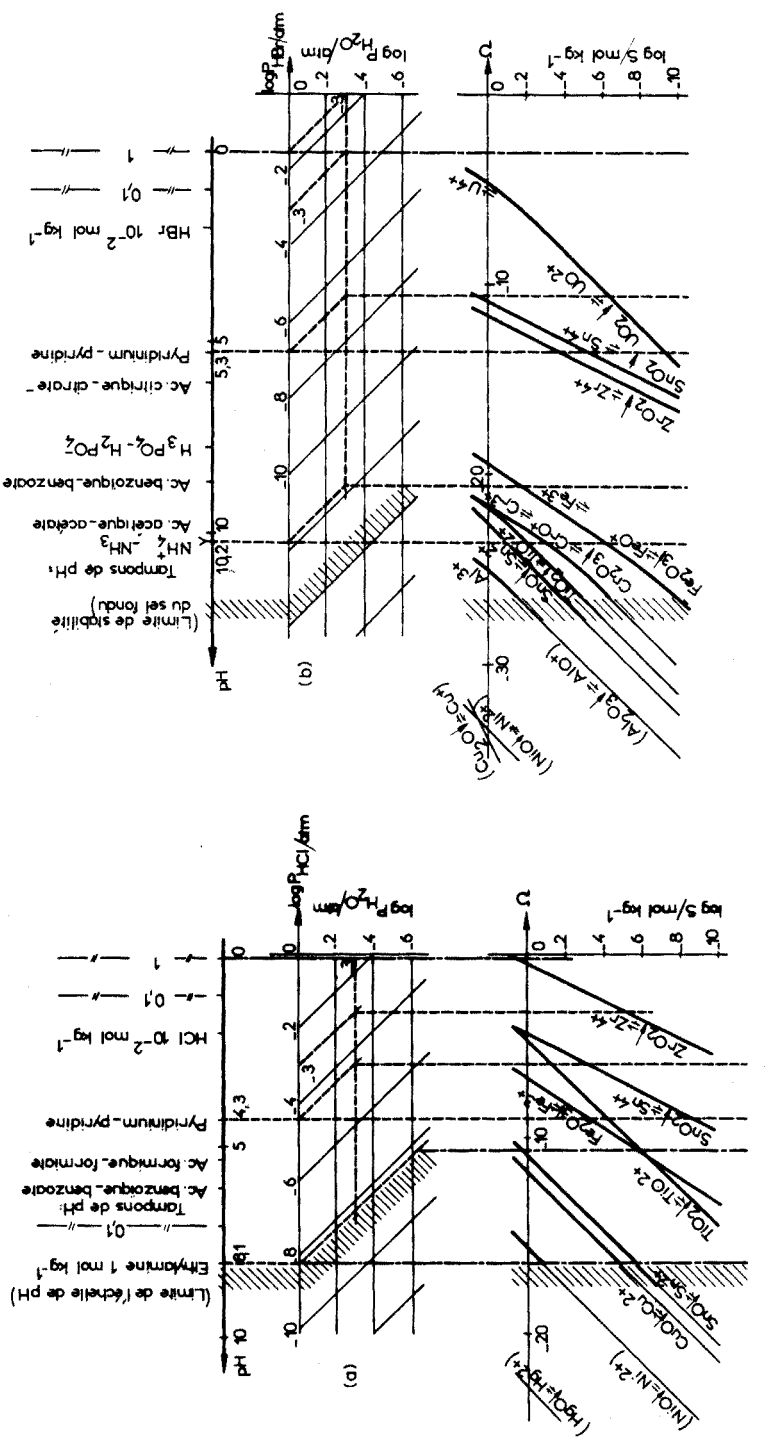

Fig. 1. Diagrammes de solubilité apparente d'oxydes métalliques en fonction de Ω et détermination de Ω en fonction du pH et de la pression de vapeur d'eau, dans le chlorure d'éthylammonium (a) et le bromure d'éthylpyridinium (b) fondus, à 127 °C.

oxydes les plus difficilement solubles tels que ZrO_2.

La limitation des échelles de pH dans les deux sels fondus entraîne celle des échelles Ω. Ainsi, le milieu de pH 8,1 dans le CEA fondu, milieu pratiquement le plus basique, correspond sous $P_{H_2O} = 0{,}1$ atm à $\Omega = 15{,}8$. Ce milieu provoque donc la dissolution spontanée de HgO et de NiO ($S \approx 0{,}1$ mol kg^{-1}) qui, par conséquent, ne peuvent précipiter par addition d'éthylamine (ni d'aucune autre base) à une solution contenant les ions Hg^{2+} et Ni^{2+} (dilués). Les oxydes CuO et SnO sont insolubles dans les mêmes conditions, mais se trouvent légèrement dissous si l'atmosphère et le sel fondu sont secs.

Dans le BEP, on constate de la même manière la solubilisation spontanée de plusieurs oxydes — notamment Al_2O_3 — par la seule action du solvant sec, même rendu basique.

Propriétés oxydoréductrices apparentes des métaux. Influence de l'acidité

Les valeurs de potentiels d'équilibre qui ont été déterminées expérimentalement [2—5] et qui sont rassemblées dans le Tableau 3, jointes aux valeurs du Tableau 2 concernant les couples oxoacide—oxobase, permettent l'établissement de diagrammes type Pourbaix représentant les variations en fonction de Ω des potentiels d'équilibre E caractérisant les couples oxydant—réducteur dans les deux sels fondus. Les Figs. 2 et 3 représentent à titre d'illustration les diagrammes correspondant au titane dans les deux sels et au chrome et au fer dans le BEP.

Le calcul du diagramme pour un élément métallique est effectué comme dans le cas des diagrammes E—pO^{2-} [6]. L'origine de potentiel est fixée dans chaque cas au potentiel de l'électrode normale à hydrogène dans le sel fondu ([HX] = 1 mol kg^{-1}, soit pH = 0, et $P_{H_2} = 1$ atm).

Sur ces diagrammes, il est intéressant de faire apparaître les limitations dues au sel fondu lui-même en raison de son oxydabilité ($X^- \rightarrow X_2$), d'une part, et de sa réductibilité, d'autre part, propriétés qui ont été précisées et décrites antérieurement [1—5]. Les limites de l'échelle Ω apparaissent naturellement aussi, variables selon la pression de vapeur d'eau régnant au-dessus de la solution, d'après le raisonnement précédent.

La présence d'eau dans le sel fondu fait que la réduction de celle-ci en hydrogène peut constituer la limite effective de l'échelle de potentiel vers les milieux réducteurs. Ce potentiel limite est alors doublement dépendant de P_{H_2O} et de Ω, donc du pH. Vers les potentiels les plus élevés, la limite en milieu oxobasique (Ω très négatif) est due à la formation d'oxygène par oxydation des ions O^{2-} (combinés), oxydation se produisant alors plus facilement que celle des ions X^- (mais ne se produit pas en atmosphère sèche dans le BEP).

On peut tirer diverses conséquences de ces diagrammes, selon les modes de prévision classiques que nous ne développerons pas. Ainsi, par exemple, pour le fer dans le BEP, on note la facilité de dissolution de Fe_2O_3 à l'état de Fe^{2+}, même par un réducteur faible, dès que l'on opère en atmosphère sèche.

TABLEAU 3

Potentiels normaux (concentrations exprimées en molalité) ou potentiels de demi-vague réversible (indiqués par*) de systèmes électrochimiques de métaux dans le bromure d'éthylpyridinium (BEP) et dans le chlorure d'éthylammonium (CEA) fondus, à 127 °C. Origine de potentiel d'électrode relatif: électrode normale à hydrogène (P_{H_2} = 1 atm, [HX] = 1 mol kg^{-1}) dans le sel fondu. D'après réfs. 2—5

Système électrochimique	E° ou $E_{1/2}$ (mV)	
	Dans BEP	Dans CEA
Ag/Ag^+	—558	—36
Au/Au^+	+110	+691
Bi/Bi^{3+}	—534	—189
Cr^{2+}/Cr^{3+}	—269*	—
$Cd(Hg)/Cd^{2+}$	—	—609*
Cu/Cu^+	—723	—278
$Cu(Hg)/Cu^+$	—805*	—375*
Cu^+/Cu^{2+}	(Cu^{2+} oxyde Br^-)	+483
Fe^{2+}/Fe^{3+}	+227*	+388*
Hg/Hg^{2+}	—498	+20
$Ni(Hg)/Ni^{2+}$	—	—357*
$Pb(Hg)/Pb^{2+}$	—	—474*
Sn/Sn^{2+}	—821	—529
Sn^{2+}/Sn^{4+}	(Irréversibilité)	(Irréversibilité)
Ti^{3+}/Ti^{4+}	—205	+209*
U^{3+}/U^{4+}	—525*	—
V^{2+}/V^{3+}	—	—420*
X^-/X_2	X=Br: + 392	X=Cl (oxydation irrév. de $EtNH_2$ en EtNHCl à $E \approx$ + 1 V)

CONCLUSION

La solubilisation des oxydes métalliques par fusion avec un sel acide, ou la corrodabilité des métaux au contact de ces mêmes sels fondus, constituent des aspects pratiques importants des phénomènes qui viennent d'être étudiés. Leur exploitation a été jusqu'ici plus empirique que raisonnée; mais le traitement précédent démontre que ces phénomènes peuvent être exploités d'une manière aussi systématique et quantitative que les réactions en solution aqueuse.

Un facteur apparaît très important pour la maîtrise des phénomènes afin d'obtenir des effets raffinés (sélectivité de séparations, par exemple): c'est le contrôle de la teneur en eau, autrement dit de l'humidité, qui est réalisable par celui de la pression de vapeur d'eau de l'atmosphère au contact des "bains fondus". Des résultats différents peuvent être atteints selon que l'on opère en milieu sec ou au contraire très humide.

Le pouvoir dissolvant des sels fondus vis-à-vis des oxydes métalliques est principalement lié à leur acidité propre: on comprend ici aisément pourquoi

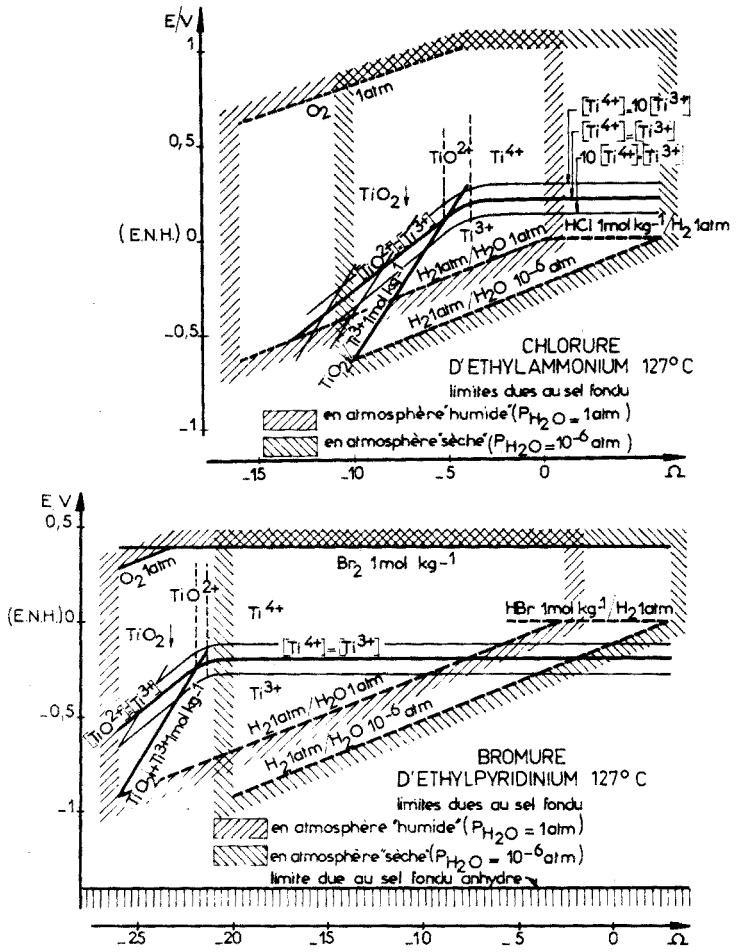

Fig. 2. Diagrammes potentiel d'équilibre en fonction de Ω pour le titane dans le CEA et le BEP fondus à 127 °C.

les sels d'ammonium non quaternaires ont un pouvoir dissolvant que n'ont pas les sels d'ammonium quaternaires et alcalins, et pourquoi le chlorure de pyridinium a été le plus exploité en raison de son efficacité [7]. Le rôle du pouvoir complexant de l'anion halogénure ne doit cependant pas être négligé: les différences de comportement entre le BEP et le CEA, qu'on peut relever à l'examen des Figs. 1—3, lui sont essentiellement imputables.

Enfin, les raisonnements développés ici pour le cas d'halogénures sont aisément transposables au cas d'autres sels similaires, tels que les hydrogénosulfates $M^+HSO_4^-$. Leur pouvoir dissolvant des oxydes métalliques ("fusions au bisulfate") découle de la forte acidité des anions HSO_4^-. Dans ce cas également, les phénomènes d'oxoacidité sont en relation avec l'acidité

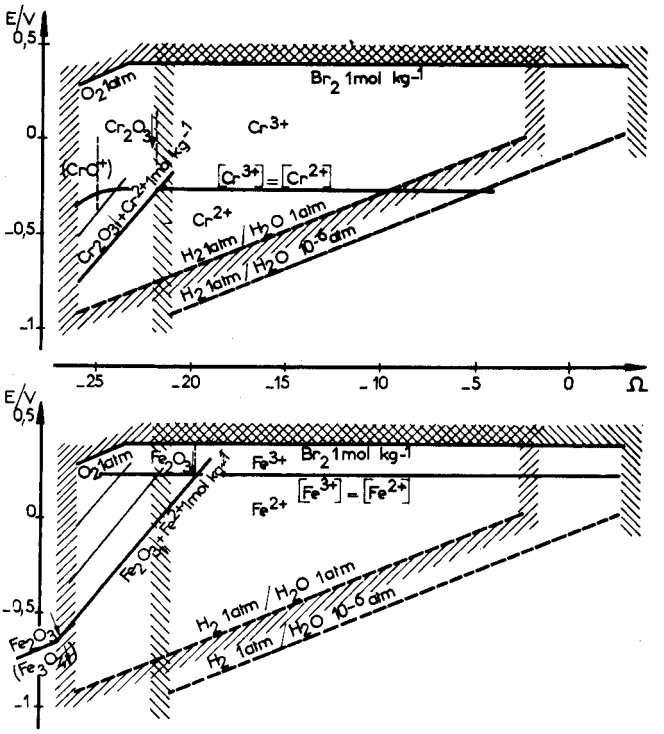

Fig. 3. Diagrammes potentiel d'équilibre en fonction de Ω, dans le BEP fondu à 127 °C, pour le chrome et le fer.

(mesurée par pH = —log $[H_2SO_4]$) et sont contrôlés par un double contrôle expérimental de la pression de vapeur de H_2SO_4 (qui fixe le pH) et de la pression de vapeur d'eau (cf. réf. 8). Il en sera de même dans le cas de l'hydrogénodifluorure de potassium fondu $K^+HF_2^-$, utilisé pour les "fusions au difluorure", dont l'acidité est contrôlée par la pression de vapeur de HF [9] et dans lequel le contrôle de l'oxoacidité nécessitera le double contrôle expérimental des pressions de vapeur de HF et de H_2O.

On remarquera pour terminer que l'on rejoint le cas des hydroxydes alcalins fondus ("fusions alcalines"), dans lesquels le contrôle de la pression de vapeur d'eau suffit pour imposer à la fois l'acidité et l'oxoacidité, car ici les deux concepts se juxtaposent de manière biunivoque en vertu de l'équilibre d'autoprotolyse particulier (*cf.* réf. 10).

Les auteurs sont reconnaissants au Dr. J. Vedel pour les discussions fructueuses qu'ils ont eues avec lui sur le sujet de ce mémoire.

BIBLIOGRAPHIE

1 J. Vedel et B. Trémillon, Bull. Soc. Chim. Fr., (1966) 220; J. Vedel, Bull. Soc. Chim. Fr., (1968) 3069.
2 M. Lapidus et B. Trémillon, J. Electroanal. Chem., 15 (1967) 371.
3 G. Picard et J. Vedel, Bull. Soc. Chim. Fr., (1975) 540.
4 G. Picard, Thèse Doct. d'Etat, no. CNRS: AO 8625, Paris, 1973.
5 G. Picard et J. Vedel, Bull. Soc. Chim. Fr. (1969) 2557; Electrochim. Acta, 17(1972) 1; J. Chim. Phys., (1975) 767.
6 B. Trémillon, Pure Appl. Chem., 25 (1971) 395.
7 A. Long et L. F. Audrieth, Trans. Ill. State Acad. Sci., 28 (1935) 121.
8 J. P. Vilaverde, G. Picard, J. Vedel et B. Trémillon, J. Electroanal. Chem., 54 (1974) 279; A. Ben Hadid, G. Picard et J. Vedel, à paraître.
9 J. Devynck, M. Sloim et B. Trémillon, J. Electroanal. Chem., à paraître.
10 B. Trémillon et R. G. Doisneau, J. Chim. Phys., (1974) 1379.

Analytica Chimica Acta, 82 (1976) 285—292
©Elsevier Scientific Publishing Company, Amsterdam — Printed in The Netherlands

THE INFLUENCE OF SOME ORGANIC COMPLEXING AGENTS ON THE POTENTIAL OF COPPER(II) - SELECTIVE ELECTRODES. APPLICATION OF THE SILICONE RUBBER-BASED ELECTRODE TO THE DETERMINATION OF CITRATE ION AND 8-HYDROXYQUINOLINE

MOHAMED FAYEZ EL-TARAS* and ERNÖ PUNGOR

Institute for General and Analytical Chemistry, Technical University of Budapest, 1502-Budapest-XI (Hungary)

GÉZA NAGY

EGYT Pharmacochemical Works, Budapest (Hungary)

(Received 20th October 1975)

SUMMARY

The behaviour of the silicone rubber-based copper(II)-selective electrode in the presence of complexing agents is discussed. The electrode shows well defined responses to several complexing agents in solutions practically free of copper(II) ions. Titrimetric determinations of citrates and 8-hydroxyquinoline with potentiometric end-point detection are described.

Recently, several reports have appeared about different copper(II) electrodes made of different materials and prepared by different methods [1]. It seems that all the copper(II) electrodes described to date which function properly, i.e. which give near Nernstian, stable and more or less selective responses to Cu^{2+} ions, belong to the group of precipitate-based ion-selective electrodes. They all are prepared with copper sulphide [2—5], copper telluride [6] or copper selenide [7] precipitate as the active ingredient.

It is well known that the presence of a complexing agent can seriously influence the electrode potential of a potentiometric sensor. There are two different mechanisms on the basis of which this effect on the electrode potential can be explained. First, the potential of a potentiometric sensor is determined by the activity of one or more ionic ingredients; any agent which forms a strong complex with (or with one of) the potential-determining species will therefore decrease its activity, and so will affect the electrode potential. Since the copper(II) ion readily forms various kinds of complex with organic and inorganic ligands, complexing agents must be seriously considered as possible interferences when copper(II)-selective electrodes are used. Secondly, in the case of precipitate-based electrodes, potentials can be affected by complexing reactions between a ligand in the solution and the active ingredient of the measuring membrane on the surface of the electrode.

---

*Present address: Faculty of Pharmacy, Cairo University (Egypt).

In special cases this second type of influence can function in the absence of the ion giving the reversible electrode response. The complexing agent can even give a reversible, well-defined and analytically applicable response at the ion-selective electrode in question.

The cyanide response of silver halide electrodes and the use of the cyanide-selective electrode in different measurements, seem to be the most studied example and the most widely used analytical application of this effect [8—12].

In the work reported here, the influence of different complexing agents on the function of the silicone rubber-based copper(II)-sensitive electrode was studied. On the basis of the experimental findings, procedures were worked out for determining citrate ion and 8-hydroxyquinoline with this electrode as detector. The applicability of the methods was proved in the analysis of some pharmaceutical products. Copper salts have been used frequently as reagents in the determination of 8-hydroxyquinoline [13—15].

EXPERIMENTAL

Apparatus

Measurements were made with an expanded scale precision pH meter (model OP-205, Radelkis, Budapest). The silicone rubber-based copper(II)-selective electrode used as indicating electrode was prepared as described earlier [3].

A saturated calomel electrode served as reference and an agar-agar potassium nitrate salt bridge ensured electrical contact.

Reagents

All reagents used were of analytical grade. The copper(II) solutions were prepared from a copper sulphate stock solution by serial dilution; the stock solution was standardized by titration with EDTA in the presence of PAN indicator. The ionic strength of the solutions used in the direct potentiometric measurements was adjusted to a constant level of 10^{-1} M with KNO_3. The pH of the solutions was adjusted with 0.1 M acetate buffer or 0.1 M sodium hydrogencarbonate.

8-Hydroxyquinoline solutions (10^{-2} M) were prepared by dissolving weighed samples in a few ml of acetic acid and diluting to volume with distilled water.

RESULTS AND DISCUSSION

Effects of complexing agents on the copper(II)-selective electrode

The potential of the copper(II)-selective electrode was measured in

solutions containing different agents which form complexes with the copper(II) ions. The relationship between the total concentration of the complexing agent and the electrode potential was observed in solutions containing originally no copper(II) and in solutions containing different activities of copper(II).

When the initial standard solutions contained no copper ions, the copper(II)-selective electrode responded to changes in the complexing agent concentration. With strong complexing agents such as citrate and tartrate, the plot of electrode potential vs. the logarithmic concentration of the complexing agent was a straight line in the range 10^{-2}—10^{-6} M; as can be seen in Fig. 1, the plot for citrate has a slope of 29 mV/decade. Since the electrode potential in citrate and tartrate solutions was found to be very stable even in the absence of copper(II), it can be concluded that the concentration of citrate ions and other reagents forming strong complexes with copper(II) can be determined by direct potentiometry with the copper(II)-selective electrode.

One complexing agent, however, can interfere with the direct potentiometric determination of another. The electrode definitely possesses some selectivity for the different complexing agents. The selectivity ratios of the copper(II) electrode with citrate as the species measured and tartrate and acetate as interfering species were determined by the method of mixed solutions [16], i.e. the concentration of citrate was kept constant and the concentration of acetate or tartrate was changed. The results are shown in Fig. 2; the calculated selectivity ratios are $K = 10^{-1}$ for tartrate and $K = 10^{-4}$ for acetate.

The copper(II)-selective electrode also showed a response in the absence of copper(II) ions to complexing agents such as glycine and serine which form less stable complexes with copper(II) ions, but the electrode potentials were less reproducible and less stable in glycine solutions than in citrate solutions. When the concentration of the glycine or serine was changed, 3—4 min were required for the electrode potential to achieve a constant value.

The dependence of the electrode potential on the logarithmic concentration of glycine is compared with that for copper(II) in Fig. 3. The absolute values

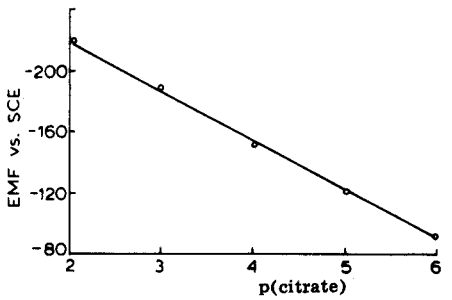

Fig. 1. Calibration curve of the copper(II)-selective electrode for citrate.

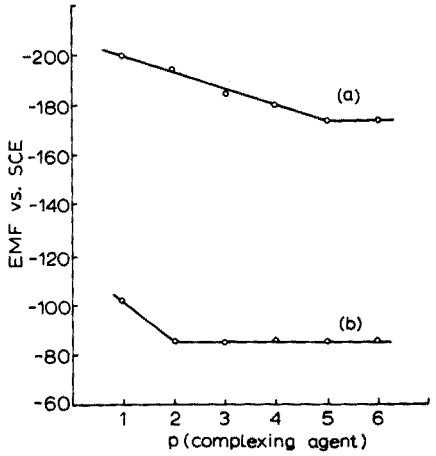

Fig. 2. Curves used to determine the selectivity ratios of the copper(II) electrode for citrate in the presence of (a) tartrate (10^{-4} M citrate), and (b) acetate (10^{-6} M citrate).

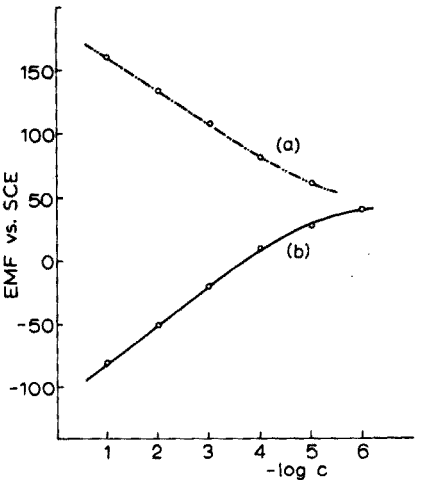

Fig. 3. Comparison of the copper(II) (curve a) and glycine (curve b) responses of the copper(II) electrode.

of the slopes of these plots for serine and glycine were much higher at the higher concentrations (10^{-1}—10^{-3} M) than that of the slope of the copper(II) calibration curve.

In solutions of complexing agents which are involved in proton exchange equilibria with the solvent, the potential of the copper(II)-selective electrode must be influenced by the pH of the solution. This dependence is shown in Fig. 4 for citrate solutions of different concentration.

The response of copper(II)-selective electrodes to the concentration of complexing agent in solutions free of copper ions may be explained on the same basis as the response of the silver halide membrane electrode to complexing agents such as cyanide. Although the theoretical understanding of the behaviour of ion-selective electrodes in the presence of complexing agents is far from complete, the interpretation is based on the dissolution of the precipitate incorporated in the sensing membrane of the electrode. Thus the potential response of the copper electrode observed in copper-free solutions is the result of the steady state of a continuous dissolution process of the CuS precipitate from the sensing surface. Copper-selective electrodes kept for 2—3 days in relatively concentrated (10^{-1}—10^{-2} M) solutions of citrate or glycine stopped functioning. This behaviour can be explained as exhaustion of the electrode surface by dissolution of the incorporated precipitate.

The potential of the copper(II)-selective electrode is also affected by the presence of complexing agents in copper (II) solutions. In Fig. 5 the dependence of the electrode potential on the glycine concentration is shown at different concentrations of copper(II). As can be seen, the effect is more

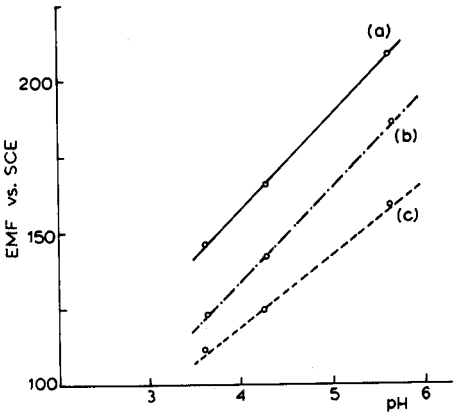

Fig. 4. The effect of pH on the citrate function of the copper(II)-selective electrode at different citrate concentrations. (a) 10^{-2} M. (b) 10^{-3} M. (c) 10^{-4} M.

pronounced at lower copper(II) concentrations. Accordingly, when the direct potentiometric method is used to determine copper(II), complexing agents can be a serious source of interference.

Use of the copper(II)-selective electrode in titrations

The copper(II)-selective electrode can be used as an end-point detector in titrimetric determinations of copper(II) with strong complexing agents as the titrant or in titrimetric determinations of compounds which form strong complexes with copper(II), with standard copper(II) solutions as the titrant.

The concentrations of solutions of sodium citrate and citric acid could be determined readily when copper sulphate solution was used as titrant. The titration curves for different concentrations of sodium citrate are shown in Fig. 6. In these titrations, 10^{-1} M sodium hydrogencarbonate was used to buffer the pH change during the titration; the distortion in the first part of the titration curve for the 10^{-1} M solution was probably caused by pH change. When 0.1 *M* acetate buffer was used in the titrations the potential jump at the end-point was poorer; this is to be expected, given the interference of acetate ions with the citrate response of the electrode.

The procedure suggested for the titration of citrate is as follows: the sample containing 30—100 mg of citrate is mixed with 10 ml of 10^{-1} M $NaHCO_3$ solution and about 50 ml of 10^{-1} M KNO_3 solution, and titrated with standardized copper sulphate solution; the silicone rubber-based copper(II)-selective electrode and a saturated calomel electrode are used to establish the end-point. Table 1 summarizes the results obtained for such titrations. Over the whole range, the average recovery was 97·9 % and the standard deviation was 0.87 %. Several commercially available pharmaceutical

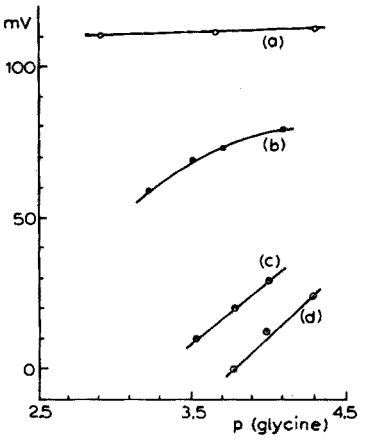

Fig. 5. The dependence of the potential on the glycine concentration at different copper(II) levels. (a) 10^{-3} M Cu^{2+}. (b) 10^{-4} M Cu^{2+}. (c) 10^{-5} M Cu^{2+}. (d) No copper(II).

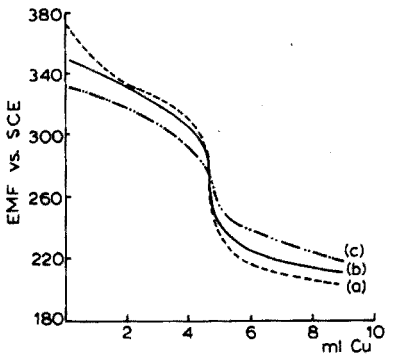

Fig. 6. Titration curves for sodium citrate solutions of different concentration with copper(II) titrant solutions. (a)10^{-1} M.(b)10^{-2} M.(c)10^{-3} M.

preparations containing citrate ion were analyzed by the proposed method. The results obtained are shown in Table 2.

8-Hydroxyquinoline can be determined by titration with copper sulphate reagent solution, and the reverse titration is also possible. For such titrations, 10^{-1} M acetate buffer pH 5.5 is most suitable. The end-points are readily located provided that the sample and titrant concentrations are not too far below 10^{-2} M. Typical titration curves are shown in Fig. 7.

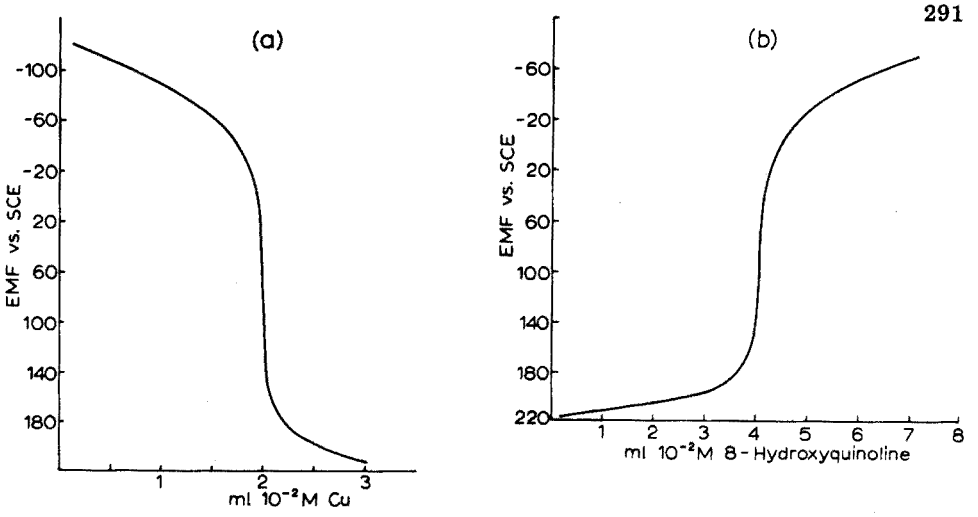

Fig. 7. Potentiometric titration curves. (a) 10^{-2} M 8-hydroxyquinoline titrated with 10^{-2} M $CuSO_4$ solution. (b) 10^{-3} M $CuSO_4$ titrated with 10^{-2} M 8-hydroxyquinoline solution.

TABLE 1

The titrimetric determination of citrate

Added (mg)	Found (mg)	Recovery (%)	Deviation
29.4	28.3	96.25	−1.61
44.10	42.95	97.4	−0.48
58.8	58.4	99.3	+1.44
73.5	72.36	98.45	+0.59
88.2	86.4	97.95	+0.09
102.9	100.7	97.80	−0.06

TABLE 2

Determination of citrate in some pharmaceutical preparations

Preparation		Stated amount (g)	Amount found[a] (g)	Recovery (%)
Potassium citrate tablet	1	0.5	0.494	98.8
	2	1.0	0.974	97.4
Sodium citrate injection		0.380	0.377	99.2
Caffeine citrate powder		48—52[b]	54.6[b]	104.1
Walirine syrup		1[c]	1.029[c]	102.9

[a]Average of at least 3 determinations.
[b]% citric acid.
[c]Weight/100 ml.

REFERENCES

1 R. P. Buck, Anal. Chem., 46 (1974) 28 R.
2 J. W. Ross Jr., In R. A. Durst (Ed.), Ion-selective Electrodes, NBS Special Publ. No. 314, Washington, 1969.
3 J. Pick, K. Tóth and E. Pungor, Anal. Chim. Acta, 61 (1972) 169.
4 J. Pick, K. Tóth and E. Pungor, Anal. Chim. Acta, 65 (1973) 240.
5 T. Anfält and D. Jagner, Anal. Chim. Acta, 56 (1971) 477.
6 K. Higashigama and H. Hirata, Ger. Offen Patent, 2,210,530, 1971.
7 J. Vesely, Collect. Czech. Chem. Commun., 36 (1971) 3364.
8 D. H. Evans, Anal. Chem., 44 (1972) 875.
9 G. P. Bound, B. Fleet, H. von Storp and D.H. Evans, Anal. Chem., 45 (1973) 788.
10 B. Fleet and H. von Storp, Anal. Chem., 43 (1971) 1575.
11 E. Pungor and K. Tóth, Analyst (London), 95 (1970) 625.
12 K. Tóth and E. Pungor, Anal. Chim. Acta, 51 (1970) 221.
13 D. J. Stoever, Pharm. Weekbl. Ned., 107 (1972) 201.
14 G. J. Van Rossum and G. den Boef, Anal. Chim. Acta, 61 (1972) 144.
15 E. Vinkler, F. Klivenyi and Simon M. Gati, Acta Pharm. Hung., 42 (1972) 141.
16 E. Pungor and K. Tóth, Anal. Chim. Acta, 47 (1969) 291.

Analytica Chimica Acta, 82 (1976) 293—309
©Elsevier Scientific Publishing Company, Amsterdam — Printed in The Netherlands

ATOMIC ABSORPTION SPECTROMETRIC DETERMINATION OF SELENIUM WITH CARBON FURNACE ATOMIZATION*

MILAN IHNAT

Chemistry and Biology Research Institute, Agriculture Canada, Ottawa, Ontario K1A OC6 (Canada)

(Received 13th August 1975)

SUMMARY

A Varian Techtron model 63 carbon rod atomizer is used for the atomic absorption spectrometric determination of nanogram quantities of selenium. The pronounced interferences from the matrices in biological digests can be obviated by isolating selenium from sample matrices by precipitation with ascorbic acid. The precision of the determination is improved by incorporating 5000 μg Ni ml^{-1} in the analytical solutions. Selenium at $\mu g\ g^{-1}$ and sub-$\mu g\ g^{-1}$ levels in a variety of biological samples can be determined. The detection limit is 25 ng Se g^{-1}.

Of the several methods available for the determination of selenium at p.p.m. and sub-p.p.m. levels, frequent use is made of a fluorimetric procedure which has proved to be precise and accurate [1, 2] and has gained official status for plant samples and foods [3]. The sample detection limit is in the region of 10 ng g^{-1}, which is adequate for many applications but unsuitable for samples containing p.p.b. levels of selenium. Flame atomic absorption spectrometry with solution aspiration is not sufficiently sensitive for most biological applications where sub-p.p.m. levels are encountered. For a variety of flames, detection limits in the range 50—3600 ng ml^{-1} have been reported [4—13]. Sensitivity can be improved by the hydride generation technique, the hydrogen selenide being introduced into an argon-hydrogen-entrained air flame [14—18]; a detection limit as low as 1 ng ml^{-1} of solution has been achieved [17]. Recent work by Goulden and Brooksbank [19] and Siemer and Hageman [20] in which the hydrogen selenide was dissociated in an electrically heated tube furnace in an atmosphere of hydrogen, oxygen and argon, brought the detection limit down to an impressive 0.1 ng ml^{-1}.

The introduction of commercial carbon furnace atomization instruments has generated widespread interest in this technique. Several reports [21—32]

*Portions of this paper were presented at the 4th International Conference on Atomic Spectroscopy, Toronto, Ontario, October 1973, Conference II, Trace Analysis in Biological Materials, Halifax, N.S., August 1974, and 1st Meeting of the Federation of Analytical Chemistry and Spectroscopy Societies, Atlantic City, N.J., November 1974.

have appeared dealing with the determination of selenium in water, waste water, alloys, and plant and animal tissues. Absolute detection limits in the range of 26—300 pg have been reported. The present paper describes a further study of the potential of this technique for determining selenium, and the application of a carbon furnace to the estimation of selenium in biological samples.

EXPERIMENTAL

Instrumentation

A commercially available carbon furnace (carbon rod atomizer model 63, Varian Techtron Pty. Ltd., Melbourne, Australia) was employed with an atomic absorption spectrophotometer (model AA5, Varian Techtron) equipped with a photomultiplier tube with R446 response. This atomization device, based on the work of Massmann [33], is a modified version of model 61 [34—37]. The atomization device was positioned on the burner holder in place of the burner head. Both tube and cup configurations of the furnace were employed in this investigation, the bulk of the work being done with the tube form. The tube and cup were suitably aligned in the spectrometer system, and source radiation was focussed in the carbon cells and refocussed in the monochromator. A masking plate with a 3-mm diameter circular aperture was positioned immediately after the sample cell to block out light other than that passing through the furnace. Nitrogen was used as an inert gas sheath at a flow rate of 4 l min^{-1}.

The light source for absorption measurements was a neon-filled selenium hollow-cathode lamp (Varian Techtron or Beckman Instruments Inc., Fullerton, California) operated at 10 mA. Non-atomic absorbance was monitored with a hydrogen hollow-cathode lamp (Varian Techtron) operated at a suitable current to match the light intensity of the selenium lamp. The monochromator wavelength was set to pass the 196.03-nm selenium line, and slit width was adjusted to 300 μm, corresponding to a spectral bandpass of 0.99 nm. A slit height attachment was fitted to the slit mechanism drum of the monochromator and set at 2 mm. The spectrometer amplifier was operated in the high gain mode, scale expansion was used as required, and damping control was set at A (least signal damping). Absorbance signals were recorded on a strip-chart recorder (Hitachi Perkin-Elmer model 056) having a 0.5-s full-scale pen response time.

Reagents and standard solutions

Nitric acid, sulfuric acid, 70 % perchloric acid, L-ascorbic acid, 30 % hydrogen peroxide and nickel nitrate hexahydrate were all reagent grade; water was singly distilled. A stock solution of nickel nitrate in water (50000 μg Ni ml^{-1})was diluted as required to introduce nickel into standard and

sample solutions. A selenium standard stock solution was prepared by dissolving with warming, 0.100 g of black elemental selenium (purity 99.9 %) in ca. 5 ml of 16 M nitric acid and diluting to 1 l with water to give 100 μg Se ml^{-1}. Working standard solutions of selenium (0.02—10 μg ml^{-1}) were prepared by serial dilution of the stock solution with water, nitric and perchloric acids and nickel stock solution to provide solutions, typically, 1.0 M in perchloric acid and 0.5 M in nitric acid, containing 5000 μg Ni ml^{-1}. Nickel and acid concentrations were altered when the effects of these components on selenium absorbance were being monitored. In all cases, bulk matrices of standard solutions matched those of the samples.

Sample preparation

The samples used were primarily selected from those used previously for a detailed fluorimetric study [2b]. All samples were prepared in dry form [2b], and except for the NBS liver, had been stored in air-tight polyethylene bottles at −18 °C since the fluorimetric analyses were completed; the liver sample was stored in its original glass container at room temperature. The fluorimetrically determined selenium results from interlaboratory analyses [2b] or the author's laboratory, and the provisionally certified levels in the NBS liver sample were taken as references for monitoring the performance of the a.a.s. procedure. Samples were not dried further either in the previous fluorimetric analyses or in the present study; moisture contents (mean ca. 6 %) were expected to remain constant, permitting direct comparison of analytical results. A correction for a 5.4 % moisture content of the NBS liver sample was made to permit comparison of the data generated in this study with the level reported by NBS for the dry sample.

Sample decomposition with nitric-perchloric-sulfuric acids

Samples were digested with nitric, perchloric and sulfuric acids under non-charring, selenium-retentive conditions to destroy organic matter [2a], as follows. Transfer an accurately weighed 1-g sample to a 30-ml Kjeldahl flask containing 3 glass beads. Add 16 M nitric acid (10 ml), and reduce the volume to ca. 3 ml by cautious heating on an electric digestion rack. After cooling, add 6.0 ml of 70 % perchloric acid and 3.0 ml of 18 M sulfuric acid, return the flask to a cool heater, and heat until perchloric acid is removed and dense white fumes of sulfur trioxide appear. Remove the flask from the heat, add 1.0 ml of 30 % hydrogen peroxide, swirl, and boil briskly until white fumes are again evolved. Repeat the addition of hydrogen peroxide and heating to fumes twice more, and finally heat for 5 min after the appearance of white fumes. Cool the solution and dilute with 3.0 ml of water.

Sample decomposition with nitric-perchloric acids

When isolation of selenium from sample matrices was not desired, the samples were digested as follows. Heat with 10 ml of 16 M nitric acid, cool, and add 70 % perchloric acid. Return the flask to a cool heater, heat until all the nitric acid is removed and the volume of perchloric acid is reduced so that a solution 1.0 M in perchloric acid results when the digest is brought to final volume (usually 3 ml). Monitor this volume of perchloric acid by weighing the digestion flask. Transfer the contents of the flask to a volumetric flask and dilute to volume with nitric acid, nickel nitrate solution, and water, to give a solution 1.0 M in perchloric acid and 0.5 M in nitric acid, containing 5000 μg Ni ml^{-1}.

For recovery studies, various weights (0.05—1.0 g) of potato, flour and swordfish were spiked in the digestion flask with 10.0 μg selenium and taken through the nitric-perchloric digestion. Digests were made to a final volume of 10.0 ml containing 1.0 M perchloric acid, 0.5 M nitric acid and 5000 μg Ni ml^{-1}. Samples with no added selenium were taken through the same procedure as reagent blanks to correct for the native levels of selenium present, which amounted to ca. 0.02, 0.68 and 3.44 μg g^{-1} for potato, flour and swordfish, respectively. A selenium standard solution and an appropriate blank solution were also processed simultaneously.

Isolation of selenium

Selenium was separated from the inorganic sample matrix remaining in the digests by reduction of the selenite to elemental selenium, as follows. Add ascorbic acid (2.0 g) to the contents of a Kjeldahl flask, and shake for 5 min on a wrist-action shaker. Allow to stand for 25 min, add 20 ml of water, and shake to dissolve the remaining ascorbic acid. Filter through a 25-mm diameter, 0.2-μm type EG Millipore membrane filter (0.8-μm type AA was also used for comparison) and wash the filter and digestion flask well with several aliquots of water. Return the filter and contents to the original Kjeldahl flask, add 1.0 ml of nitric acid and warm to dissolve the filter. Complete the digestion of the filter plus selenium by adding 0.26 ml of 70 % perchloric acid and heating to fumes. Add a little water to rinse down the wall of the flask, and again heat to fumes of perchloric acid. Transfer the resulting solution quantitatively to a 3-ml volumetric flask containing 0.10 ml of 16 M nitric acid and 0.30 ml of a 50000 μg Ni ml^{-1} solution to give an analytical solution 1.0 M in perchloric acid and 0.5 M in nitric acid containing 5000 μg Ni ml^{-1}. Samples containing $\lesssim$ 1 μg Se g^{-1} are made up to a final volume of 1 ml. To obviate transfer problems with such small volumes, prepare the solutions directly in the digestion flask. In these cases, use 90 μl of perchloric acid for the second digestion, and then add 30 μl of 16 M nitric acid, 0.10 ml of 50000 μg Ni ml^{-1} solution and 0.78 ml of water. The resulting volume was found to be 1.07 ± 0.03 ml; corrections

for weights of inorganic ash remaining from samples were found to be negligible. An appropriate selenium standard solution (based on preliminary estimation or known selenium level in sample) and a reagent blank must be taken, along with the sample, through the entire procedure.

Determination procedure

Introduce a 5-μl aliquot of solution into the carbon tube or cup furnace with an Autopette pipet fitted with an Eppendorff polypropylene tip; these tips are narrower at the dispensing end than those supplied with the pipet and fit better into the sample introduction orifice of the carbon tube. Use a depth guide to aid in depositing the droplet reproducibly in the same position within the carbon tube. The furnace is then automatically taken through the usual three temperature steps to dry, ash and atomize the sample.

Power supply voltage and time settings were adjusted for every furnace to give optimal performance; typical voltage setttings and durations for the drying, ashing and atomization steps were: 5 (0.9 V), 8 s; 8 (3.0 V), 5 s; and 10 (9 V), 1 s, respectively. The analytical signal was taken from the height of the peak recorded during the atomization step. Dry and ash step absorbances were also routinely recorded, and this pattern together with the behavior of the atomization peak was used to set voltage and time parameters. Sample runs were bracketted by those of the standard solution.

Atomization step absorbances, with both the selenium and hydrogen continuum lamps were determined for the sample, standard and reagent blank. Sample and standard absorbances were corrected for reagent blank and non-atomic absorption, and comparison of the net absorbances yielded the selenium content of the sample. Occasional decontamination firings were made to ensure that complete volatilization of analyte occurred during determination. An untreated selenium solution was incorporated into the set to monitor the behavior of the furnace and to provide a reference for calculating recoveries.

RESULTS AND DISCUSSION

Optimization of parameters

Instrumental parameters such as nitrogen gas flow rate, and monochromator slit height, once optimized were left undisturbed for all experiments. Other parameters such as monochromator slit width and selenium hollow-cathode lamp current were set at optimal values as determined by previous experimentation. Variation of nitrogen flow rate from 1 to 4 l min^{-1} had no significant effect on sensitivity; the flow rate of 4 l min^{-1} recommended by the manufacturer was used for both cup and tube furnaces. As the least damped mode of operation was required to permit faithful recording of the transient absorption responses, amplifier damping was set at A. The hydrogen

hollow-cathode lamp current was adjusted each time a non-atomic absorbance measurement was made, to match its intensity to that of the selenium hollow-cathode lamp fixed at 10 mA. Carbon furnace power supply settings for voltage and time of the drying, ashing and atomization steps could not be assumed to be identical for each cup or tube used. These six parameters were adjusted for each carbon furnace to give optimum absorbance behavior as described in the operating manual. They also depended somewhat on the nature of the solution being analyzed (particularly with digested, non-precipitated samples) and were optimized for each sample.

Performance of furnace

The pronounced characteristic of both cup and tube furnace performance was signal variability. Typical behavior of a carbon tube is depicted in Fig. 1 where the atomization step absorbance of a selenium standard solution is plotted as a function of firing number. With a new furnace, the absorbance changed substantially during the initial several dozen firings before settling down to a moderately erratic response superimposed on longer term variation over the remaining lifetime. A rapid fall-off of signal and/or physical deterioration of the furnace signalled the end of its usefulness. On average, some 30 firings, with as many introductions of standard solution to monitor behavior, were required for the furnace to behave; with a small number of tubes no indication of good behavior was evident even efter 100 firings and the tubes were discarded. The average lifetimes were approximately 150 and 300 firings for the cup and tube furnaces, respectively (cup experiments conducted

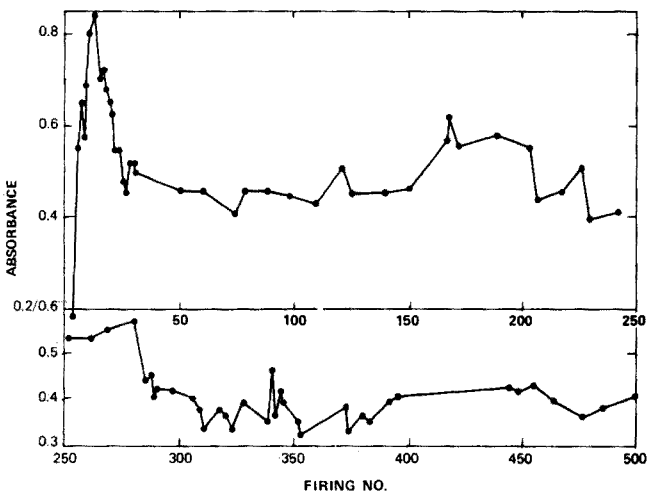

Fig. 1. Behavior of carbon tube. Atomization step absorbance is plotted as a function of firing number. 0.8 μg Se ml^{-1}; matrix 1.0 M perchloric acid, 0.5 M nitric acid and 5000 μg Ni ml^{-1}. New applications of 5 μl of solution were made before each firing depicted.

without nickel, data for tubes from experiments with nickel present) with a range from only several to over 500. Excluding the initial conditioning firings, the absorbance of a given solution measured in a given tube varied over a two-fold range throughout the life of the tube. Mean absorbances obtained with different tubes also exhibited a two-fold variation. Decontamination firing absorbances were constant, indicating that the observed variability did not arise from analyte memory effects, but rather was due to the inherent behavior of the furnace and perhaps the volatility of the analyte.

As the condition of the furnace deteriorated with firing, it was observed that the portions of the support electrodes adjacent to the tube also deteriorated, losing surface lustre and becoming thinner. Even though the electrodes could be used with more than one tube, a new pair of support electrodes was installed with each tube change in the hope that this would improve performance. It was also suspected that the position of the sample solution droplet within the tube, may have had an effect on the atomization rate and therefore on peak height [38]. An attempt was made to minimize possible uncertainty from this source by setting up a depth guide for the micropipet to locate the drop more reproducibly in the tube furnace; the micropipet tip then always came to rest in the same position and did not contact the wall. A side benefit of this procedure was that it obviated the problem of small carbon particles being picked up by the tip and deposited elsewhere within the tube causing partial blockage of the light path. Whether the use of this technique was of any consequence is uncertain. However, for selenium, the operation of this particular carbon furnace proved to be troublesome. Another problem of a minor nature was the short life span of the selenium hollow-cathode lamps, which lasted for 1/5 of the rated 5 A-hours when operated at 10 mA, a current below the maximum permissible, and 5 lamps were required during this project.

Response variability was a problem when quantitative results were desired. A standard calibration curve could not be used for reliable determinations, and bracketting of samples with standard solutions was resorted to as described above. Standard curve linearity, a preferred prerequisite for this procedure, was demonstrated for the concentration range of interest.

Interferences

Acid matrices. The behavior of selenium in several mineral acids was investigated to ascertain their suitability as bulk matrices for furnace atomization. Most of these studies were conducted with the carbon cup and solutions without nickel. Good response of the element dissolved in 0.5 M sulfuric acid contrasted with the very poor absorbance obtained after digestion of standards with nitric-perchloric-sulfuric acids ending up with solutions 0.5 M in sulfuric acid. This behavior was traced to the presence of traces of residual perchloric acid which depressed the signal; concentrations of 0.05—0.1 M completely suppressed it. Nitric and perchloric acids were

superior matrices, with the absorbances of standards being higher in mixtures of the two than in either acid alone. At constant nitric acid concentration (Fig. 2A), the absorbance increased with perchloric acid concentration to give a plateau over the range 0.2 to $\geqslant$ 1.4 M perchloric acid with a gradual decrease at high molarities (Fig. 2B). In solutions containing perchloric acid fixed at 0.5 M, the absorbance was optimum in the range 0.3—0.6 M nitric acid. Analogous detailed studies were not repeated for the tube and it cannot be stated whether this behavior was reproducible in that configuration. In the presence of 5000 μg Ni ml^{-1}, however, it appeared that in the tube, absorbances of standard solutions were similar in 0.5 M and 1.0 M nitric acid, 1.0 M perchloric acid and mixtures containing 1.0 M perchloric and 0.5 M nitric acids. The latter acid matrix was selected for the main analytical effort.

Three reports [22, 30, 31] on the determination of selenium with a graphite atomizer have mentioned acid effects. Baird et al. [22], using a Techtron CRA model 61 carbon rod atomizer, reported depression of peak height in the presence of perchloric acid, which was eliminated by the incorporation of nitric acid.

Sample matrices. Previous work in this laboratory [27] with a carbon cup and without nickel addition demonstrated a signal depression depending on the weight and type of the sample. Apparent recoveries of selenium added to various weights of potato and swordfish before nitric-perchloric acid digestion were 102—72 % and 85—37 % respectively, for sample concentrations of

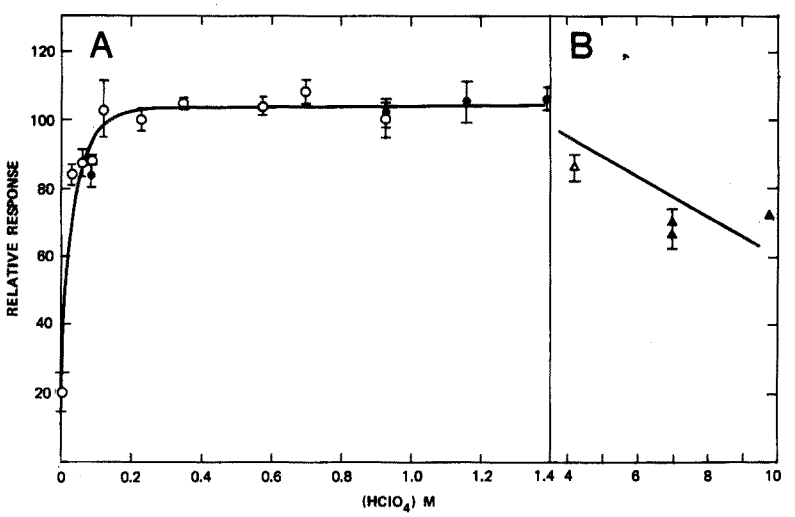

Fig. 2. Effect of perchloric acid on absorbance of selenium standard solution in carbon cup furnace without nickel. A: Nitric acid concentration constant at 1 M. B: Nitric acid concentration constant at 0.5 M. Data obtained with 4 different cups.

0.2—20 mg ml^{-1}. The relative recovery from flour at 20 mg ml^{-1}, however, was near 100 %. Inorganic matrix amounting to several percent of the above concentrations remaining after digestion of sample thus caused severe complications in the determination of selenium under the previous experimental conditions [27]. Little or no analyte signal was seen for the high (ca. 3 $\mu g\ g^{-1}$) native selenium levels present in swordfish.

Similar studies in the tube furnace, with swordfish and flour sample solutions in the absence of nickel, indicated either the absence of native selenium (known, by fluorimetric analysis, to be present) or very low contents with large attendant variabilities. A substantial improvement was realized when nickel at 5000 $\mu g\ ml^{-1}$ was added. The measured selenium contents of two flour samples agreed well with fluorimetrically determined levels, while levels in three different samples of swordfish, although much better, were still 1/3 lower than the corresponding fluorimetric data. An oat cereal sample and NBS standard liver sample taken through an identical treatment exhibited high non-atomic absorbances and were not amenable to analysis.

Matrix effects on analyte signals have been noticed by other workers with carbon furnace atomic absorption spectrometry and have been discussed [22, 30, 31, 39—41]. It appears that these interferences are common, at times severe and dependent on the nature of the furnace. Various mechanisms are responsible including the change in rate of atomization of the analyte in the presence of the sample matrix, and of the matrix contribution to non-atomic absorption by light scattering and broadband molecular absorption. As all analyte absorbance signals have been corrected for non-atomic absorbance, the latter factor is not responsible for the present results. An interesting comparison of the behavior of three carbon furnaces, Perkin-Elmer, Varian-Techtron and Woodriff, has been reported by Koirtyohann [39] who pointed out the dependence of performance on construction. Using a bone sample as the source of matrix material, he observed the Techtron furnace to show the most severe matrix effects, low non-atomic absorption and the highest absolute sensitivity; the Perkin-Elmer atomizer gave the highest precision but had severe non-atomic absorption, whereas the Woodriff furnace was relatively free from matrix and background problems.

Recovery of selenium

Recoveries, measured with the carbon tube in the presence of nickel, of 10 μg of selenium added as selenite to various weights of several food samples before digestion with nitric-perchloric acids, were independent of sample type and weight. The recoveries from 0.2 and 1.0 g of flour, and from 0.05, 0.2 and 1.0 g of potato and swordfish averaged 99 % (standard deviation, $s = 9$, degrees of freedom, $f = 7$) relative to a similarly treated standard solution. This behavior differs from the behavior of native selenium in swordfish mentioned above, and differs from the dependence of recovery on sample type and weight observed in early work with the carbon cup form

of the furnace and without added nickel. These data suggested that some sample matrices (remaining after digestion) impair the performance of this carbon furnace. It was felt that separation of the analyte from the sample matrix before the determination step would improve the performance of the method. Analyte isolation, accomplished by precipitation with ascorbic acid, is discussed later.

Effect of nickel

During this investigation, it was reported [24] that the incorporation of nickel into the analytical solutions improved the precision for selenium. Utilization of nickel decreases the volatility of selenium [24, 27, 29] by the formation of a higher boiling nickel selenide which behaves more reproducibly than the more volatile compounds of the element. Reduction by nickel oxide of SeO_2, formed by decomposition of selenite or selenate, to the less volatile element is another possibility. Henn [31] chose molybdenum to overcome the depressant effect of acid and sample matrix on selenium and stabilize it in the furnace, and speculated that the mode of action could be explained by selenide or heteropolymolybdate formation.

The effect of nickel was studied by conducting experiments with solutions to which nickel nitrate had been added (5000 μg Ni ml^{-1}) and comparing their behavior with samples containing no nickel. Repeated determinations in carbon tubes on standard solutions (in 1.0 M $HClO_4$ and 0.5 M HNO_3) in the absence of nickel gave a mean relative standard deviation (s_r) of 36 % (162 observations, 4 tubes) whereas the mean s_r for solutions with nickel was 15 % (531 observations, 9 tubes). An improvement by a factor of 2.4 was realized because of the stabilizing effect of nickel. These large standard deviations are in part due to taking absorbance readings during a long span of the life of a tube, so that long-term variations contributed. They serve for comparison of precision, but do not represent the precision attainable in actual analyses where interpolated standard absorbances are used to minimize effects of long-term variations.

The precision of the determination (carbon tube, 5000 μg Ni ml^{-1}) for digested samples containing native and added selenium is depicted in Fig. 3 as a function of the mean level of selenium found. When bracketting with standards is used, the s_r value drops to a respectable 7 % for selenium concentrations above ca. 0.5 μg ml^{-1}. The overall s_r for the combined digestion-precipitation-redigestion and determination steps was 4 % for NBS liver (1.0 μg g^{-1}), 9 % for halibut (2.9 μg g^{-1}) and 27 % for swordfish (2.6 μg g^{-1}). It was observed that once nickel was introduced into the carbon tube, traces lingered through subsequent firings influencing the behavior of selenium. To obviate such contamination problems, all experiments with a given tube were conducted first with nickel-free solutions.

Although standard calibration curves could not be used in the analytical scheme, a curve based on average absorbances could be constructed and

used to estimate sensitivity. Over the range 0—1.3 μg Se ml^{-1}, the data were represented by the equation $A_{NET} = 0.45c$ (536 determinations with 10 different carbon tubes, 1.0 M perchloric acid, 0.5 M nitric acid, 5000 μg Ni ml^{-1}) where A_{NET} is the net absorbance, and c is the concentration of selenium in μg ml^{-1}. No dependence of non-atomic absorbance on analyte level was observed with an average absorbance of 0.068 (s = 0.013, f = 135, 9 tubes).

A plot for standard solutions without nickel exhibited non-linearity and diminished sensitivity. Again, non-atomic absorbance was concentration-independent over the range 0—6.3 μg ml^{-1}, with a mean of 0.022 (s = 0.015, f = 44, 4 tubes). The average standard reagent blank absorbance for solutions with nickel was 0.072 (s = 0.020, s_r = 28 %, f = 79, 5 tubes) compared to 0.017 (s = 0.012, s_r = 67 %, f = 39, 4 tubes) in the absence of nickel, indicating a significant four-fold contribution of nickel to reagent blank readings. The respective blank and non-atomic absorbances were identical, suggesting that reagent blank absorbances are essentially non-atomic in nature. Nickel was also observed to contribute an ashing peak which was absent when pure standard solutions were run.

Sensitivities and detection limits for standard selenium solutions with or without nickel are compared in Table 1. Sensitivities were computed from the slopes of mean calibration curves discussed above, the limiting slope near zero concentration being used for the curvilinear behavior of standards without nickel. It can be seen that nickel improves both sensitivity and detection limit, the former by a factor of 3.4, the latter by a factor of 2. This enhancement of sensitivity compares with reported values of 1.88 [30], 1.86 [31] and ca. 3—6 [24]. Baseline peak-to-peak noise was 0.0025 absorb-

TABLE 1

Sensitivities and detection limits for selenium in carbon tube furnace[a]

	Solutions with 5000 μg Ni ml^{-1}	Solutions without Ni
Sensitivity (ng ml^{-1})[b]	10	34
Absolute sensitivity (ng)[c]	0.050	0.17
Detection limit (ng ml^{-1})[d]	90 (25)[e]	185
Absolute detection limit (ng)[c]	0.45 (0.13)[e]	0.93

[a]Based on untreated standard solutions and on pooled performance of several tubes (except e); all solutions contain 1.0 M perchloric acid, 0.5 M nitric acid and 5000 μg Ni ml^{-1}.
[b]Sensitivity defined as concentration of selenium giving a net absorbance (absorbance corrected for reagent blank and non-atomic absorbance readings) of 0.0044.
[c]Based on 5-μl injections.
[d]Detection limit defined as concentration of selenium giving a net absorbance equal to twice the standard deviation of blank readings.
[e]From analyses of samples containing native and added selenium; equal to concentration and weight of selenium which can be determined with a relative standard deviation of 50 %.

ance units corresponding to 6 ng ml^{-1} (0.030 ng per 5 μl) for solutions with nickel. This would indeed be a good value for the detection limit if detection limits were governed solely by baseline noise. Detection limits estimated from actual analyses of biological samples containing native and added selenium (acid digestion, measurement in carbon furnace, bracketting with standard) and nickel in the analytical solution, are also included in Table 1. These data are from a more realistic situation. A detection limit of 25 ng Se ml^{-1}, corresponding to an absolute detection limit of 0.13 ng, was obtained from the curve in Fig. 3. The detection limits determined in this study are comparable to or somewhat larger than those reported [21, 22, 24, 26, 30, 31], or determined earlier with a carbon cup (27), or the 20 ng ml^{-1} and 0.10 ng specified by Varian Techtron.

Isolation of selenium from sample matrices

Of the various methods described in the literature for isolating selenium from sample matrices, or for its determination, precipitation with ascorbic acid is often favored [42—48], and was chosen for the present work. It was thought that this procedure would be advantageous in providing a clean solution containing selenium with only possible traces of other coprecipitated or adsorbed elements and a small but constant contribution of trace

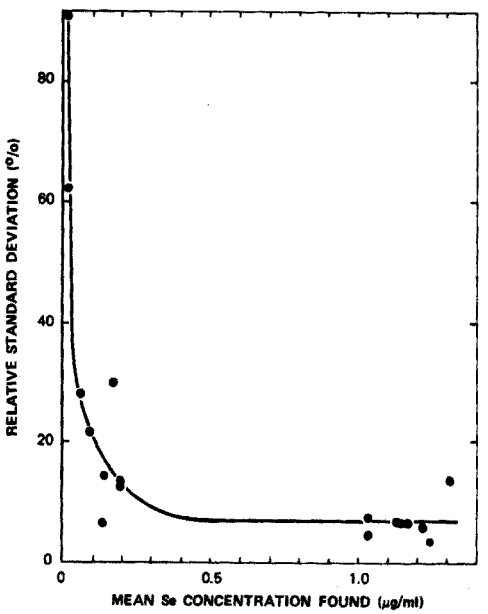

Fig. 3. Precision of determination step in the analysis of digested samples. Samples of potato, flour and swordfish containing native and added selenium were digested with nitric and perchloric acids. Final solutions containing 1 M perchloric acid, 0.5 M nitric acid and 5000 μg Ni ml^{-1} were each analyzed 6 times with a carbon tube.

elements from the digested membrane filter, in an acid matrix of known composition. Ascorbic acid was effective in reducing the selenium species in solution to red elemental selenium. The matrix removal simplified the dry and ash absorbance pattern and enhanced the selenium atomization signal [27].

In early work when nitric and perchloric acids were used for sample digestion, and precipitation was effected from a perchloric acid medium [46, 47], low and erratic recoveries were obtained. This was due to incomplete volatilization of nitric acid from the solution; traces of the order of 10^{-3} M were found to reduce substantially the precipitation yield of selenium. To obviate this problem, the earlier procedure [27] specified heating the digest to perchloric acid fumes to ensure that all nitric acid was boiled off. For most of the work reported here, selenium was precipitated from the sulfuric acid medium resulting from digestion with nitric-perchloric-sulfuric acids [2a]; this had the advantages of providing a nitric acid-free acid medium, and of converting the selenium in the sample to selenite which is more easily reduced than selenate. This digestion procedure had previously been shown [2a, b] to retain selenium quantitatively.

Several aspects of the precipitation were investigated to optimize selenium recovery; both carbon furnace a.a.s. and fluorimetry were used for monitoring purposes. The efficiencies of 0.2 and 0.8-μm membrane filters were assessed by precipitating the analyte from standard solutions containing sulfuric acid, filtering through a 0.8-μm filter and passing the filtrate through a 0.2-μm filter. Based on the initial 300—3000 ng of selenium taken, it appeared that 3 % (number of determinations, n = 9, fluorimetry) of the precipitate passed through the 0.8-μm filter and was retained by the 0.2-μm filter, while an additional 3 % of the selenium was recovered in the second filtrate passing through 0.2-μm. The performance of both filters was thus fairly equivalent; the 0.2-μm type was used for most sample analyses, whereas many of the other studies were carried out with 0.8-μm filters. When precipitation was carried out from 9 M sulfuric acid, the solution was diluted before filtration to prevent acid attack on the filter.

Precipitation from 9 M sulfuric acid of 100—3000 ng of selenium effected by 0.5—2.0 g of ascorbic acid over a time of 0.5—16 h gave an average recovery of 89.7 % (s = 9.3, f = 45, 0.8-μm filter, fluorimetry). With 20 ng of selenium, the recovery was lower (76 %) with higher variability (s = 34, f = 7). To enhance the reliability of fluorescence readings at this low level, 5 separately precipitated 20-ng samples were filtered through one membrane filter which was then digested and analyzed; the 8 determinations in the above average thus include 40 separate precipitations. Recoveries from several determinations of 200—3000 ng of selenium with a carbon furnace, (precipitation from sulfuric acid, 0.2-μm filter, determination in nitric-perchloric-nickel medium) gave a mean of 99.0 % (s = 10.3, f = 8).

Data accumulated during earlier studies with perchloric acid [27] at levels of 100—30000 ng of selenium gave a precipitation recovery averaging 85.8 % (s = 17.8, f = 73, collection on 0.8-μm filters, determinations with carbon

cup in nitric-perchloric matrix without nickel). This result, obtained with nitric-perchloric digested standard solutions, agrees closely with the value of 89.7 % observed for a sulfuric acid medium. Additional experiments indicated that heating the nitric-perchloric digests of standards with hydrochloric acid [49] before precipitation, to reduce selenium to Se(IV) increased recoveries. For 7 pairs of standard solutions containing 1—5.5 μg of selenium, the mean recoveries were 67.0 % (s = 12.7, f = 6) without the HCl treatment, and 83.2 % (s = 11.6, f = 6) with it. These recoveries are significantly different (t test, p = 0.05) and suggest that oxidation occurs during nitric-perchloric digestion. For this reason and the superior recoveries reported from a sulfuric acid medium, the nitric-perchloric-sulfuric digestion mixture with a final hydrogen peroxide treatment was preferred.

Analysis of samples including selenium isolation

An example of a typical determination sequence and absorbance behavior during the 3 heating stages is presented in Fig. 4. The selenium standard and

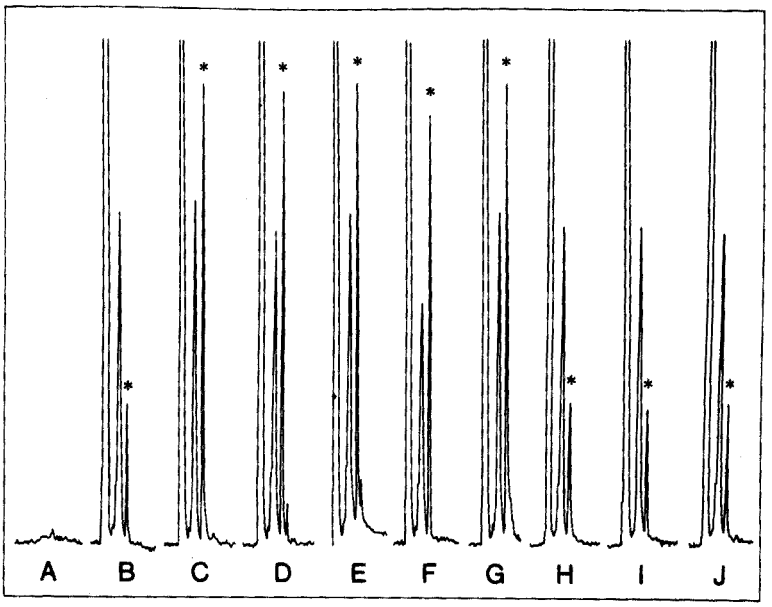

Fig. 4. Example of determination sequence and absorbances at the three heating stages of a carbon tube. A: decontamination; B and H reagent blank; C, G and I, Se standard solution containing 0.333 μg Se ml^{-1}; D—F and J, NBS liver sample solution containing 0.333 g of sample per ml. Absorbances for firings A—G were measured with a selenium hollow-cathode lamp; H—J were measured with a hydrogen continuum lamp. Identical procedures of digestion-precipitation-redigestion were followed for all solutions. The matrix was 1 M perchloric acid, 0.5 M nitric acid and 5000 μg Ni ml^{-1} for all solutions. The three major absorbance peaks are associated with, L to R, drying, ashing and atomization steps, the latter peaks being indicated by asterisks.

reagent blanks were taken through the same procedure as the sample and all determinations were with a carbon tube, on solutions containing nickel.

Natural levels of selenium in a variety of biological samples determined in the early stages of the work with a carbon cup (no nickel), were on average 0.85 as large as those obtained by fluorimetry [27]. More recent analyses by the procedure described here (determination with carbon tube on solutions containing nickel) of halibut, swordfish, NBS liver, flour, oat cereal, and round steak containing 0.2—3 μg Se g^{-1} are summarized in Table 2. Levels determined by fluorimetry are included for comparison. In general, the sample concentrations determined by carbon furnace atomic absorption spectrometry agree well with those measured by fluorimetry, suggesting that the carbon furnace technique can provide acceptable data. The excellent agreement of the level of 1.00 μg g^{-1} for the NBS liver sample obtained with the carbon furnace, with 1.04 μg g^{-1} calculated from the provisionally certified NBS value obtained by neutron activation analysis and spark-source mass spectrometry is encouraging. The swordfish sample exhibited the poorest performance having a difference of −23% and a large relative standard deviation of 27 %. The average deviation from the fluorimetrically determined levels including all samples, was −8%.

Pronounced sample matrix interferences limit the usefulness of this particular type of carbon furnace in the direct determination of selenium in

TABLE 2

Levels of selenium in biological samples determined by carbon tube furnace atomization with prior separation of selenium[a]

Sample	Selenium content μg g^{-1}							
	Carbon furnace				Fluorimetry			
	Mean	n[b]	s	$s_{\bar{x}}$	Mean	n	s	$s_{\bar{x}}$
Halibut	2.90	3	0.27	0.16	2.83[c]	17	0.29	0.07
Swordfish	2.64	5	0.72	0.32	3.44	3	0.28	0.16
NBS Liver (SRM 1577)	1.00	3	0.04	0.02	1.04[d]	—	—	—
Flour	0.76	2	(0.76, 0.75)[e]		0.72[c]	16	0.05	0.01
Oat cereal	0.36	2	(0.35, 0.38)[e]		0.40[c]	17	0.05	0.01
Round steak	0.20	2	(0.22, 0.18)[e]		0.24[c]	17	0.04	0.01

[a]Sample (1 g) digested with nitric-perchloric-sulfuric acids, Se precipitated with ascorbic acid and redigested with nitric-perchloric acids. Analytical solutions contain 1.0 M perchloric acid, 0.5 M nitric acid and 5000 μg Ni ml^{-1}.

[b]n denotes the number of analyses; s is the standard deviation; $s_{\bar{x}}$ is the standard error of the mean.

[c]Data from interlaboratory study (2b); n denotes number of laboratories.

[d]Provisionally certified NBS value corrected for moisture content; determination by neutron activation analysis and spark-source mass spectrometry.

[e]Individual values.

biological sample digests. More success, however, is realized with prior separation of selenium from interfering matrices, and the inclusion of this step enhances considerably the potential of the method. The detection limit, on a sample basis, is similar to the detection limits obtained by fluorimetry and selenide generation-flame atomic absorption spectrometry. Processing a 1-g sample to give the selenium content in 1 ml of solution leads to a sample detection limit of 25 ng g^{-1} based on the analytical solution detection limit of 25 ng ml^{-1}. Hydrogen selenide generation procedures require 20—50 ml of solution; if such a solution contains 1 g of sample, the detection limit on a sample basis, lies the range of 2—50 ng g^{-1} based on the solution detection limit of 0.1—1 ng ml^{-1}. Fluorimetry can detect 10 ng of selenium in a 1-g sample. Thus, the present carbon furnace technique exhibited a detection limit similar to that obtainable with other sensitive techniques. The small solution volume requirements of the carbon furnace method suggest that sample detection limits can be reduced by concentrating the analyte into volumes similar to those required for the determination step. A volume of 0.1 ml would suffice for 19 replicate determinations on 5-μl aliquots. The isolation of selenium by precipitation is convenient, but its efficacy at very low levels requires further study. The solution of these points coupled with improvement of precision and reliability should make the determination of selenium at the p.p.b. level a reality.

The author is indebted to Robert J. Westerby for his invaluable technical assistance and perseverance in the solution of experimental difficulties

REFERENCES

1 O. E. Olson, J. Ass. Offic. Anal. Chem., 52 (1969) 627.
2 a. M. Ihnat, J. Ass. Offic. Anal. Chem., 57 (1974) 368.
b. M. Ihnat, J. Ass. Offic. Anal. Chem., 57 (1974) 373.
3 Official Methods of Analysis, 12th edn., A.O.A.C. Washington, D.C., 1975, Sect. 3.074—3.078; 25.117—25.120.
4 W. Slavin, S. Sprague and D. C. Manning, At. Absorption Newslett., 3 (1964) 1.
5 R. M. Dagnall, K. C. Thompson and T. S. West, At. Absorption Newslett., 6 (1967) 117.
6 H. L. Kahn and J. E. Schallis, At. Absorption Newslett., 7 (1968) 5.
7 C. L. Chakrabarti, Anal. Chim. Acta, 42 (1968) 379.
8 G. F. Kirkbright, M. Sargent and T. S. West, At. Absorption Newslett., 8 (1969) 34.
9 P. Johns, Spectrovision, 24 (1970) 6.
10 G. F. Kirkbright and L. Ranson, Anal. Chem., 43 (1971) 1238.
11 B. C. Severne and R. R. Brooks, Anal. Chim. Acta, 58 (1972) 216.
12 B. C. Severne and R. R. Brooks, Talanta, 19 (1972) 1467.
13 S. Ng, M. Munroe and W. McSharry, J. Ass. Offic. Anal. Chem., 57 (1974) 1260.
14 F. J. Fernandez and D. C. Manning, At. Absorption Newslett., 10 (1971) 86.
15 D. C. Manning, At. Absorption Newslett., 10 (1971) 123.
16 Y. Yamamoto, T. Kumamaru, Y. Hayashi and M. Kanke, Anal. Lett., 5 (1972) 717.
17 F. J. Schmidt and J. L. Royer, Anal. Lett., 6 (1973) 17.

18 J. Y. Hwang, P. A. Ullucci, C. J. Mokeler and S. B. Smith, Jr., Amer. Lab., 5 (1973) 43.
19 P. D. Goulden and P. Brooksbank, Anal. Chem., 46 (1974) 1431.
20 D. D. Siemer and L. Hageman, Paper presented at the First National Meeting of the Federation of Analytical Chemistry and Spectroscopy Societies, Nov., 1974, Atlantic City, N.J.
21 J. P. Matousek, Amer. Lab., 3 (1971) 45.
22 R. B. Baird, S. Pourian and S. M. Gabrielian, Anal. Chem., 44 (1972) 1887.
23 G. F.Kirkbright, Paper 1A, Eastern Analytical Symposium, Nov., 1973, New York, N.Y.
24 R. D. Ediger, S. Slavin and F. J. Fernandez, Paper 1D, cf. ref. 23.
25 D. P. Sandoz, C. Parker, B. Culver and J. Sanders, Paper 1E, cf. ref. 23.
26 R. B. Baird and S. M. Gabrielian, Appl. Spectrosc., 28 (1974) 273.
27 M. Ihnat and R. J. Westerby, Anal. Lett., 7 (1974) 257.
28 W. B. Barnett, Paper presented, at cf. ref. 20.
29 R. D. Ediger, Paper presented, cf. ref. 20.
30 G. G. Welcher, O. H. Kriege and J. Y. Marks, Anal. Chem., 46 (1974) 1227.
31 E. L. Henn, Anal. Chem., 47 (1975) 428.
32 S. Slavin, G. E. Peterson and P. C. Lindahl, Paper 40, Pittsburgh Conference, March, 1975, Cleveland, Ohio.
33 H. Massmann, Spectrochim. Acta, Part B, 23 (1968) 215.
34 M. D. Amos, Amer. Lab., 4 (1972) 57.
35 J. P. Matousek and K. G. Brodie, Anal. Chem., 45 (1973) 1606.
36 C. R. Parker, J. Rowe and D. P. Sandoz, Amer. Lab., 5 (1973) 53.
37 B. R. Culver, J. F. Lech and N. K. Prodhan, Food Technol., 29 (1975) 16.
38 J. F. Chapman, L. S. Dale and J. W. Kelly, Anal. Chim. Acta, 69 (1974) 207.
39 S. R. Koirtyohann, Paper presented at the Fourth International Conference on Atomic Spectroscopy, Oct. 29—Nov. 2, 1973, Toronto, Ontario.
40 R. B. Cruz and J. C. Van Loon, Anal. Chim. Acta, 72 (1974) 231.
41 R. Woodriff, Appl. Spectrosc., 28 (1974) 413.
42 M. N. Rudra and S. Rudra, Current Sci., 21 (1952) 229.
43 V. Simon and V. Grim, Chem. Listy, 48 (1954) 1774.
44 D. N. Fogg and N. T. Wilkinson, Analyst (London), 81 (1956) 525.
45 L. M. Cummins, J. L. Martin, G. W. Maag and D. D. Maag, Anal. Chem., 36 (1964) 382.
46 C. L. Newberry and G. D. Christian, J. Ass. Offic. Anal. Chem., 48 (1965) 322.
47 G. D. Christian, E. C. Knoblock and W. C. Purdy, J. Ass. Offic. Anal. Chem., 48 (1965) 877.
48 R. Ripan and G. Tautu, Stud. Univ. Babes-Bolyai, Ser. Chem., 17 (1972) 59. Chem. Absts. 78 (1973) 105665j.
49 J. H. Watkinson, Anal. Chem., 38 (1966) 92.

Analytica Chimica Acta, 82 (1976) 311—320
©Elsevier Scientific Publishing Company, Amsterdam — Printed in The Netherlands

THE DETERMINATION OF BERYLLIUM IN GEOLOGICAL AND INDUSTRIAL MATERIALS BY ATOMIC-ABSORPTION SPECTROMETRY AFTER CATION-EXCHANGE SEPARATION

J. KORKISCH and A. SORIO

Institute for Analytical Chemistry, Analysis of Nuclear Raw Materials Division, University of Vienna, Währingerstrasse 38, A-1090 Vienna (Austria)

(Received 26th September 1975)

SUMMARY

A method is described for the determination of beryllium in geological and industrial samples. After dissolution of the sample in mineral acids, beryllium is separated from the matrix elements by chloroform extraction of its acetylacetonate from a solution of pH 7 containing ascorbic acid and EDTA. Beryllium is separated from the organic extract and from co-extracted aluminium by means of a column of the strongly acidic cation-exchanger Dowex 50; beryllium is adsorbed from a medium consisting of 60 % (v/v) tetrahydrofuran, 30 % (v/v) chloroform and 10 % (v/v) methanol containing hydrochloric acid, aluminium is removed with 0.4 M oxalic acid and after elution with 6 M hydrochloric acid, beryllium is determined by atomic-absorption spectrometry with a nitrous oxide-acetylene flame. The method was used to determine p.p.m. and sub-p.p.m. quantities of beryllium in geochemical reference materials, U_3O_8 and yellow cake samples, and manganese nodules.

Determinations of p.p.m. and sub-p.p.m. quantities of beryllium in geological materials are gaining increased importance with respect to studies directed towards measuring the degree of pollution of the environment by this toxic element. Also of significance are determinations of beryllium in secondary nuclear raw materials, such as samples of yellow cake and uranium oxides, because of the neutron-absorbing properties displayed by this element.

The methods most frequently used for the assay of beryllium in both geological and industrial materials are based on the chloroform extraction of beryllium acetylacetonate followed by spectrophotometry or fluorimetry [1]. Atomic-absorption spectrometry can also be used to determine very small amounts of beryllium, and this technique can be combined successfully with the chloroform extraction of beryllium acetylacetonate and the isolation of beryllium, directly from the organic extract, by cation-exchange. A description of this method is presented in the present paper.

EXPERIMENTAL

Solutions and reagents

Ion-exchange resin. The strongly acidic cation-exchanger Dowex 50-X8 (100-200 mesh H^+-form) was used. Slurry the resin (4 g) with a few ml of the THF—$CHCl_3$—methanol—HCl-mixture (see below) and after 30 min, pour into an ion-exchange column filled with the same mixture. Subsequently wash the resin bed with 20 ml of the mixture (pre-treatment of the resin).

Standard beryllium solutions. Dissolve an exactly weighed amount of beryllium nitrate tetrahydrate in 1 M nitric acid to obtain a stock solution containing 630 p.p.m. of beryllium. From this solution prepare standard solutions in 0.1 M nitric acid and 0.6 M hydrochloric acid containing from 0.063 to 630 p.p.m. of beryllium.

THF—$CHCl_3$—methanol—HCl-mixture. Prepare this mixture (of overall acidity 0.1 M) by mixing 60 ml of tetrahydrofuran, 30 ml of chloroform and 10 ml of methanol—HCl-mixture (of overall acidity 1.0 M; see below).

Methanol—HCl-mixture. Dilute 83 ml of 12 M hydrochloric acid with methanol to 1 l. The overall acidity of the resulting solution is 1.0 M. To obtain the mixture of overall acidity 0.1 M used to wash the resin bed during the ion-exchange separation of beryllium (see later), dilute 10 ml of this solution with methanol to 100 ml.

THF—methanol—HCl-mixture. This mixture (of overall acidity 0.1 M) consists of 90 % (v/v) tetrahydrofuran and 10 % (v/v) methanol—HCl-mixture (of overall acidity 1.0 M).

Other reagents. Acetylacetone (undiluted), chloroform, solid ascorbic acid, solid EDTA (disodium salt), solid *ortho*-boric acid, aqueous 25 % (w/v) sodium hydroxide and 0.4 M aqueous oxalic acid were used as well as dilute and concentrated solutions of hydrochloric, hydrofluoric, nitric, and perchloric acids.

Apparatus and operating conditions

A Perkin—Elmer atomic-absorption spectrophotometer 303 (equipped with a Hitachi Perkin—Elmer Recorder 56 connected to a read-out accessory) was used with the following instrumental settings:

Grating	Ultraviolet
Wavelength	234.9 nm
Scale expansion	Up to 30X
Slit	5 (3 mm; 2 nm spectral bandpass)
Source	Beryllium hollow cathode lamp
Lamp current	30 mA
Burner	One-slit burner for the acetylene-N_2O-flame
Acetylene pressure	8 psig; 14 on flowmeter (arbitrary scale)
N_2O pressure	30 psig; 6 on flowmeter (arbitrary scale)
Noise suppression	Up to 5

When the measurements were carried out in 0.6 M hydrochloric acid, the sensitivity was 0.015 p.p.m. of beryllium for 1 % absorption.

The separations of beryllium were performed in ion-exchange columns of the type and dimensions described earlier [2].

The Teflon "bombs" (Perkin—Elmer Corporation) used for the dissolution of samples are cylindrical, thick-walled Teflon containers, of about 50 ml capacity, equipped with Teflon screwcaps.

Determination of distribution coefficients

The weight distribution coefficients (K_d values) of beryllium and other elements were determined by the batch- and column methods [1].

Procedure

Dissolution of samples. Transfer 0.5—2 g of the sample to a Teflon "bomb" and add, for each gram of sample, 1 ml of water, 10 ml of 40 % hydrofluoric acid and 5 ml of 72 % perchloric acid. Close the screwcap tightly and heat the bomb for 24 h at 110 °C in an oven. Allow to cool to room temperature, open the bomb, and transfer its contents to a platinum dish; use 5 ml of 40 % hydrofluoric acid as a rinse. Evaporate the solution on a steam-bath until hydrofluoric acid is removed, add 10 ml of perchloric acid, and evaporate to dryness on a sand bath. Dissolve the residue in 10 ml of 12 M hydrochloric acid and evaporate to dryness on the steam-bath. Repeat the latter treatment with the same volume of hydrochloric acid. Finally take up the residue in 6 M hydrochloric acid, allow to stand overnight, filter off any insoluble residue, rinse it with 6 M hydrochloric acid and dilute the filtrate with the same acid to 25, 50 or 100 ml.

This dissolution procedure was used for the geochemical reference samples from the Centre de Recherches Pétrographiques et Géochimiques, National Institute for Metallurgy, Johannesburg, and Geological Survey of Canada.

To dissolve the U_3O_8-samples from the National Institute for Metallurgy, use the same procedure including the evaporation step on the sand-bath in

the presence of 10 ml of 72 % perchloric acid. Then dissolve the residue in 10 ml of 16 M nitric acid and evaporate to dryness on the steam-bath. Repeat this treatment using the same volume of nitric acid. Finally take up the residue in 6 M nitric acid and treat the solution exactly as described above for the geochemical reference samples, except that 6 M nitric acid is used in place of 6 M hydrochloric acid.

To dissolve the sodium diuranates (yellow cake samples), treat 0.5—2 g of the sample with 2 ml of water and 15 ml of each of concentrated nitric and hydrofluoric acids. Evaporate the mixture on a steam-bath, add to the residue 10 ml of concentrated nitric acid and about 0.5 g of boric acid, and evaporate to dryness on the steam-bath. Take up the residue in 6 M hydrochloric acid, filter, and dilute the filtrate with 6 M hydrochloric acid to 25 or 50 ml.

The diuranates, and samples of manganese nodules, can also be dissolved with hydrochloric acid only. Add 50 ml of 12 M hydrochloric acid to 0.5—2 g of the sample, and, after heating on the steam-bath for about 3 h, evaporate the solution to dryness under an IR lamp, dissolve the residue in 10 ml of 12 M hydrochloric acid, and again evaporate to dryness. Finally take up the residue in 10 ml of 6 M hydrochloric acid, allow to stand overnight, filter, and dilute the filtrate with 6 M hydrochloric acid to 25 or 50 ml.

Solvent extraction of beryllium. Dilute a suitable aliquot of the 6 M hydrochloric acid or 6 M nitric acid solution of the sample (see above) with water to about 350 ml, add 3 g of ascorbic acid and 5 g of EDTA, and shake until these reagents are dissolved completely. Carefully add aqueous 25 % sodium hydroxide solution until a pH of about 7 is obtained, add 5 ml of acetylacetone, and readjust the pH to 7. Shake the mixture for about 5 h, allow to stand overnight, and transfer to a 2-l separatory funnel. Extract beryllium acetylacetonate by shaking first for 1 min with 20 ml of chloroform and then, after separation of the organic extract, by shaking for 30 s each time with two 8-ml portions of chloroform. Combine all chloroform extracts (about 30 ml) and mix with 60 ml of tetrahydrofuran and 10 ml of methanol—HCl-mixture (overall acidity 1.0 M) to obtain the sorption solution.

Ion-exchange separation of beryllium. Pass the sorption solution (see above) through an ion-exchange column containing 4 g of the cation-exchanger (pretreated with 20 ml of the THF—$CHCl_3$—methanol—HCl-mixture) at a flow-rate which corresponds to the back-pressure of the resin bed (about 0.75 ml min^{-1}). Afterwards, wash the resin bed with 5 ml of the THF—methanol—HCl-mixture and then with 10 ml of the methanol—HCl-mixture (of overall acidity 0.1 M). Remove residual organic solvents by washing with 5 ml of 0.1 M hydrochloric acid and then elute co-adsorbed aluminium with 100 ml of 0.4 M oxalic acid. Subsequently wash the resin bed with 10 ml of 0.1 M hydrochloric acid and elute beryllium with 50 ml of 6 M hydrochloric acid (beryllium eluate).

Determination of beryllium. Evaporate the beryllium eluate (see above) under an IR lamp, dissolve the residue (not completely dry) in 0.6 M hydrochloric acid and transfer to a 10-ml measuring flask; use 0.6 M hydrochloric acid both as a rinse and to adjust the volume of the solution to 10 ml. Subsequently aspirate the solution into the acetylene-N_2O flame. Construct a calibration curve by aspirating suitable beryllium standard solutions (prepared in exactly the same way as the samples) before and after each batch of samples. In the determination of very small quantities of beryllium (less than about 0.1 p.p.m.), run a reagent blank through the whole procedure (starting with the dissolution of the sample).

RESULTS AND DISCUSSION

Extraction of beryllium

The chloroform extraction of beryllium acetylacetonate is carried out in the presence of EDTA in order to prevent, to a large extent, the co-extraction of most major and trace constituents of both geological and industrial materials [1]. This was found, however, to give relatively low beryllium recoveries in the presence of large amounts of iron, aluminium, titanium and uranium which, on neutralization of the sample solutions with sodium hydroxide, gave rise to precipitates even in the presence of excess of EDTA. Adsorption on or co-precipitation [1] with these precipitates explains why often only a small fraction of the beryllium was recovered.

Beryllium recoveries in the range 95—100 % can be achieved, however, if ascorbic acid is added to the solution to be extracted. This acid either reduces or forms complexes with iron, titanium, uranium and other elements thus preventing their precipitation as hydroxides when the sample solution is neutralized to pH 7. The addition of citric or oxalic acid in place of ascorbic acid proved to be much less effective.

Low beryllium recoveries (less than 75 %) were also obtained when beryllium acetylacetonate was extracted with chloroform immediately after readjustment of the pH which follows the addition of acetylacetone. Beryllium recoveries of 95—100 % were obtained consistently, however, if the beryllium was left in contact with acetylacetone first for 5 h (shaking period) and then for about 10—12 h (overnight standing period).

After this extraction of beryllium acetylacetonate the chloroform extracts contained large amounts of co-extracted aluminium and iron (about 25 % and 10 %, respectively, of the total amounts originally present in the sample solutions). Of these two elements aluminium interferes with the atomic-absorption determination of beryllium, and so does chloroform. Attempts to remove chloroform by evaporation led, through the volatility of beryllium acetylacetonate, to considerable losses of beryllium (especially when sub-microgram amounts were present) even when the evaporation was carried out at low heat and in the presence of concentrated mineral acids. The

interference by aluminium increased with increasing aluminium concentration. Thus, in the presence of 1, 2, and 3 mg of aluminium per 1 ml of 0.6 M hydrochloric acid, the readings of beryllium absorption (0.063 μg of Be ml^{-1}) were lower by 8, 15 and 17 %, respectively. At aluminium concentrations below 1 mg ml^{-1} the interference was negligible.

Cation-exchange separation of beryllium

For the reasons mentioned above, experiments were carried out to separate beryllium from both the co-extracted aluminium and the chloroform. As a result, the cation-exchange method utilizing adsorption of beryllium on Dowex 50 from the mixed tetrahydrofuran—chloroform—methanol medium containing hydrochloric acid was developed. In this mixture the presence of tetrahydrofuran is necessary to obtain a homogeneous solution while methanol is the component regulating the flow-rate through the ion-exchange column. In the absence of methanol the viscosity of the sorption solution is extremely low so that a flow-rate is attained at which complete adsorption of beryllium is not guaranteed. Hydrochloric acid must be present so that beryllium is in the ionic form which is adsorbed on the cation exchanger together with co-extracted aluminium and iron(II).

From the results of determinations of distribution coefficients and elution characteristics of beryllium and of other elements it is evident (see Table 1) that a simple separation of beryllium from the co-adsorbed aluminium cannot be achieved in this medium because of the closeness of the distribution coefficients of these two elements. Therefore, during the treatment of the resin column with the THF—methanol—HCl and methanol—HCl solutions, the chloroform which interferes with the a.a.s. determination of beryllium is removed. Acetylacetone is also eliminated completely; it is co-extracted simultaneously with beryllium, aluminium and iron and, if present in the

TABLE 1

Distribution coefficients of beryllium and other elements in the $CHCl_3$—THF—methanol—HCl-mixture (1 g Dowex 50; 1 mg load)[a]

Metal ion	BTV	K_d	EV	Metal ion[b]	BTV	K_d	EV
Be(II)		1650		Cu(II)	(1)	2	(10)
Al(III)		900		Zn(II)	(1)	2	(10)
Mg(II)		880		Cr(III)	(1)	2	(30)
Ca(II)		120		Co(II)	(2)	3	(50)
Fe(III)[b]	(1)	2	(5)	Ni(II)	(3)	5	(100)
UO_2(II)[b]	(1)	2	(20)	Mn(II)	(10)	20	(100)

[a]BTV = Breakthrough volume (ml); K_d = Distribution coefficient; EV = Elution volume (ml).
[b]The column method [1] was used to determine the distribution coefficients of these metal ions. The experiments were carried out on 1-g columns of the resin.

beryllium eluate, may give rise to low beryllium recoveries, because of the volatility of beryllium acetylacetonate.

For the separation of beryllium from co-adsorbed aluminium and iron(II) (iron(III) as well as other elements that readily form anionic chloride complexes such as UO_2(II), Cu(II) and Zn(II) pass into the effluent during the sorption process; see Table 1), 4 M oxalic acid proved to be a very effective eluant. Thus, on washing the resin column with 100 ml of this eluant, about 99 % of the adsorbed aluminium (when 50 mg were present) is removed from the resin, so that in practically all cases the aluminium content of the 6 M hydrochloric acid—beryllium eluate is very low. Consequently in the 10 ml of 0.6 M hydrochloric acid in which beryllium is determined after evaporation of the eluate, the aluminium concentration is always below 1 mg ml^{-1}, so that it will not interfere with the determination of beryllium by a.a.s. This also occurs when 1-g samples of materials of high aluminium content (10% or higher) such as bauxites are analysed, but experiments showed that beryllium recoveries are below 95 % when beryllium is extracted from solutions of such samples. This is because the large amounts of aluminium present compete with the beryllium for the acetylacetone chelating agent so that reaction and extraction are incomplete even after the many hours of shaking and standing time allowed. Thus, beryllium recoveries of 93, 90 and 88 % were obtained in the presence of 100, 200 and 300 mg of aluminium, respectively.

The passage of 0.1 M hydrochloric acid through the resin bed before and after the elution of aluminium serves to remove residual amounts of methanol and oxalic acid. The latter may cause interferences on evaporation of the beryllium eluate.

Application to geological and technical materials

Investigations of the influence of the beryllium concentration (in the range 0.063—63 μg of beryllium) on the recovery of beryllium from solutions containing concentrations similar to those encountered in geological and technical samples of similar composition (listed in Table 2) showed that beryllium recovery was always in the range 95—100 %.

Good results were also obtained when the described procedure was applied to the analysis of geochemical reference samples (compare the results shown in columns B and C with those of column D in Table 2). When the results in columns B and C are compared, it is also evident that the added amounts of beryllium were recovered quantitatively in practically all cases. Table 2 also shows that the results obtained by direct a.a.s. determination of beryllium (see column A) are much lower in virtually all cases than those obtained after application of the combined solvent-extraction—ion-exchange separations of beryllium described in the procedure. Thus, the presence of the matrix elements causes a considerable depression of the beryllium absorption, which appears to be caused to a large extent by the presence of aluminium; the

TABLE 2

Results of beryllium determinations in geochemical reference samples and in U_3O_8 samples

A = Results obtained by direct a.a.s. determination of beryllium in samples after dissolution in hydrofluoric-perchloric acids, unless otherwise noted.
B = Results obtained by a.a.s. determination of beryllium after extraction and cation-exchange from samples dissolved in hydrofluoric-perchloric acids.
C = Same as B, but after deduction of known amounts of beryllium added to the samples before their dissolution. The number in parentheses shows the amount of beryllium (in μg) which was added.
D = Results or ranges obtained in other laboratories, and given by the supplier (see footnotes).

Sample	p.p.m. Beryllium			
	A	B	C	D
Granite GA[a]	2.48	3.40	3.65 (3.15)	4
Granite GH[a]	3.45	5.10	5.50 (6.30)	6
Basalt BR[a]	1.20	1.35	1.09 (1.26)	1
Biotite mica—Fe[a]	4.70	7.95	8.10 (6.30)	10
Phlogopite mica—Mg[a]	0.21	0.28	0.40 (0.63)	—
Diorite DR—N[a]	1.20	1.60	1.80 (1.26)	<3; 2; 3; 5
Serpentine UB—N[a]	0.098	0.12	0.10 (0.63)	<1; 3; 3
Bauxite BX—N[a]	5.10	6.75	6.30 (6.30)	<3; 7
Disthène DT—N[a]	0.57	0.75	0.70 (0.63)	<2; <3
MRG-1[b, c] (Gabbro)	0.38	0.50	0.55 (0.63)	<2
SY-2[b, c] (Syenite rock)	10.25	10.70	10.45(12.6)	16—29
SY-3[b, c] (Syenite rock)	10.20	11.60	11.85(12.6)	16—31
NIM-D (Dunite)[d]	0.41	0.40	0.45 (0.63)	<1; <3 (<3)[e]
NIM-G (Granite)[d]	3.96	5.80	6.20 (6.30)	<8; 13.5 (10)[e] 1; 6; 10
NIM-L (Lujavrite)[d]	13.85	18.00	16.95(18.9)	<8; 20; 2; (20)[e] 31; 14
NIM-N (Norite)[d]	0.63	0.85	0.92 (0.63)	<1; 1; (<3)[e] <3; <3
NIM-P (Pyroxenite)[d]	0.33	0.30	0.27 (0.63)	<1; <3; <3; (<3)[e]
NIM-S (Syenite)[d]	1.19	1.55	1.50 (1.26)	<3; <3; 2 (<3)[e]
NIM-1[c, d, f]	4.30	4.85	4.60 (6.30)	5
NIM-2[c, d, f]	2.50	2.25	2.20 (3.15)	2.5
NIM-3[c, d, f]	1.52	1.10	1.05 (1.00)	1.2
NIM-4[c, d, f]	1.40	0.75	0.70 (1.00)	0.6
NIM-5[c, d, f]	0.25	0.17	0.20 (0.63)	<0.3

[a]Supplied by Centre de Recherches Pétrographiques et Géochimiques [3].
[b]Supplied by Canadian Standard Reference Project [4].
[c]The samples were dissolved in hydrofluoric, perchloric and nitric acids.
[d]Samples from the National Institute for Metallurgy, Johannesburg, South Africa.
[e]The values in parentheses are those cited in the N.I.M. certificates of analysis.
[f]U_3O_8 samples.

beryllium values listed in column A of Table 2 for dunite and pyroxenite are in the same range as the corresponding results listed in columns B and C. According to the certificates of analysis, these samples contain relatively little aluminium [0.44 % Al_2O_3 (dunite) and 4.38 % Al_2O_3 (pyroxenite)] while NIM-G, NIM-L, NIM-N and NIM-S have Al_2O_3 contents of 12.08 %, 13.93 %, 16.64 % and 17.33 %, respectively. The samples of basalt BR and serpentine UB-N also have considerably lower aluminium contents than the other samples listed in Table 2, and the beryllium values in column A are very close to those of columns B and C.

That the presence of large amounts of uranium has the opposite effect to that of aluminium on the absorption of beryllium is demonstrated by the results for U_3O_8 and sodium uranate (column A of Tables 2 and 3) which show that beryllium concentrations in the range from about 0.02 to 2 p.p.m. cannot be determined accurately in the presence of the matrix elements (predominantly uranium); the accuracy decreases with decreasing beryllium concentration. The difference between the beryllium values in columns A or B of Table 3 and those of column C is about one order of magnitude. However, good results were obtained for the samples of U_3O_8 and sodium diuranate (yellow cake obtained from alkaline leach solutions of uranium ores found in the State of Chihuahua, Mexico) by the recommended method; compare the results shown in columns B, C and D of Table 2 and the two sets of beryllium values of column C in Table 3.

TABLE 3

Results of beryllium determinations in samples of yellow cake (sodium diuranate)

A = Results obtained by direct a.a.s. determination in samples after dissolution in hydrochloric acid.

B = Results obtained by direct a.a.s. determination in samples after dissolution in hydrofluoric—nitric acids.

C = Results obtained by a.a.s. determination after separation by extraction and cation-exchange from samples dissolved in hydrofluoric—nitric acids. The values in parentheses indicate the results obtained after deduction of 0.063 μg of beryllium which was added before dissolution of the sample.

Sample	p.p.m. Beryllium		
	A	B	C
1	0.295	0.440	0.029 (0.035)
2	0.300	0.350	0.022 (0.015)
3	0.300	0.450	0.038 (0.040)
4	0.285	0.400	0.040 (0.035)
5	0.295	0.410	0.035 (0.040)
6	0.290	0.360	0.034 (0.030)
7	0.295	0.380	0.025 (0.020)
8	0.285	0.410	0.040 (0.035)
9	0.295	0.400	0.035 (0.040)
10	0.300	0.450	0.028 (0.030)

The procedure was also applied to the determination of beryllium in 20 samples of manganese nodules collected in the South Pacific; values within the range 1.4—2.8 p.p.m. beryllium were found.

This research was supported by the Fonds zur Förderung der wissenschaftlichen Forschung, Vienna, Austria, which help is gratefully acknowledged. The following institutions generously supplied sample material: National Institute for Metallurgy, Johannesburg, Republic of South Africa; Centre de Recherches Pétrographiques et Géochimiques, Vandoeuvre-lès-Nancy, France; Comision Nacional de Energia Nuclear, Mexico D.F., Mexico; Geological Survey of Canada, Ottawa, Canada; University of California, Scripps Institution of Oceanography, La Jolla, California, U.S.A. (Prof. Dr. Gustaf Arrhenius).

REFERENCES

1 J. Korkisch, Modern Methods for the Separation of Rarer Metal Ions, Pergamon, Oxford, 1969.
2 W. Koch and J. Korkisch, Mikrochim. Acta, (1972) 687.
3 H. de la Roche and K. Govindaraju, Revue du GAMS, Centre de Recherches Pétrographiques et Géochimiques, Vandoeuvre-lès-Nancy, 7(4) (1971) 314.
4 Canadian Standard Reference Materials Project, Geological Survey of Canada, Ottawa, Canada.
5 B. G. Russell, R. G. Goudvis, G. Domel and J. Levin, National Institute for Metallurgy Res. Johannesburg, S. A., Rep. No. 1351, 1972.

Analytica Chimica Acta, 82 (1976) 321—327
© Elsevier Scientific Publishing Company, Amsterdam — Printed in The Netherlands

A RAPID METHOD FOR THE DETERMINATION OF MERCURY IN AIR BY FLAMELESS ATOMIC ABSORPTION SPECTROMETRY

DORIS GARDNER*

Oceanography Department, University of Liverpool, P.O. Box 147, Liverpool L69 3BX (England)

(Received 17th September 1975)

ABSTRACT

A rapid method for the determination of total gaseous mercury in the atmosphere is described. A simple, inexpensive sampling device is used; the collection time for mercury levels above 5 ng m^{-3} is less than 25 min; less than 10 min is then needed to determine the mercury by flameless atomic absorption. For subnanogram levels longer sampling periods are used, but air polluted with mercury can be monitored in a few minutes. Data obtained for different samples are presented.

Since the first mercury pollution disaster [1] scientists have become increasingly aware of the need for accurate monitoring of environmental samples for this metal. Because mercury vapour is rapidly adsorbed into the blood stream from the lungs, and some early signs of poisoning are apparent long before they become medically evident [2], atmospheric contamination by mercury is of particular concern. The concentration of mercury in the atmosphere is extremely variable and is controlled by physical and geographical factors such as altitude, barometric pressure, and proximity to mercury sources such as ore bodies. Values reported range from $1—20 \cdot 10^5$ ng m^{-3} Hg in mercury mines at Idria, Yugoslavia, and $0.6—9.7 \cdot 10^5$ ng m^{-3} in a mercury processing plant [3], to 0—20 ng m^{-3} in samples from non-mineralized, non-polluted areas [4, 5].

Most methods for the determination of atmospheric mercury employ elaborate and expensive equipment [6—10] or require lengthy periods to trap detectable quantities of mercury [6, 7, 11—15]. However, many of these methods are restricted to heavily polluted environments such as mines and processing plants. Because the ambient mercury concentrations of environmental air samples may fall to very low levels, a method having a detection level of < 2 ng m^{-3} is desirable, and as these levels also vary greatly over small intervals of time, the analysis must be completed in a short period. This paper describes a rapid, simple and efficient technique that fulfills these conditions.

---

*Present address: CSIRO Division of Fisheries & Oceanography, P.O. Box 21, Cronulla, N.S.W. 2230 (Australia).

EXPERIMENTAL

Apparatus

The mercury trapping system is shown in Fig. 1. The all-glass absorption trap A consists of a tube containing the absorbant (25 ml) surmounted by the splash bulbs (250 ml). The deep lip at each joint prevents loss of the absorbant at the high flow rates required, while the sinter (porosity 0) ensures maximal contact between air and reagent. To prevent excessive evaporation of the absorbant on hot, dry days, the tube may be immersed in an ice bath G and be preceded in the line by an air saturation bottle B which contains dilute tin(II) chloride solution. The diaphragm pump C (William & James Model G2353) draws air through the system and is protected from occasional reagent splashes by the trap D. The flow is controlled at 40 l min^{-1} by a needle valve and measured with a GEC Elliot 1100 rotameter E. To prevent large particles entering the system the inlet is protected by a 15 cm plug of glass-wool F (a glass fibre filter pad may be used if it is necessary to sample the particulates).

The trapped mercury was measured with a Unicam SP 90A, Series 2 atomic absorption spectrophotometer using a cold-vapour technique [16]. The equipment was set up as shown in Fig. 2. The mercury vapour, liberated by adding tin(II) chloride to the 25-ml measuring cylinder A, is pumped through a short drying column B of magnesium perchlorate into the 15-cm fused silica cell C in the light path of the atomic absorption spectrophotometer by means of a peristaltic pump D (flow-rate, 130 ml min^{-1}). Dead space was kept to a minimum by making all connecting tubing as short and narrow as possible.

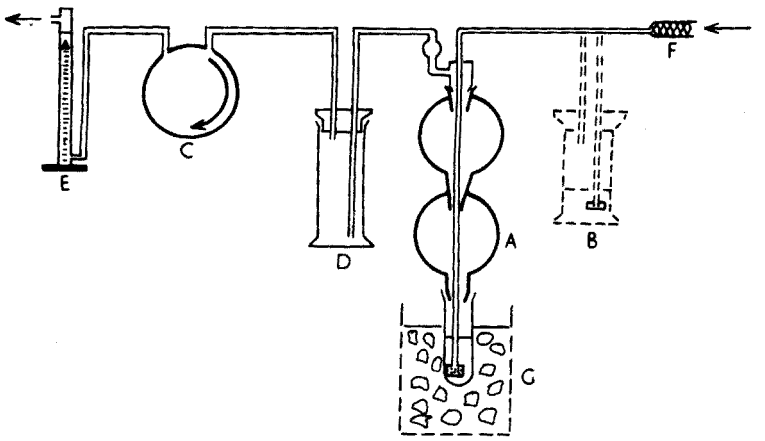

Fig. 1. The mercury trapping apparatus.

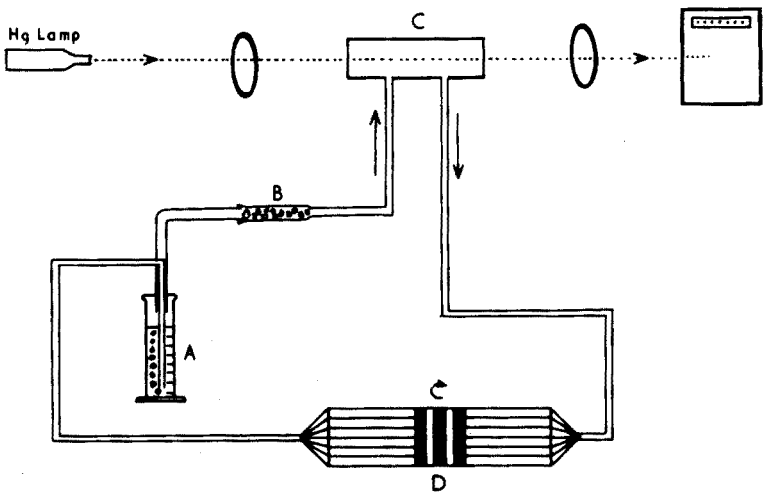

Fig. 2. The mercury detecting apparatus.

Reagents

Reagents were prepared with mercury-free water obtained by all-glass distillation followed by passage through a cation-exchange resin (Dowex AG50-W-X8) in its hydrogen form. Analytical-grade chemicals were employed, and were tested for mercury contamination before use.

Absorbant. This solution was prepared daily by mixing 25 ml of 4 % potassium permanganate solution with 25 ml of 10 % sulphuric acid and diluting to 100 ml with distilled water.

Hydroxyammonium chloride solution. A 20 % (w/v) solution was purified by repeated extraction with 0.05 % dithizone in redistilled carbon tetrachloride.

Tin(II) chloride reagent. Tin(II) chloride dihydrate (30 g) was dissolved in 30 ml of 5 M HCl which had been purified by passage through a column of Deacidite FF anion-exchange resin (500—100 mesh). The solution was then diluted to 50 ml with distilled water, and purified by bubbling nitrogen through it to remove mercury. The reagent was prepared fresh daily.

Standard mercury solution

A 10^6 ng ml^{-1} stock solution was prepared by dissolving 0.1354 g of mercury(II) chloride in 100 ml of 5 M HCl. A standard solution of 10^2 ng ml^{-1} was prepared daily by dilution.

Glassware

All glassware was cleaned with a mixture of concentrated nitric and hydrochloric acids (1:1) and rinsed with mercury-free water before use.

METHOD

Set up the trapping system shown in Fig. 1 and add 25 ml of the absorbant to the mercury absorption trap. Using the vacuum pump, draw air at 40 l min^{-1} through the trap for 25 min. Disconnect the pump, allow the trap to drain, then transfer the contents to a 25-ml stoppered measuring cylinder. Wash the trap with 1 ml of 20 % hydroxyammonium chloride solution, then with distilled water, and add the washings to the cylinder. Adjust the volume to 24 ml with water. Immediately before analysis by atomic absorption spectrophotometer, add a further 1 ml of hydroxyammonium chloride solution and mix until colourless. Add 1 ml of 30 % tin(II) chloride solution, fit the bubbling head on the cylinder immediately, then pass air through the closed circuit by means of the peristaltic pump, and measure the maximum absorbance at 253.7 nm. A steady state should be attained after 30 s. Measure a blank value for the reagents and prepare a calibration graph for standard mercury solutions.

RESULTS AND DISCUSSION

Experiments were performed to devise an efficient trapping system for mercury. The type and concentration of the absorbing reagent for mercury, and the flow rate of the sample through this reagent, are important. For these experiments ^{203}Hg was used for convenience; in the final stages, natural mercury was used to test the method under optimum conditions. Known mercury concentrations were released, from a gas wash bottle upstream of the trapping systems, by 30 % $SnCl_2$ in 5 M HCl.

Low flow rates for long periods gave mercury losses of up to 7 % as a result of adsorption onto the walls of the trapping system. Since the ^{203}Hg could only be recovered completely by rinsing the trap with concentrated nitric acid, it was preferable to use higher flow rates for shorter periods; a mixture (1:1:2) of 10 % (v/v) H_2SO_4:4 % (w/v) $KMnO_4$:H_2O was used. Figure 3 shows the recovery of ^{203}Hg from the absorption tubes of two traps arranged in series, as the mixed reagent concentration is increased.

These conditions have been used in the standard method outlined above to monitor atmospheric samples in which the concentration of mercury can vary greatly, depending on the area under investigation. It has also been used to monitor laboratory air samples and both land-based and shipboard environmental studies which will be discussed elsewhere. Under normal conditions mercury from 1 m^3 of air was collected; after rainstorms, however, mercury levels were so low that it was necessary to pass at least 2 m^3 of air

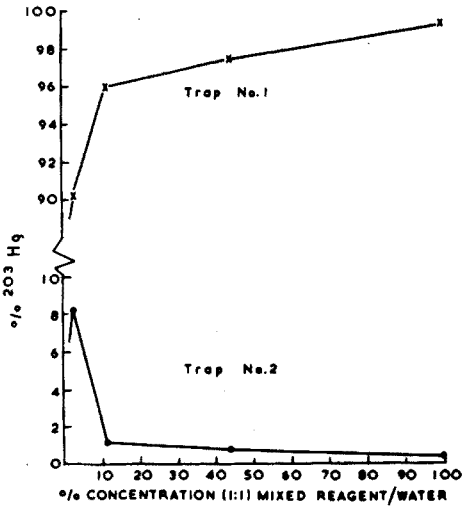

Fig. 3. Mercury trapped vs. concentration of trapping reagent.

through the absorbing solution. Smaller sample volumes of air were required in polarographic laboratories as the calibration graph obtained with the standard samples was not linear above 500 ng of mercury.

Published methods for mercury analysis in air report standard deviations on replicate samples ranging from 1 % [6] to 20 % [11]. It is not known if these reflect experimental errors (the majority $\simeq$ 10 %) or changes in the atmospheric concentration during prolonged sampling periods. During this series of experiments, however, it was found that unless a common inlet was used for replicate sample analyses run in parallel, the standard deviation could be up to 30 %, because of large variations in the mercury concentration over short periods and over small areas. The use of a common inlet gave variations of less than 1 % (P. D. Jones, personal communication).

With this sampling equipment secured to a portable frame, and aliquots of fresh reagent mixed ready in stoppered measuring cylinders, this technique gives a fast, cheap and accurate method of measuring the ambient mercury concentrations in any locality. Table 1 indicates the enormous range of ambient mercury levels found in different environments; potentially dangerous working areas e.g., polarographic laboratories and processing plants etc., can be monitored frequently. Although the maximum permissible concentration allowable for public exposure in the U.S.A. is $1 \cdot 10^3$ ng m^{-3} [17] threshold limit values from $5 \cdot 10^3$ ng m^{-3} for alkyl mercury to $1 \cdot 10^5$ ng m^{-3} for metallic mercury in working environments are tolerated in other countries. When more than $5 \cdot 10^3$ ng Hg m^{-3} was found in and around an unvented polarographic laboratory, an extractor fan reduced that concentration quickly to tolerable levels. The concentrations found outdoors ranged from 0 to 70 ng m^{-3}, but tended to be much higher on misty and foggy days;

TABLE 1

Mercury concentrations in various environments under differing conditions

Place and time			Mercury (ng m^{-3})	Comment
OUTDOOR (Liverpool)	March	02.00	0	Raining
	March	09.30	62	Fine
	March	16.45	150	Misty
	March	20.11	1.2	Raining
	June	10.00	9	Wind-Drizzle
	June	16.30	10	Fine
INDOOR	Research Laboratory 1		350	Broken thermometer found
	Research Laboratory 2		148	—
	Polarographic Laboratory		>5000	Unvented, large volumes of Hg used
	Outside Polarographic Laboratory		4900	—
	Library		510	Situated above Polarographic Lab.
	Polarographic Laboratory		178	Vented for 10 min with extraction fan
	Offices away from laboratories		70	—

levels of $18 \cdot 10^3$ ng m^{-3} in smog in the vicinity of busy highways [20] have been recorded.

The author wishes to thank Professor J. P. Riley, and NERC for financial support for this work.

REFERENCES

1 K. Irukayama, Advan. Water Pollut. Res., 3 (1966) 153.
2 D. B. Shaffin, D. B. Dinman, J. M. Miller, R. G. Smith and D. H. Zoltine, Final Report — N.I.O.S.H. contact, 1973.
3 G. A. Neville, Can. Chem. Educ., 3 (1967) 4.
4 Y. A. Sergeev, Int. Geol. Rev., 3 (1961) 93.
5 J. H. McCathy, Jr., W.W. Vaughan, R.E. Learned and J.L. Meuschke, U.S., Geol. Surv. Circ., (1969) 609.
6 G. L. Corte, R. S. Thomas, L. Dubois and J. L. Monkman, Sci. Total Environ., 2 (1973) 251.
7 S. J. Long, D. R. Scott and R. J. Thompson, Anal. Chem., 45 (1973) 2227.
8 D. A. Church and T. Hadeishi, Appl. Phys. Lett., 24 (1974) 185.
9 D. Siemer, J. Lech and R. Woodriff, Appl. Spectrosc., 28 (1974) 68.
10 T. Hadeishi, D. A. Church, R. D. McLaughlin, B. D. Zak, M. Nakamura and B. Chang, Science, 187 (1975) 348.
11 P. F. Svistov and Yu. I. Turkin, Anal. Metody Geokhim Issled Mater Geokhim Konf. 4th 1970 (1972) 77.

12 J. Panek, Cesk. Hyg., 18 (1973) 244.
13 A. Sugimae, Bunseki Kagaku, 22 (1973) 1350.
14 F. P. Scaringelli, J. C. Puzak, B. I. Bennett and L. D. Robert. Anal. Chem., 46 (1974) 278.
15 J. Scullman and G. Widmark, Int. J. Environ. Anal. Chem., 2 (1972) 29.
16 D. Gardner and J. P. Riley, J. Cons. Int. Exp. Mer., 35 (1974) 202.
17 Anon, Environ. Protect. Agen. Pub. APTD 0753, Dec. 1971.
18 A. V. Roschin and L. A. Timofeevskaya, Ambio, 4 (1975) 30.
19 M. Winell, Ambio, 4 (1975) 34.
20 Y. Fujimura, Jap. J. Hyg., Series No. 7, 2nd Report, 18 (1974) 10.

Analytica Chimica Acta, 82 (1976) 329—336
©Elsevier Scientific Publishing Company, Amsterdam — Printed in The Netherlands

A SEMI-AUTOMATED METHOD FOR THE DETERMINATION OF ARSENIC IN SOIL AND VEGETATION BY GAS-PHASE SAMPLING AND ATOMIC ABSORPTION SPECTROMETRY

P. N. VIJAN, A. C. RAYNER, D. STURGIS and G. R. WOOD

Air quality laboratory, Ministry of the Environment, 880 Bay Street, Toronto, Ontario (Canada)

(Received 19th August 1975)

ABSTRACT

A semi-automated method for the determination of arsenic in soil and vegetation is described. The samples are digested with a perchloric—nitric acid mixture, and the diluted solutions are treated with sodium borohydride solution in a Technicon sampler fitted with a proportioning pump. The resulting mixed stream of gases and solutions is swept into a gas—liquid separator by an argon stream. The gas phase is passed through a heated quartz cell aligned in the optical path of an atomic absorption spectrometer equipped with an arsenic hollow-cathode lamp. The atomic absorption at 193.7 nm is recorded. Forty samples a day can be analyzed. Relative standard deviations are less than 4 % for vegetation samples, and 7 % for soil samples. The detection limit is 0.15 $\mu g\ g^{-1}$ for both vegetation and soils.

The widespread occurrence of arsenic in minerals of economic importance and in arsenical pesticides, etc. leads to its dispersal in air, water, and soil, thereby posing possible public health problems. The analytical methods for the determination of trace amounts of arsenic have been well documented [1]. However, they lack the speed, simplicity, precision and accuracy for routine analysis with a large daily throughput of samples. The use of the silver diethyldithiocarbamate — pyridine reagent for determining arsenic is a definite improvement over the classical semi-quantitative Gutzeit method, but it is too slow and cumbersome for a heavy workload and involves too many variables to obtain precise results.

Conventional atomic absorption methods are not very sensitive, and suffer from chemical and spectral interferences resulting in poor precision. Graphite tube atomization techniques, although more sensitive, have similar drawbacks. Since the report by Holak [2] in 1969, many workers have applied the gas-sampling technique to the determination of arsenic by atomic absorption [4—7].

Kan [3] used sodium borohydride solution to reduce arsenic to arsine which was passed into an argon—hydrogen-entrained air flame. Goulden and Brooksbank [4] used a slurry of aluminium with KI and $SnCl_2$ as a reductor

and passed the evolved hydride through a heated silica tube for atomization. The replacement of flame by heated silica tube significantly improved the sensitivity and precision of the measurement. Schmidt and Royer [5] report a conversion efficiency of close to 100 % for arsenic to arsine by the use of sodium borohydride.

Vijan and Wood [6] combined the desirable features of these methods and applied them successfully to the analysis of suspended air particulate matter. The present work is an adaptation of this method to the determination of arsenic in vegetation and soils. The principal advantages of the gas-sampling technique are: (a) arsenic is converted to arsine and isolated from the matrix elements; (b) all the arsine evolved is available for atomization; and (c) the heated quartz tube provides a more efficient container for atomization and affords longer residence time.

EXPERIMENTAL

Reagents

Digestion Mixture. Mix 4 parts of nitric acid (A.C.S. 70—71 %) and 1 part of perchloric acid (A.C.S. 70—72 %), and store in a glass-stoppered pyrex bottle.

Sodium Borohydride Solution. Dissolve 0.8 g of sodium hydroxide in 400 ml of distilled water, add 4.0 g of sodium borohydride and stir until dissolved.

Background Acid Solution. Dilute 500 ml of the digestion mixture to 2.5 l.

Stock Standard Solution of Arsenic (1000 p.p.m.). Dissolve 1.3203 g of As_2O_3 in a minimum volume of 20 % sodium hydroxide, neutralize with nitric acid and dilute to 1 l. Prepare working standard solutions (5—100 ng As ml^{-1}) by serial dilution of the stock standard with background acid solution.

Instrumentation and Apparatus (Fig. 1)

An atomic-absorption spectrometer capable of giving a stable signal at the 193.7-nm arsenic wavelength is required. A Techtron AA5 was used with a 2—10-mV variable range strip chart recorder. The Technicon modules used were a sampler, a proportioning pump, and a manifold tray. The quartz cell was 16 cm long and of 1.3 cm internal diameter with an inlet tube (4-mm diameter) fused in the middle. The cell was wound with 4 m of Chromel-C wire (resistance 1.06 ohms ft^{-1}) and insulated with asbestos tape and string, the temperature being controlled by a Variac transformer (0—110 V).

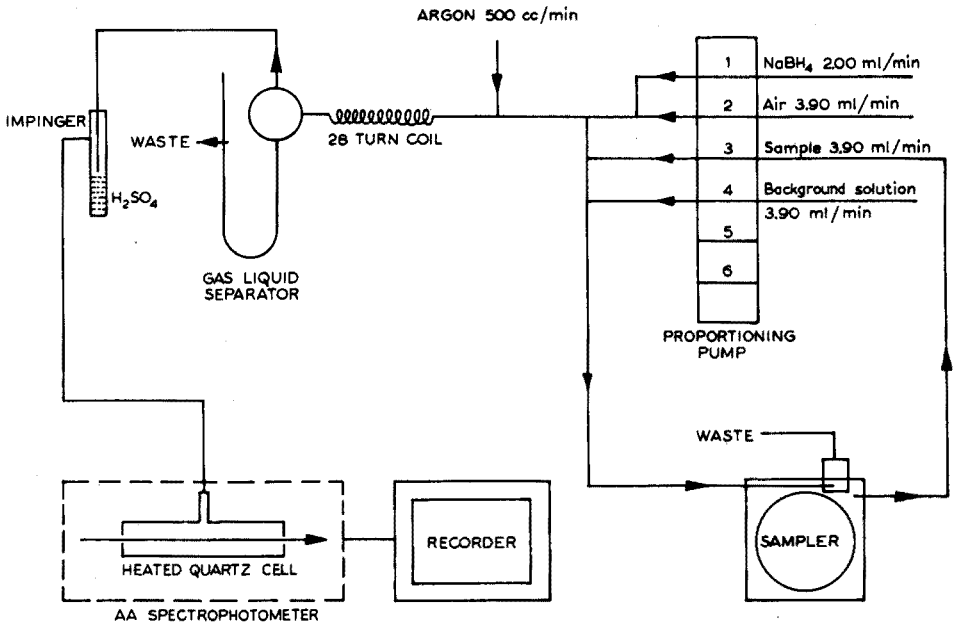

Fig. 1. Autoanalyser — a.a.s. system for arsenic.

Procedure

Sample Preparation. Weigh 0.100 g of vegetation or soil sample on a piece of weighing paper and transfer to a dry 18 × 150-mm borosilicate glass test-tube with a calibration mark at 15 ml. Add 3 ml of acid digestion mixture and allow to stand in an aluminium heating block [6] under a fume hood. Prepare a batch of 35 samples in like manner and place them in the heating block. Include a reagent blank and a series of arsenic standards with each batch. Leave the loaded block for 1 h at room temperature. Transfer the block to a hot-plate set at 250 °C for 3 h or until a clean solution with a slight yellowish tinge is obtained. (The block is, preferably, left overnight at 250 °C.) The samples at this stage are completely dissolved except for a white residue of silicic acid. Allow the samples to cool to room temperature and dilute to the 15-ml mark with distilled water. Seal the test-tubes with Parafilm or use polyethylene caps and mix the contents thoroughly. Allow the siliceous residue to settle, and pour the supernate into the appropriately numbered cups held in the sampler tray for analysis.

Determination of arsenic. Allow the instrument to warm up for 20—30 min. Set the lamp current at 8 mA, or as recommended by the manufacturer. Set the wavelength at 193.7 nm and the slit width at 300 nm or as recommended by the manufacturer. Insert the quartz cell assembly into the

burner-head holder of the spectrometer, and heat it to 700—800 °C. Turn the mode switch to absorbance and the damping to maximum (D on the Techtron AA5). Close the vent to the lowest position in order to prevent air turbulence in front of the cell openings. (Any draft will result in a noisy baseline.) Set the recorder at 2-mV full scale deflection and the chart speed at 0.5 cm min^{-1}

Insert the reagent lines into the appropriate bottles as indicated in Fig. 1 and start the proportioning pump. Allow the U-tube of the gas—liquid separator as well as the sampling probe well to fill up with the solution. Turn on the argon with a delivery pressure set at 5 p.s.i. and a flow rate of 500 ml min^{-1}. Adjust the spectrometer to give zero absorbance. Turn on the sampler and start recording the standard and sample peaks.

Measure the peak heights of the standards, to prepare a calibration curve and read off the sample concentrations in p.p.b. arsenic. For arsenic in the initial sample, μg As g^{-1} = p.p.b. As in sample solution × 0.15.

RESULTS AND DISCUSSION

The NBS Orchard Leaves Standard (Control A) and a typical vegetation sample (Control B) were run as controls with every batch of samples analysed by the proposed method. The standard and the sample chosen had arsenic values that differed by an order of magnitude so that an assessment of data would encompass moderate as well as high levels of arsenic. The mean of 24 analyses of Control A was 9.05 $\mu g\ g^{-1}$ with a standard deviation (s) of 0.36 and a relative standard deviation (s_r) of 3.93. The mean of 27 analyses of Control B was 127.52 $\mu g\ g^{-1}$ (s = 5.05; s_r = 3.96). The s_r values for these two materials are very close, which indicates that the 40-mesh ground vegetation is sufficiently homogeneous for the analysis. The As analyses were done on 30 days over a period of 3 months, and so provide a fair estimate of the performance of the method.

The NBS certified arsenic value for Control A is 11 ± 2 $\mu g\ g^{-1}$. Applying a moisture correction factor of 5 % gave a mean value of 9.4 $\mu g\ g^{-1}$ by the present method. Results of neutron activation analysis by McMaster University, Hamilton, and of the SDDC spectrophotometric analysis, which is a slightly modified version of the AOAC method, done in this laboratory, showed good agreement with those obtained by the present method (9.8 ± 0.9 $\mu g\ g^{-1}$ and 9.4 ± 1 $\mu g\ g^{-1}$, respectively, based on the average of five results by each method). All three methods gave results within the limits of the NBS certified value.

The effects of interferences, gas flow rates and furnace temperature, types and concentration of acids, and strength of borohydride solution on the determination of arsenic have already been discussed [6].

Under similar experimental conditions, standard solutions containing arsenic(V) generate signals which are 25—30 % lower than those from arsenic(III) but the normalizing effect of the decomposition treatment of both samples and standards practically eliminates this difference.

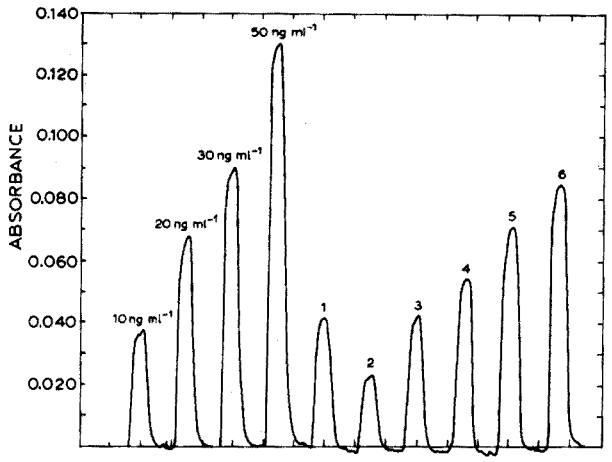

Fig. 2. Typical recorder tracings for arsenic.

The calibration curve constructed from standard solutions ranging from 20 to 100 ng As ml^{-1} covered sample values up to 15 μg As g^{-1}. For samples with higher arsenic levels, the digests must be diluted to give a suitable arsenic level. Figure 2 shows typical recorder tracings.

A set of 27 vegetation samples covering arsenic concentrations between 0.4 and 540 μg g^{-1} was analysed by the neutron activation method at McMaster University. Each sample was then analysed in duplicate by the SDDC spectrophotometric method and by the present method. The results are presented in Table 1.

The analysis of 74 samples of vegetation by the present method and by the SDDC method showed that the proposed method gives slightly higher results than the SDDC method. The least-squares regression equation was calculated for the two sets of data. The slope of the regression line was 0.900 and the intercept was −1.00.

Three typical soil samples containing 6.0, 45 and 97 p.p.m. arsenic representing low, medium and high levels were spiked with known amounts of arsenic and then taken through the procedure. The results (Table 2) show a mean recovery of 101.5 %; the amounts of arsenic added up to 150 μg g^{-1} of sample were recovered quantitatively.

Precision data for the measurement of arsenic at three levels commonly occurring in soil samples are given in Table 3; it can be seen that the within-run precision is almost twice as good as the day-to-day precision. Table 4 contains the results of analysis of soil samples obtained by the present method and the SDDC colorimetric method. The agreement is reasonably good. The mean % deviation is 2.58 % for the a.a.s. method and 11.1 % for the SDDC method.

Up to eighty samples can be easily analysed by one technician over two working days; one day is used for weighing samples and decomposition, and

TABLE 1

Determination of arsenic in 27 vegetation samples by three methods
(All results are given as p.p.m. As)

Present method (mean)	N.a.a.	SDDC method (mean)	Present method (mean)	N.a.a.	SDDC method (mean)
4.3	3.7	4.3	3.4	2.9	3.3
3.2	2.8	2.7	2.7	2.1	2.4
1.2	0.8	0.9	1.3	1.2	1.1
0.7	0.5	0.5	17	15	18
3.1	2.8	2.7	19	11	14
2.1	1.0	1.2	22	20	20
1.1	1.6	1.4	341	329	364
0.9	1.1	1.2	142	143	155
0.9	1.1	1.1	412	350	387
3.3	N.D.	3.4	144	134	136
0.4	0.8	0.5	547	479	537
1.0	1.2	1.5	192	182	193
215	184	219	235	212	209
47	37	40			

TABLE 2

Recovery of added arsenic in soil samples

Description of sample	As found (p.p.m.)	As recovered (p.p.m.)	% Recovery
Sample X	6.0		
Sample X + 3 p.p.m. As	8.8	2.8	93.3
Sample X + 6 p.p.m. As	12.1	6.1	101.7
Sample X + 9 p.p.m. As	14.6	8.6	95.6
Sample Y	45.0		
Sample Y + 30 p.p.m. As	71.0	26.0	86.7
Sample Y + 60 p.p.m. As	103.0	58.0	96.7
Sample Y + 90 p.p.m. As	136.0	91.0	101.1
Sample Z	97.0		
Sample Z + 60 p.p.m. As	154.0	57.0	95.0
Sample Z + 90 p.p.m. As	211.0	114.0	126.7
Sample Z + 150 p.p.m. As	272.0	175.0	116.7

the other day for running the samples through the analysis system and computing results. The argon flow rate is critical and should be closely reproduced each time the instrument is used.

When drastic reduction in the peak height of a standard solution or a noisy

TABLE 3

Precision test for arsenic in soil
(Mean, standard deviation and relative standard deviation for 8 determinations in each set are given)

Conc. range (p.p.m. As)	Within-run			Day-to-day		
	$\bar{X}$	s	s_r	$\bar{X}$	s	s_r
Low	5.8	0.15	2.6	6.0	0.27	4.5
Med.	44	0.83	1.9	45	2.8	6.2
High	96	4.7	4.9	93	6.6	7.1

TABLE 4

Results obtained by the a.a.s. and SDDC method for arsenic in soils

Present method p.p.m. As[a]	% Deviation from mean	SDDC method p.p.m. As[a]	% Deviation from mean
9.4	3.7	10.1	12.9
6.0	1.7	6.1	1.6
22.0	2.3	21.0	14.3
25.0	—	23.5	13.2
7.5	—	7.3	17.8
5.2	5.8	6.0	10.0
27.0	—	25.2	13.1
59.0	—	58.9	13.4
36.0	2.8	31.2	13.5
40.0	3.7	42.2	5.2
78.0	5.8	83.0	12.8
70.0	5.0	73.5	2.0
6.7	1.5	6.3	11.1
6.0	3.5	7.3	1.4
45.0	6.7	48.2	17.0
23.0	—	24.8	16.1
115.0	4.3	125.0	4.0
55.0	3.6	58.7	20.9
92.0	2.2	88.0	9.1
4.8	3.1	5.2	7.7
5.5	5.4	6.5	16.9
20.0	2.5	19.0	13.7
11.0	—	14.1	9.9
28.0	3.6	31.1	5.5
57.0	—	57.9	9.7
30.0	5.0	31.4	21.0
290.0	—	293.0	14.7
370.0	—	355.0	2.2

[a]Mean of duplicate results.

baseline occurs, the problem may be related to deterioration of the proportioning pump tubes which should be replaced. The 10 ml of concentrated sulphuric acid in the impinger should be replaced every 2—3 days. A light colored deposit builds up in the quartz cell over a period of time; when this happens the cell should be cleaned or replaced.

The lower limit of determination on the system built around the Techtron AA5 atomic absorption spectrophotometer is 0.25 p.p.m. based on 0.100-g sample.

CONCLUSIONS

The method presented offers speed and convenience of operation for the routine analysis of large numbers of vegetation and soil samples for arsenic. The precision and accuracy are at least as good as those of conventional methods. The sample size offers the advantage of streamlining the decomposition procedure in conveniently sized batches. The subsequent procedure being automatic, the operator is freed for other work. The recorder tracings provide a permanent record and help in evaluation and interpretation of the results.

REFERENCES

1 P. F. Reay, Anal. Chim. Acta, 72 (1974) 145.
2 W. Holak, Anal. Chem., 41 (1969) 1712.
3 Kwok-Tai Kan, Anal. Lett., 6 (1973) 603.
4 P. D. Goulden and P. Brooksbank, Anal. Chem., 46 (1974) 1431.
5 F.J. Schmidt and J.L. Royer, Anal. Lett., 6 (1973)17.
6 P. N. Vijan and G. R. Wood, At. Absorption Newslett., 13 (1974) 33.
7 Official Methods of Analysis of the Association of Official Analytical Chemists, 25.016, 11th edn., Washington D.C., 1970, p. 402.

Analytica Chimica Acta, 82 (1976) 337—342
©Elsevier Scientific Publishing Company, Amsterdam — Printed in The Netherlands

DETERMINATION OF TRACE AMOUNTS OF TIN IN GEOLOGICAL MATERIALS BY ATOMIC ABSORPTION SPECTROMETRY

E. P. WELSCH and T. T. CHAO

U.S. Geological Survey, Denver, Colorado 80225 (U.S.A.)

(Received 4th August, 1975)

SUMMARY

An atomic absorption method is described for the determination of traces of tin in rocks, soils, and stream sediments. A dried mixture of the sample and ammonium iodide is heated to volatilize tin tetraiodide which is then dissolved in 5 % hydrochloric acid, extracted into TOPO-MIBK, and aspirated into a nitrous oxide—acetylene flame. The limit of determination is 2 p.p.m. tin and the relative standard deviation ranges from 2 to 14 %. Up to 20 % iron and 1000 p.p.m. Cu, Pb, Zn, Mn, Hg, Mo, V, or W in the sample do not interfere. As many as 50 samples can be easily analyzed per man-day.

Colorimetric methods have been used in the determination of tin in geological materials for geochemical exploration. Several of the methods involve sample decomposition by heating with ammonium iodide to volatilize tin as the tetraiodide, and its reaction with a coloring agent such as gallein [1—4]. The released tin may also be determined by atomic absorption measurement in an air-hydrogen flame [5], or a nitrous oxide—acetylene flame [6]. Burke's work [7] with aluminum-, iron-, and nickel-base alloys has demonstrated that tin can be quantitatively extracted into a 5 % trioctylphosphine oxide (TOPO) in MIBK from 10 % hydrochloric acid in the presence of iodide and ascorbic acid. Ascorbic acid maintains the dissolved iron in the iron(II) state, thus minimizing its extraction into the organic layer. Thus, the TOPO—MIBK extraction may be adaptable to the determination of tin in geological materials. Mensik and Seidemann [8] have determined tin at percent concentrations in rocks and ores by combining the TOPO—MIBK extraction with ammonium iodide sublimation-fusion using an air condenser to trap the volatile tin tetraiodide. The method proposed in this paper is similar to that of Mensik and Seidemann [8], except that trace levels of tin in a sample are volatilized and condensed in the same sample tube by heating with ammonium iodide at a controlled temperature. The tolerance to some interfering metals that may be present in samples has been determined.

EXPERIMENTAL

Apparatus

A Perkin—Elmer 103 atomic absorption spectrophotometer was used with a tin hollow-cathode lamp. Neither the Perkin—Elmer nor the Westinghouse tin electrodeless-discharge lamp proved to have any advantage over the tin hollow-cathode lamp. In addition, use of the Perkin—Elmer 360, while providing greater sensitivity, resulted in the same signal-to-noise ratio as the Perkin—Elmer 103. The Varian nitrous oxide burner produced a stable flame and the stainless steel nebulizer was found to be essential for optimal sensitivity.

A Pyropot 10 heater (Pyroco Products, Margat, Queensland, Australia 4019) provided the controlled heat source for the sample decomposition with ammonium iodide.

Operation of the Perkin—Elmer 103 spectrophotometer

Set the lamp current at 10 mA and the slit at 0.7 nm, and isolate the 286.3-nm tin line. Adjust the burner to about 7 mm below the bottom of the light beam. With the nitrous oxide and air regulators set at 35 psi, turn the oxidant-flow dial to 13:50. Set the acetylene regulator at 8 psi and the fuel flow dial at 13:50, turn on air and acetylene controls, and light the burner. Make the acetylene flow very rich by setting the fuel dial at about 12:20 and switch to nitrous oxide. Dip the nebulizer capillary tube into methyl isobutyl ketone (MIBK) and enrich the flame further until a tall pink flame is achieved (fuel dial at about 11:80). Allow a 5-min warm-up and optimize the aspiration rate, paying constant attention to the flame condition. With all the adjustments in order, the 20 μg Sn ml^{-1} (in MIBK) standard (see below) should read about 0.14 absorbance or 14 % of the scale without expansion. With MIBK as the blank, expand the scale until this standard reads 100 %.

Reagents and standards

Ascorbic acid solution. Prepare daily by dissolving 10 g of ascorbic acid in 100 ml of 5 % hydrochloric acid.

TOPO (trioctylphosphine oxide)-MIBK (methyl isobutyl ketone). Dissolve 4 g of TOPO in 100 ml of MIBK.

Tin stock and standard solutions. Prepare the 1000 μg Sn ml^{-1} stock solution by dissolving 1.000 g of reagent-grade tin metal in 1 l of 50 % (v/v) hydrochloric acid. To prepare the 100 μg Sn ml^{-1} standard solution in 5 % hydrochloric acid, transfer 10 ml of the stock solution to a 100-ml

volumetric flask and dilute to volume with deionized water. This solution is stable for at least 2 weeks. A (1 + 9) dilution of this standard with 5 % hydrochloric acid will yield the 10 μg Sn ml^{-1} solution required for preparing the organic tin standards.

Organic tin standard solutions in MIBK (1, 5, 10, and 20 μg Sn ml^{-1}). Pipet 0, 1, 5, 10, and 20 ml of the above 10 μ g Sn ml^{-1} solution to each of five 125-ml separatory funnels along with 3 g of ascorbic acid and enough 5 % hydrochloric acid to make a total volume of 90 ml. Shake to dissolve the ascorbic acid, add 10 ml of TOPO—MIBK solution, and shake for 30 s. Drain away the aqueous phase and transfer the organic tin extracts to 16 × 150-mm test tubes.

With a 1.0-g sample taken for analysis, the range of tin concentrations in the sample that can be determined with the above standard solutions is 2—40 p.p.m. A set of high-tin organic standards may be prepared by using 0, 1, 2, 3, 4, and 5 ml of the 100 μg Sn ml^{-1} solution (corresponding to 0, 10, 20, 30, 40, 50 μg Sn ml^{-1} in MIBK). This set of standards will cover tin concentrations in the sample up to 100 p.p.m. Samples containing as much as 1000 p.p.m. Sn can be determined by simple dilution of the organic extract with the TOPO—MIBK reagent. Above this amount a smaller sample size is recommended.

Procedure

Weigh 1.0 g of less than 100-mesh soil, rock, or stream-sediment sample into a 25 × 200-mm screw-cap tube along with 4 g of dry powdered ammonium iodide, and mix thoroughly. Dry the mixture overnight at 105 °C in an electric oven. Allow to cool and then heat the sample for 15 min in the Pyropot, which has been pre-heated to 500 °C. After cooling, add 12 ml of 5 % hydrochloric acid and 6 ml of ascorbic acid solution, and heat in a boiling water bath for 15 min. Mix while hot on a tube vibrator until the sample is finely dispersed. After thorough cooling in a cold-water bath, add 2 ml of TOPO—MIBK to each sample, secure the screwcap, and shake for 30 s. Decant the contents into a 16 × 150-mm test tube, centrifuge, and aspirate the organic layer into the nitrous oxide—acetylene flame of the spectrometer. Determine the tin concentration of the sample by comparing with a tin calibration curve. As many as 50 samples per man-day can be analyzed by this method.

The above volatilization procedure is very effective in releasing tin from cassiterite. For samples containing tin occluded by or substituting in the silicate minerals, destruction of the silicate structure is necessary for the release of tin. The 1.0-g sample is evaporated to dryness in a 100-ml Teflon beaker with 20 ml of hydrofluoric acid (50 %) and 5 ml of nitric acid (*d*, 1.42). The residue is then quantitatively transferred with the powdered ammonium iodide to a 25 × 200-mm screw-cap test tube and treated as above.

RESULTS AND DISCUSSION

Sample decomposition

Various methods of sample decomposition were examined, but none proved as simple and effective as the volatilization with ammonium iodide for extracting tin from cassiterite. The use of the Pyropot 10 heater makes this method of decomposition even more attractive, inasmuch as it provides a better controlled temperature. The reaction of cassiterite with ammonium iodide is as follows:

$$SnO_2 + 4NH_4I \rightleftharpoons SnI_4 + 4NH_3 + 2H_2O$$

Since water is a product of the reaction, obviously the sample—ammonium iodide mixture must be as dry as possible for maximum efficiency. Any excess of water would tend to reverse the reaction. The temperature and duration of heating in the Pyropot are critical and must be controlled in order to obtain reproducible results. A heating temperature of 500 °C was found optimal for the samples used; this agrees with the results of Heffernan et al. [5] in their determination of tin in cassiterite ores. However, the duration of heating has been increased from their 5 min to 15 min, because of the larger sample size.

Sensitivity

With the instrument scale expanded so that the 20 μg Sn ml^{-1} standard read 100 % as previously mentioned, a sensitivity of 0.2 μg Sn ml^{-1} per scale division is possible. Where rapid analysis of a large number of samples is desired, 1.0 μg Sn ml^{-1} or 2 p.p.m. Sn in a 1-g sample is the convenient limit of determination. The zero setting with MIBK may vacillate 1 scale division, owing to slight variation of fuel and nitrous-oxide flow. The highly flame-sensitive nature of tin makes gas regulation critical for achieving maximum sensitivity and minimum noise. This means that gaskets, O-rings, valves, and any other fittings that may affect the condition of the flame must be properly maintained.

MIBK is the preferred blank because it will clean the mixing chamber of any precipitated TOPO. At the proposed instrument scale expansion, a reagent blank will read one-half scale division higher than MIBK. For more precise work, this can be compensated for by simply adjusting the auto zero to read minus one-half division when MIBK is aspirated. A small screw at top center of the readout scale facilitates this adjustment.

Figure 1 shows a slight curvature in a plot of a series of high-tin standard solutions (0—50 μg Sn ml^{-1} in MIBK). For rapid semiquantitative screening of geological samples, this slight curvature can be ignored. For the plot shown, the 50 μg Sn ml^{-1} standard was set to read 100 % by scale expansion, and each scale division was equivalent to 0.5 μg Sn ml^{-1}. The concentration

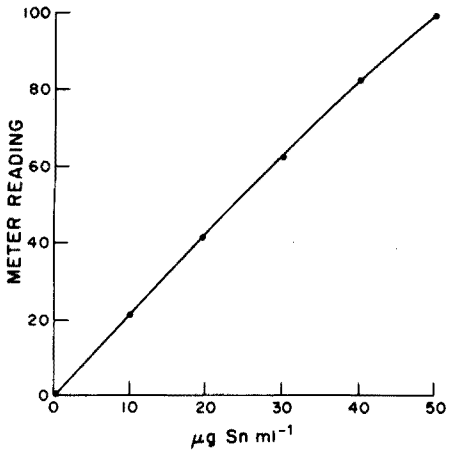

Fig. 1. Calibration curve relating meter reading to tin concentration.

of tin in parts per million in a sample is then equal to the scale reading when a 1-g sample is taken for analysis.

Analytical data

Six replicates of six samples of varying matrices yielded relative standard deviations ranging from 2 to 14 % (Table 1).

Recovery of added known amounts of Specpure SnO_2 to a tin-free matrix of major elements is presented in Table 2. The average recovery ranged from 93 to 127 %. Samples with lower tin concentrations consistently gave higher recovery values, probably because of greater background noise and matrix effects. Samples containing higher tin concentrations gave lower recoveries, which probably reflects the fusion and extraction efficiency of the method.

TABLE 1

Six replicate determinations of tin in various samples

Sample no.	Material	Range (p.p.m.)	Mean (p.p.m.)	s_r (%)
T-2	Cassiterite and quartz	26—32	28.8	9.0
GXR-1	Jasperoid	54—56	54.8	1.8
4	Cu mill tailings	4—5	4.8	8.8
284598	Stream sediment	1450—1700	1566.7	13.9
581	Stream sediment	16—23	19.3	11.2
613	Stream sediment	165—185	172.0	4.4

TABLE 2

Recovery of tin from samples prepared with additions of known amounts of Specpure SnO_2 to a matrix containing Si, Al, Fe, Ca, Mg, Na, and K in approximate crustal abundance concentrations

Sample no.	Sn added (μg)	Sn recovered (μg)	Recovery (%)
1	2.2	2.8	127
2	4.6	5.3	115
3	10.0	9.2	92
4	215.0	200.0	93
5	1574.0	1520.0	97

INTERFERENCES

Nine pairs of standard solutions containing 4 and 40 μg Sn were spiked individually with 1000 μg Cu, Pb, Zn, Mn, Hg, Mo, V, W, and the equivalent of 20 % Fe in a 1-g sample. The solutions were analyzed for tin by the proposed procedure. A slight suppression by zinc and an enhancement by iron were noted on the 224.6-nm tin line, but not on the 286.3-nm tin line. Considerable suppression was found from tungsten on both tin lines. However, since tungsten minerals are unlikely to be decomposed by the sample fusion and acid dissolution of this method, significant interference from tungsten should be uncommon. The specific fusion temperature, as well as the low acid concentration used, presumably reduces the amounts of the above tested elements that can actually be put into solution from a sample. For this reason, the proposed method described probably tolerates considerably larger quantities of these elements.

REFERENCES

1 G. A. Wood, Sym. Geol. Expl. (20th Internat. Geol. Congr., Mexico, 1956) (1958) 461.
2 R. E. Stanton and A. J. McDonald, Bull. Inst. Min. Met., 659 (1961) 29.
3 R. N. Ward, H. W. Lakin, F. C. Canney, and others, U.S. Geol. Surv. Bull., 1152 (1963) 74.
4 A. Y. Smith, Geol. Surv. Can., Pap., 67—50 (1967).
5 B. J. Heffernan, R. O. Archbold and T. J. Vickers, Proc. Aust. Inst. Mining Met., 223 (1967) 65.
6 J. A. Bowman, Anal. Chim. Acta, 42 (1968) 285.
7 K. E. Burke, Analyst (London), 97 (1972) 19.
8 J. D. Mensik and H. J. Seidemann, Jr., At. Absorption Newslett., 13 (1974) 8.

Analytica Chimica Acta, 82 (1976) 343—348
©Elsevier Scientific Publishing Company, Amsterdam — Printed in The Netherlands

DETERMINATION OF LEAD IN ROCKS BY RADIOMETRIC ISOTOPE DILUTION AND SUBSTOICHIOMETRIC EXTRACTION

PHILIP ARUSCAVAGE

U.S. Geological Survey, Reston, Va. 22092 (U.S.A.)

(Received 21st July 1975)

SUMMARY

A rapid procedure is described for the determination of lead in rocks by an isotope-dilution substoichiometric method. After the sample has been digested with acid in the presence of ^{210}Pb tracer, the lead is separated by dithizone extractions. After the lead has been back-extracted into aqueous solution, it is reacted with a substoichiometric amount of EDTA. Excess of unreacted lead is removed by extraction with dithizone in carbon tetrachloride, and the specific activity of the aqueous complex is determined by counting ^{210}Pb. The standard deviation of the method is less than 10 % for replicate determinations of lead in several U.S. Geological Survey standard rocks. The agreement with literature values indicates that the method is accurate.

The routine determination of lead in rock samples for geochemical studies requires a method that is rapid and that has sufficient sensitivity to determine easily the low concentrations found in many rocks. Some sensitive determinations of lead in rocks have been outlined, the methods being based on atomic absorption spectrometry [1—3] and isotope-dilution mass spectrometry [4, 5].

The present method describes a substoichiometric isotope-dilution method; the highly selective reaction of dithizone with lead in basic cyanide solution is used as the basis for the separation, followed by reaction with a substoichiometric amount of EDTA. The theory of the substoichiometric isotope-dilution method has been described and procedures have been given for many elements [6—10]. Briefly, the method is based on the reaction of the element and equilibrated isotopic tracer and a substoichiometric amount of reactant, quantitative separation of the excess element, and determination of the specific activity of the separated product. Because separations preceding the determination of the specific activity need not be quantitative, the analytical separations can often be shortened and advantage taken of separations that, although not quantitative, are fast and specific.

EXPERIMENTAL

Reagents

Standard lead solution (1 mg Pb ml^{-1}). Dissolve 1.342 g of $PbCl_2$ in 100 ml of 2 M hydrochloric acid. Dilute to 1 l with water in a volumetric flask. Prepare a 10 μg Pb ml^{-1} solution by diluting 1.0 ml of this standard lead solution to 100 ml with 0.2 M hydrochloric acid in a volumetric flask.

EDTA solution (0.01 M). Dissolve 1.860 g of sodium ethylenediaminetetracetate in 500 ml of water. Prepare a 10^{-5} M solution of EDTA by diluting 0.1 ml of this solution to exactly 100 ml with water. A 0.25-ml aliquot of this reagent will now complex about 0.5 μg of lead.

Tracer solution. Dilute commercially available carrier-free ^{210}Pb with dilute hydrochloric acid so that 0.1 ml yields about 40000 c.p.m.

Dithizone—xylene solution (0.01 % w/v). Dissolve 50 mg of dithizone in 500 ml of xylene. Prepare a 0.001 % dithizone solution by diluting 50 ml of the above with 450 ml of xylene. Store both solutions in dark bottles.

Dithizone—carbon tetrachloride solution (0.01 % w/v). Dissolve 50 mg of dithizone in 500 ml of carbon tetrachloride. Prepare daily a 0.0001 % solution by diluting 3 ml of the above to 300 ml with carbon tetrachloride.

Potassium cyanide solution (10 % w/v). Dissolve 50 g of potassium cyanide in 100 ml of water. Remove lead by extraction with small portions of 0.001 % dithizone in carbon tetrachloride until the organic layer remains green. Remove excess of dithizone from the aqueous solution by extracting with a small portion of carbon tetrachloride. Dilute the aqueous solution to 500 ml with water.

Sodium citrate solution (50 % w/v). Dissolve 100 g of sodium citrate in 200 ml of water. Adjust the pH to 9 with dilute ammonia solution and extract lead with small portions of 0.001 % dithizone in carbon tetrachloride until the organic layer remains green. Remove excess of dithizone by making the aqueous layer slightly acid with dilute hydrochloric acid and extracting with a small portion of carbon tetrachloride.

Ammonia solution. Prepare a ca. 6 M isothermally distilled solution by placing two large plastic beakers, one containing concentrated ammonia liquor and the other 500 ml of redistilled water, in a desiccator or other suitable closed container for 1 week. Store in a polyethylene bottle. (Note: Because the concentration of the ammonia may vary according to conditions, the amount of 6 M ammonia specified in the procedure may vary and must be adjusted to give the proper pH for each extraction step.)

Apparatus

Counting system. A 10 × 10 cm sodium iodide detector coupled to a single-channel analyzer was set to count the 0.046 MeV γ-ray of ^{210}Pb.

Solvent extraction apparatus. Extractions were performed by mixing the phases in a separatory funnel with a stream of nitrogen gas as described by Greenland and Campbell [9]. Removal of the upper phase after extraction was facilitated by using a suction-tube apparatus as described by Lillie and Greenland [11].

Procedure

Transfer 0.1 g of rock sample to a Teflon beaker. Prepare standards of 1, 2, 4, and 5 μg of lead by pipetting appropriate amounts of standard lead solution. To each beaker add 0.1 ml of ^{210}Pb tracer, 1 ml of 72 % perchloric acid (lead-free), 3 ml of concentrated redistilled nitric acid, and 10 ml of 40 % hydrofluoric acid.

Heat the samples overnight on a hot plate at 120 °C. Dissolve the residue in 10 ml of 2 M hydrochloric acid, add 2 ml of sodium citrate solution, and transfer to a 60-ml separatory funnel. Add 5 ml of the 6 M ammonia solution and extract the lead from the solution (pH 9) into 15 ml of 0.01 % dithizone—xylene solution. Discard the aqueous phase. Wash the organic phase three times with 5-ml portions of a weak ammoniacal solution (pH 9). Rinse the funnel once with water. Add 10 ml of 10^{-3} M hydrochloric acid and back-extract lead for 5 min. Discard the upper organic layer by using the suction-tube apparatus. Wash once with 5 ml of xylene and discard the organic layer. Add 0.5 ml of 2 M hydrochloric acid and mix thoroughly. Add 1.0 ml of 10 % potassium cyanide solution and extract lead from the aqueous phase (pH 9) by using 10 ml of 0.001 % dithizone—xylene solution. Discard the aqueous phase. Wash twice with 5-ml portions of weakly ammoniacal solution (pH 9) and finally rinse the funnel once with water.

Transfer the organic phase to a clean 60-ml separatory funnel, add 5.0 ml of 10^{-3} M hydrochloric acid, and back-extract lead for 5 min. Discard the upper organic layer. Add 0.50 ml of redistilled 6 M hydrochloric acid and 0.25 ml of 10^{-5} M EDTA solution and mix thoroughly. Add 1 ml of 6 M ammonia and, while mixing by bubbling nitrogen through, heat each sample to boiling, using a hot-air blower to ensure reaction of EDTA. Allow to cool to room temperature and add 0.2 ml of 6 M ammonia. Add 5 ml of 0.0001 % dithizone—carbon tetrachloride solution and extract the excess of lead from the aqueous phase (pH 9) for 2 min. Discard the organic phase. Repeat the extractions with fresh portions of reagent solution until the organic phase remains distinctly green. Drain the aqueous phase into a suitable counting vial. Count samples and standards in the well of a sodium iodide detector for 2—3 min each. Prepare a calibration curve by plotting the mass of lead in the standard solutions against A/a, where A is the counting rate of 0.1 ml of

tracer diluted to 5 ml and a is the counting rate of the processed standards. Determine the amount of lead in the samples by reference to this curve.

RESULTS AND DISCUSSION

The principles of the substoichiometric isotope-dilution method have been previously described [6—10, 12]. Briefly, as described by Greenland and Campbell [9], after the samples have been decomposed in the presence of isotopic tracer, the specific activity of the solution is given by the equation $A/(m+m_b)$, where A is the counting rate of the tracer and m and m_b are the masses of lead in the sample and in the reagents, respectively. After separation of the lead, reaction with EDTA, and removal of excess of lead by extraction, the lead—EDTA complex still retains this same original specific activity regardless of any losses of lead that occurred during the separations. This is true because, after equilibration, a proportionate amount of radioactive lead is lost with the inactive lead. Therefore, after extraction of the excess of lead, the complex has a specific activity equal to a/m_c, where a is the counting rate of the aqueous solution of the lead—EDTA complex and m_c is the mass of lead complexed by EDTA. Equating the original condition with the final, and solving for m gives $m = (A/a)\, m_c - m_b$. Plotting A/a against the known m of the standards yields a calibration curve having the slope equal to the amount of lead in the EDTA complex and an intercept equal to the blank.

The tracer counting standard contains an appreciable quantity of activity due to bremsstrahlung from ^{210}Bi ($t_{1/2}$ = 5.01 d), the daughter of ^{210}Pb. If this activity is not subtracted from the total activity, the slope of the curve and thus the theoretical mass of lead complexed by a given amount of EDTA would be altered. For example, if half the total activity was due to ^{210}Pb and half was due to ^{210}Bi, the slope would be twice as large as that of a pure ^{210}Pb standard. As after chemical separation, the final activity is due to ^{210}Pb only, if counting is done immediately, and as standards are processed along with samples, subtraction of the ^{210}Bi activity is only of theoretical importance. The calibration curves of standards taken through the procedure were in agreement with theoretical values when bismuth was removed from the counting standard by an extraction from 4 M hydrochloric acid solution with diethylammonium dithiocarbamate in carbon tetrachloride [6].

The choice of the dithizone extraction method was based on the selectivity of the reaction, which assures a fast efficient separation of lead from a rock matrix. The choice of solvents was made for convenience in discarding layers. The few elements that would be expected to follow lead through the procedure (Tl, In) are usually much lower in concentration in rocks than lead and thus offer no problem in the determination. An important point of the procedure is adequate washing of the organic phase to remove thoroughly iron, aluminum, and other elements that would compete with lead for EDTA.

The agreement of literature values of lead in the U.S. Geological Survey

standard rocks with the present method confirms the absence of interference from other elements and the reproducibility of the method. The recoveries of lead from most rocks were usually 75—95 %. However, yields from ultramafic rocks, e.g., DTS-1 and PCC-1, were often 50 % or less because of the large amount of nickel, which consumes the dithizone before lead can be extracted. In such cases it may be desirable to use additional extractions by means of fresh dithizone to insure that the amount of lead recovered is sufficient for a substoichiometric reaction with EDTA. The choice of EDTA as the complexing reagent instead of simply extracting lead by using a substoichiometric amount of dithizone as described by Ruzicka and Stary [6] was based on calculations from equations and data given in the literature [6, 13]. These indicate that because of the relatively low extraction constant of lead when dithizone in carbon tetrachloride is used, the threshold pH for substoichiometric extraction would have to be controlled very closely to give reproducible results at the 1-μg level. However, when EDTA is the complexing reagent, calculations based on the equations given by Greenland and Campbell [10] and Briscoe and Dodson [12] indicate that the reaction could theoretically be applied below 0.1 μg of lead. However, problems of blanks,even under the best conditions, together with problems of reaction rates at these levels, would most likely limit the usefulness of the method to about 0.1 μg of lead.

The extraction of excess of lead was a problem initially. Equations given by Briscoe and Dodson [12] and data in the literature [14] indicate that extraction with 5 ml of 10^{-5} M dithizone (equivalent to 5 μg of lead) should be well below the maximum allowed before a breakdown of the EDTA—lead complex occurs at the $5 \cdot 10^{-7}$ M EDTA level. Reproducibility was improved by using a lower concentration of dithizone and by performing several extractions.

The reaction of lead with EDTA at room temperature produced erratic results at lower concentrations of lead. As reproducible results were obtained upon heating, the problem was probably due to the slowness of the reaction between EDTA and lead at the 1-μg level. A hot-air dryer was found to be useful by allowing the solution to be heated to boiling in about 1 min without removing the contents from the separatory funnel. When higher concentrations of lead and EDTA are used, heating should not be necessary if a reasonable time is allowed for reaction.

By using the mixing procedure described by Greenland and Campbell [9], where the phases in the separatory funnel are mixed by using a 1-mm i.d. capillary tube connected to a compressed air source, or, in this case, compressed nitrogen, it is easy to perform separations on 18 samples within 4 h.

Analysis of standard rocks

The accuracy and precision of the method was estimated by determining lead in replicate splits of eight U.S. Geological Survey standard rocks and comparing these results with the literature values.

It can be seen from Table 1 that the standard deviation for the method is less than 10 % for the range of concentration in the various rock types. The accuracy of the method by comparison with the literature values appears to be good.

TABLE 1

Lead ($\mu g\ g^{-1}$) in U.S. Geological Survey standard rocks

Rock	Lead concn. mean	No. of detns.	Standard deviation	Flanagan [13] averages	Isotope-dilution mass spectrometry
G-2	30.5	6	1.3	31.2	30.8 [15]
AGV-1	36.1	6	0.8	35.1	36.53 [17]
GSP-1	56.2	7	3.8	51.3	58.7 [16]
BCR-1	14.6	6	0.8	17.6	13.56 [14]
W-1	7.3	9	0.7	7.8	—
G-1	44.9[a]	3	—	48	—
DTS-1	9.7[a]	3	—	14.2	—
PCC-1	10.2[a]	2	—	13.3	—

[a]Ranges were 43.7—46.3 for G-1, 9.1—10.4 for DTS-1, and 10.1—10.3 for PCC-1.

REFERENCES

1 J. Korkish and H. Gross, Talanta, 21 (1974) 1025.
2 R. Moldan, I. Rubeska and M. Miksovsky, Anal. Chim. Acta, 50 (1970) 342.
3 C. Iida and K. Yamasaki, Anal. Lett., 5 (1970) 251.
4 J. W. Arden and N. H. Cole, Anal. Chem., 46 (1974) 2.
5 T. J. Barnes, J. W. Murphy, J. W. Gramlich and W. R. Shields, Anal. Chem., 45 (1973) 1881.
6 J. Růžička and J. Stary, Substoichiometry in Radiochemical Analysis, Pergamon Press, Oxford, 1968.
7 J. Stary and J. Růžička, Talanta, 18 (1971) 1.
8 J. Růžička and J. Stary, Talanta, 11 (1964) 691.
9 L. P. Greenland and E. Y. Campbell, Anal. Chim. Acta, 60 (1972) 159.
10 L. P. Greenland and E. Y. Campbell, Anal. Chim. Acta, 67 (1973) 29.
11 E. G. Lillie and L. P. Greenland, Anal. Chim. Acta, 69 (1974) 313.
12 G. B. Briscoe and A. Dodson, Talanta, 14 (1967) 1051.
13 F. J. Flanagan, Geochim. Cosmochim. Acta, 37 (1973) 1189.
14 A. Ringbom, Complexation in Analytical Chemistry, Interscience, New York, 1963.
15 B.R. Doe, M. Tatsumoto, M. Delevaux and Z.E. Peterman, as cited by F.J. Flanagan, ref. 13.
16 Z. E. Peterman, B. R. Doe and A. Bartel, as cited by F. J. Flanagan, ref. 13.
17 M. Tatsumoto, as cited by F. J. Flanagan, ref. 13.

Analytica Chimica Acta, 82 (1976) 349—367
©Elsevier Scientific Publishing Company, Amsterdam — Printed in The Netherlands

EXTRACTION PAR SOLVANTS FONDUS: I — ÉQUILIBRES DE DISTRIBUTION DU ZINC(II) ENTRE LE THIOCYANATE DE POTASSIUM ET LE PHÉNANTHRÈNE FONDUS (À 195 °C)

G. DURAND, M. BILLON et B. TRÉMILLON

Laboratoire d'Electrochimie Analytique et Appliquée, associé au CNRS, ENSCP, 11 rue Pierre-et-Marie-Curie, 75231 Paris Cedex 05 (France)

(Reçu le 26 Septembre 1975)

RÉSUMÉ

L'étude de la distribution de cations métalliques entre un sel fondu, le thiocyanate de potassium, et une phase organique fondue non miscible, le phénanthrène, a été entreprise, en commençant par l'ion Zn^{2+}. La température d'équilibre était de 195 °C. Le zinc(II) a été extrait sous l'influence de ligands organiques dissous dans le phénanthrène; trois dérivés organophosphorés — oxyde de tri-*n*-octylphosphine (TOPO), oxyde de triphénylphosphine (TPPO) et hexaméthylphosphorotriamide (HMPT) — et deux dérivés pyridiniques — 2, 2'-bipyridyle (bipy) et 1,10-phénanthroline (phen) — ont été utilisés comme agents d'extraction. L'étude de la variation du coefficient de distribution D_{Zn} en fonction de la concentration de ligand dans la phase organique a permis de déterminer la constitution des espèces extraites: $Zn(TOPO)_2(SCN)_2$, $Zn(HMPT)_2(SCN)_2$, $Zn(TPPO)_3(SCN)_2$, $Zn(bipy)(SCN)_2$ et $Zn(bipy)_2(SCN)_2$. Les constantes des équilibres d'extraction correspondants ont été déterminées. La valeur du coefficient de distribution peut être abaissée par complexation du zinc(II) par l'ion cyanure dans la phase saline. Les espèces extraites par les agents organophosphorés et le 2,2'-bipyridyle sont les mêmes. Deux associations $Zn(phen)(SCN)_2$ et $Zn(phen)_3(CN)_2$ ont pu être mises en évidence dans ces conditions. Les constantes de formation des complexes zinc(II)-cyanure dans KSCN fondu ont été tirées des variations du coefficient de distribution.

Une représentation graphique, permettant l'exploitation pratique des résultats, des équilibres de distribution du cation métallique entre les deux phases liquides, variant sous l'influence du ligand organique $\bar{L}$ et du complexant inorganique CN^-, est proposée (diagrammes $\log [\bar{L}] = f(\log [CN^-])$ à D_{Zn} constant).

SUMMARY

A study of the distribution of cations between a molten salt, potassium thiocyanate and an immiscible molten organic phase, phenanthrene, has been undertaken with Zn^{2+} ions. The equilibrium temperature was 195 °C. Zinc(II) can be extracted by organic ligands dissolved in phenanthrene; three organophosphorus compounds — trioctylphosphine oxide (TOPO), triphenylphosphine oxide (TPPO) and hexamethylphosphorotriamide (HMPT) — and two pyridine-type compounds — 2,2'-bipyridyl (bipy) and 1,10-phenanthroline (phen) — can be used as extracting agents. A study of the variation of the distribution coefficient D_{Zn} in terms of ligand concentration in the organic phase has allowed the formulae of the extracted species to be determined as $Zn(TOPO)_2(SCN)_2$,

$Zn(HMPT)_2(SCN)_2$, $Zn(TPPO)_3(SCN)_2$, $Zn(bipy)(SCN)_2$ and $Zn(bipy)_2(SCN)_2$. The corresponding extraction equilibria constants have been determined. The value of the distribution coefficient may be lowered by complexing zinc(II) with cyanide ion in the salt phase. The species extracted with organophosphorus compounds and 2,2'-bipyridyl are the same. Two associations, $Zn(phen)(SCN)_2$ and $Zn(phen)_3(CN)_2$, have been found under these conditions. The formation constants of zinc(II)-cyanide complexes in molten KSCN have been deduced from distribution coefficient variations.

The use of a diagram which allows the results to be compared conveniently is proposed for the distribution equilibria of a metal cation between two liquid phases when an organic ligand $\overline{L}$ and an inorganic complexing agent CN^- are varied ($\log [\overline{L}] = f(\log [CN^-])$, with constant D_{Zn}).

L'extraction d'éléments métalliques dissous dans des sels fondus est un sujet d'intérêt suscité à la fois par la perspective de réaliser des séparations à haute température et par celle, plus spéculative, d'en tirer des connaissances sur les propriétés dans les sels fondus, selon une méthodologie largement éprouvée et exploitée pour l'étude des solutions aqueuses.

Les études de distribution d'ions mettant en jeu un sel fondu sont généralement classées en trois catégories, selon la nature de l'autre phase liquide non miscible [1].

En premier lieu, celle-ci peut être de nature organique, constituée par un agent d'extraction organique dilué dans un solvant organique fondu. En deuxième lieu, on peut envisager un second sel fondu pratiquement immiscible avec le premier, [2], en général sel ionisé, le second présentant alors un caractère covalent [3]. Enfin, la troisième catégorie correspond à la distribution entre un sel fondu et un métal liquide; généralement réalisés à haute température, ces équilibres ont été exploités pour des extractions de métaux notamment dans le domaine de l'énergie nucléaire [4, 5]. Ils font naturellement intervenir des phénomènes d'oxydoréduction et pas seulement des phénomènes de distribution.

Dans le cas de l'emploi d'une phase organique, celle-ci impose une température de travail relativement basse afin d'éviter sa dégradation ou sa volatilisation. C'est pourquoi les solvants organiques les plus fréquemment employés ont été des mélanges de polyphényles [6—17]. Herzog [18] a pour sa part utilisé une huile de silicone. Les sels fondus employés ont été le plus souvent des mélanges, de composition proche de celle d'un eutectique, de nitrates [6—28], de chlorures [29—31] ou de thiocyanates alcalins fondus [32—35]. La plupart des travaux effectués se rapportent à la distribution de cations métalliques, principalement des actinides et des lanthanides [6, 17—19, 22—24, 27, 34], mais quelques études ont été consacrées à la distribution d'anions [8, 36]. Certains travaux ont mis en évidence l'existence du phénomène de synergisme à haute température [14, 15, 17]. Par ailleurs, la possibilité de réaliser des électrodes sélectives fonctionnant en milieu fondu a été démontrée [16].

L'étude que nous avons réalisée concerne la distribution de cations métalliques entre le thiocyanate de potassium et le phénanthrène fondus,

sous la double influence, d'une part, de ligands dissous dans la phase organique et, d'autre part, d'un complexant des cations, l'ion cyanure, en phase inorganique. Le thiocyanate de potassium a été choisi comme phase inorganique parce que son point de fusion relativement bas, 173 °C, est compatible avec l'utilisation d'un solvant organique comme phase antagoniste. D'autre part, il a déjà fait l'objet de plusieurs études électrochimiques, notamment celles réalisées dans notre laboratoire [37—39], à la température de 195 °C. Afin de pouvoir utiliser ces connaissances, nous avons travaillé à la même température; celle-ci présente en outre l'avantage d'être éloignée de la température de début de décomposition du sel fondu (270 °C).

Le comportement des cations métalliques dans le thiocyanate de potassium fondu présente une double particularité. En premier lieu, on constate qu'ils sont très fortement "solvatés" par l'anion SCN^-; aussi, seuls des complexants plus puissants peuvent-ils le déplacer et s'associer aux cations métalliques; c'est le cas de l'ion cyanure. En second lieu, il a été constaté [39] qu'en solution concentrée, et parfois même diluée, de nombreux cations métalliques provoquent la décomposition de l'anion SCN^-, avec apparition de soufre, de cyanogène et d'un précipité de sulfure métallique. Le cation Zn^{2+} est l'un de ceux qui, au moins en solution diluée, ne provoquent pratiquement pas cette décomposition; c'est la raison pour laquelle nous avons choisi de commencer l'étude par la distribution de ce cation. Dans un mémoire suivant, nous compléterons par la description des résultats obtenus avec d'autres cations.

Le solvant organique que nous avons utilisé est le phénanthrène; il ne l'avait jamais été auparavant pour une telle étude. Il présente l'avantage d'être inerte chimiquement, thermiquement stable et surtout d'avoir une tension de vapeur suffisamment faible à 195 °C: 25 mm de Hg. Les divers agents d'extraction utilisables doivent naturellement être suffisamment solubles dans le phénanthrène et stables thermiquement. C'est le cas des dérivés organophosphorés et des dérivés pyridiniques que nous avons choisis. Le pouvoir d'extraction de ces molécules est lié à leur caractère de ligand vis-à-vis des cations métalliques. Avec les dérivés organophosphorés (oxyde de tri-*n*-octylphosphine (TOPO), oxyde de triphénylphosphine (TPPO) et hexaméthylphosphorotriamide (HMPT)), la liaison est assurée par les doublets d'électrons de l'atome d'oxygène [40]. La force de cette liaison dépend des substituants liés à l'atome de phosphore; l'action de ceux-ci se fait sentir de deux manières: d'une part par un effet inductif qui s'exerce sur le site donneur d'électrons, d'autre part par un effet stérique qui peut modifier l'accessibilité de ce site. La nature des complexes extraits dépend donc de ces deux actions [41]. Les propriétés chélatantes des deux composés pyridiniques que nous avons utilisés [2,2′-bipyridyle (bipy) et 1,10-phénanthroline (phen)] sont dues aux doublets d'électrons des deux atomes d'azote de ces molécules.

Un tel système biphasé n'ayant fait jusqu'à présent l'objet d'aucune recherche publiée, nous avons tout d'abord vérifié l'immiscibilité des deux solvants, condition évidemment nécessaire pour que le système soit utilisable

pour réaliser des extractions. Nous avons déterminé, après agitation des deux phases puis décantation, la solubilité du phénanthrène dans la phase inorganique à 195 °C; cette solubilité est inférieure à 5.10^{-3} mol kg^{-1}. De la même manière, nous avons observé que la solubilité du thiocyanate de potassium dans le phénanthrène à la même température est de l'ordre de 10^{-5} mol kg^{-1}.

PARTIE EXPERIMENTALE

Produits

Le thiocyanate de potassium que nous avons utilisé est le produit Merck de qualité "pour analyses". Le sel a été séché à l'étuve vers 150 °C pendant 12 h, puis conservé en dessiccateur. La masse volumique du thiocyanate de potassium fondu à 195 °C est 1,68 g cm^{-3} [42]. Le phénanthrène (Prolabo "pur") a été employé comme solvant organique sans traitement préalable. Il se liquéfie à 101 °C. Sa masse volumique à 195 °C est 1,00 g cm^{-3} [42]. Les agents d'extraction ont été utilisés sans purification préalable.

Dispositif expérimental

Nous avons réalisé une enceinte thermorégulée à 195 ± 1 °C en utilisant un bain de sable fluidisé Techne type SBL2, au sein duquel étaient plongées des cellules d'extraction en verre pyrex. Une pièce de verrerie en forme de pipette et comportant à sa partie inférieure des pales hélicoïdales permettait d'effectuer à la fois l'agitation des deux phases jusqu'à l'établissement de l'équilibre puis, après décantation, le prélèvement, à la température opératoire, d'une partie aliquote de l'une ou l'autre phase.

Méthodes analytiques mises en oeuvre

Le zinc(II) présent dans la phase saline a été dosé par absorption atomique (spectrophotomètre Perkin Elmer,type 303) après mise en solution aqueuse d'une partie aliquote de la phase inorganique. La limite de détection accessible par cette méthode est de l'ordre de 10^{-6} M; l'irreproductibilité des mesures conduit à une incertitude de 10 % sur la détermination du coefficient de distribution.

Les espèces présentes dans la phase organique (solidifiée) ont été dosées après réextraction par une solution aqueuse, en procédant ainsi: une partie aliquote de la phase organique est dissoute dans le tétrachlorométhane ou dans le chloroforme (dans le cas de la 1,10-phénanthroline) puis agitée en présence d'une solution aqueuse d'EDTA 0,1 M. Le complexe Zn(II)—EDTA, les ions K^+, SCN^- et CN^- sont ré-extraits; seuls les ligands organiques demeurent dans le tétrachlorométhane ou dans le chloroforme. Les dosages de zinc(II) et de potassium ont été effectués par absorption atomique. En ce

qui concerne le cyanure, du fait de la présence simultanée d'un grand excès d'anions thiocyanate, nous avons utilisé la méthode de Fischer et Brown [43], qui est sensible et sélective. Le produit coloré de la réaction a été dosé par absorptiométrie à l'aide d'un spectrophotomètre Cary 14.

RESULTATS ET INTERPRETATION

Extraction du thiocyanate de potassium

Nous avons constaté que la présence de ligands organiques dissous dans le phénanthrène modifie la miscibilité du thiocyanate de potassium avec la phase organique. Celle-ci augmente avec la concentration de ligand. Cela s'explique par la formation d'une association entre le thiocyanate de potassium et le ligand, soluble dans le phénanthrène.

En présence d'un ligand L, la distribution du thiocyanate de potassium peut être exprimée par l'équilibre

$$K^+ + SCN^- + p\bar{L} \leftrightharpoons \overline{K(L)_pSCN}$$

(les barres désignent les espèces en phase organique).

L'application de la loi d'action de masses à cet équilibre donne la relation

$$K = \overline{[K(L)_pSCN]}/[K^+][SCN^-][\bar{L}]^p$$

Les concentrations de potassium et de thiocyanate étant initialement très élevées (10 mol kg^{-1}), on peut estimer qu'elles demeurent constantes au cours de l'extraction; on définit alors une constante apparente $K_{KSCN} = K[K^+][SCN^-]$. On peut écrire cette nouvelle constante sous une forme logarithmique, d'où

$$\log [\overline{K(L)_p(SCN)}] = \log K_{KSCN} + p \log [\bar{L}]$$

En représentant graphiquement cette expression pour chacun des ligands utilisés (Fig. 1), on détermine grâce à la pente des droites obtenues la formule des espèces extraites, et l'importance de l'extraction du thiocyanate de potassium. Les résultats obtenus sont rassemblés dans le Tableau 1.

On constate que, dans le domaine de concentration de ligand exploré, l'extraction du thiocyanate de potassium n'est jamais négligeable et qu'une proportion appréciable de ligand est associée à KSCN dans le phénanthrène. C'est avec la 1,10-phénanthroline que le phénomène est le plus marqué: un calcul montre qu'il subsiste seulement 74 % de ligand "libre", c'est-à-dire non associé au thiocyanate de potassium (cette valeur ne dépend pas de la concentration de phénanthroline ajoutée dans la phase organique; cela est également vrai pour le bipyridyle, mais ne l'est pas pour les trois autres ligands).

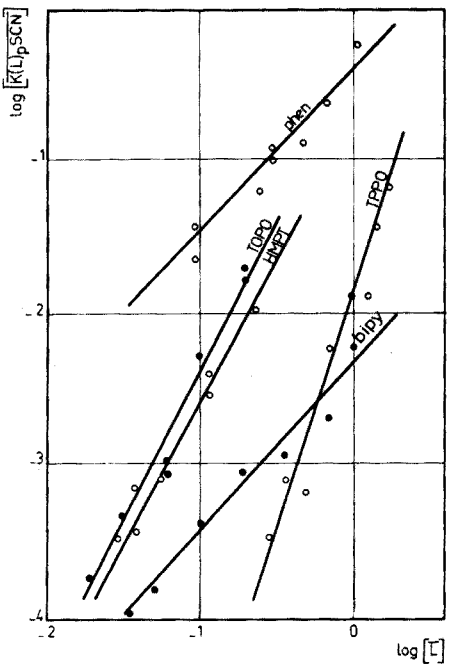

Fig. 1. Extraction du thiocyanate de potassium par les ligands organiques dissous dans le phénanthrène, à 195 °C.

TABLEAU 1

Extraction du thiocyanate de potassium par des ligands organiques L dissous dans le phénanthrène, à 195 °C

L	p	Formule de l'espèce extraite	$\log K_{KSCN}$ (conc. exprimées en mol kg^{-1})
TOPO	2,0 ± 0,4	$K(TOPO)_2(SCN)$	−0,4 ± 0,2
HMPT	1,8 ± 0,3	$K(HMPT)_2(SCN)$	−0,8 ± 0,4
TPPO	3,0 ± 0,5	$K(TPPO)_3(SCN)$	−1,9 ± 0,3
phen	1,1 ± 0,2	K(phen)(SCN)	−0,4 ± 0,1
bipy	1,1 ± 0,2	K(bipy)(SCN)	−2,4 ± 0,2

Extraction du cyanure de potassium dissous dans KSCN fondu

Le cyanure de potassium utilisé pour complexer le zinc(II) dans la phase inorganique peut, de la même manière que le thiocyanate de potassium, être partiellement extrait par les ligands dissous dans le phénanthrène.

En pratique, nous avons constaté que la 1,10-phénanthroline seule extrait notablement le cyanure de potassium, selon l'équilibre

$K^+ + CN^- + \overline{phen} \leftrightharpoons \overline{K(phen)CN}$

avec

$K = [\overline{K(phen)CN}]/[K^+][CN^-][\overline{phen}]$

Pour les mêmes raisons que lors de l'extraction du thiocyanate de potassium, on définit une constante apparente $K_{KCN} = K[K^+]$. L'expérience fournit la valeur $\log K_{KCN} = -0{,}80 \pm 0{,}15$. Cette valeur est suffisamment petite pour que l'adjonction de cyanure à KSCN fondu ne modifie pratiquement pas la proportion de phénanthroline libre dans le phénanthrène.

Extraction du zinc(II) dissous dans KSCN fondu, à l'aide d'agents organophosphorés et de dérivés pyridiniques

D'une façon générale, le zinc(II) en solution dans le thiocyanate de potassium est extrait par un ligand L selon l'équilibre

$Zn^{2+} + n\overline{L} + m SCN^- + (m-2)K^+ \leftrightharpoons \overline{Zn(L)_n K_{(m-2)} SCN_m}$

(en supposant qu'on n'extrait pas de complexes polynucléaires. Zn^{2+} symbolise l'ion zinc(II) solvaté par SCN^-, en réalité $Zn(SCN)_x^{2-x}$).

L'équilibre est caractérisé par la constante apparente K_{Zn}

$K_{Zn} = [\overline{Zn(L)_n K_{(m-2)}(SCN)_m}]/[Zn^{2+}][\overline{L}]^n$

L'expression du coefficient de distribution étant par définition

$D_{Zn} = [\overline{Zn(L)_n K_{(m-2)}(SCN)_m}]/[Zn^{2+}]$

On a finalement

$\log D_{Zn} = \log K_{Zn} + n \log [\overline{L}]$

Pour chacun des ligands *organophosphorés* utilisés, nous avons étudié la variation du coefficient de distribution du zinc(II) en fonction de la concentration du ligand; les résultats obtenus sont représentés Fig. 2.

L'analyse des droites obtenues permet de déterminer le nombre de molécules de ligand associées à un ion Zn^{II} et la valeur de la constante K_{Zn} de l'équilibre d'extraction. Par ailleurs, en comparant les quantités de potassium dosées dans le phénanthrène en présence et en l'absence de zinc(II), nous avons constaté qu'aucune des espèces extraites ne contient de potassium. Pour les trois ligands organophosphorés, l'équilibre de distribution est donc

$Zn^{2+} + 2SCN^- + n\overline{L} \leftrightharpoons \overline{Zn(L)_n(SCN)_2}$

avec n=2 pour L=TOPO et HMPT, et n=3 pour L=TPPO. Les résultats sont rassemblés dans les Tableaux 2 et 3.

Dans le cas du *2,2'-bipyridyle*, nous avons constaté que la variation du coefficient de distribution du zinc n'est linéaire que pour des concentrations de ligand inférieures à 0,3 mol kg^{-1}; dans cette zone, il se forme donc le

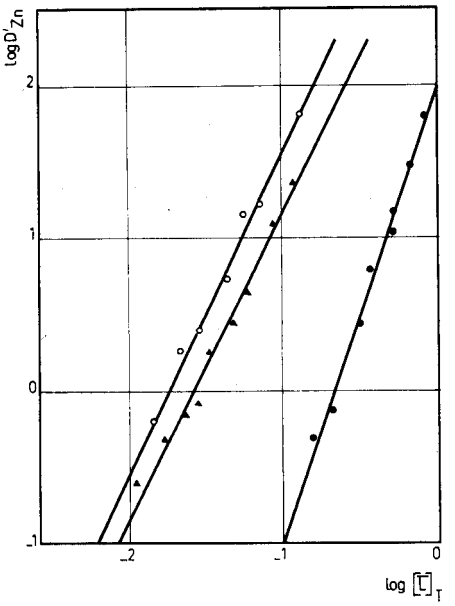

Fig. 2. Distribution du zinc(II) entre KSCN fondu et des solutions de ligands organophosphorés dans le phénanthrène (à 195 °C).
• TPPO ○ TOPO ▲ HMPT

TABLEAU 2

Caractéristiques des droites de régression correspondant à l'analyse statistique de $\log D_{Zn} = f(\log [\bar{L}]_T)$
(incertitude déterminée pour un taux de confiance de 95 %)

L	n	$\log K_{Zn}$ (ordonnée à l'origine, conc. exprimées en mol kg^{-1})
TPPO	3,0 ± 0,2	2,0 ± 0,1
TOPO	2,1 ± 0,2	3,8 ± 0,2
HMPT	2,0 ± 0,2	3,2 ± 0,3

complexe 1:1 (n = 1,10 ± 0,05, $\log K/\text{kg mol}^{-1}$ = 1,6 ± 0,1). Par dosage de potassium dans la phase organique, il a été montré que l'espèce extraite est $Zn(bipy)(SCN)_2$. Pour les concentrations de 2,2'-bipyridyle supérieures à 0,3 mol kg^{-1}, l'infléchissement de la courbe suggère qu'un complexe supérieur (1:2 ou même 1:3) apparaît, ce qui a été ensuite vérifié.

La *1,10-phénanthroline* extrait pratiquement quantitativement Zn^{II} et il n'a pas été possible de réaliser l'étude directe de l'équilibre de distribution avec ce ligand. En effet, les quantités de zinc demeurant en phase

TABLEAU 3

Potassium extrait par les ligands organophosphorés dans le phénanthrène

L	$[\overline{L}]$ (mol kg^{-1})	$[\overline{Zn^{2+}}]$ (mol kg^{-1})	$[\overline{K^+}]$ (mol kg^{-1})
TPPO	0,503	0	$(0,7 \pm 0,1).10^{-3}$
		$0,8.10^{-3}$	$(0,6 \pm 0,1).10^{-3}$
TOPO	0,021	0	$(1,8 \pm 0,9).10^{-4}$
		$1,0.10^{-3}$	$(1,8 \pm 0,9).10^{-4}$
HMPT	0,028	0	$(3,4 \pm 0,1).10^{-4}$
		$0,55.10^{-3}$	$(3,6 \pm 0,2).10^{-4}$

inorganique sont alors trop petites pour que la méthode de dosage utilisée fournisse le coefficient de distribution avec suffisamment de précision.

Extraction du zinc(II) en présence de cyanure dissous dans le thiocyanate de potassium

L'extraction du zinc(II) par les différents ligands organiques précédents peut être modifiée par complexation du cation métallique dans le thiocyanate de potassium par l'ion cyanure, celle-ci provoquant une régression de l'extraction, fonction de la stabilité des complexes Zn^{II}—cyanure dans KSCN.

Outre cette action sur le cation métallique dans la phase inorganique, le cyanure peut également modifier l'équilibre d'extraction en s'associant au zinc(II) dans la forme extraite. L'équilibre de distribution peut alors s'écrire

$$Zn(CN)_r^{(2-r)} + mSCN^- + (m + s - 2)K^+ + n\overline{L}$$
$$\rightleftharpoons \overline{Zn(L)_n(SCN)_m(CN)_sK_{(m+s-2)}} + (r - s)CN^-$$

Influence du cyanure sur l'extraction du zinc(II) par les dérivés organophosphorés

La variation du coefficient de distribution D'_{Zn} en présence de cyanure à la concentration 0,1 mol kg^{-1}, en fonction de la concentration de chacun des ligands dans le phénanthrène, est représentée sur la Fig. 3. Les pentes des droites obtenues étant les mêmes qu'en l'absence de complexant, la stoechiométrie des complexes zinc(II)—ligand organique n'a donc pas varié (Tableau 4).

Les quantités de potassium et de cyanure dosées dans le phénanthrène étant sensiblement les mêmes en présence et en l'absence de zinc(II) (Tableau 5), aucune des espèces extraites ne contient ces ions. La nature des composés extraits est donc la même qu'en l'absence de cyanure.

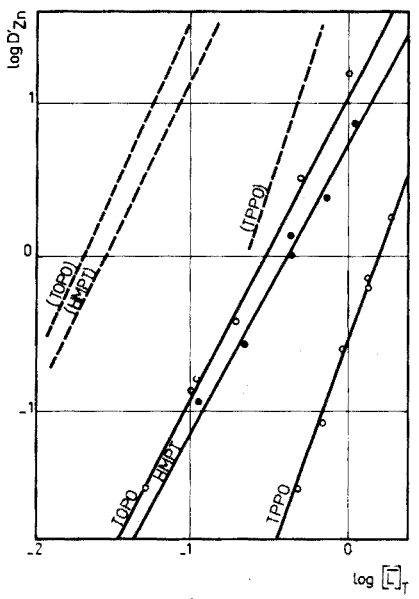

Fig. 3. Influence du cyanure de potassium dissous dans KSCN fondu sur l'extraction du zinc(II) par les ligands organophosphorés,
---------- En l'absence de KCN
———— En présence de KCN 0,1 mol kg^{-1}

TABLEAU 4

Caractéristiques des droites de régression correspondant à l'analyse statistique de $\log D'_{Zn} = f(\log [\bar{L}]_T)$
(Incertitude déterminée pour un taux de confiance de 95 %)

L	n	$\log K'_{Zn}$ (ordonnée à l'origine) (conc. exprimées en mol kg^{-1})
TOPO	2,0 ± 0,2	1,1 ± 0,1
TPPO	2,8 ± 0,3	−0,63 ± 0,07
HMPT	1,8 ± 0,3	−0,7 ± 0,1

Influence du cyanure sur l'extraction du zinc(II) par les dérivés pyridiniques

La présence de cyanure en phase inorganique diminuant la valeur des coefficients de distribution du zinc, il a été possible de mesurer D'_{Zn} à forte concentration de ligand en phase organique. Cela a permis de confirmer l'existence d'un complexe 1:2 du zinc(II) avec le 2,2′-bipyridyle et d'étudier l'équilibre d'extraction du zinc(II) par la 1,10-phénanthroline.

TABLEAU 5

Potassium et cyanure extraits par les ligands organophosphorés dans le phénanthrène

L	$[\overline{L}]$ (mol kg^{-1})	$[\overline{Zn^{2+}}]$ (mol kg^{-1})	$[\overline{K^+}]$ (mol kg^{-1})	$[\overline{CN^-}]$ (mol kg^{-1})
TOPO	0,102	0	$(2,5 \pm 0,1)10^{-3}$ [a]	[b]
		$1,25.10^{-3}$	$(2,4 \pm 0,1)10^{-3}$	[b]
HMPT	0,114	0	$(2,9 \pm 0,1)10^{-3}$	[b]
		$1,10.10^{-3}$	$(3,2 \pm 0,1)10^{-3}$	[b]
TPPO	0,144	0	$(3,8 \pm 0,1)10^{-2}$	5.10^{-4}
		$5,18.10^{-3}$	$(3,9 \pm 0,2)10^{-2}$	$7,5.10^{-4}$

[a] Incertitude déterminée pour un taux de confiance de 95 %.
[b] Concentration inférieure à 2.10^{-5} mol kg^{-1}, limite de détection de la méthode de dosage.

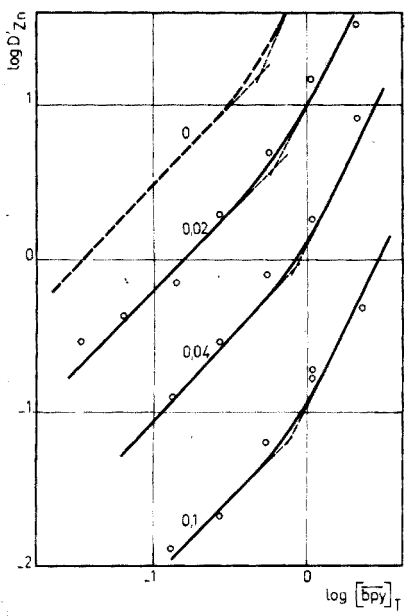

Fig. 4. Influence de la complexation du zinc(II) par le cyanure sur l'extraction par le 2,2'-bipyridyle. (Sur chaque courbe est portée la concentration de cyanure dans le thiocyanate de potassium (en mol kg^{-1})).

2,2'-Bipyridyle

Les courbes $\log D'_{Zn} = f(\log [bipy]_T)$ obtenues (Fig. 4) montrent que deux complexes sont extractibles, selon la concentration du ligand: complexe 1:1 au-dessous de 0,7 mol kg^{-1} et complexe 1:2 au-dessus. Aucun d'eux ne contient de potassium ni de cyanure, quelle que soit la concentration du

cyanure dans KSCN. Les formules des espèces extraites sont donc les mêmes que précédemment: $Zn(bipy)(SCN)_2$ et $Zn(bipy)_2(SCN)_2$. Les deux équilibres d'extraction correspondant à ces associations sont caractérisés chacun par une constante, respectivement K'_1 et K'_2. De ces deux constantes on déduit l'équation de chacune des deux parties linéaires du diagramme $\log D'_{Zn} = f(\log [\overline{bipy}])$ de la Fig. 4, soit

$$\log D'_{Zn} = \log K'_1 + \log [\overline{bipy}] \quad ([\overline{bipy}] \ll 0{,}7 \text{ mol kg}^{-1})$$

$$\log D'_{Zn} = \log K'_2 + 2 \log [\overline{bipy}] \quad ([\overline{bipy}] \gg 0{,}7 \text{ mol kg}^{-1})$$

Pour une concentration donnée de cyanure, l'intersection des deux segments de droites a lieu pour une concentration de ligand telle que

$$\log [\overline{bipy}] = \log K'_1 - \log K'_2 = -0{,}16$$

L'abcisse du point d'intersection est donc indépendante de la concentration de cyanure dans le thiocyanate de potassium.

1,10-Phénanthroline

La variation de $\log D'_{Zn}$ en fonction de $\log [\overline{phen}]$ pour différentes concentrations de cyanure dans KSCN (Fig. 5) met en évidence la possibilité

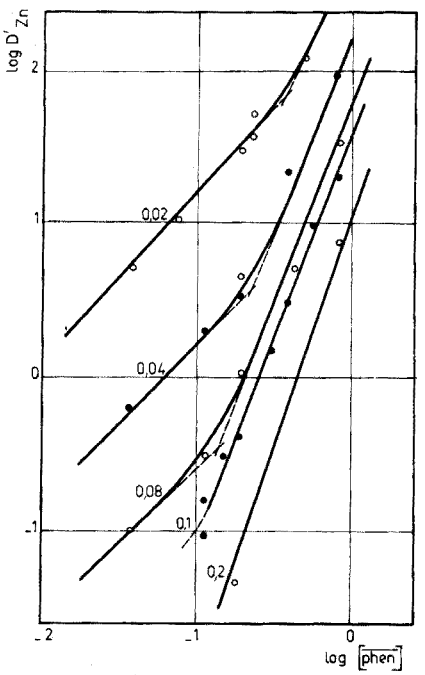

Fig. 5. Influence de la complexation du zinc(II) par le cyanure sur l'extraction par la 1,10-phénanthroline. (Sur chaque courbe est portée la concentration de cyanure dans le thiocyanate de potassium (en mol kg^{-1})).

TABLEAU 6

Caractéristiques des droites de régression correspondant à l'analyse statistique de $\log D'_{Zn} = f(\log [\overline{phen}])$, en présence de KCN dans KSCN.
(Incertitude déterminée pour un taux de confiance de 95 %)

$[CN^-]$ (mol kg^{-1})	n	$\log K$ (ordonnée à l'origine) (conc. exprimées en mol kg^{-1})
0,02	1,1 ± 0,1	2,3 ± 0,3
0,1	2,8 ± 0,3	1,7 ± 0,2

TABLEAU 7

Détermination de la constitution des espèces extraites par la 1,10-phénanthroline, en présence de cyanure dans KSCN.
(Concentrations exprimées en mol kg^{-1}. Incertitude déterminée pour un taux de confiance de 95 %)

$[CN^-]$	$[\overline{phen}]$	$[\overline{Zn^{2+}}]$	$[\overline{K^+}]$	$[\overline{CN^-}]$	Formule de l'espèce extraite
0,02		0	$(1,1 \pm 0,1)10^{-1}$	2.10^{-4}	
	0,303	$1,9.10^{-3}$	$(1,0 \pm 0,1)10^{-1}$	3.10^{-4}	$Zn(phen)(SCN)_2$
		0	$(2,6 \pm 0,1)10^{-1}$	$3,7\ 10^{-3}$	
0,1	0,71	$1,7.10^{-3}$	$(2,6 \pm 0,1)10^{-1}$	$7,2\ 10^{-3}$	$Zn(phen)_3(CN)_2$

d'extraire deux complexes respectivement 1:1 et 1:3 (Tableau 6). La détermination de la formule complète des espèces extraites est réalisée grâce au dosage du cyanure et du potassium dans le phénanthrène, en présence et en l'absence de zinc(II) (Tableau 7). On constate qu'aux fortes concentrations de cyanure dans KSCN deux anions CN^- sont associés à chaque ion zinc(II) extrait.

Ainsi, selon la concentration de cyanure en phase inorganique, on peut écrire (au moins) deux équilibres d'extraction:

— en présence de cyanure 0,02 mol kg^{-1} par exemple, on a

$$Zn(CN)_r^{(2-r)} + 2SCN^- + \overline{phen} \rightleftharpoons \overline{Zn(phen)(SCN)_2} + r\ CN^-$$

d'où

$$\log D'_{Zn} = \log K'_1 + \log [\overline{phen}] - r \log [CN^-] \qquad (1)$$

— en présence de cyanure 0,1 mol kg^{-1}, on a

$$Zn(CN)_r^{(2-r)} + 3\ \overline{phen} \rightleftharpoons \overline{Zn(phen)_3(CN)_2} + (r-2)\ CN^-$$

d'où

$$\log D'_{Zn} = \log K'_3 + 3 \log [\overline{phen}] - (r-2) \log [CN^-] \qquad (2)$$

Pour chaque concentration de cyanure, nous avons extrapolé jusqu'à leur intersection les droites vérifiant les relations (1) et (2). L'abscisse de cette intersection, qui a pour expression

$$\log [\overline{\text{phen}}] = \tfrac{1}{2}(\log K'_1 - \log K'_3) - \log [CN^-],$$

doit varier avec la concentration de cyanure dans la phase inorganique, ce que l'expérience confirme (Fig. 5).

CONCLUSIONS

Une première conclusion suggérée par les formules des complexes extraits par le phénanthrène est la variation de la coordinence de l'ion Zn^{II} selon la nature du ligand, ainsi que celle de l'anion complexant associé. En admettant que les ligands phosphorylés sont monodentés et les deux autres bidentés, on trouve ainsi des nombres de coordinence de 4 [$Zn(TOPO)_2(SCN)_2$, $Zn(HMPT)_2(SCN)_2$, $Zn(bipy)(SCN)_2$, $Zn(phen)(SCN)_2$]; de 5 [$Zn(TPPO)_3(SCN)_2$]; de 6 [$Zn(bipy)_2(SCN)_2$]; et même de 8 [$Zn(phen)_3(CN)_2$]. S'il est courant d'attribuer à Zn^{II} les nombres de coordinence 4 et 6, les autres valeurs sont plus surprenantes. On peut néanmoins noter que la coordinence 5 a déjà été signalée dans le cas de liaisons zinc^{II}—oxygène; une étude par rayons X de l'acétylacétonate de zinc trimérisé, $Zn_3(acac)_9$, a en effet montré que deux des ions Zn^{2+}y possèdent la coordinence 5 tandis que le troisième y possède la coordinence 6 [44].

La coordinence de 5 a été également observée dans le monohydrate $Zn(acac)_2(H_2O)$ [45, 46].

La possibilité de coordinence 8 de Zn^{2+}n'est pas encore clairement établie, bien qu'elle ait été signalée pour des associations telles que $Zn(bipyO_2)_3(ClO_4)_2$ (où $bipyO_2$ = *N*, *N'*-dioxyde-2,2'bipyridyle) [47], ainsi que dans le cas de liaisons zinc(II)—azote: le complexe $Zn(NH_3)_6Br_2$ est connu (sa structure cubique a été établie), également $Zn(en)_3Cl_2$ (en = éthylènediamine). Ainsi, les associations Zn^{2+}—ligand—anion que nous avons mises en évidence dans le phénanthrène sont en accord avec ces résultats antérieurs.

En second lieu, il a été possible de déduire de la variation du coefficient de distribution conditionnel D'_{Zn} (mesuré à concentration variable de cyanure en phase inorganique et à concentration constante de ligand en phase organique), les constantes de formation des complexes zinc—cyanure dans le thiocyanate de potassium fondu. Celles-ci ont été calculées à partir de la relation

$$D'_{Zn} = D_{Zn}/F_o(CN)$$

où D_{Zn} est le coefficient de distribution mesuré en l'absence de cyanure et

$$F_o(CN) = \sum_{i=0}^{i=r} (\beta i [CN^-]^i)$$

TABLEAU 8

Constantes de formation des complexes zinc—cyanure (Concentrations en mol kg^{-1})

Formule	Mesures de distribution	Mesures électrochimiques [39]
$ZnCN^+$	$\log \beta_1 = 2{,}1$	
$Zn(CN)_2$		$\log \beta_2 = 5{,}1$
$Zn(CN)_3^-$	$\log \beta_3 = 5{,}7$	$\log \beta_3 = 6{,}6$
$Zn(CN)_4^{2-}$		$\log \beta_4 = 8{,}6$

La résolution mathématique du système d'équation $F_o = f([CN^-])$ par calcul de la courbe polynomiale des moindres carrés a mis en évidence deux complexes $ZnCN^+$ et $Zn(CN)_3^-$ dans le domaine de concentration étudié et permis de calculer leur constante de formation (Tableau 8).

Ces résultats sont en contradiction avec ceux qui ont été obtenus antérieurement par polarographie [39]. Ayant redéterminé les contantes des complexes zinc—cyanure par électrochimie (polarographie et potentiométrie), nous avons pu constater leur concordance avec les résultats d'Eluard et Tremillon (Fig. 6). Il apparaît que pour une même concentration de cyanure

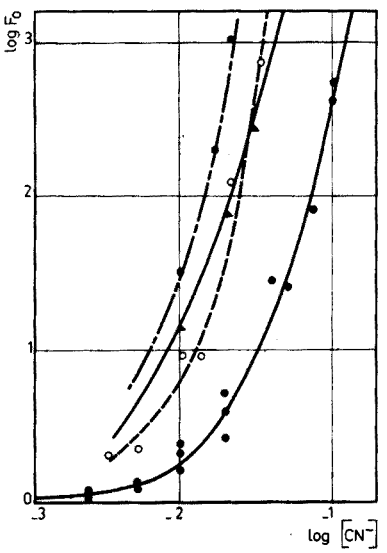

Fig. 6. Détermination des constantes de formation des complexes zinc(II)—cyanure par électrochimie et extraction,

—●— Extraction.

------○------ Extraction en présence de mercure.

———— Polarographie [39].

- —●— - Voltampérométrie avec une électrode d'argent amalgamé.

▲ Potentiométrie à courant nul avec une électrode de zinc amalgamé.

ajoutée, la valeur de F_0 obtenue est plus élevée par polarographie que par extraction. Des deux hypothèses envisageables pour expliquer cet écart—déterminations polarographiques exactes et résultats de l'extraction faussés par une réaction annexe consommant des ions CN^-; ou valeurs exactes par extraction et résultats erronés par polarographie car une réaction parasite produit du cyanure—seule la seconde a été retenue.

En effet, la réaction lente de décomposition du thiocyanate par le mercure a déjà été signalée [39]; elle conduit à la formation de cyanure en solution

$$Hg\downarrow + SCN^- \rightarrow HgS\downarrow + CN^-$$

Dans les conditions de la polarographie (présence au fond de la cellule de mercure provenant de la chute des gouttes) il n'a pas été possible de mettre en évidence une augmentation de la concentration de cyanure en solution. La réaction a lieu uniquement lorsqu'une importante quantité de mercure est agitée avec peu de thiocyanate (respectivement 100 g pour 20 g). Il faut donc supposer que les mesures polarographiques sont faussées par la formation de cyanure au niveau de la couche de diffusion. Cela s'est trouvé confirmé par une étude voltampérométrique réalisée avec une électrode d'argent amalgamé; dans ce cas le mercure de l'électrode n'étant pas renouvelé, il a été constaté qu'à la fin du tracé d'une courbe courant—potentiel la surface de l'électrode est recouverte d'une pellicule noire de sulfure mercurique; par ailleurs c'est avec une telle électrode que les valeurs de $F_0(CN)$ s'éloignent le plus de celles obtenues par extraction (Fig. 6).

Une confirmation de la justesse des mesures de distribution est fournie par la comparaison des valeurs calculées des constantes conditionnelles d'extraction $\log K'_1$ et $\log K'_2$ (obtenues à partir de $\log K_1$ et $\log K_2$) aux valeurs expérimentales correspondantes. L'accord entre les 2 séries de valeurs est bon (Tableau 9). Dans le cas présent l'extraction est donc une méthode de détermination des constantes de formation plus fiable que la polarographie.

TABLEAU 9

Comparaison des valeurs calculées et des valeurs expérimentales des constantes K'_1 et K'_2 (Résultats calculés à partir des mesures polarographiques (1) et de distribution (2). Concentrations exprimées en mol kg^{-1}).

		[CN^-]			
		0	0,02	0,04	0,1
$\log K'_1$ [=$\log K_1 - \log F_0(CN)$]	calc. (1)		−0,5	−1,5	−3,0
	calc. (2)		0,72	0,05	−1,11
	exp.	$\log K_1 = 1,6$	0,8	0,0	−1,0
$\log K'_2$ [=$\log K_2 - \log F_0(CN)$]	calc. (1)		−0,3	−1,3	−2,8
	calc. (2)		0,92	0,25	−0,91
	exp.	$\log K_2 = 1,8$	1	0,2	−0,8

En dernier lieu, une exploitation commode de nos résultats est possible grâce à l'établissement de diagrammes qui rendent compte de la double influence sur les équilibres de distribution des deux facteurs considérés: la concentration du ligand organique L dissous dans le phénanthrène et celle de l'ion cyanure dissous dans le thiocyanate de potassium. Ces diagrammes permettent de mettre en évidence les domaines de prédominance des différentes espèces dans chacune des phases, en fonction de ces deux facteurs; on peut alors en déduire des courbes de variation du rendement d'extraction de l'ion zinc(II).

En effet, pour chacun des exemples que nous avons considéré, on peut écrire l'équilibre d'extraction sous la forme simplifiée (faisant abstraction des ions SCN^- dont l'activité ne varie pas):

$$M(CN)_r^{-} + n\,\overline{L} \leftrightharpoons \overline{M(L)_n} + r CN^-$$

On en déduit:

$$\log [\overline{L}] = \frac{\log D'_{Zn}}{n} - \frac{\log K'_{Zn}}{n} + \frac{r}{n} \log [CN^-] \qquad (1)$$

Ainsi, connaissant r, n et $\log K'_{Zn}$ d'après l'étude réalisée, on peut établir à l'aide de la relation (1) un abaque de courbes $\log [\overline{L}] = f(\log [CN^-])$ dont

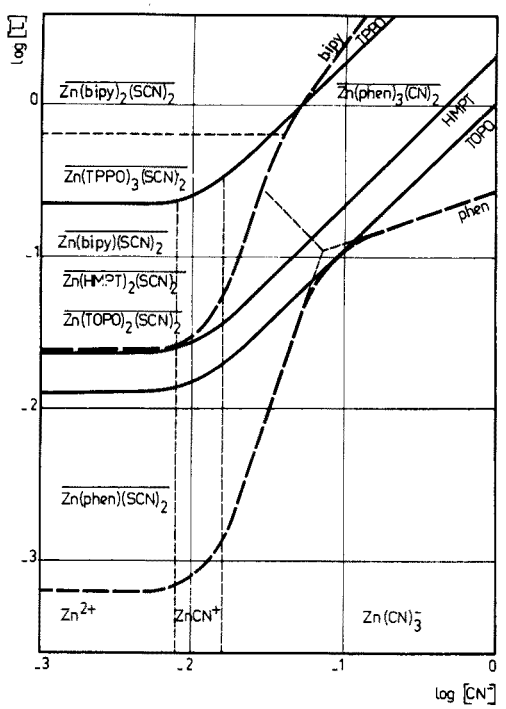

Fig. 7. Diagramme $\log [\overline{L}] = f(\log [CN^-])$ à $D'_{Zn} = 1$ (rendement d'extraction de 50 % pour des masses égales des 2 phases liquides).

chacune correspond à une valeur fixée du coefficient de distribution D'_{Zn}. Un point de l'une de ces courbes donne les valeurs de $[\bar{L}]$ et de $[CN^-]$ permettant d'obtenir la valeur correspondante de D'_{Zn}, donc une valeur du rendement d'extraction. De l'abaque, il est aisé de déduire comment varie le rendement d'extraction du zinc dans le système considéré, soit en fonction de log $[\bar{L}]$ à $[CN^-]$ fixé (notamment $[CN^-] = 0$), soit en fonction de log $[CN^-]$ à $[\bar{L}]$ fixé.

La Fig. 7 représente les courbes correspondant uniquement à $D'_{Zn} = 1$. Ces courbes séparent le plan en deux régions: d'un côté le domaine (log $[\bar{L}]$ $-$ log $[CN^-]$) où $D'_{Zn} > 1$ — le zinc est préférentiellement dans la phase organique; de l'autre, le domaine où $D'_{Zn} < 1$ — le zinc est préférentiellement dans le sel fondu.

BIBLIOGRAPHIE

1 Y. Marcus, dans D. Dyrssen, J. O. Liljenzin et J. Rydberg (Éds.) Solvent Extraction Chemistry, North Holland Pub. Co, Amsterdam, 1967, p. 555.
2 Y. Marcus, dans J. Braunstein, G. Mamantov et G. P. Smith (Éds.) Advances in Molten Salt Chemistry, vol. 1, Plenum Press, New York, 1971, p. 82.
3 K. F. Guenther, J. Inorg. Nucl. Chem., 27 (1965) 1427.
4 C. F. Baes Jr., dans W. R. Grimes U.S.A.E.C., Rep. ORNL 3708 (1964) 311.
5 L. M. Ferris, J. C. Mailen, F. J. Smith, E. D. Nogueira, J. H. Shaffer, D. M. Moulton, C. J. Barton et R. G. Ross, dans Proc. 3rd Intern. Protoact. Conf., Elmau, 1969.
6 D. H. Gruen, S. Fields, P. Graaf et R. L. McBeth, Proc. 2nd Intern. Conf., Genève (1958) 112 et 940.
7 O. Vittori, Thèse, Lyon, 1971.
8 I. J. Gal, J. Mendez et J. W. Irvine Jr., Inorg. Chem., 7 (1968) 985.
9 M. Zangen et Y. Marcus, Isr. J. Chem., 2 (1964) 49, 155.
10 M. Zangen, Isr. J. Chem., 2 (1964) 91; J. Phys. Chem., 69 (1965) 1835; Inorg. Chem., 7 (1968) 131, 138, 1202; J. Inorg. Nucl. Chem., 31 (1969) 867.
11 M. Zangen, dans A. S. Kertes et Y. Marcus (Éds.) Solvent Extraction Research, Wiley Interscience, New York, 1968, p. 151; et dans D. Dyrssen, J. O. Liljenzin et J. Rydberg (Éds.) Solvent Extraction Chemistry, North Holland Pub. Co, Amsterdam, 1966, p. 581.
12 Y. Marcus, M. Liquornik, L. F. Friedman et M. Zangen, Israel A.E.C. Report, 1963.
13 O. Vittori et M. Porthault, C. R. Acad. Sci. Ser. C, 271 (1970) 1362.
14 O. Vittori et M. Porthault, Bull. Soc. Chim. Fr., 7 (1971) 2789.
15 J. Targhetta, J. Inorg. Nucl. Chem., 36 (1974) 445.
16 J. Mesplede, Thèse, Lyon, 1972.
17 J. Foos, Thèse, Paris, 1974.
18 D. Herzog, Thèse, Paris, 1963; Rapport CEA-R-2628 (1964).
19 O. Vittori et M. Porthault, C. R. Acad. Sci. Ser. C, 269 (1969) 967; 267 (1968) 383.
20 C. Gonnet, O. Vittori et M. Porthault, C. R. Acad. Sci. Ser. C, 267 (1968) 714.
21 J. Mesplede et M. Porthault, C. R. Acad. Sci. Ser. C, 269 (1969) 1036; Bull. Soc. Chim. Fr., 10 (1970) 3771.
22 O. Vittori et M. Porthault, Bull. Soc. Chim. Fr., 11 (1970) 4169.
23 J. Mesplede et M. Porthault, J. Inorg. Nucl. Chem., 33 (1971) 4275.
24 C. Gonnet et M. Porthault, Bull. Soc. Chim. Fr., 11 (1970) 4157.
25 M. Guillermier, O. Vittori et M. Porthault, C. R. Acad. Sci. Ser. C, 271 (1970) 1565.

26 R. Giroud et M. Porthault, Bull. Soc. Chim. Fr., 6 (1971) 2371.
27 J. Foos et J. Mesplede, J. Inorg. Nucl. Chem., 34 (1972) 2051.
28 J. Foos et R. Guillaumont, Bull. Soc. Chim. Fr., 6 (1971) 3129.
29 Z. Borkowska, M. Mielcarski et M. Taube, Nucléonika, 10 (1966) 31.
30 M. Mielcarski et M. Taube, Nucléonika, 7 (1962) 595.
31 Z. Borkowska et M. Taube, Nature (London), 192 (1961) 745.
32 K. S. de Haas, P. A. Brink et P. Crowther, J. Inorg. Nucl. Chem., 33 (1971) 4301.
33 J. G. V. Lessing, P. A. Brink et K. F. Fouche, J. Inorg. Nucl. Chem., 35 (1973) 2009.
34 J. David et M. Zangen, dans A. S. Kertes et Y. Marcus (Éds.) Solvent Extraction Research, Wiley Interscience, New York, 1968, p. 219.
35 M. Zangen, J. David-Auslaender et A.S. Kertes, J. Inorg. Nucl. Chem., 36 (1974) 218.
36 Z. C. Tan et J. W. Irvine Jr., Inorg. Chem., 11 (1972) 1701.
37 G. Metzger, Thèse, Paris, 1964; Rapport CEA-R-2566 (1964).
38 A. Eluard, Thèse, Paris, 1965.
39 A. Eluard et B. Tremillon, J. Electroanal. Chem., 13 (1967) 208.
40 J. C. White, dans Symposium on Solvent Extraction in the Analysis of Metals, ASTM Spec. Tech. Publ. no 238, 1958.
41 D. D. Perrin, Organic Complexing Reagents, Interscience, New York, 1964.
42 M. Billon, Thèse, Paris, 1974.
43 F. B. Fischer et J. S. Brown, Anal. Chem., 24 (1952) 1440.
44 M. J. Bennett, F. A. Cotton, R. Eiss et R. Elder, Nature (London), 213 (1967) 174.
45 E. L. Lippert et M. R. Truter, J. Chem. Soc., (1960) 4996.
46 H. Montgomery et E. C. Lingafelter, Acta Crystallogr. 16 (1963) 748.
47 P. G. Simpson, A. Vinciguerra et J. V. Quagliano, Inorg. Chem. 2 (1963) 282.

Analytica Chimica Acta, 82 (1976) 369—375
©Elsevier Scientific Publishing Company, Amsterdam — Printed in The Netherlands

CHELATING ION-EXCHANGERS CONTAINING N-SUBSTITUTED HYDROXYLAMINE FUNCTIONAL GROUPS PART III. HYDROXAMIC ACIDS

F. VERNON and H. ECCLES

The Ramage Laboratories, Department of Chemistry and Applied Chemistry, University of Salford, Salford M5 4WT (England)

(Received 14th August 1975)

SUMMARY

The synthesis of a poly(hydroxamic acid) ion exchange resin from cross-linked poly-(acrylonitrile) is described. This ion exchanger is highly selective for vanadium, iron and mercury; its fast equilibration rate makes it suitable for column work. Curves showing the dependence of the total capacity against pH are presented for nine metal species. This ion exchanger is more stable to loading — acid washing cycles than the hydroxamic acid resins reported previously.

In 1869, Lossen [1] reported that diethyl oxalate reacts with hydroxylamine to give a compound which he named oxalohydroxamic acid. The hydroxamic acids have since been prepared by many methods; the most general reaction is that between an ester and hydroxylamine. The hydroxamic acids form chelate complexes of high stability with a wide range of metal ions, e.g. the iron(III)—tris—acetohydroxamic acid complex has a log stability constant [2] of 11.42, whereas the value for the aluminium complex [3] is 4.4. The copper(II) complex has a log stability constant [2] of 7.9, suggesting that an iron—copper separation is feasible with this ligand.

A variety of techniques for the production of polymeric hydroxamic acids has been proposed. Kern and Schulz [4] prepared a linear polyhydroxamic acid from poly(methyl methacrylate) and hydroxylamine in the presence of sodium methoxide with an 80 % conversion of polyester groups to hydroxamic acid. The linear polymeric ligand gave precipitates with a variety of metal ions.

As described in part II [5], several workers [6—8] attempted the preparation of polyhydroxamic acids from conventional cross-linked polycarboxylic acid cation exchangers. The conversion of carboxylic acid to acid chloride, prior to reaction with hydroxylamine, is the controlling factor in the synthesis. Since poor conversions were obtained, an alternative preparation of a poly(acid chloride) was given [5] and the controlling factor in the production of a poly(acylphenylhydroxylamine) ion exchanger was reported to be the limited stability of phenylhydroxylamine. It appeared that the

much more reactive hydroxylamine would yield a better product, albeit a poly(hydroxamic acid). Marshall [9] had attempted to prepare such a chelate ion exchanger from polyacrylonitrile fibres by hydrolysis, acid chloride formation, and reaction with hydroxylamine. A one-stage synchronous reaction of linear polyacrylonitrile fibres with sodium hydroxide and hydroxylamine yielded a fibrous polymer with iron(III) and copper(II) capacities of 1.3 and 5 mmol g^{-1}, respectively.

Linear amidoxime polymers were produced by Schouteden [10] by treating polyacrylonitrile solution with hydroxylamine in dimethylformamide. A commercial preparation of acrylamide from acrylonitrile [11] involves hydrolysis of the latter with 90 % sulphuric acid. Consequently, the route to a macroporous, cross-linked poly(hydroxamic acid) ion exchanger appears to involve acid hydrolysis of the corresponding acrylonitrile — divinylbenzene copolymer to the amide, and reaction of the resulting acid amide with hydroxylamine. Such a synthesis is described here. The resulting polymer is vastly superior to those poly(hydroxamic acids) previously reported and which are described [12], as unstable toward relatively concentrated acids and bases and undergo rearrangements during regeneration. The cross-linked poly(hydroxamic acids) are selective for iron(III), vanadium(V) and mercury(II) and are completely stable when treated with 5 M hydrochloric or sulphuric acids. Preliminary results suggest that the resin is also stable in 1 M sodium hydroxide solution.

EXPERIMENTAL

Preparation of polyhydroxamic acid resin

Acrylonitrile (135 g) was passed through a column of activated alumina to remove inhibitors, 15 g of 54 % divinylbenzene solution was added, and the mixture was heated to 68—69 °C in a constant temperature bath. α,α-Azobisisobutyronitrile (0.6 g) dissolved in 30 ml of toluene was added, and the mixture was stirred at constant temperature for 18—19 min. At the first appearance of milkiness, the mixture was poured rapidly into 1 l of 20 % sodium chloride solution containing 10 g of sodium lauryl sulphate. The suspension was heated to 75 °C with efficient stirring and maintained at this temperature for 1 h to complete the polymerization. The suspension was then stirred at 90 °C for 8 h; the polymer, which changed from white to a creamy colour was then filtered, washed with water to remove the soap and with methanol to remove the toluene, and was washed finally with water. The macroporous, cross-linked polyacrylonitrile was then hydrolysed.

The polymer (70 g) was stirred for 16 h at 70—80 °C with 50 % (v/v) sulphuric acid. The hydrolysed polymer was filtered, washed thoroughly with water, and treated for 18 h at 80—85 °C with 1 l of 1 M sodium acetate solution containing 66 g of hydroxylamine. The resulting white polymer was washed with water, sulphuric acid solution, and again with water until

sulphate-free. A small sample was vacuum-dried for elemental microanalysis; the bulk was stored in the fully swollen form for metal capacity determinations.

Procedures

Sodium capacity. A sample of the moist polymer (0.5 g), equilibrated with 25 ml of 0.25 M sodium bicarbonate solution for 12 h, was filtered and washed thoroughly with distilled water. The total filtrate was acidified with 25 ml of 0.25 M hydrochloric acid, boiled to expel carbon dioxide, and back-titrated with 0.25 M sodium hydroxide solution.

Multivalent metal capacities. The behaviour of Fe(III), Fe(II), Co(II), Ni(II), Cu(II), V(V), UO_2(II), Hg(II), and Pb(II) was studied by the methods reported previously [5, 13].

Water regain. The fully swollen resin was dried at 105 °C overnight to determine the weight of water associated with 1 g of resin.

Equilibration rate. This was determined as reported previously [14]. The time to 50 % equilibration ($t_{\frac{1}{2}}$) for the resin in contact with a 14 mM iron(III) solution was taken as the equilibration rate. The effect of ionic concentration on the rate was examined by determining the value for a 5 mM iron(III) solution, and the effect of changing the metal ion was studied with 14 mM copper solution.

Resin stability. A sample of the moist exchanger (0.5 g) was equilibrated with 100 ml of 0.02 M iron(III) ammonium sulphate solution for 48 h; after washing, the iron was eluted with 5 M hydrochloric acid for 24 h and the iron content was determined spectrophotometrically. The regenerated resin was re-equilibrated with a further ion solution and subsequently eluted by 5 M hydrochloric acid; this procedure was repeated 20 times. Iron capacities at pH 2.7 were thus obtained for 20 loading—acid washing cycles, and the variations were studied for resin instability.

Diffuse reflectance spectroscopy. The polyhydroxamic acid resin in the hydrogen form is cream coloured; the copper, iron, and vanadium forms are green, red and brown respectively. The contributions of the hydroxamic and carboxylic acid groupings present in the metal-loaded resins, together with the corresponding metal-loaded polycarboxylic resins and the metal—propionohydroxamic acid complexes, were studied by diffuse reflectance spectroscopy. All spectra were recorded on a Unicam SP800 with SP890 diffuse reflectance accessory. The copper, iron and vanadium forms of the polyhydroxamic acid resin were examined undiluted, as was the copper—propionohydroxamic acid complex. The iron and vanadium—

propionohydroxamic acid complexes were adsorbed from solution on sodium sulphate, which was dried and ground. The copper and iron forms of a polycarboxylic resin were ground and diluted with magnesium oxide.

RESULTS AND DISCUSSION

Table 1 summarizes the properties of the poly(hydroxamic acid) ion exchanger. The sodium—hydrogen exchange from sodium hydrogen carbonate solution is a measure of the carboxylic acid groups produced by hydrolysis of the nitrile beyond the amide stage. The hydroxamic acid units are incapable of reacting with hydrogen carbonate; this was verified by determining the sodium capacity of the copper-loaded resin produced by equilibrating the exchanger with copper sulphate solution at pH 4. The hydroxamic groups are complexed, whereas the carboxylic groups cannot take up copper at this pH. The sodium capacity of the copper-loaded form of the resin was also 3.3 mmol g^{-1}. The vanadium capacity at pH 3 determines only the oxime-carbonyl grouping and not the carboxylic content. The vanadium capacity of 1.7 mmol g^{-1} is a measure of the "available" hydroxamic acid groups, and is not of much use in determining the structure of the ion exchanger. The sodium capacity shows that 25 % of the original nitrile units have been converted into carboxylic acids; if the remainder were unchanged a nitrogen content of 18.0 % would be found but if the nitrile groups had been converted completely to hydroxamic acids, a nitrogen content of 11.25 % would result. The experimental value of 13.0 % nitrogen indicates 75 % conversion of nitrile groups to hydroxamic units; therefore in the resin 25 % nitrile groups have been hydrolysed, 19 % remain as nitrile, and 56 % have been converted to hydroxamic acid. The equilibration rate of 10 min to 50 % saturation was obtained by equilibrating resin samples with 14 mM solutions of iron(III). The rate was highly dependent on metal ion concentration and also on the nature of the ion; 5 mM iron(III) solution gave $t_{\frac{1}{2}}$ = 50 min whilst 14 mM copper(II) solution gave a value of 45 min.

The polyhydroxamic resin was completely stable to loading and acid washing with 5 M hydrochloric acid. Iron(III) capacities for the first and twentieth cycle were 1.26 mmol g^{-1}, with all values in 20 determinations lying between 1.18 and 1.38 mmol g^{-1}.

TABLE 1

Physical and chemical characteristics of the polyhydroxamic acid resin

Percent cross-linking	5
Water regain	1.53 $g.g^{-1}$
Particle size (95 %)	0.7—1.7 mm diam
Sodium—hydrogen exchange capacity	3.3 mmol g^{-1}
Vanadium capacity at pH 3	1.7 mmol g^{-1}
Equilibration rate ($t_{\frac{1}{2}}$)	10 min

The diffuse reflectance studies gave rather inconclusive results for copper and iron. Table 2 lists the absorbance maxima of the various species examined. Only for vanadium is there a clear indication of chelate complexing by the hydroxamic group. The copper reflectance maxima gave more information than the absorbance maxima when it was found that the polyhydroxamic acid, polycarboxylic acid and propionohydroxamic acid complex of copper had reflectance maxima of 529, 500 and 519 nm respectively.

Metal ion capacity

The total capacity versus pH contours for the metals studied are shown in Fig. 1. The resin demonstrates high selectivity for vandium, as would be expected from the solvent extraction behaviour of benzohydroxamic acid with this element. The curves suggest three different forms of vanadium-resinate depending on pH. The optimum conditions for two of these forms are well-defined. Figure 2 shows a capacity maximum for vanadium from

TABLE 2

Diffuse reflectance spectroscopic results

Species		λ_{max} (for absorbance) (nm)
Iron(III)	resinate	455
	propionohydroxamate	470
	carboxylate	415, 472, 528
Copper(II)	resinate	787
	propionohydroxamate	685
	carboxylate	813
Vanadium(V)	resinate	472
	propionohydroxamate	465
	carboxylate	—

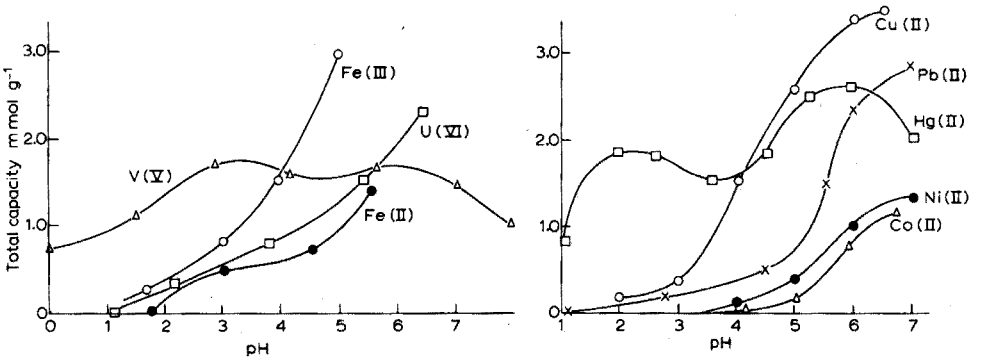

Fig. 1. Total capacity versus pH curves for metal ions and the poly(hydroxamic acid) ion exchanger.

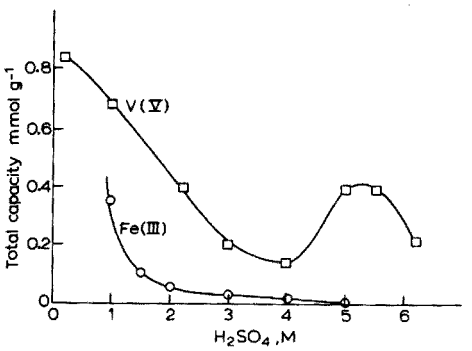

Fig. 2. Total capacity of the exchanger for vanadium(V) and iron(III) as a function of sulphuric acid molarity.

5 M sulphuric acid, under which conditions the metal would appear to be separated from all other metals studied. If this is the 1 : 1 complex, the sterically unlikely 1 : 2 complex would be responsible for the maximum at pH 3. The ill-defined maximum at pH 6 could result from the carboxylate groupings in the resin. The material also demonstrates high selectivity for iron(III) and its separation from copper, cobalt and nickel is possible. The third metal for which the material demonstrates selectivity is mercury(II); it should be possible to isolate mercury from all other species, except vanadium, by employing column operation at pH 1. This resin therefore combines the useful property of differentiating between iron(III) and iron(II), demonstrated by the polymeric aroyl—phenylhydroxylamine described earlier [13], with the selectivity for mercury demonstrated by the alkyl—phenylhydroxylamine resin [5]. Separations of copper from cobalt and nickel at pH 3.5 are possible. The high capacity for uranium from almost neutral solutions could be utilized as a specific technique for this element with a sodium carbonate eluant.

The high affinity of the resin for vanadium poses a problem, as the only way to recover all the vanadium is by destruction of the resin. Several eluting systems were evaluated for vanadium, the residual metal on the resin being determined by wet-ashing; the capacity for vanadium was as high as 0.2 mmol g^{-1} from 10 M sulphuric acid. The percentages of vanadium recovered from other eluting systems were: 4 M sulphuric acid, 69 %; 5 M hydrochloric acid, 74 %; 5 M ammonia, 27 %; 20 mM citric acid, 40 %. Preliminary experiments suggest that 1 M sodium hydroxide may be the most effective eluant.

The effect of a competing ligand in solution was studied with citrate and EDTA. Only small reductions in the total capacity for vanadium and uranium were caused by citrate, whereas the total capacities for iron, copper, cobalt and nickel were greatly reduced in the presence of this ligand. The extent of the competing ligand effect may be seen from the case of iron(III), where the total capacities at pH 3.0 in the presence of sulphate, acetate, EDTA and citric acid were 1.4, 0.7, 1.3 and 0.6 mmol g^{-1}, respectively.

Conclusions

The hydroxamic acid ion exchanger produced from macroporous cross-linked polyacrylonitrile demonstrates high selectivity for vanadium, iron and mercury. A fast equilibration rate is an advantageous feature of the chelating ion exchanger which, in contrast to previous hydroxamic acid exchangers, was completely stable to metal loading and acid washing cycles. The simple preparation from relatively cheap materials invites comparison with the commercially available imino-diacetic acid ion exchanger, but the nature and extent of their metal capacities suggests that these two chelating ion exchangers are complementary rather than competitive. Whereas the iminodiacetic acid exchanger is most useful for blanket extraction of metal ions above pH 5, the potential of the hydroxamic acid exchanger appears to lie in its ability to separate multivalent ions, e.g. iron from copper at pH 1.5, and copper from cobalt and nickel at pH 3.5. Future parts of this series will be concerned with such separations and with the analytical applications suggested.

REFERENCES

1 H. Lossen, Justus Liebigs Ann. Chem., 150 (1869) 314.
2 G. Anderegg, F. L'Eplattenier and G. Schwarzenbach, Helv. Chim. Acta, 46 (1963) 1400.
3 G. Anderegg, F. L'Eplattenier and G. Schwarzenbach, Helv. Chim. Acta, 46 (1963) 1409.
4 W. Kern and R. C. Schulz, Angew. Chem. Int. Ed. Engl., 69 (1957) 153.
5 F. Vernon and H. Eccles, Anal. Chim. Acta, 79 (1975) 229 (Part II).
6 G. Petrie, D. Locke and C. E. Meloan, Anal. Chem., 37 (1965) 919.
7 J. P. Cornaz, K. Hutschneker and H. Deuel, Helv. Chim. Acta, 40 (1957) 2015.
8 J. P. Cornaz and H. Deuel, Experientia 10 (1954) 137.
9 G. R. Marshall, Ph.D. Thesis, Bristol (1965).
10 F. L. M. Schouteden, Makromol. Chem. 24 (1957) 25.
11 R. E. Friedrich, G. D. Jones and S. N. Heiny, U.S. Patent, 3,130,229 (1964).
12 H. A. Flaschka and A. J. Barnard (Eds.), Chelates in Analytical Chemistry, Vol. I, Edward Arnold, London, 1967, p. 64.
13 F. Vernon and H. Eccles, Anal. Chim. Acta, 77 (1975) 145.
14 F. Vernon and H. Eccles, Anal. Chim. Acta, 72 (1974) 331.

Analytica Chimica Acta, 82 (1976) 377—390
© Elsevier Scientific Publishing Company, Amsterdam — Printed in The Netherlands

THE KINETICS AND MECHANISM OF THE CHROMOGENIC AND FLUOROGENIC INTERACTION BETWEEN NITRATE AND BIANTHRONYL IN CONCENTRATED SULFURIC ACID

M. MARCANTONATOS and B. NAWRATIL

Department of Inorganic and Analytical Chemistry, University of Geneva, Geneva (Switzerland)

(Received 6th July 1975)

SUMMARY

The chromogenic interaction between nitrate and bianthronyl ([9,9′-bianthracene]-9,9′-hydro-10,10′-dione) in 96 % sulfuric acid, which has been recently applied to the determination of nitrate traces, is investigated. It is shown that bianthronyl first degrades, via a bianthronyl—nitronium CT complex, to anthronyl cation and anthrone, the latter being oxidized to an anthronyl radical cation; and that both anthronyl cation and radical convert, by different oxidative paths, to anthraquinone. Analysis of the kinetic and spectral data suggests a catalytic action of nitronium ions, and the experimental results are fitted by an eleven-step reaction mechanism.

Traces of nitrate in natural waters can be readily determined [1] by a colorimetric method based on a red-colored intermediate formed in the reaction between bianthronyl (9,9′-bianthracene-9,9′-hydro-10,10′-dione) and nitrate in 96 % sulfuric acid. The general sequence of this reaction was described in the original communication [1]. In this paper, results from kinetic investigations, as well as data from absorption, fluorescence, phosphorescence and e.s.r. determinations, are summarized and discussed. Although the reaction is highly complex, it is possible, by analysis of the kinetic and spectral data, to propose a mechanism consistent with the experimental results.

EXPERIMENTAL

Apparatus

A Unicam SP 8000 spectrophotometer, a JES ME e.s.r. spectrometer (model ME-X), and an Aminco—Keirs phosphorimeter with a Houston Omnigraph recorder for phosphorescence decay determinations, were used. Mean lifetimes of the reacting mixture were obtained from total phosphorescence emission (P_t) decays, which were found to follow a $P_t = P_1^0 e^{-t/\tau_1} + P_2^0 e^{-t/\tau_2}$ relationship, except at the end of the reaction, where $\ln P_t = P_0 e^{-t/\tau}$ (emission of anthraquinone).

Reagents

Bianthronyl (Aldrich) and potassium nitrate (Merck G. R.) were purified as described previously [1]. Sulfuric acids were prepared from concentrated sulfuric acid (d = 1.84) and oleum (30 % SO_3) (Merck G. R.) and were checked conductometrically. Anthrahydroquinone was prepared by dithionite reduction of anthraquinone [2].

RESULTS AND DISCUSSION

Spectral investigations

As has been reported [1], the general reaction sequence is:

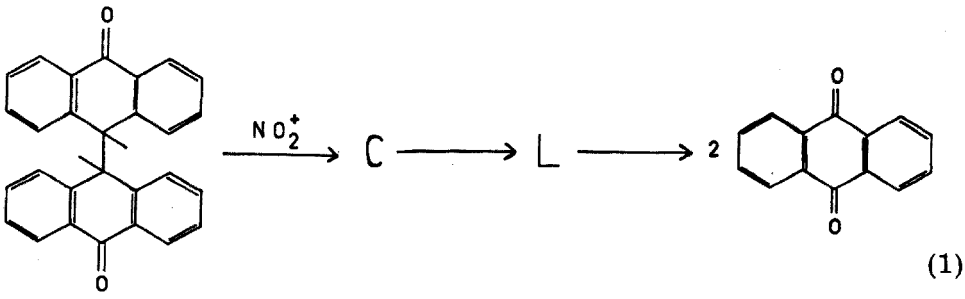

(1)

where C is the coloured species and L the luminescent compound, which in subsequent steps yields anthraquinone.

Kinetically, species C appears as a first intermediate, formed by a rate-determining step. To elucidate its nature, the electronic absorption spectrum of bianthronyl plus nitrate in sulfuric acid, at the beginning of the reaction, was compared with those of anthrone (A) and bianthrone (BA), which may be assumed as being C species or of closely related structure:

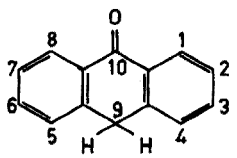

(A)

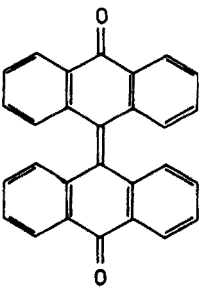

(BA)

As can be seen from Fig. 1, the general modification of the spectrum of

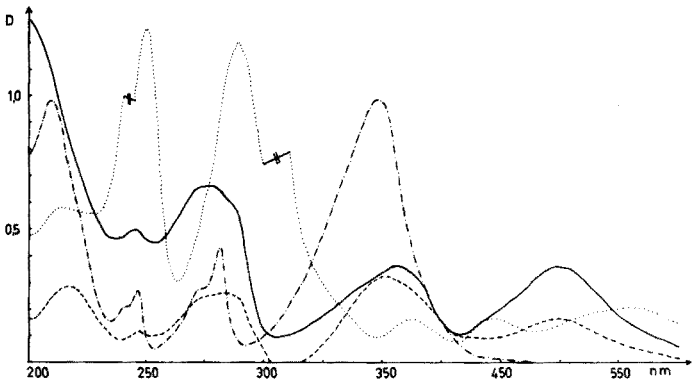

Fig. 1. Absorption spectra. Species C in 96 % H_2SO_4 (———). Bianthronyl, 10^{-5} M + 10^{-3} M NO_3^- in 100 % H_2SO_4 (- - - -). Bianthrone 10^{-5} M in 96 % H_2SO_4 (· · · ·). Anthrone $2 \cdot 10^{-5}$ M in 96 % H_2SO_4 (—·—·—). (* D > 2).

bianthronyl (B) and the hypo- and bathochromic shift of its characteristic, broad and intense, electron transfer band (347 nm), cannot be assigned, as was done by Meyer [3], to the formation of bianthrone. In fact, with the exception of the 200-nm band, which is distorted by the presence of nitrate, the 200—400-nm spectrum of the initially reacting system is closer to that of anthrone, and its visible absorption is quite different from the spectrum of bianthrone, indicating scission of bianthronyl to species of anthronyl structure.

Further support for this assignment comes from the more informative e.s.r. spectra of anthrone plus nitrate and bianthronyl plus nitrate in sulfuric (96 %) solutions. Figure 2 shows that the two spectra are identical, both being characterized by a triplet and a secondary doublet. These spectra, recorded at room temperature, are quite surprising, since one would expect an a (4H) quintet (positions 2,3,6,7), two a (2H) triplets (positions 4,5 and 1,8) and one a (1H) doublet, if one of the 9 position protons lies perpendicular to the *p*-orbitals of the π system (lack of splitting constant associated with this proton). However, detailed structural studies by e.s.r. spectroscopy were out of the scope of the present work, and further e.s.r. investigations, especially at low and variable temperatures, in order to obtain better hyperfine structures, were not undertaken.

What is noteworthy, from a mechanistic point of view, is the fact that the anthronyl radical cation is not the red species C. In fact, Fig. 3 shows that its formation is consecutive to C, since the point of inflexion of the e.s.r. signal intensity vs. time curve appears about the maximum of the A_{500} vs. time variation.

Stabilization of the red color for a long period can be achieved when the bianthronyl—nitrate reaction takes place in 99 % sulfuric acid. Moreover, red 96 % or 99 % sulfuric solutions present interesting thermochromic effects,

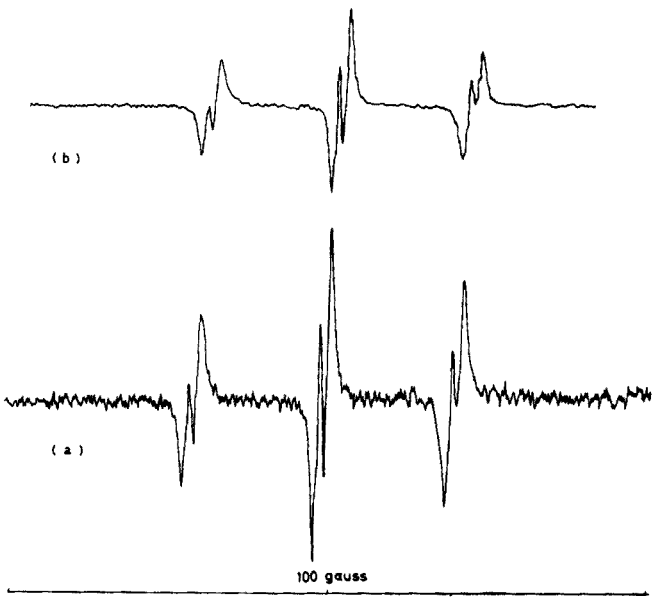

Fig. 2. E.s.r. spectra of bianthronyl + NO_3^- (a) and anthrone + NO_3^- (b) in 96 % H_2SO_4 (room temp.).

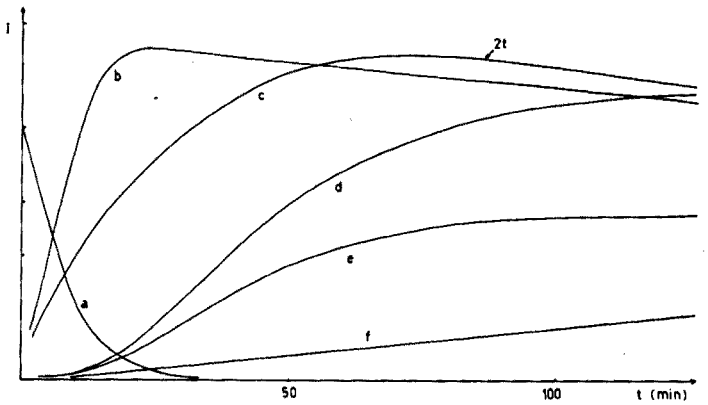

Fig. 3. Intensity vs. time curves. a: Bianthronyl u.v. absorption at 347 nm. b and c: Red-coloured species absorption at 500 nm in 96 % and 99 % H_2SO_4. d: Fluorescence emission at 457 nm. e: E.s.r. signal. f: U.v. absorption at 273 nm (anthraquinone); 96 % H_2SO_4.

both solutions changing reversibly to pale-yellow when the temperature is changed from 25 °C to 77 K.

The closeness of the absorption spectra of anthrone/H_2SO_4 and bianthronyl—nitrate/H_2SO_4 (Fig. 1) and the stabilization of the 500-nm absorbance with increasing sulfuric acid concentration, can probably be

attributed to the presence of the red anthronyl cation (A^+), formed simultaneously with anthrone in the first steps of the reaction.

The observed thermochromic effect also favors this assignment, since one could expect that, with a change of temperature to 77 K, an $A^+ \bar{O}SO_3H$ contact complex would convert to an association complex with a significant stability constant, in which charge delocalization would be considerably depressed:

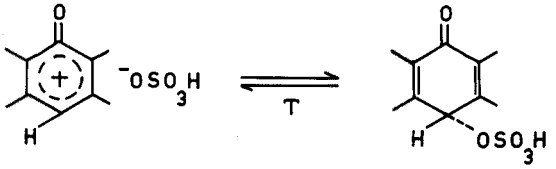

(2)

Consequently, it seems plausible to assume the following reactions as initial steps in the bianthronyl—nitrate interaction:

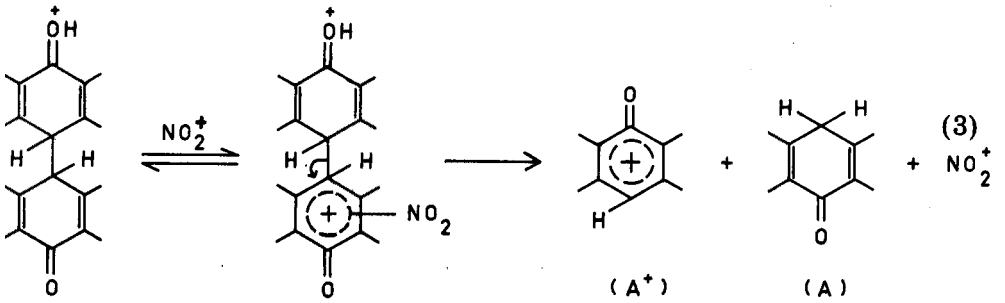

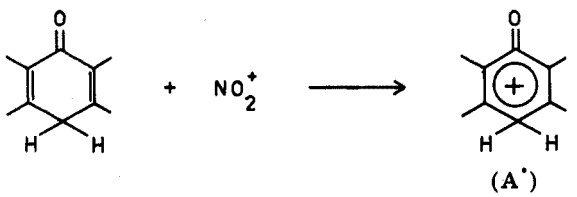

(4)

As indicated in Fig. 3, the fluorescent species is formed consecutively to the red cation A^+ and, strikingly enough, parallel to the radical cation $A^{\cdot}$. It is not however evident that this radical is the luminescent species, since it cannot be excluded that the latter originates, by a rapid step, from the anthronyl cation A^+.

If 96 % sulfuric solutions of bianthronyl and nitrate are, at about the time of maximum red color intensity, frozen to 77 K, the "cryochromic" effect is accompanied by photoluminescence. The 99 % sulfuric acid solutions do not exhibit any detectable emission, but as the 99 % acid is affected by atmospheric humidity, luminescence emission appears slowly from the top

of the solid matrix. This suggests that hydrated solvent species react rapidly (and probably reversibly) with the anthronyl cation to give the luminescent compound. Further support in favor of this behavior comes from the abrupt diminution of the red color and the increase of emission intensity when the solvent is changed from 96 % to lesser percentages of sulfuric acid.

It cannot be suggested that solvated water molecules $H_2O(H_3O^+)$ accomplish the transformation of carbocation to luminescent compound, since, in 96 % sulfuric acid, their activity is very low (ca. 10^{-5}) [4]. Yet, the relevant ionization equilibria for numerous ROH compounds are given [5] by:

$$ROH + 2H_2SO_4 \rightleftharpoons R^+ + H_3O^+ + 2HSO_4^- \qquad (5)$$

and the pK_{ROH} values of some of them allow values of the J_0 acidity function up to 98.9 % sulfuric acid to be calculated. Consequently, it is not implausible to assume the reaction:

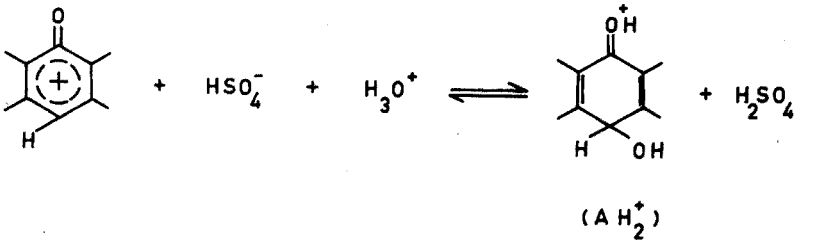

(6)

as a possible step in the bianthronyl—nitrate interaction. In fact, in 99 % sulfuric acid, the red carbocation is not totally stabilized but decays less rapidly than in 96 % acid (Fig. 3). This may account for step (6), since oxanthrone can be readily oxidized by dissolved oxygen to anthraquinone, so that the rate of carbocation (A^+) decay must depend on the $[HSO_4^-][H_3O^+]/[H_2SO_4]$ ratio, which is lower in 99 % than in 96 % sulfuric acid [6].

Attempts to prepare sufficiently pure oxanthrone (AH), in order to compare spectroscopically its sulfuric solutions with the bianthronyl—nitrate reaction mixture, were unsuccessful.

The fluorescence and 77-K phosphorescence spectra of anthrahydroquinone (9,10-dihydroxyanthracene), prepared by dithionite reduction of anthraquinone [2], were examined, because this compound should have spectroscopic characteristics close to those of oxanthrone. Anthrahydroquinone solutions were prepared in 96 % sulfuric acid, through which high-purity nitrogen had been passed in order to avoid oxidation to anthraquinone. Figure 4 shows that the excitation and emission spectra of the bianthronyl—nitrate, taken at the maximum of fluorescence emission intensity (Fig. 3), lie intermediately between those of anthrone and anthrahydroquinone. However, it is noteworthy (Table 1) that the longest radiative $T_1 \rightarrow S_0$ lifetime (1.55 s) of the reaction mixture at the maximum

TABLE 1

Radiative $T_1 \rightarrow S_0$ mean lifetimes at 77 K

Reaction mixture or compound in H_2SO_4	Excitation (nm)	Emission (nm)	τ_1[a] (s)	τ_2[a] (s)
Bianthronyl	360	494	0.65	—
R.m.[b] at maximum color	362 280	492 425	0.65 —	1.6 2.3
R.m. at maximum fluorescence	362 282	492 425	0.7 —	1.55 2.4
Final product	286	422	2.5	—
Anthrone	378	492	1.8	—
Anthrahydroquinone	353	492	3.5	—
Anthraquinone	285	420	2.5	—

[a]See experimental. [b]R.m.: reaction mixture.

of luminescence intensity, is less than the τ value for anthrahydroquinone (3.5 s), but very close to that of anthrone. This also suggests that the intermediate consecutive to the red compound is probably oxanthrone, since one would expect a lower τ value caused by a >CO group, which is absent in anthrahydroquinone.

As can be seen from Table 1, the results from phosphorescence lifetime determinations, at different stages of the bianthronyl—nitrate reaction, generally appear to be in accord with the deductions from the spectral investigations.

From many experiments it was established that the conversion of bianthronyl to anthraquinone by nitrates is quantitative. This indicates that the anthronyl radical cation $A^{\cdot}$ formed in the first steps of the bianthronyl—nitrate reaction, is also quantitatively converted to anthraquinone.

Oxanthrone can be readily oxidized to anthraquinone by dissolved oxygen, but the data obtained here are insufficient to make any precise assumption about the mechanism of the anthronyl radical conversion to anthraquinone. Nitrogen dioxide was detected by a diazotization-coupling reaction [7], when high-purity nitrogen was bubbled through the bianthronyl—nitrate mixture, hence nitrogen dioxide and dissolved oxygen might accomplish this conversion.

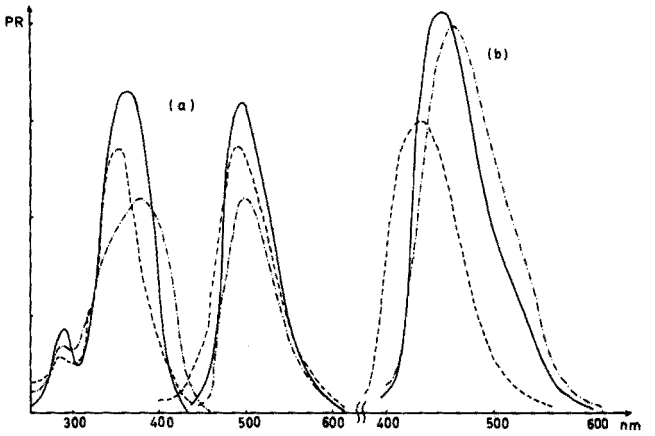

Fig. 4. Excitation—phosphorescence emission (a) and fluorescence (b) spectra. Luminescent compound L (———) ([bianthronyl]. = $[NO_3^-]$. = $5 \cdot 10^{-6}$ M). Anthrone $2 \cdot 10^{-5}$ M (—·—·—). Anthrahydroquinone $2 \cdot 10^{-5}$ M (- - - -). All in 96 % H_2SO_4.

A possible succession of reaction path is:

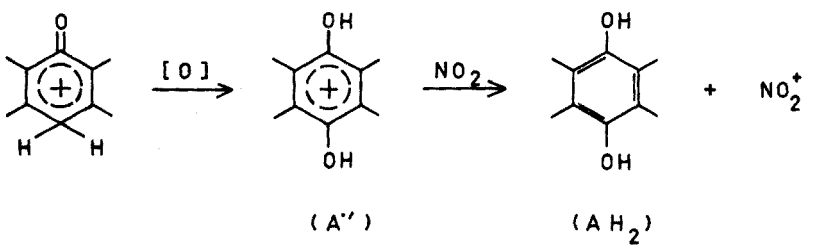

(7)

where anthrahydroquinone (AH_2), resulting from the interaction of the anthraquinonyl radical ($A^{\bullet}$) with nitrogen dioxide, is finally oxidized by dissolved oxygen to anthraquinone. If these latter steps are rapid enough, AH_2 should be in very low concentrations, satisfying steady-state conditions and thus accounting for the lack of long phosphorescence decays (see Table 1) Also the radical $A^{\bullet}$ should satisfy steady-state conditions, and in fact, the e.s.r. spectra for bianthronyl—nitrate and anthrone—nitrate mixtures, recorded at different reaction stages and near the time of the e.s.r. signal disappearance, do not display any modification; this is what one would expect if the assumed anthraquinonyl radical is highly reactive and consequently in very low concentrations.

Proposal of mechanism

From the preceding discussion, one may consider the following reaction mechanism:

$$NO_3^- + H_2SO_4 \xrightarrow{k_1} NO_3H + HSO_4^- \quad (8)$$

$$NO_3H + 2H_2SO_4 \overset{K_2}{\rightleftharpoons} H_3O^+ + 2HSO_4^- + NO_2^+ \quad (9)$$

$$\underset{(B)}{OAH{-}HAO} + H_2SO_4 \overset{K_3}{\rightleftharpoons} \underset{}{\overset{+}{H}OAH{-}HAO} + HSO_4^- \quad (10)$$

$$\underset{(BH)}{\overset{+}{H}OAH{-}HAO} + NO_2^+ \overset{k_4}{\underset{k_{-4}}{\rightleftharpoons}} \underset{(BN)}{[HOAH{-}HA(NO_2)O]^{2+}} \quad (11)$$

$$[HOAH{-}HA(NO_2)O]^{2+} \xrightarrow{k_5} \underset{(A^+)}{\overset{+}{O}AH} + \underset{(A)}{OAH_2} + NO_2^+ \quad (12)$$

$$\overset{+}{O}AH + H_3O^+ + HSO_4^- \overset{K_6}{\rightleftharpoons} \underset{(AH_2^+)}{\overset{+}{H}OAH(OH)} + H_2SO_4 \quad (13)$$

$$\overset{+}{H}OAH(OH) + O + H_2SO_4 \xrightarrow{k_7} \underset{(AQ)}{\overset{+}{H}OAO} + HSO_4^- + H_3O^+ \quad (14)$$

$$OAH_2 + NO_2^+ \xrightarrow{k_8} \underset{(A^\bullet)}{\overset{+}{O}A^\bullet H_2} + NO_2 \quad (15)$$

$$\overset{+}{O}A^\bullet H_2 + O \xrightarrow{k_9} \underset{(A^{\bullet\prime})}{\overset{+}{A}^\bullet(OH)_2} \quad (16)$$

$$\overset{+}{A}^\bullet(OH)_2 + NO_2 \xrightarrow{k_{10}} \underset{(AH_2)}{A(OH)_2} + NO_2^+ \quad (17)$$

$$A(OH)_2 + O + H_2SO_4 \xrightarrow{k_{11}} \overset{+}{H}OAO + H_3O^+ + 2HSO_4^- \quad (18)$$

giving as the overall reaction:

$$NO_3^- + 6H_2SO_4 + OAH{-}HAO + 3[O] \longrightarrow 2OA\overset{+}{O}H + 6HSO_4^- + 2H_3O^+ + NO_2^+ \quad (19)$$

According to the above mechanism, the rate expressions for the decomposition of protonated bianthronyl BH and for the formation of species BN and A^+, are:

$$-\frac{d[BH]}{dt} = k_4[BH][NO_2^+] - k_{-4}[BN] \quad (20)$$

where $[BH] = [B]_0 - [BN] - [A^+] - S$

$([B]_0 = (1 + K_3'^{-1})[BH] + [BN] + [A^+] + S =$

$[BH] + [BN] + [A^+] + S;\ K_3' \gg 1)$

$S = [AH_2^+] + \frac{1}{2}[AQ],$

$$\frac{d[BN]}{dt} = k_4([B]_0 - [BN] - [A^+] - S)[NO_2^+] - (k_{-4} + k_5)[BN]) \quad (21)$$

and as equilibrium (13) cannot be considered as rate-determining,

$$\frac{d[A^+]}{dt} = k_5[BN] - \frac{d[AQ]}{dt}. \quad (22)$$

However,

$$\frac{d[AH_2]}{dt} = k_{10}[A^{\cdot\prime}][NO_2] - k'_{11}[AH_2] \quad (23)$$

where $k'_{11} = k_{11}[O][H_2SO_4]$

and

$$\frac{d[NO_2]}{dt} = k_8[A][NO_2^+] - k_{10}[A^{\cdot\prime}][NO_2] \quad (24)$$

Since it was assumed (see the discussion under reaction (7)) that steps (17) and (18) are rapid, the rate of formation of anthraquinone (AQ) is given by:

$$\frac{d[AQ]}{dt} = k'_7[AH_2^+] + k_8[A][NO_2^+] \quad (25)$$

(where $k'_7 = k_7[O][H_2SO_4]$)

and this relation is immediately obtained, starting from $d[AQ]/dt = k'_7[AH_2^+] + k'_{11}[AH_2]$ and introducing steady-state conditions for AH_2 and NO_2 (see eqns. (23) and (24)).

If it is now assumed that $d[BN]/dt \simeq O$, and as $[NO_2^+] = [NO_2^+]_0 - [BN] - [NO_2] \simeq [NO_2^+]_0 - [BN]$, where $[NO_2^+]_0$ = initial nitronium concentration, then

$$[BN] = \frac{k_4([B]_0 - [A^+] - S)[NO_2^+]_0}{k_{-4} + k_5 + k_4([B]_0 - [A^+] - S) + k_4[NO_2^+]_0} \quad (27)$$

which leads to

$$\frac{-d[BH]}{dt} = \frac{k_5 K'_2 k_4([B]_0 - [A^+] - S)[NO_3H]_0}{k_{-4} + k_5 + k_4([B]_0 - [A^+] - S) + K'_2 k_4[NO_3H]_0} \quad (28)$$

and

$$\frac{d[A^+]}{dt} = -\frac{d[BH]}{dt} - [K'_6 k'_7[A^+] + k_8[A]([NO_2^+]_0 - [BN])] \quad (29)$$

where $K'_2 = K_2[H_2SO_4]^2/[H_3O^+][HSO_4^-]^2$ (30)

A comparative spectral study between sulfuric solutions of bianthronyl and anthrone or anthraquinone, immediately showed that monitoring the

kinetics colorimetrically at the bianthronyl absorption bands, was impossible without serious distortion of the kinetic curves. Undistorted absorbance vs. time evolutions could, however, be recorded at the visible band (500 nm) of the anthronyl cation A^+, for a sufficiently long period to permit analysis of the recorded kinetic curves.

Computations indicated that the $[A^+]$ vs. time variations for different initial concentrations of bianthronyl and nitrate and large time intervals, followed a reaction model involving two consecutive first-order steps:

$$BH \longrightarrow A^+ \longrightarrow AQ \tag{31}$$

where the deviations were statistically acceptable.

If it is assumed that (i) the second of the bracketed kinetic terms in eqn. (29) is much less important than the others, and (ii) after a certain reaction time, k_4 ($[B]_0 - [A^+] - S$) becomes much smaller than the constants in the denominator of eqn. (28), then the system of eqns. (28) and (29) undoubtedly fits the model shown in eqn. (31).

As far as point (i) is concerned, it should be noted that the second kinetic term in brackets of eqn. (29) contains a product of concentrations. Also, k'_7 is probably larger than k_8, since it is the product of k_7, solvent concentration and oxygen concentration, which is quite important (cm^3O_2/cm^3 solution = 0.0275, at 21 °C in 95.4 % sulfuric acid [8]). Moreover, K'_6 may not have a low value. In fact, step (13) may be detailed as follows (where AH is the unprotonated oxanthrone):

$$H_3O^+ + HSO_4^- \rightleftharpoons H_2O + H_2SO_4;\ K' = [H_3O^+]\,[HSO_4^-]/[H_2O]\,[H_2SO_4] \tag{31a}$$

$$A^+ + H_2O \rightleftharpoons AH + H^+;\qquad K_{A^+} = [A^+]\,[H_2O]/[AH]\,[H^+] \tag{31b}$$

$$AH + H^+ \rightleftharpoons AH_2^+;\qquad K_{AH_2^+} = [AH]\,[H^+]/[AH_2^+] \tag{31c}$$

giving (from eqns. 31a to 31c):

$$[AH_2^+]/[A^+] = K'_6 = [H_3O^+]\,[HSO_4^-]/K_{AH_2^+} \cdot K_{A^+} \cdot K'\,[H_2SO_4]$$

In 96 % sulfuric acid, the ratio $[H_3O^+]\,[HSO_4^-]/K'\,[H_2SO_4]$ can be evaluated from the data of Kaandorp et al. [6] as ca. $4.9 \cdot 10^{-4}$. The value of $K_{AH_2^+}$ can be taken roughly as the K_{RH^+} value of anthraquinone, which is $10^{8.3}$ [9], so that $K'_6 \approx 10^{-13}/K_{A^+}$. The K_{A^+} value of oxanthrone is unknown, but the K_{R^+} values (corresponding to $1/K_{A^+}$) of the indicators used by Deno et al. [10] to measure ionization ratios in 84—96 % sulfuric acid range between $10^{16.3}$ and $10^{17.4}$; thus, even if one assumes that the hydroxylic oxygen of oxanthrone is more basic than that of the above indicators, K'_6 may still be higher than unity.

With regard to point (ii), it is noteworthy (Fig. 5) that the calculated curves fit the experimental curves after a reaction time which is the shorter the greater is the initial concentration of nitrate; this supports the assumption made on the relative magnitude of the kinetic term $k_4([B]_0 - [A^+] - S)$.

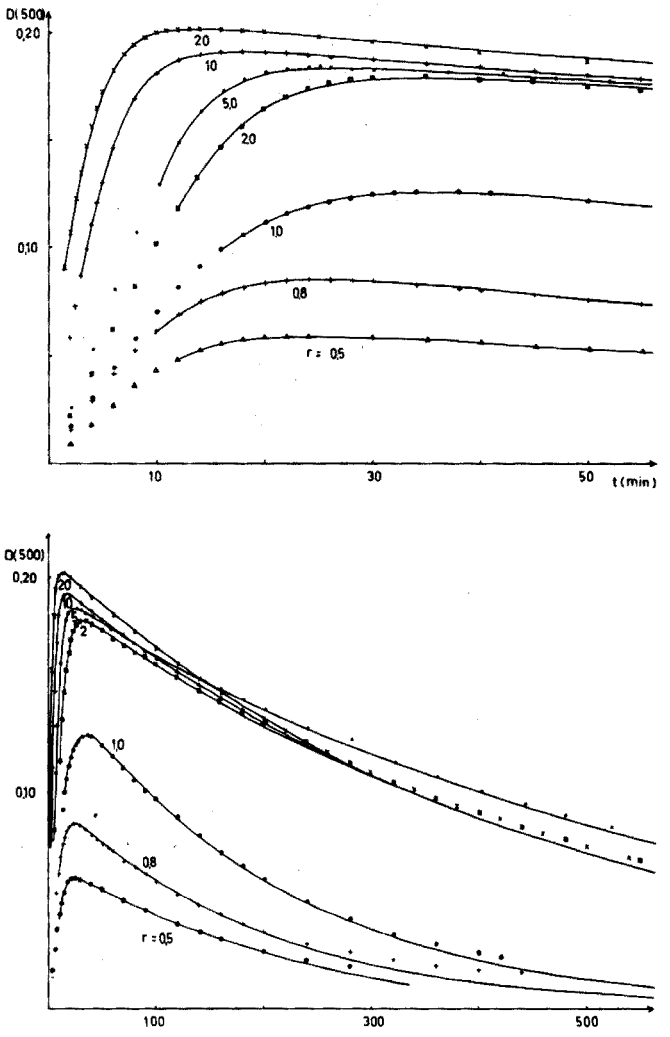

Fig. 5. Experimental points and calculated D vs. t curves for $[NO_3^-]_0/[\text{bianthronyl}]_0$ = 0.5 to 20. $[\text{Bianthronyl}]_0 = 10^{-5}$ M. 96 % H_2SO_4.

On the basis of the above assumptions, after some initial time of interaction:

$$\frac{d[A^+]}{dt} = k_N[BH]' - k'_{67}[A^+] \tag{32}$$

where $[BH]' = [B]_0 - [A^+] - S$ (33)

$$k_N = k_5 K'_2 k_4 [NO_3H]_0/k_{-4} + k_5 + K'_2 k_4 [NO_3H]_0 \tag{34}$$

$$k'_{67} = K'_6 k'_7,$$

and from the SS approximation $d[BN]/dt \simeq O$ and relations (20) and (33):

$$-\frac{d[BH]'}{dt} = k_N[BH]' \tag{35}$$

so that the solutions of (35) and (32) are, respectively:

$$[BH]' = [B]_0 \exp(-k_N t) \tag{36}$$

$$\text{and } [A^+] = [B]_0[k_N(k'_{67} - k_N)^{-1}][\exp(-k_N t) - \exp(-k'_{67} t)] \tag{37}$$

At the maximum intensity of the red color:

$$k_N [BH]'_{max} = k'_{67} D_{max} (\epsilon_{A^+} l)^{-1}$$

where D is the absorbance. Equation (37) then takes the form ($l = 1$):

$$D = [B]_0 \left[\frac{[BH]'_{max}}{D_{max}} \left(1 - \frac{k_N}{k'_{610}}\right) \right]^{-1} [\exp(-k_N t) - \exp(-k'_{67} t)] \tag{38}$$

Analysis of the ln D vs. t data at about the end of the decay of the 500-nm absorbance yields approximate values of k'_{67} and D values at any time can be calculated by using eqn. (38) and determining k_N and $[BH]'_{max}$ by iteration.

As shown in Fig. 5, the calculated D vs. t curves fit the experimental ones well, for long reaction times. Deviations at the beginning of the reaction, for initial conditions $0.5 \leqslant [NO_3^-]_0/[B]_0 \leqslant 20$, have already been explained, while negative deviations at the end of the reaction come from the contribution of the absorbance of anthraquinone, which is significant at 500 nm.

Values of k_N (Table 2) for $[NO_3^-]_0$ concentrations of $5 \cdot 10^{-6}$ and $8 \cdot 10^{-6}$ are imprecise, because eqns. (35) and (33) become valid near the $[A^+]_{max}$. However, for $[NO_3^-]_0 > 8 \cdot 10^{-6}$, the k_N values verify eqn. (34), since $k_N^{-1} = 7.4 \cdot 10^{-5} [NO_3^-]_0 + 2.73$, with a linear regression coefficient $r = 0.998$.

Finally, since k'_{67} is, for a given percentage of sulfuric acid, a function of the dissolved oxygen concentration only, significant variations of this constant are not expected to occur.

TABLE 2

Calculated k_N and k'_{67} (min^{-1}) ($[B]_0 = 10^{-5}$ M; H_2SO_4 = 96 %)

$[NO_3^-]_0$ ($\cdot 10^{-3}$ M)	k_N	k'_{67} ($\cdot 10^{-3}$)
0.005	0.172	5.1
0.008	0.165	5.4
0.01	0.1	5.0
0.02	0.152	2.0
0.05	0.23	2.7
0.2	0.31	2.1
1.0	0.4	2.2

REFERENCES

1 B. Nawratil, M. Marcantonatos and D. Monnier, Anal. Chim. Acta, 68 (1974) 217.
2 E. Grandmougin, Ber., 39 (1906) 3563.
3 H. Meyer, Monatsschr., 33 (1912) 1447.
4 P. A. H. Wyatt, Trans. Faraday Soc., 56 (1960) 490.
5 C. H. Rochester, Acidity Functions, Academic Press, London, New York, 1970, p. 72.
6 A. W. Kaandorp, H. Cerfontain and F. L. Sixma, Rec. Trav. Chim., 81 (1962) 969.
7 F. Celardin, M. Marcantonatos and D. Monnier, Anal. Chim. Acta, 68 (1974) 61.
8 Landolt-Börnstein, Springer-Verlag, Berlin 1962, Vol. 2, pp. 1—36.
9 M. A. Paul and F. A. Long, Chem. Rev., 57 (1957) 1.
10 N. C. Deno, J. J. Jaruzelski and A. Schriesheim, J. Amer. Chem. Soc., 77 (1955) 3044.

Analytica Chimica Acta, 82 (1976) 391—399
©Elsevier Scientific Publishing Company, Amsterdam — Printed in The Netherlands

EXTRACTION—PHOTOMETRIC DETERMINATION OF INDIUM IN ZINC-BASE ALLOYS WITH BROMOPYROGALLOL RED

S. G. JADHAV, P. MURUGAIYAN and CH. VENKATESWARLU

Analytical Chemistry Division, Bhabha Atomic Research Centre, Bombay-400 085 (India)

(Received 14th April 1975)

SUMMARY

The extraction—photometric determination of indium at the 5 p.p.m. level in high-purity zinc and zinc-base alloys is described. After a preliminary separation of indium by isopropyl ether extraction from hydrobromic acid medium, indium is determined by extraction into benzyl alcohol of its complex with bromopyrogallol red at pH 9.0. It is shown that 2 : 1, 1 : 1 and 1 : 2 complexes can be formed in aqueous and water—ethanol media; the 1 : 3 complex reported earlier was not found. The composition of the complexes extracted into benzyl alcohol from aqueous solutions at pH 6.5 and 9.0, was found to be 1 : 2.

Dithizone [1], arsenazo [2], pyridylazoresorcinol [3, 4], morin/quercetin [4], salicylfluorone/disulphophenyl fluorone [5], stilbazo [6], rhodamine 6F [7] and 5,7-dibromo-8-hydroxyquinoline [8] have been suggested as reagents for the photometric determination of indium in minerals, zinc compounds or similar matrices. In all these cases, a prior separation of indium from associated elements is necessary; extractions have been done with isopropyl ether [1, 2] or butyl acetate [4] in hydrobromic acid medium, ethyl ether in iodide medium [3, 5, 8], chloroform in the presence of antipyrine and iodide [4], and mixtures of tri-n-butyl phosphate and alkyl phosphoric acids in sulphuric acid medium [7]. Indium can be preconcentrated by coprecipitation with cadmium [6]. However, only one of these methods [4] is applicable for the determination of indium at the 5-p.p.m. level in zinc-base alloys as used in the die-casting industry.

Bromopyrogallol red (BPR) has been reported as a sensitive spectrophotometric reagent for indium, forming 1 : 1 [9, 10] and 1 : 3 [10] complexes, but the procedure has not been applied to any specific problem. This system was reinvestigated to elucidate further the composition of the complexes formed. An extraction—photometric method was then developed for the determination of indium in high-purity zinc and zinc-base alloys, after a preliminary extraction with isopropyl ether from bromide medium.

EXPERIMENTAL

Reagents

Indium solutions. AnalaR indium metal (0.100 g) was dissolved in 2 ml of 12 M hydrochloric acid and the solution was diluted to 100 ml. This solution was diluted appropriately just before use to give a 10 μg ml^{-1} solution. ^{114m}In tracer solution, prepared by the n, γ reaction, was supplied by the Isotope Division of this Research Centre.

Bromopyrogallol red solution. A 0.01 % solution (BDH) was prepared in 2 % (w/v) ammonium acetate solution. In some experiments, dye solutions in 50 % ethanol—water and in dilute ammonia solution in the presence of 2 % *L*-ascorbic acid were used.

All other reagents were of analytical grade.

Instrumentation

Absorbance measurements were made with matched 10-mm optical cells in a Beckman spectrophotometer (Model DU). Since the reaction between indium and BPR is slow, aqueous mixtures were kept overnight before measurement. In extraction studies, however, equilibration for 3 min was adequate. Ascorbic acid was used to minimise oxidation of BPR in alkaline solutions.

Beckman Expandomatic SS-2 pH meter was used in the normal mode. A medical spectrometer, made by the Electronics Division, BARC, was used to measure the γ-activity of ^{114m}In.

Development of the method

The optimal pH for the reaction of BPR with indium has been reported as 3.5 [9] and 5.5 [10]. To clarify this point, spectra of mixtures of indium with excess of BPR (prepared in ammonium acetate solution) at different pH values were scanned from 500 to 630 nm against the corresponding reagent blanks, and pH—absorbance curves at different wavelengths were prepared. The curve at 610 nm (Fig. 1, curve 1) shows that the absorbance of the dye is little affected by change of pH at this wavelength. The λ_{max} of the complexes lies at about this wavelength; a blue complex was formed quantitatively by pH 4.0 and a claret one beyond pH 5.5. The molar absorptivity of the blue complex ($3 \cdot 10^4$ l mol^{-1} cm^{-1}) at 610 nm is higher than that ($5.2 \cdot 10^3$ l mol^{-1} cm^{-1}) of the claret complex. However, it was found that the matrix element, zinc, interfered even at the 1.0-mg level and could not be masked at pH 4.0 by potassium cyanide. Hence it was concluded that BPR could not be used in aqueous medium. During these studies, the formation of a mixed ligand complex of indium with

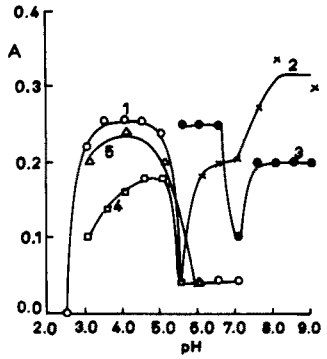

Fig. 1. pH—absorbance curves for the indium—BPR system. Measured at 610 nm for curves 1, 4 and 5; and 540 nm for curves 2 and 3.

Curve	[In] ($\cdot 10^{-6}$ M)	[BPR] ($\cdot 10^{-5}$ M)	[NH_4Cl] (M)	Vol. of org. phase (ml)
1	8.7	3.5	—	—
2	5.8	5.8	—	10
3	Tracer (3.2)	5.8	0.22	20
4	8.7	3.5 (in NH_4OH)	—	—
5	8.7	(in 50 % ethanol)	0.15	—

1,10-phenanthroline and BPR was observed.

Preliminary experiments showed that the indium—BPR complexes could be extracted into polar solvents like nitrobenzene, n-butanol and benzyl alcohol. Because of the ease of phase separation and the amount of indium extracted, benzyl alchohol was selected for further experiments. To establish the optimal pH of extraction, mixtures (30 ml) of indium ($5.8 \cdot 10^{-6}$ M) with excess of BPR ($5.8 \cdot 10^{-5}$ M) at different pH values were equilibrated with 10 ml (or 20 ml) of benzyl alcohol; the spectra of the extracted species were scanned against corresponding reagent blanks, and pH—absorbance curves at different wavelengths were prepared. The λ_{max} of the extracted species occurs at 540 nm, and the pH—absorbance curve at this wavelength (Fig. 1, curve 2) shows the extraction of one species around pH 6.0 and another at 8.0. Since the ammonium ion concentration is known to influence the formation of BPR complexes with metals, a similar experiment was carried out in the presence of 0.22 M ammonium chloride (with $3.2 \cdot 10^{-6}$ M indium and 20 ml of benzyl alcohol). This pH—absorbance curve (curve 3) shows the extraction of one complex with a constant absorbance between pH 5.5 and 6.5, and another with a different absorbance between pH 7.5 and 9.0; a minimum occurs at pH 7.0. A comparison of curves 2 and 3 shows a considerable increase in absorbance when ammomium chloride is present around pH 6.5.

When indium was extracted at pH 6.5 from solutions with varying concentrations of ammonium chloride, the absorbances increased as the ammonium chloride concentration increased up to 0.15 M and remained

constant thereafter. In the presence of 0.2 M ammonium chloride, a linear calibration curve was obtained over the range 2.5—20 μg of indium, with a molar absorptivity of 46000 l mol^{-1} cm^{-1} (assuming quantitative extraction of indium). However, even under these conditions, 1 mg of the matrix element zinc caused a positive interference despite masking with cyanide. Hence, these experimental conditions were also considered unsuitable.

Since potassium cyanide is a better masking agent in alkaline medium, the influence of buffer concentration on the extraction of indium was studied at pH 9.0 by adding varying volumes of buffer (0.13 M NH_4Cl + 0.8 M NH_4OH) to mixtures of indium and BPR, extracting with benzyl alcohol (10 ml) and measuring the absorbances of the organic phase against a corresponding reagent blank. Maximal constant absorbance was obtained when the volume of buffer was 5.0—7.5 ml. With this optimal concentration of buffer (6.5 ± 1.0 ml), a linear calibration curve was obtained for 15—30 μg of indium, the molar absorptivity being 42500 l mol^{-1} cm^{-1}.

The effects of masking agents and of some cations are shown in Table 1. Oxalate, tartrate, phosphate and EDTA interfere, while cyanide and fluoride do not. Cyanide masks Zn, Cu, Ni, Co and Cd at the 1.0-mg level and iron(III) at the 100-μg level. Aluminium and gallium interfere even in the presence of fluoride. Therefore it was decided to separate indium from the bulk of zinc and other associated elements by means of isopropyl ether

TABLE 1

Effects of anions and cations in presence of masking ions
(In taken = 20 μg; A_{540} = 0.370)

Ion	Amount added (mg)	A_{540}	Error %
Tartrate	50	0.310	−16.2[a]
Oxalate	50	0.300	−18.9[a]
EDTA	25	0.020	−94.6
Phosphate	25	0.258	−30.3[a]
Fluoride	100	0.365	−1.4
Cyanide	150	0.360	−2.7
Al[b]	0.01	0.123	−37.0[a]
Ga[b]	0.01	0.256	−30.8[a]
Zn[c]	1.0	0.375	+1.4
Fe^{3+}[c]	0.1	0.360	−2.7
Fe^{3+}[c]	1.0	0.060	−83.8
Cu[c]	1.0	0.380	+2.7
Ni[c]	1.0	0.380	+2.7
Co[c]	1.0	0.375	+1.4
Cd[c]	1.0	0.350	−5.4

[a] Blue residue observed at the interface.
[b] Fluoride (50 mg) added as masking agent.
[c] Cyanide (150 mg) added as masking agent.

extraction from hydrobromic acid medium.

Preliminary experiments indicated that indium can be separated from iron in the isopropyl ether extraction step either by selectively stripping indium with 7—8 M hydrochloric acid or by reducing iron(III) with ascorbic acid before the extraction. The separation of aluminium was quantitative only when the extracted aluminium and indium were stripped into an aqueous phase and indium was reextracted. Finally synthetic samples were prepared with known amounts of indium and analyzed by the procedure given below. The results are given in Table 2. To check the validity of the present method, one zinc sample was analyzed by separating indium with isopropyl ether extraction and determination with oxine [11]. The results in Table 2 indicate good agreement between the two methods.

Procedure

Weigh 4.0 g of the sample into a beaker, cover with water and heat with 30 ml of concentrated hydrobromic acid on a hot water bath. After complete dissolution of the sample, evaporate to dryness. Dissolve the residue in a known amount of hydrobromic acid and transfer to a separating funnel; the aqueous phase (50 ml) should be 5.5 M in hydrobromic acid. Extract indium

TABLE 2

Determination of indium in synthetic samples of high-purity zinc and zinc-base alloys

Nature of sample[a]	Indium added (p.p.m.)	Indium found (p.p.m.)	
		Present method	Oxine method
Zinc	20.0	22.7 ± 0.3[b]	22.5, 23.0, 23.0
Zinc (purified)	0.0	0.0	
	15.0	15.0	
	25.0	25.0	
	30.0	30.5	
Distilled zinc	—	nil	
	5.0	4.9, 5.0	
Hindustan zinc	—	nil	
	5.0	4.7, 4.9	
General Electric zinc	—	nil	
	5.0	4.8, 4.8	
Zone refined zinc	—	nil	
	5.0	5.0 ± 0.11 (one σ for 8 values)	
Zinc-base alloy[c]	—	nil	
	5.0	5.0, 5.5, 5.5	

[a]The weight of sample taken was 1.0 g for the first 5 tests and 4.0 g for the rest.
[b]Standard deviation from 12 results.
[c]See Anal. Chim. Acta, 57 (1971) 67 for composition.

with 25 ml of isopropyl ether, wash the organic phase with 10 ml of 6.0 M hydrobromic acid, and back-extract indium with two 10-ml portions of water. (In the case of zinc-base alloys, add 1 g of ascorbic acid to this aqueous indium solution. After 15 min, transfer the solution to a separating funnel with hydrobromic acid so that the aqueous phase is 50 ml and 6.0 M in HBr. Extract indium with 25 ml of isopropyl ether, and then back-extract the indium with two 10-ml portions of water.)

Evaporate the aqueous solution to dryness, and destroy organic matter by fuming with 4 ml of (1 + 1) 60 % perchloric—16 M nitric acid. Remove excess of perchloric acid by fuming, cool the residue and treat with 1 ml of 2 % ascorbic acid, 3 ml of 5 % potassium cyanide and 6 ml of the above-mentioned ammonia buffer; adjust the pH of the solution to 9.0. Transfer to a separating funnel containing 10 ml of 0.01 % BPR in 2 % ammonium acetate (this order of addition of reagents is essential), dilute the solution to 30 ml, and extract indium with 20 ml of benzyl alcohol. Filter the organic phase through a dry filter paper, and measure the absorbance at 540 nm against a corresponding reagent blank. Calculate the amount of indium from a calibration curve obtained by running the standards through the entire procedure.

DISCUSSION

BPR, like all the other reagents cited earlier, is not selective enough for a direct determination of indium in zinc-base alloys even in the presence of masking agents. Hence, isopropyl ether extraction from hydrobromic acid medium was resorted to for the separation of indium from associated elements.

Experiments with ^{114m}In showed that only about 60 % of the indium is extracted into benzyl alcohol as the BPR complex under the conditions reported. Despite this, satisfactory results were obtained for the indium content in samples, when standards were run through the whole procedure. The sensitivity of this reagent is better than that of oxine, but lower than those of morin and quercetin [4].

In the extraction of indium into benzyl alcohol, if BPR is added before the pH adjustment, iron is not masked by cyanide. Because of the traces of iron introduced during the destruction of organic matter, only the extraction—photometric method at pH 9.0 can be applied for the final determination.

BPR has been reported to form 1:1 [9, 10] and 1:3 [10] complexes in weakly acidic medium, but not the intermediate 1:2 complex. The effects of acetate and alcohol on complex formation in most of the BPR systems have not been generally studied, though the dye is usually dissolved in ammonium acetate or in alcohol. The pH—absorbance curve (curve 1, Fig. 1) obtained with the dye in ammonium acetate solution indicated the formation of one complex at about pH 4.0 and another complex beyond

pH 5.5. Curve 4, obtained with the dye dissolved in ammonium hydroxide solution, showed that the degree of complex formation was lower. When this experiment was repeated, without ammonium acetate but with an equivalent amount of ammonium chloride, the curve coincided with curve 1, showing that ammonium ions enhance complex formation and that acetate has no influence. This effect was not observed in the presence of an equivalent amount of sodium chloride. Curve 5 in ethanol (10 %)—water medium, shows that the degree of complex formation is less in the presence of ethanol despite the presence of the ammonium chloride.

Composition of the complexes

The continuous variations method in equimolar solutions gives a maximum at $X = 0.55$ (curve 1, Fig. 2) at 610 nm and pH 4.0. The maximum occurs at 0.67 at 560 nm (curve 2), and at 0.50 with a break at 0.65 at 610 nm (curve 3), and pH 6.5. These curves indicate the formation of a 1:1 complex (blue) at pH 4.0, and 1 : 1 and 1 : 2 (claret) complexes at pH 6.5 depending on the concentration of BPR. Their spectra against corresponding reagent blanks are shown in Fig. 3 (curves 1 and 2). When Job's method was applied at pH 9.0, the curve at 610 nm showed a maximum at about 0.4 with a break around 0.67 (curve 4) while that at 560 nm (not given) showed a minimum at 0.67. From these results it is concluded that only 1 : 1 and 1 : 2 complexes are formed in this system.

When indium and BPR are mixed at about pH 4.0, a pink complex is formed immediately, and then slowly changes to a blue complex. The spectrum of a mixture of indium ($2.30 \cdot 10^{-5}$ M) and BPR ($1.15 \cdot 10^{-5}$ M) at pH 3.0 in water—ethanol medium was scanned 30 min after the solutions had been mixed (curve 3, Fig. 3). This spectrum shows a maximum at about 560 nm and is different from the spectra of the 1 : 1 and 1 : 2 complexes (curves 1 and 2). The Job curve at this pH (curve 5, Fig. 2) shows a maximum at 0.55 and a break around 0.33. It is therefore inferred that a polynuclear 2 : 1 species can also be formed in this system. Similar polynuclear species have been reported by others for silver [12] and bismuth [13]. Mole ratio curves showed breaks at [BPR]/[In] values of 1.5 at pH 4.0 and 2.0 at pH 6.5, confirming the conclusions drawn from the continuous variations method. The break at 1.5 in the mole ratio curves at pH 4.0 and the maximum at 0.55 in the continuous variations curves are attributed to the influence of the polynuclear complex forming simultaneously. Similar compositions could be deduced by the two methods when ethanol was present, and when acetate was absent. In view of the present findings, the 1 : 3 composition reported by Kish [10] in ethanol—water medium is considered erroneous.

It has been stated that metal—BPR complexes are extracted into nitrobenzene [14]. The present studies show that extraction of indium—BPR species into other polar solvents like n-butanol and benzyl alcohol is also possible. The pH—absorbance (of the organic phase) curves with benzyl

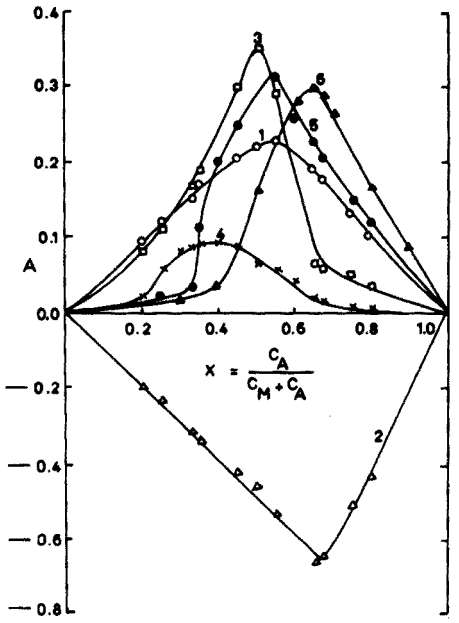

Fig. 2. Continuous variations (Job's) curves. BPR in 50 % ethanol and 0.15 M NH_4Cl were used in curve 5. The volume of the organic phase is 10 ml in curve 6.

Curve	[In] + [BPR] ($\cdot 10^{-5}$ M)	pH	λ (nm)
1	1.7	4.0	610
2	3.5	6.5	560
3	3.5	6.5	610
4	1.7	9.0	610
5	3.5	3.0	610
6	2.9	6.5	540

alcohol (curves 2 and 3, Fig. 1) indicate the extraction of two different species one below and another above pH 7.0. The continuous variations method indicated that the extracted species is a 1 : 2 complex at pH 6.5 as well as 9.0. However, the non-superimposable spectra (curves 4 and 5, Fig. 3) show that the two complexes are not identical. The continuous variations curve at pH 6.5 (curve 6, Fig. 2) further indicates that the formation of the 1 : 1 complex in the aqueous phase hinders the extraction of the 1 : 2 complex, when insufficient BPR is present. Mole ratio methods (data not given) confirmed the compositions of the extracted species.

The authors are grateful to Dr. M. Sankar Das, Head, Analytical Chemistry Division, for his interest and useful discussions during this work.

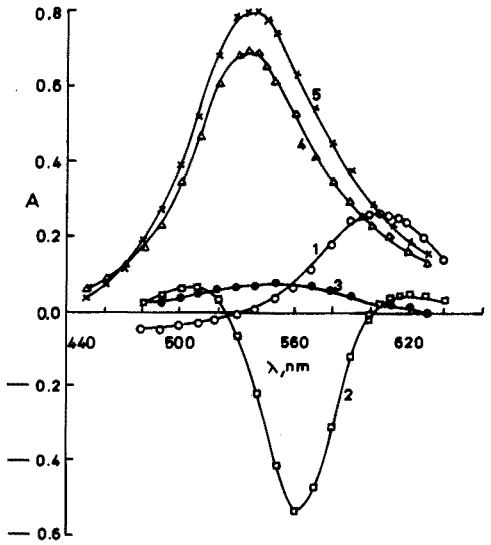

Fig. 3. Spectra. The volume of the organic phase is 10 ml in curves 4 and 5.

Curve	pH	[In] ($\cdot 10^{-5}$ M)	[BPR] ($\cdot 10^{-5}$ M)	[NH_4Cl] (M)
1	4.0	0.87	3.5	—
2	6.5	0.87	3.5	—
3	3.0	2.3	1.15 (in 50 % ethanol)	0.15
4	9.0	0.58	5.8	0.03 (+ 0.18 M NH_4OH)
5	6.5	0.58	5.8	0.22

REFERENCES

1 T. A. Collins, Jr. and J. H. Kanzelmeyer, Anal. Chem., 33 (1961) 245.
2 T. Matsumae, Bunseki Kagaku, 8 (1959) 167; cf. I.M. Kolthoff, P.J. Elving and E.B. Sandell (Eds.), Treatise on Analytical Chemistry, Part II, Vol. 2, Interscience Publishers, New York, 1962, p. 52.
3 P. P. Kish and S. T. Orlovskii, Zh. Anal. Khim., 17 (1962) 1057.
4 N. L. Olenovich, L. T. Kovalchuk and E. P. Lozitskaya, J. Anal. Chem. (USSR), 29 (1974) 32.
5 V. A. Nazarenko and R. V. Ravitskaya, Zavod. Lab., 31 (1965) 1301.
6 M. Z. Yampolskii, Peredovye Metody Khim. Tekhnol. Kontr. Proizvod. Tr. Vses. Konf. Rab. Met. Khim. Prom. Sotrudnikov Vuzov, 178 (1964).
7 I. S. Levin and T. G. Azarenko, Zh. Anal. Khim., 20 (1965) 452.
8 Z. Gregorowicz and M. Marczak, Chem. Anal. (Warsaw), 14 (1969) 159.
9 Sh. T. Talipan, Kh. S. Abdullaeva and G.P. Gorkovayca, Uzb. Khim. Zh., 6 (1962) 16.
10 P. P. Kish, Nauk. Zap. Uzhgorod. Derzh. Univ., 49 (1962) 70.
11 K. Bansho and Y. Umezaki, Bunseki Kagaku, 14 (1965) 72.
12 R. M. Dagnall and T. S. West, Talanta, 8 (1961) 711.
13 V. Suk and M. Smetanova, Coll. Czech. Chem. Commun., 30 (1965) 2532.
14 B. W. Bailey, J. E. Chester, R. M. Dagnall and T. S. West, Talanta, 15 (1968) 1359.

Analytica Chimica Acta, 82 (1976) 401—408
©Elsevier Scientific Publishing Company, Amsterdam — Printed in The Netherlands

SPECTROPHOTOMETRIC DETERMINATION OF DISSOLVED SILICA BASED ON α-MOLYBDOSILICIC ACID FORMATION

KIKUO KATO

Water Research Institute, Nagoya University, Nagoya 464 (Japan)

(Received 30th June 1975)

SUMMARY

Dissolved silica reacts with molybdate to form the α- and β-acids in the pH range below 4.1, but only the α-acid in the pH range 4.1—4.5. The maximum absorbance of molybdosilicic acid in the determination based on the mixed acids is maintained in a temporary steady-state condition by formation of the α- and β-acids and conversion of the β-acid to the stable α-acid. A spectrophotometric determination of dissolved silica based on the formation of the α-acid alone is possible at pH 4.2 when a 2 M acetate buffer solution is used. Maximum absorbance is achieved within15 min at 20 ± 1 °C, and the absorbance remains constant for 10 days.

Jolles and Neurath [1] suggested in 1898 a colorimetric method for the determination of silica based on the reaction of silica and molybdate to form yellow molybdosilicic acid. In 1923, Diénert and Wandenbulcke [2] applied this method to the analysis of natural waters. Isaacs [3] first reported that reducing agents convert yellow molybdosilicic acid to molybdenum blue, which has a much larger absorbance. Many modifications of these methods have been described [4—26].

In 1952, Strickland [27] first reported the existence of two forms of molybdosilicic acid giving different absorption spectra and termed them α- and β-molybdosilicic acids. The β-acid is unstable in solution and, when formed, is transformed spontaneously and irreversibly to the α-acid [18, 27]. This change is accelerated by high pH, elevated temperature and dissolved electrolytes in the solution [16, 18, 27]. These facts suggest that the determination based on the β-acid would, in principle, be irreproducible. However, the rate of formation of the stable α-acid and the rate of transformation of the β-acid to the α-acid are low, and complete formation and transformation take too long [15, 18, 27], so that there has been considerable difficulty in devising an analytical method based on the stable α-acid only. Although attempts have been made in which the reaction solution is heated at about 100 °C [14, 15] or is stored for several hours [18], those procedures are not appropriate for the analysis of natural waters.

In this work, the conditions for the formation of molybdosilicic acid were investigated, and an attempt was made to obtain a reproducible determination of the disssolved (molybdate-reactive) silica.

EXPERIMENTAL

Apparatus

A Hitachi Perkin-Elmer 139 spectrophotometer and a Hitachi 356 dual-wavelength double-beam spectrophotometer were used with 10 mm cells. A Beckman 1019 pH meter was also used.

Reagents and solutions

All chemicals were of analytical-reagent grade. All solutions were stored in polyethylene bottles.

Standard silica solution. Fuse 500 mg of pure powdered silica dried at about 700 °C, with 4.0 g of anhydrous sodium carbonate and dissolve the melt in 5.00 l of distilled water. Prepare working solutions by suitable dilution with distilled water.

Preliminary procedure

Add 2 ml of sulfuric acid of known molarity and 2 ml of aqueous 10 % (w/v) ammonium molybdate solution to solutions (50 ml) containing 4.7 mg SiO_2 l^{-1} in polyethylene bottles at 20 ± 1 °C. Determine the absorbance of the solution at 400 and 330 nm against a blank solution. Measure the pH of the solution after the addition of the reagent solutions.

THE FORMATION OF α- AND β-MOLYBDOSILICIC ACIDS

In order to elucidate the formation of the molybdosilicic acids, the absorption spectra of the α- and β-acids should be exactly known. However, as Strickland [27] has reported, a solution of the β-acid without some α-acid present cannot be obtained. Figure 1 shows the absorption spectra of the α-acid solution and of the solution during maximum color development at pH 1.2, in which the β-molybdosilicic acid predominates (see Fig. 2). The absorption spectra below 350 nm (Fig. 1) are not in agreement with those given in previous work [14, 15, 27, 28], although some of the earlier spectra [15, 27] are in fairly good agreement with spectra which were measured against water instead of the blank solution. From Fig. 1, it can be seen that the absorbance of the α-acid equals that of the β-acid at ca. 333 nm and exceeds that of the β-acid at wavelengths below 333 nm. In this work, the absorbances were measured at both 400 and 330 nm.

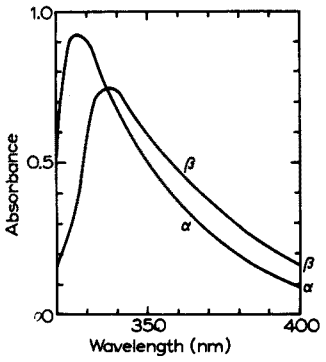

Fig. 1. Absorption spectra of molybdosilicic acid solution. 2 ml of 2.5 M sulfuric acid added. (α) the α-acid solution and (β) the silica solution during maximum color development at pH 1.2.

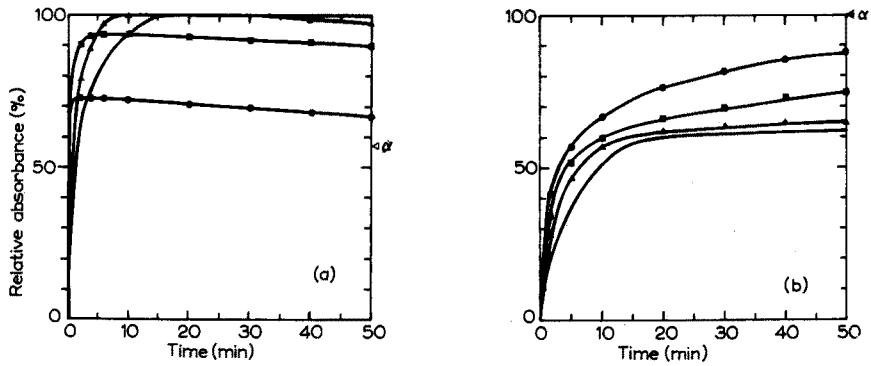

Fig. 2. The change with time in the absorbance of molybdosilicic acid at various pH values (adjusted with H_2SO_4) at 20 ± 1 °C. (•) pH 2.7, (▪) pH 1.8, (▲) pH 1.4 and (—) pH 1.2. α indicates the maximum absorbance of α-acid solution. (a) Measured at 400 nm. (b) Measured at 330 nm.

Formation of β-molybdosilicic acid

Figure 2(a) shows the change with time in the absorbance at 400 nm of molybdosilicic acid at various pH values. These pH values were taken as representative of the reported methods based on the β-acid [2—13, 16, 17, 19—26]. At any pH, the absorbance of the molybdosilicic acid exceeds that of the α-acid within 5 min of adding the reagent solutions, and decreases after showing a maximum. Thus the β-acid can be formed at any of these pH values.

The maximum absorbances of the solutions at pH 1.2 and pH 1.4 are the same, and exceed those at pH 1.8 and 2.7, which indicates that the β-acid predominates during the maximum color development at pH 1.2—1.4.

Possibly only the β-acid is formed at pH 1.2—1.4, though both the α-acid and the β-acid are formed at pH 1.8—2.7.

Formation of α-molybdosilicic acid at pH 1.2—1.4

The change with time in the absorbance at 330 nm of molybdosilicic acid was measured simultaneously with the measurements at 400 nm. The results (Fig. 2(b)) differ greatly from those in Fig. 2(a). The absorbance at 330 nm increases simply with time at any pH value and with decreasing pH value at any time. However, the maximum absorbance at 400 nm and pH 1.2 is the same as the maximum absorbance at 400 nm and pH 1.4. Thus the β-acid must be transformed to the stable α-acid even during the period showing maximum absorbance at 400 nm.

These data cannot be explained only by the initial formation of the β-acid and its gradual conversion to the α-acid but show that some α-acid is also formed originally. The maximum absorbance at 400 nm in the solution at pH 1.2—1.4 is considered to be maintained by a temporary steady-state condition based on formation of the α- and β-acids and conversion of the β-acid to the α-acid. Therefore, the determination of dissolved (molybdate-reactive) silica by measuring the absorbance of the stable α-acid alone became the aim of this work.

Effect of pH on the formation of α- and β-molybdosilicic acids

For ultimate measurement of the α-acid only, either the α- and β-acids are formed and the β-acid is converted to the α-acid [14, 15, 18], or only the α-acid is formed initially. Figure 3 shows the maximum absorbance at 400 nm of solutions at various pH values, measured 30 h after the addition of the reagent solutions to the silica solution. Clearly, both the α- and β-acids are formed below pH 3.9, whereas the α-acid alone is probably formed above pH 3.9.

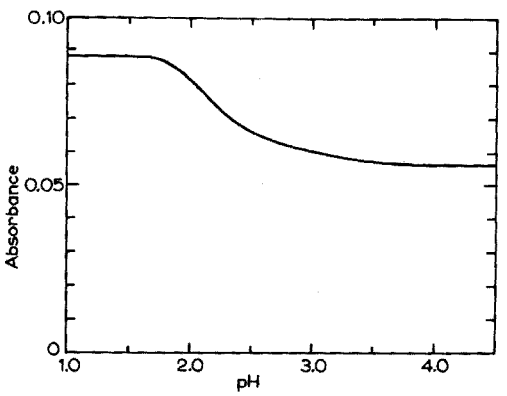

Fig. 3. Maximum absorbance at 400 nm of molybdosilicic acid at various pH values (adjusted with H_2SO_4) measured 30 h after reagent addition.

The conversion of the β-acid to the α-acid is very slow (Figs. 2(a) and 3), as reported by previous authors [14, 15, 18], who attempted to overcome the problem of obtaining only α-molybdosilicic acid by heating the solution at about 100 °C [14, 15] or by storing it for several hours [18]. These procedures are not appropriate for the analysis of natural waters containing various forms of silicon compounds [12, 29]. Dissolved silica should be determined within at least 1 h and at room temperature for routine analysis. Further studies showed that acetic acid accelerates the formation of α-acid in the pH range 3.9—4.5.

MOLYBDOSILICIC DETERMINATION BASED ON THE FORMATION OF α-MOLYBDOSILICIC ACID ALONE

Preliminary procedure

Acetate buffer solution (2 ml) of different pH values and 10 % ammonium molybdate solution (2 ml) were added to 50 ml of a solution containing 4.7 mg SiO_2 l^{-1}; the pH was checked and the absorbance was measured at 400 and 330 nm against a blank solution. The buffer was prepared by mixing 2.0 M sodium acetate and 2.0 M acetic acid.

Optimal pH range and time for color development

Although the maximum absorbance of molybdosilicic acid is constant in the pH range 3.9—4.5, the molybdosilicic acid formed in this pH range may not be the α-acid alone. The existence of the β-acid at pH 3.9—4.5 was therefore examined. The change with time in the absorbance at 400 nm of molybdosilicic acid (Fig. 4) indicated the formation of the β-acid even at

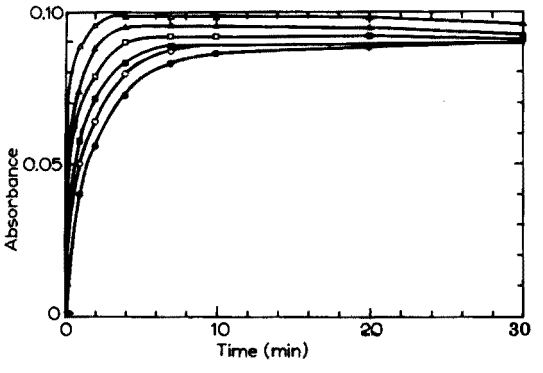

Fig. 4. The change with time in the absorbance at 400 nm of molybdosilicic acid at different pH values (acetate buffer). (△) pH 3.8, (▲) pH 3.9, (□) 4.0, (■) pH 4.1, (○) pH 4.2 and (●) pH 4.5.

pH 3.9. However, at pH 4.1 and above, only the α-acid was formed; this was confirmed by measuring the change with time in the absorbance of molybdosilicic acid at pH 4.1 and above, at both 400 and 330 nm. The curves at 400 and 330 nm (Fig. 5) are exactly similar, which is to be expected if only the α-acid is formed.

The time required to attain maximum absorbance with the α-acid formed at pH 4.1 was about 10 min, but the time increased with increasing pH; pH 4.2 was selected for further work.

The effect of the acetate buffer concentration was then examined, under the general conditions of the preliminary procedure. The results (Fig. 6) showed that when the buffer solution added was more than 2.0 M, maximum absorbance was achieved within 10 min of adding the reagent solutions; a 2.0 M acetate buffer was therefore selected.

Applicability of Beer's Law and reproducibility

Figure 7 shows the calibration curves for the determination of dissolved silica by the proposed method. Beer's law is valid at 330 or 400 nm, the range being selected according to the content of dissolved silica in the sample solution. Replicate (5) analyses of solutions containing various amounts of dissolved silica showed standard deviations of less than 0.5 % and 2 % for the ranges 1.0—100 mg l^{-1} and 0.2—0.5 mg l^{-1}, respectively.

The absorbances shown in Fig. 7 were constant over a period of 10 days, which confirms that the molybdosilicic acid formed is the α-acid alone, and indicates that this is a stable and reproducible method for the determination of dissolved silica.

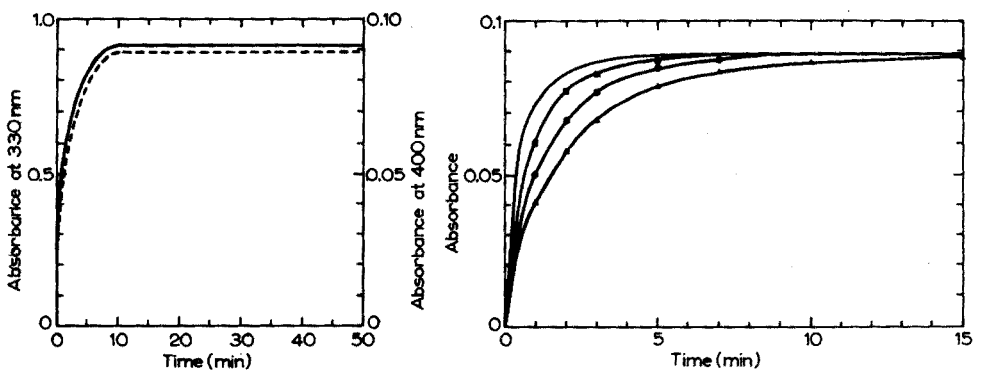

Fig. 5. The change with time in the absorbance of molybdosilicic acid at 400 and 330 nm. Buffer pH 4.2. (—) 330 nm. (---) 400 nm.

Fig. 6. The change with time in the absorbance of molybdosilicic acid at 400 nm, with different acetate buffer concentrations at pH 4.2. (▲) 1.0 M, (■) 2.0 M, (●) 3.0 M and (—) 4.0 M.

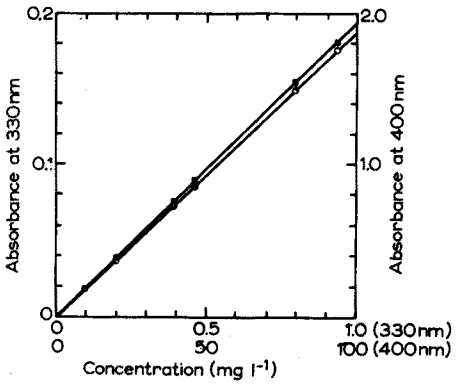

Fig. 7. Calibration curves for the determination of dissolved silica by the proposed method. (■) 330 nm. (○) 400 nm.

Recommended procedure for dissolved silica

To 50 ml of sample solution, add 2 ml of buffer pH 4.2 (prepared by mixing 150 ml of 2 M acetic acid and 50 ml of 2 M sodium acetate) and 2 ml of aqueous 10 % (w/v) ammonium molybdate solution. Check that the pH is 4.2 and leave the solution for 15 min at 20 °C. Measure the absorbance against a blank solution at 330 — 400 nm according to the color intensity of the solution. The interference of phosphate can be diminished by adding 2 ml of 20 % (w/v) oxalic acid to the solution just before measuring the absorbance.

The author is greatly indebted to Prof. Y. Kitano of the Water Research Institute, Nagoya University, for his valuable advice.

REFERENCES

1 H. Jolles and F. Neurath, Z. Angew. Chem., 11 (1898) 315.
2 F. Diénert and F. Wandenbulcke, Compt. Rend., 176 (1923) 1478.
3 M. L. Isaacs, Bull. Soc. Chim. Biol., 6 (1924) 157.
4 W. R. G. Atkins, J. Mar. Biol. Ass., U.K., 14 (1926) 89.
5 E. J. King and H. Stantial, Biochem. J., 27 (1933) 990.
6 R. J. Robinson and H. J. Spoor, Ind. Eng. Chem., Anal. Ed., 8 (1936) 455.
7 R. J. Robinson and T. G. Thompson, J. Mar. Res., 7 (1948) 48.
8 J. A. Brabson, H. C. Mattraw, G. E. Maxwell, A. Darrow and M. F. Needham., Anal. Chem., 20 (1948) 504.
9 A. Saeki, J. Oceanogr. Soc. Japan, 6 (1950) 39.
10 F. A. J. Armstrong, J. Mar. Biol. Ass., U.K., 30 (1951) 149.
11 O. A. Kenyon and H. A. Bewick, Anal. Chem., 25 (1953) 145.
12 D. T. Chow and R. J. Robinson, Anal. Chem., 25 (1953) 646.
13 L. B. Mullin and J. P. Riley, Anal. Chim. Acta, 12 (1955) 162.
14 L. H. Andersson, Acta Chem. Scand., 12 (1958) 495.
15 A. Ringbom, P.E. Ahlers and S. Siitonen, Anal. Chim. Acta, 20 (1959) 78.

16 I. E. Morrison and A. L. Wilson, Analyst (London), 88 (1963) 88, 100, 446.
17 L. Trudell and D. F. Boltz, Anal. Chem., 35 (1963) 2122.
18 K. Grasshoff, Deep Sea Res., 11 (1964) 597.
19 A. L. Wilson, Analyst (London), 90 (1965) 270.
20 D. R. Schink, Anal. Chem., 37 (1965) 764.
21 K. Kato and Y. Kitano, J. Earth Sci., (Nagoya Univ.), 14 (1966) 151.
22 P. G. Brewer and J. P. Riley, Anal. Chim. Acta, 35 (1966) 514.
23 J. D. H. Strickland and T. R. Parsons, A Practical Handbook of Sea Water Analysis, Fisheries Research Board of Canada, Bulletin No. 167, 1968, p. 65.
24 L. G. Hargis, Anal. Chim. Acta, 52 (1970) 1.
25 P. Pakalns, Anal. Chim. Acta, 54 (1971) 281.
26 K. A. Fanning and M. E. Q. Pilson, Anal. Chem., 45 (1973) 136.
27 J. D. H. Strickland, J. Amer. Chem. Soc., 74 (1952) 862, 868, 872.
28 H. E. Garrett and A. J. Walker, Analyst (London), 89 (1964) 642.
29 I. Iwasaki, T. Katsura and T. Tarutani, Bull. Chem. Soc. Jap., 24 (1951) 227.

Analytica Chimica Acta, 82 (1976) 409—413
©Elsevier Scientific Publishing Company, Amsterdam—Printed in The Netherlands

Short Communication

ION-SELECTIVE ELECTRODES BASED ON METAL COMPLEXES OF THE TYPE $M_x[N(II)L_4]$

D. E. RYAN and M. T. CHEUNG

Trace Analysis Research Centre, Chemistry Department, Dalhousie University, Halifax, Nova Scotia B3H 4J1 (Canada)

(Received 25th July 1975)

Metal complexes used as sensors for ion-selective electrodes have not been widely studied. Scibona et al. [1] detected zinc(II) or palladium(II) by means of liquid membranes formed by benzene solutions of alkylammonium tetrachlorozincate(II) or tetrachloropalladate(II) salts. Cattrall and Pui Chin-Poh [2] determined iron(III) with the tetrachloroferrate(III) salt of the quaternary ammonium compound, Aliquat 336S. Fogg et al. [3] investigated liquid state, heterogeneous silicone rubber and carbon paste electrodes based on brilliant green tetrathiocyanatozincate(II) in *o*-dichlorobenzene. Lebl and Vesely [4] studied the functional layers of the ion-selective electrodes with $Ag_2[HgI_4]$, $Cu_2[HgI_4]$ and $Tl_2[HgI_4]$ as sensors.

The ion-selective electrodes studied here are mainly heterogeneous membrane electrodes based on polyvinyl chloride as the inert support binder. The active materials used are the precipitates of metal complex salts of the type, $M_xN(II)L_4$, where L is a ligand (SCN^-, I^-), M is Ag(I), Cu(I), Cu(II), Pb(II), Hg(II) or malachite green, and N is Hg(II), Zn(II), Co(II), or Ni(II). Manipulation of ion-selective electrodes of the liquid membrane type is more cumbersome than that of solid-state electrodes and attention is focused mainly on solid-state membrane electrodes of the heterogeneous type.

Experimental

Apparatus. A Fisher Accumet Model 320 Expanded Scale Research pH Meter was used for potential measurements. The temperature of the measuring solutions was regulated by a Haake thermostated water bath.

Preparation of metal complexes. $Pb[Hg(SCN)_4]$, and $Cu[Hg(SCN)_4]$ were prepared by adding the stoichiometric amount of $Pb(ClO_4)_2$ or $Cu(ClO_4)_2$ to $K_2[Hg(SCN)_4]$ solutions (prepared by mixing stoichiometric ratios of potassium thiocyanate and mercury(II) nitrate solutions at pH 1.8).

$Ag_2[HgI_4]$, $Cu_2[HgI_4]$, and the $Ag_{1.14}Cu_{0.86}[HgI_4]$ eutectoid were made by simultaneous precipitations from solutions containing stoichiometric amounts of reactants as reported by Suchow and Pond [5]. Aqueous

solutions containing either copper(II) or silver nitrate with a total metal content of 0.4 M were added to boiling solutions of ca. 0.1 M $K_2[HgI_4]$ (prepared from solutions containing stoichiometric ratios of mercury(II) nitrate and potassium iodide and a sufficient amount of potassium iodide to reduce Cu(II) to Cu(I); for $Ag_2[HgI_4]$ the excess of potassium iodide is not necessary. The resulting mixture was evaporated almost to dryness in order to remove the iodine formed and to decrease the material remaining in the solution.

$Hg[Co(SCN)_4]$, malachite green $[Zn(SCN)_4]$, and $Ag_2[Ni(SCN)_4]$ were prepared in the same manner as the tetrathiocyanatomercurates.

Pb[PbY] was precipitated by addition of a 0.1 M solution of the disodium salt of ethylenediaminetetraacetic acid (H_4Y, EDTA) to a 0.5 M lead perchlorate solution.

All precipitated compounds were filtered, washed and dried at room temperature before use.

Membrane preparation. The general procedure was to use one drop of vinyl plastic repair cement (Lepage No. 330) and two drops of either dibutylphthalate or dioctylphthalate, and to mix thoroughly with an equal volume of the metal complex. The mixture was placed on one end of a glass tube (5 mm i.d.) or a medicine dropper to form a membrane ca. 2 mm thick. The membrane was allowed to dry for 5—10 h.

Electrodes. The internal solutions for these electrodes were 0.1 M solutions of the chloride, iodide or thiocyanate of the metal ion being measured; contact was made with this internal solution with a silver—silver halide wire. The external reference electrode was a saturated calomel electrode. A 0.15 M KNO_3 solution was used in the salt bridge from the test solution to the reference electrode.

The plastic membrane electrode was soaked in a 10^{-3} M solution of the measured ion for at least 12 h before use. All measurements were made on solutions prepared by successive five-fold or ten-fold dilution of a 0.1 M cation or anion stock solution.

Results and Discussion

Responses of the $Pb[Hg(SCN)_4]$ electrode towards each individual component, namely Hg(II), SCN^-, Pb(II), and $HgSCN_4^{2-}$, were studied to establish the behaviour of this electrode towards each of these species. Response to mercury(II) and thiocyanate was evident only at concentrations greater than 10^{-2} M; the change per decade was ca. 15 m V for both ions. Lead tetrathiocyanatomercurate(II) is present as ionized species in solutions as:

$$Pb[Hg(SCN)_4] \rightleftarrows Pb^{2+} + Hg(SCN)_4^{2-}$$

The concentrations of these ions depend on the solubility of the salt in

solution. However, the $Hg(SCN)_4^{2-}$ anion will dissociate further:

$$Hg(SCN)_4^{2-} \underset{\leftarrow}{\overset{k_4}{\rightarrow}} Hg(SCN)_3^- + SCN^- \underset{\leftarrow}{\overset{k_3}{\rightarrow}} Hg(SCN)_2 + SCN^- \underset{\leftarrow}{\overset{k_2}{\rightarrow}} HgSCN^+ + SCN^- \underset{\leftarrow}{\overset{k_1}{\rightarrow}} Hg^{2+} + SCN^-$$

The $p(k_1k_2)$ is 17.7, pk_3 is 1·68 and pk_4 is 0.62, and the concentration of each species in solution depends on the total concentration of potassium thiocyanate and mercury(II). The question therefore arises as to whether a $Pb[Hg(SCN)_4]$ electrode will respond to any given species from Hg(II) to $Hg(SCN)_x$ ($x = 1$—4) or just to one particular species existing in solution. Experiments showed that there is non-Nernstian response to Hg(II) and thiocyanate or to Hg(II) at low concentrations of thiocyanate. However, when Hg(II) predominantly exists as $Hg(SCN)_4^{2-}$, as in solutions having a thiocyanate concentration of 7.5 M, the response is near Nernstian (29 mV per decade change in concentration of $Hg(SCN)_4^{2-}$).

Heterogeneous membrane electrodes prepared from other complex thiocyanates behave similarly. Electrodes containing malachite green—$[Zn(SCN)_4]$, $Ag_2[Ni(SCN)_4]$ or $Hg[Co(SCN)_4]$ are suitable for determining Zn(II), Ni(II) or Co(II) in solutions containing a large excess of thiocyanate (Fig. 1); the relatively high solubility of the membrane compounds limits their sensitivity. These electrodes also give a Nernstian response to the

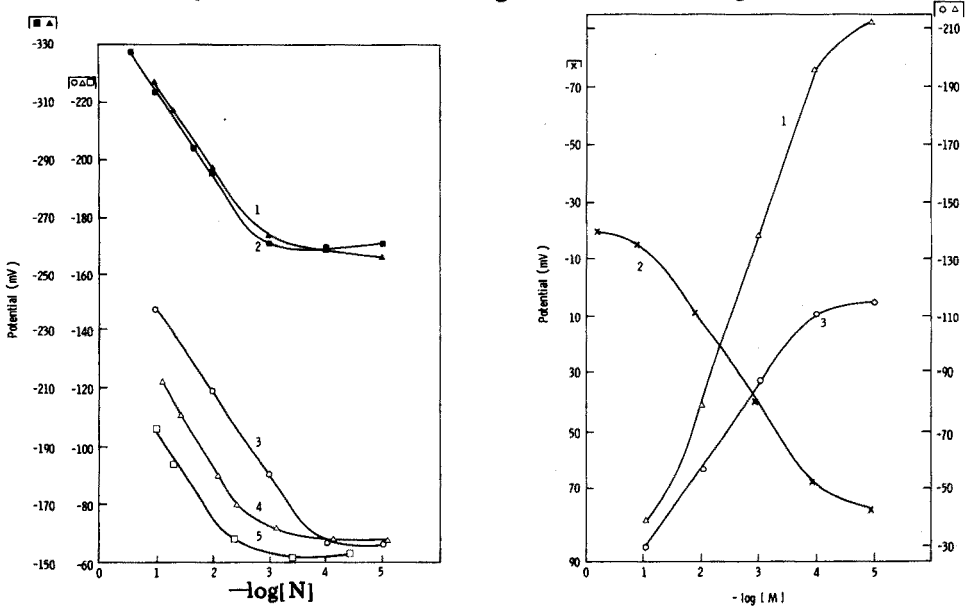

Fig. 1. Electrode response in the presence of excess of thiocyanate at 25 °C. 1, $Ag_2[Ni(SCN)_4]$ sensor and Ni(II); 2, $Hg[Co(SCN)_4]$ and Co(II); 3, malachite green $[Zn(SCN)_4]$ and Zn(II); 4, $Ag_2[Hg(SCN)_4]$ coating on copper wire and Hg(II); 5, $Pb[Hg(SCN)_4]$ and Hg(II).

Fig. 2. Electrode response to M^{n+} at 25 °C. 1, $Ag_2[Hg(SCN)_4]$ and Ag(I); 2, $Pb[Hg(SCN)_4]$ and Pb(II); 3, $Cu[Hg(SCN)_4]$ and Cu(II).

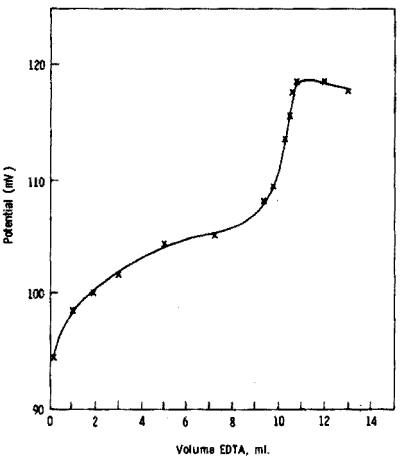

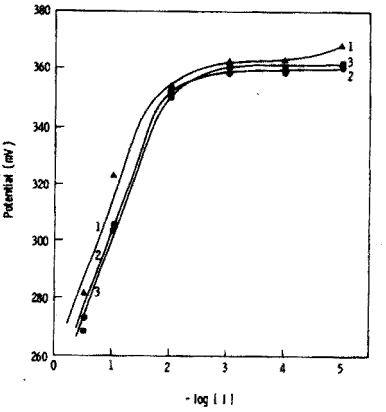

Fig. 3. Potentiometric titration of Pb(II) with EDTA using $Pb[Hg(SCN)_4]$ electrode.

Fig. 4. Electrode response to iodide. 1, $Cu_2[HgI_4]$ and I^- at 45.5 °C (▲); 2, $Ag_{1.14}Cu_{0.86}[HgI_4]$ eutectoid and I^- at 36 °C (●); 3, $Ag_{1.14}Cu_{0.86}[HgI_4]$ eutectoid and I^- at 45.5 °C (■).

M_x cation of the sensor material (Fig. 2); the sensitivity limit of about 10^{-4} M is indicative of compound solubility. The reason for the negative slope observed for Pb(II) has not yet been determined.

The $Pb[Hg(SCN)_4]$ electrode was used in the potentiometric titration of lead(II) with EDTA to determine its value as an indicator electrode. Figure 3 shows the results obtained in the titration of 20 ml of ca. 0.1 M lead perchlorate in about 100 ml of solution at pH 4.0 with 0.1 M $Na_2H_2Y_2$. There is a noticeable break in the titration curve about the equivalence point. The test titration is not a particularly good one because of the nature of the Pb[PbY] precipitate (bulky, high capacity for water, and solubility). For lead compounds with a solubility of ca. 10^{-5} mol l^{-1} a break of ca. 40 m V would be expected within 1 % of the equivalence point. These kinds of electrodes should be useful for potentiometric titration if more insoluble compounds (or compounds whose complex ions have a metal:ligand ratio of 1:1) can be prepared.

Figure 1 also shows the results obtained with an electrode prepared by simply coating the end of a plastic-insulated 16-gauge copper wire with membrane material. The wire coated with $Ag_2[Hg(SCN)_4]$—vinyl mixture gave a good response to Hg(II) in solutions containing excess of thiocyanate, but the response was slower than with electrodes containing an internal reference solution, and there was some sensitivity to inductive effects.

Figures 4 and 5 show the results obtained with $Ag_2[Hg\ I_4]$, $Cu_2[Hg\ I_4]$ and $Ag_{1.14}\ Cu_{0.86}[Hg\ I_4]$ eutectoid electrodes. The response to iodide is Nernstian (Fig. 4) but over only a very narrow range. The response to silver ion was instantaneous but inconsistent (Fig. 5); the mV change in decade change in concentration was greater than Nernstian in some cases and was

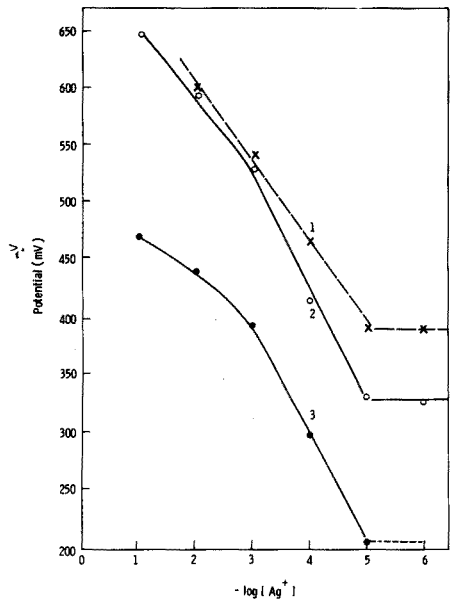

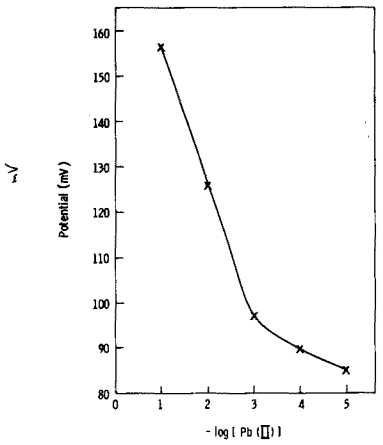

Fig. 5. Electrode response to silver(I). 1, $Ag_{1.14}Cu_{0.86}[HgI_4]$ eutectoid and Ag^+ at 26 °C; 2, $Ag_{1.14}Cu_{0.86}[HgI_4]$ eutectoid and Ag^+ 45.5 °C; 3, $Ag_2[HgI_4]$ and Ag^+ at 45.5 °C.
Fig. 6. Electrode response to Pb(II). Pb[PbY] (Y=EDTA) electrode.

irreproducible from day to day. In solutions containing excess of iodide (1 M), these sensors gave a Nernstian response (29 mV per decade) to Hg(II) from 10^{-2} to 10^{-4} M but gave a much greater change (ca. 60 mV) at higher concentrations. It is evident that these thermochromic, high-conductivity [5] compounds, which can undergo changes in stoichiometry, warrant further investigation.

Figure 6 shows a plot of potential against the negative logarithm of the concentration of lead(II) with a Pb[PbY] electrode. Since the electrode responds to variation in pH, the acidity was controlled at pH 4.0 for all measurements; a Nernstian response (30 mV/decade) to lead(II) was observed over a narrow range. The Pb[PbY] compound was prepared because it is the only well characterized slightly soluble compound containing a 1:1 EDTA—metal complex ion. The rapid response of a Pb[PbY] electrode to lead ion is probably due to the lead cation but if other slightly soluble M[NY] compounds can be made, sensitive sensors for N(II) should be possible.

This work was supported by a grant from the National Research Council of Canada.

REFERENCES

1 G. Scibona, L. Mantella and P. R. Danesi, Anal. Chem., 42 (1970) 844.
2 R. W. Cattrall and Pui Chin-Poh, Anal. Chem., 47 (1975) 93.
3 A. G. Fogg, M. Duzinkewzcz and A. S. Pathan, Anal. Lett., 6 (12) (1973) 1101.
4 M. Lebl and J. Vesely, Czech. 151, 872 (Cl B01 k), 15 Jan. 1974 Appl. 1911—70, 23 March 1970.
5 L. Suchow and G. R. Pond, J. Amer. Chem. Soc., 75 (1953) 518, 5242.

Analytica Chimica Acta, 82 (1976) 415—420
©Elsevier Scientific Publishing Company, Amsterdam—Printed in The Netherlands

Short Communication

MATRIX EFFECTS IN THE FLAMELESS ATOMIC ABSORPTION DETERMINATION OF TRACE AMOUNTS OF BARIUM IN SILICATES

R. CIONI

Istituto di Mineralogia e Petrografia dell'Università, Centro di Geologia Strutturale e Dinamica dell'Appennino, C.N.R., Pisa (Italy)

A. MAZZUCOTELLI

Istituto di Petrografia, Università di Genova, Genoa (Italy)

G. OTTONELLO

Scuola Normale Superiore di Pisa, Pisa (Italy)

(Received 2nd September 1975)

Strong matrix effects cause difficulties in determining trace amounts of barium by atomic absorption spectrometry [1—5], though the problems can be overcome in flame systems by ion-exchange separations [6]. Flameless atomic absorption spectrometry (f.a.a.s.) has been used for determinations of barium in gunshot residues [7, 8] and in silicate rocks [9], but no detailed consideration of interferences has been published. Direct f.a.a.s. determinations of barium in rock and mineral standards confirmed the existence of severe interference phenomena from complex matrices, and the work reported here was undertaken to evaluate such interferences, which may differ from those encountered in the flame method owing to the disparate atomization processes. To evaluate real interferences and to improve sensitivity, it was necessary to prevent the formation of barium carbide during atomization; for this purpose, an inner lining of titanium dioxide in the graphite tube was studied.

Experimental

The Perkin-Elmer Model 303 spectrometer used was equipped with a HGA-70 graphite furnace, an Intensitron hollow-cathode lamp and a Hitachi Perkin-Elmer Model 165 recorder. The conditions were as follows: wavelength 553.5 nm; slit width 2 nm; drying for 40 s at ca. 100 °C; charring for 30 s at ca. 1100 °C, atomization for 20 s at ca. 2550 °C (10V).

The tendency of barium to form carbides during atomization in the graphite furnace was pointed out by Renshaw [7], who eliminated the effect by using a tantalum foil to line the graphite tube; however, the vaporization of tantalum at high temperature makes it impossible to reach the optimal atomization temperature provided by the instrument (10 V).

For the lined graphite tube used here, a suspension of titanium dioxide was injected and then dried. Before use, the tube was heated several times to maximum temperature to form an inner lining of TiC_2 (m.p. 3140 ± 90 °C). The formation of barium carbide was thus limited, and absorbance and reproducibility were enhanced (Table 1). The sensitivity with the TiC_2 lining was less than that obtained with the tantalum lining [7] but sufficed for the range of barium in silicate rocks.

TABLE 1

Characteristics for modified and unmodified graphite tubes

	Sensitivity $\mu g\ ml^{-1}$ (1 % Abs)	Detection limit ($\mu g\ ml^{-1}$)	Reproducibility[a]		
			$\bar{x}$	σ	c%
Unmodified	0.06	0.01	0.154	0.012	7.6
Modified	0.04	0.004	0.201	0.004	1.9

[a]Data for 10-μl aliquots of a 1 p.p.m. barium solution.

Study of single and matrix interferences

The effects of the major elements in silicate rocks on the determination of barium by f.a.a.s. were studied in hydrochloric and nitric acid media (Fig. 1); the tube lined with titanium carbide was used. The anti-ionization effects of sodium and potassium were evident for both acid media, but were more marked in nitric acid; in the latter medium, the potassium "plateau zone" was reached only after very copious additions. In hydrochloric acid, the effect of caesium was greater than that of the other alkali metals, because of its lower ionization potential. Aluminium also caused enhancement, probably because of molecular interaction with barium compounds. Magnesium and iron showed a trend that can be attributed to a similar kind of interference. The strong depressing effect of iron in hydrochloric media may have been due to loss of barium along with volatilization of iron chloride during the charring stage. The effects of calcium were completely different in the two acid media. With barium and calcium in hydrochloric acid solutions, undissociated compounds such as calcium tetrachlorobariate [10], were probably formed during the charring state; in nitric acid solutions, oxides were probably formed in the initial atomization step [11], so that calcium merely assisted the dissociation of the barium compound [12]. No titanium interference was observed in hydrochloric acid media. Lanthanum, which has been used as a releasing agent in f.a.a.s. [2, 4], did not interfere at the Ba—La ratios present in rocks, but had a suppressing effect similar to that of calcium, if added copiously.

The effects of different acids are reported in Fig. 2; only phosphoric acid interfered, even when present in low concentrations.

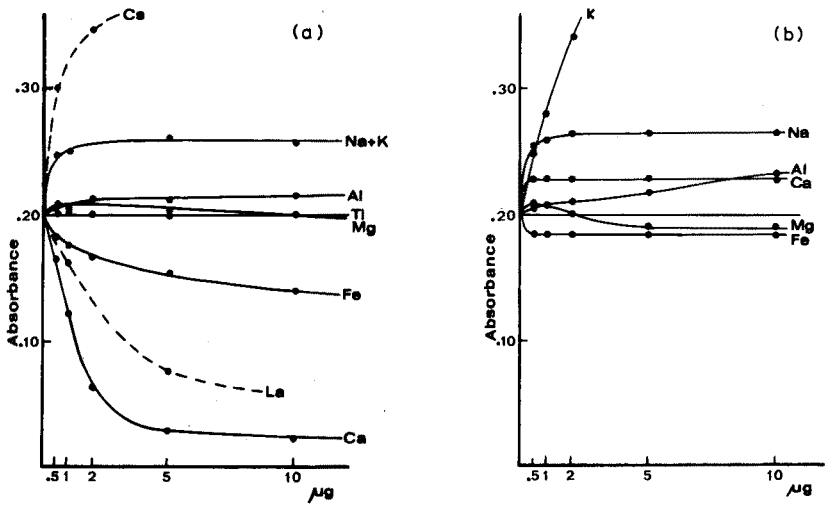

Fig. 1. Effects of various elements on the absorbance of 10 ng Ba (10μl of 1μg Ba ml^{-1} solution). (a) In 20 % (v/v) hydrochloric acid media. (b) In 20 % (v/v) nitric acid media.

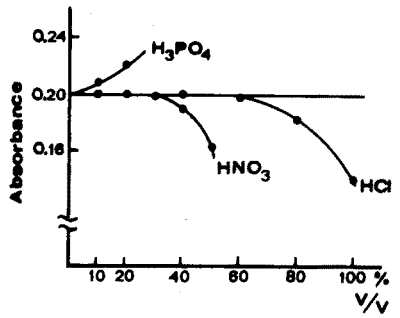

Fig. 2. Interferences of acids on the absorbance of 10 ng Ba.

The complex composition of silicate rocks makes a simple interferences study inadequate for evaluating the real interelemental effects encountered during atomization. Figure 3 shows multielement interactions on the pairs Ba—K and Ba—Ca in hydrochloric acid media. Potassium and calcium were selected as fixed elements because of their strong interferences on barium; all the elements were added in ratios corresponding to their contents in common silicate rocks. The anti-ionization effect of potassium was enhanced by aluminium, reduced by magnesium and iron, and completely masked by calcium. The depressing effect of calcium was unchanged by sodium, magnesium and potassium, reduced by iron and titanium, and eliminated by aluminium.

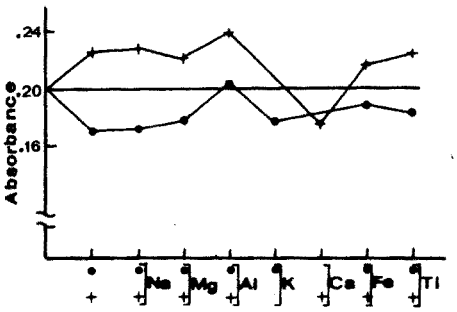

Fig. 3. Effects of various elements on the Ba—Ca and Ba—K pairs in hydrochloric acid media. (•) = 10 ng Ba + 500 ng Ca; (+) = 10 ng Ba + 2500 ng K; Na, K = 250 ng; Mg = 400ng; Al = 1000 ng; Ca Fe = 500 ng; Ti = 50 ng.

The Ca—Al—Ba—Cl interactions suggested the possibility of using aluminium as a releasing agent. The effects of 100—2500 ng of aluminium on the absorbance of 10 ng Ba + 500 ng Ca were studied in hydrochloric acid media. An Al:Ca ratio of 1:2.5 had no effect on the barium absorbance; this ratio corresponds to $AlCl_3:CaCl_2$ =2:3. When the amount of aluminium exceeded 500 ng, a "plateau zone" was reached, but the enhancing effect was quite small. Aluminium did not modify the interfering effect of calcium in nitric acid media.

Determination of barium in silicate rocks

The above interference studies made it clear that the concentration ratios of interfering elements with barium and the ratios of interfering elements between themselves, must be taken into account in evaluating the "matrix effect" for silicate rocks. Moreover, it was evident that the general effect could not be evaluated quantitatively. In most silicate rocks, barium cannot be considered as a trace element, its concentration being transitional between a "trace" and "minor" constituent. The barium measurement is therefore very dependent on rock composition. This problem was confirmed by measurements on standard silicate rocks; both nitric and hydrochloric acid sample solutions gave erroneous results, whether a calibration or a standard addition method was used. The failure of the standard addition method can be explained by the variation of interference effects with the ratio of interfering elements to barium. When large amounts of interfering elements (aluminium and potassium) were added to standardize the ratios, the reproducibility in hydrochloric acid media became poor.

Potassium and calcium added to nitric acid solutions, slightly improved the results, and some satisfactory values were obtained for barium in basic rocks. However, removal of the matrix by ion-exchange chromatography [6]

seemed the only reliable way of determining barium in rock and mineral samples by f.a.a.s. The following method is therefore recommended.

Procedure. Treat the finely powdered sample (100—500mg) with a hydrofluoric—perchloric acid mixture in a PTFE dish. Evaporate the solution to dryness and take up the residue with hydrochloric acid [6]. Bauxite and disthene are not amenable to acid attack and require a fusion procedure with 5:1 sodium carbonate—boric oxide mixture [6]. Pass the solution through a Dowex 50-X8 column (200—400 mesh, H^+ form). Elute all interfering elements with 3 M hydrochloric acid in 20 % ethanol, and then elute barium quantitatively with aqueous 3 M hydrochloric acid [6, 13, 14]. Evaporate the eluate to ca. 25 ml, and dilute to volume in a 100-ml volumetric flask. Dilute an aliquot of this solution to reach the optimal concentration range for the graphite furnace (0.5—1.5 $\mu g\ ml^{-1}$). Inject 10 μl aliquots with an Eppendorf pipette. Run blanks to compensate for any contamination during dissolution and separation. Establish the barium content from a suitable calibration graph.

The results obtained for various international standard rocks and minerals are summarized in Table 2. The agreement with literature data is considered very good.

TABLE 2

Results for barium in standard rock and minerals

Sample	p.p.m. Barium found	Recommended value	Median value
AGV-1 (Andesite)	1144	1208[a]	—
BCR-1 (Basalt)	684	675[a]	—
GH (Granite)	21	22[a]	—
GA (Granite)	773	850[a]	—
BR (Basalt)	990	1050[a]	—
DTS-1 (Dunite)	4.3	2.4[a]	—
BX-N (Bauxite)	38	—	30[b]
DT-N (Disthene)	45	—	40[b]
W-1 (Diabase)	154	160[a]	—
PCC-1 (Peridotite)	3.9	—	1.2[b]
UB-N (Serpentine)	56	—	40[b]
DR-N (Diorite)	355	360[b]	—
GSP-1 (Granodiorite)	1231	1300[a]	—
GR (Granite)	1134	1050[a]	—

[a]Ref. 15; [b]Ref. 16.

REFERENCES

1 L. Capacho-Delgado and S. Sprague, At. Abs. Newslett., 4 (1965) 362.
2 S. R. Koirtyohann and E.E. Pickett, Spectrochim. Acta, Part B, 23 (1968) 673.
3 T. Maruta, T. Takeuchi and M. Suzuki, Anal. Chim. Acta, 58 (1972) 452.
4 C. O. Ingamells, N. H. Suhr, F. C. Tan and D. H. Anderson, Anal. Chim. Acta, 53 (1971) 345.
5 B. Fleet, K. V. Liberty and T. S. West, Talanta 17 (1970) 203.
6 R. Frache and A. Mazzucotelli, Talanta 22 (1975).
7 G. D. Renshaw, At. Abs. Newslett., 12 (1973) 158.
8 J. H. Sherfinsky, At. Abs. Newslett., 14 (1975) 26.
9 H. Heinrichs and J. Lange, Fortschritte Mineralogie, 50 (1972) 35.
10 J. W. Mellor, Comprehensive Treatise on Inorganic and Theoretical Chemistry, Vol. 3, Longmans, London, (1952), p. 720.
11 C. Riandey and M. Pinta, Analusis, 2 (1973) 179.
12 B. V. L'Vov Atomic Absorption Spectrochemical Analysis, A. Hilger, London, (1970).
13 F. W. E. Strehlow, Anal. Chem., 40 (1968) 928.
14 R. Frache, A. Dadone and F. Baffi, Annal. Chim., 64 (1974) 387.
15 F. J. Flanagan, Geochim. Cosmochim. Acta, 33 (1969) 81.
16 H. de La Roche and K. Govindaraju, Analusis, 2 (1973) 59; Bull. Soc. Fran. Ceram. 100 (1973) 49.

Analytica Chimica Acta, 82 (1976) 421—425
© Elsevier Scientific Publishing Company, Amsterdam — Printed in The Netherlands

Short Communication

LINEARIZATION OF CALIBRATION CURVES WITH THE HGA-72 FLAMELESS CUVETTE FOR THE DETERMINATION OF LEAD IN BLOOD

T. A. KILROE-SMITH

Department of Biochemistry, National Research Institute for Occupational Diseases of the South African Medical Research Council, P.O. Box 4788, Johannesburg, 2000 (South Africa)

(Received 29th August 1975)

The standard conditions specified in the handbook for the Perkin—Elmer flameless cuvette give a non-linear curve when absorbance is plotted against amount of lead in the cuvette. It is possible [1] to obtain linear calibration graphs with the Beckman Model 444 when opacity instead of absorbance is plotted against the amount of lead, but when this was applied to the Perkin—Elmer HGA-72, particularly with gas stop, the linear range of the calibration graphs was limited. The shape of the graph was observed to depend on the heating conditions; this communication describes the optimization of the working conditions for linear graphs based on opacity.

Experimental

A Perkin—Elmer Model 503 atomic absorption spectrometer fitted with an HGA-72 heated-graphite atomizer was used; a Perkin—Elmer Model 056 recorder was used with no scale expansion and the recorder input was in the absorbance mode. The settings on the Model 503 were: wavelength 283.3 nm; current on low-intensity lamp 10 mA; slit 4; damping 1; repeat mode, with energy meter at 70 % of full scale. Lead standards were prepared from standard lead solution (1000 p.p.m. (w/v) Pb in 0.1 M $HClO_4$; Hopkin and Williams Ltd.) diluted to 0.1—0.4 p.p.m. with the required diluent. Three different matrices (a) 0.01 M hydrochloric acid, (b) 0.01 M nitric acid, (c) diluted precipitating mixture [2] were used. The mixture was prepared as follows: 3 parts of 72 % perchloric acid, 9 parts of 5 % trichloracetic acid, and 164 parts of water. This was used to dilute a 10 p.p.m. standard Pb solution in 0.01 M hydrochloric acid to give standards of 0.1—0.4 p.p.m. in diluted precipitating mixture. A Hamilton micro-syringe (25 μl) was used to inject the samples.

Results and discussion

Figure 1 shows the effect of atomization temperature on the normal working curves for lead in 0.01 M hydrochloric acid. These non-linear graphs are difficult to use in practice [3]. Much more satisfactory graphs are obtained when β — defined as $(I_0/I) - 1$, where I_0/I is the opacity — is plotted against the amount of lead (Fig. 2). The linear range is then limited largely by the heating conditions, and the peak height is independent of the volume of sample used up to a maximum of 50 μl for a particular set of conditions. Above 50 μl, readings are affected by excessive spread of solution in the cuvette. As can be seen from Fig. 2, when the atomization temperature is adjusted correctly, the graph can be made linear up to 8 ng of lead (correlation coefficient > 0.99, coefficient of variation < 1.3 %). If the temperature is higher than 2000 °C, the graphs curve down significantly.

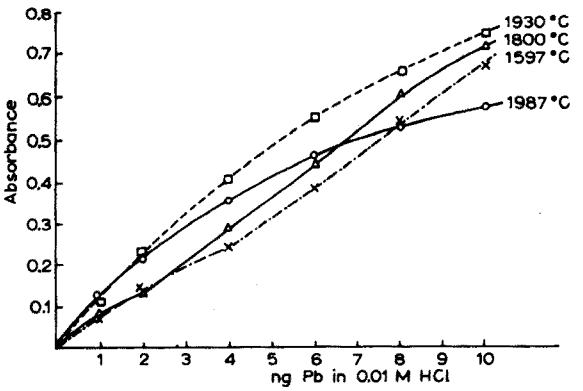

Fig. 1. Effect of atomization temperature on the absorbance at different lead concentrations. Conditions: dry, 100 °C for 30 s; ash, 450 °C for 10 s; atomization temperature given for each curve.

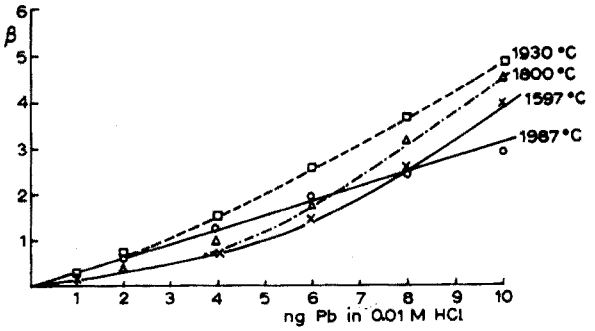

Fig. 2. Variation of curve shape with temperature of atomization — β vs. Pb. Conditions as for Fig. 1.

The reason for the change in the slope of the curve is obscure; the temperature gradient set up along the cross-section of the tube may make the metal atoms concentrate in the centre of the tube which is cooler and where most of the light absorption takes place. The rate at which this concentration effect occurs will depend on the amount of metal placed in the cuvette so that, the larger the amount of metal, the more rapidly it will tend to concentrate at the centre, resulting in an upsweep in the graph. Conversely, raising the temperature of the wall of the cuvette causes a more rapid movement of heat to the centre of the tube, and hence there is less tendency for the centre of the tube to be below the boiling point of the metal. This counteracts the tendency of metal atoms to condense along the centre axis of the cuvette and gives a more uniform distribution of the atoms so that Beer's law is obeyed more closely.

The optimum conditions required with the gas stop differ from those when it is not used. With the gas stop, a higher atomization temperature is required to obtain linearity over a reasonable range of concentration (Table 1). With precipitation mixture as matrix, it was not possible to achieve a temperature with the gas stop mode that was sufficiently high to give a linear graph beyond 3 ng Pb. In practice, this is not a disadvantage as the gas stop mode is only required when greater sensitivity is needed for low concentrations of lead. Up to 3 ng the graph is perfectly linear in diluted precipitation mixture for the following conditions: dry at 100 °C for 30 s; ash at 740 °C

TABLE 1

Optimum conditions for the determination of lead[a]

	Ashing		Atomization		Slope
	Setting	°C[b,c]	Setting	°C[b]	β per ng Pb
(a) Without gas stop					
Pb (0.01 M HCl)	106	450	475	1987	0.299
Pb (0.01 M HCl)	160	740	380	1747	0.325
Pb (0.01 M HNO_3)	106	450	480	1998	0.25
Pb (pptn. mixture)	126	550	600	2231	0.23
Pb (pptn. mixture)	160	740	500	2040	0.23
(b) With gas stop					
Pb (0.01 M HCl)	106	450	600	2231	0.785
Pb (0.01 M HNO_3)	106	450	600	2231	0.758
Pb (pptn. mixture)	126	550[d]	950	2650	0.81

[a]In all cases argon was the purging gas and drying was at 100 °C for 30 s.
[b]The temperature was obtained from the tables supplied by the manufacturers, and not read on the meter.
[c]The ashing time was 10 s in all cases, except for the tests without gas stop with the lead in precipitation mixture when a 20-s ashing time was used.
[d]An additional step after ashing was introduced before atomization, viz. temperature programming at rate 6 (125 digital values min^{-1}) to a setting of 190 (= 950 °C), i.e. 35.5 s to rise to 950 °C.

for 10 s; temperature programme 6 up to 950 °C; atomization at 2650 °C for 5 s. Without the gas stop the graph can be made linear up to at least 8 ng of lead. Table 1 shows that the slope varies for the different matrices, but to a lesser extent when the gas stop is used.

To obtain optimum curves, it is necessary to control the atomization temperature carefully. The temperature in the tube when maximum peak height is reached depends on the previous history of heating before atomization. When the heating current is applied to the tube, the time required for the interior of the tube to reach the same temperature as the walls depends on the dimensions of the tube; the smaller the diameter of the tube, the shorter the time required. If, however, the time required to reach an equilibrium temperature is longer than the time to reach peak absorbance, there will be a temperature gradient in the tube with the lowest temperature in the centre. In the Perkin—Elmer instrument the concentrated light beam is usually adjusted along the central axis of the tube, so that the temperature of the axis is of major importance. Since it is not possible to get an equilibrium temperature in this region before peak height is reached, a compromise has to be made and conditions so arranged that the gradient in temperature applied at the start of the atomization stage results in the optimum temperature being reached at the central axis exactly at the time when peak absorbance is read. Thus when the ashing temperature is higher, the nominal atomization temperature has to be lower. It was also found that increasing the ashing time decreases the optimum atomization temperature. Thus, ashing at setting 160 (740 °C) for 60 s and atomization at setting 380 (1747 °C) gave an almost identical regression curve to that obtained with ashing at 160 (740 °C) for 10 s and atomization at setting 400 (1800 °C).

There is a very good correlation (Fig. 3) between the reciprocal of the peak absorbance and the square of the time taken to reach peak value. The correlation coefficient is 0.999 in this case (9 degrees of freedom), with a coefficient of variation of 1.5 %. When gas stop is used, the time to reach

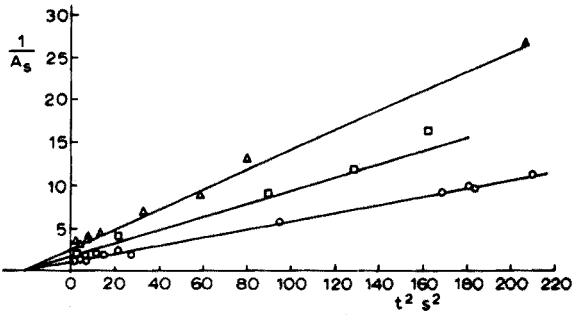

Fig. 3. Graph $1/A_s$ vs. t^2, where t = time (s) to reach peak absorbance and A_s = peak absorbance. Conditions: dry, 100 °C for 20 s; ash, 450 °C for 10 s; atomize, varying temperatures. △, 4 ng Pb without gas stop; □, 2 ng Pb with gas stop; ○ 4 ng Pb with gas stop.

peak maximum is very much longer and hence the slope is much lower. In these graphs, the equation $1/A_s = bt^2 + 1/a$ applies, where a is a theoretical absorbance obtained when the sample is atomized instantaneously, and the peak height is recorded immediately.

Another conclusion is that the general assumption that some lead is lost when ashing is carried out above 550 °C is not necessarily correct. The apparent loss of lead is to be attributed rather to a disturbance of the temperature conditions. Heating at 740 °C for 60 s gave no loss of lead in the hydrochloric or nitric acid solutions; with the precipitation mixture, there was no loss on heating at 850 °C for 60 s. Ashing at 950 °C caused considerable loss of lead in all the solutions tested.

REFERENCES

1 T. A. Kilroe-Smith, Clin. Chem., 21 (1975) 630.
2 Ö. Einarsson and G. Lindstedt, Scand. J. Clin. Lab. Invest., 23 (1969) 367.
3 P. Baily and T. A. Kilroe-Smith, Anal. Chim. Acta, 77 (1975) 29.

Analytica Chimica Acta, 82 (1976) 427—430

©Elsevier Scientific Publishing Company, Amsterdam — Printed in The Netherlands

Short Communication

DETERMINATION OF MERCURY IN FINGER NAILS AND BODY HAIR

CHRISTINE A. HELSBY

Department of Conservative Dentistry, University of Manchester, Manchester 15 6FH (England)

(Received 27th September 1975)

Contamination of dental personnel with mercury has been estimated from the analysis of finger nails, toe nails and body hair by neutron activation analysis [1, 2], but this technique is expensive for screening work. Recently, the flameless cold-vapour atomic absorption technique described by Hatch and Ott [3] has been used for the analysis of a number of body tissues. Hair has been analyzed after digestion either with a mixture of concentrated nitric and sulphuric acids and potassium permanganate at room temperature [4] or with sodium hydroxide solution (11.2 M) at 125 °C [5]. Other body tissues have been analysed after similar lengthy digestions with concentrated acids and strong oxidants [6], or after digestion in a Uni-Seal decomposition vessel with nitric acid at 150 °C for 30—60 min [7]. Biological materials have been analysed by Schöniger oxygen flask combustion and the cold-vapour technique applied either directly [8, 9] or after an amalgamation step [10]. Ure and Shand [9] replaced the conventional platinum basket of the Schöniger method with a perforated tantalum basket to overcome any interference from platinum in the subsequent determination.

The procedure described below involves Schöniger flask combustion of nails and hair followed by flameless cold-vapour analysis. The method is considerably cheaper and faster than neutron activation analysis. An additional advantage is the use of the combustion flask as an aeration flask so that the possibility of transference losses is eliminated.

Experimental

Instrumentation. A Perkin-Elmer model 303 atomic absorption spectrophotometer was fitted with a recorder-readout accessory and a Hitachi 165 recorder. The spectral source was a mercury Intensitron hollow-cathode lamp operated at 253.65 nm.

Aeration apparatus. Air (1.5 l min^{-1}) was pumped (Charles Austen Capex Mark II pump) through a Drechsel bottle head (porosity 2 glass filter) into a 250-ml Quickfit conical flask. The outlet from the flask was connected to a

drying tube containing magnesium perchlorate. The air then passed into a 15-cm gas cell of 10-mm diameter fitted with silica windows and positioned in the optical path of the spectrometer. The air returned to the pump to complete the closed circuit. The circuit contained a 3-way valve by which the air stream could be passed through a scrubbing tube containing activated charcoal, which removed any mercury vapour from the air-stream after absorption measurements had been completed.

Reagents and preparation. All new glassware was boiled in 6 M nitric acid for 20 min before use. After washing, all glassware was rinsed several times with 10 % (v/v) nitric acid; no organic solvents were used. All the acids were Aristar grade and the other chemicals were Analar grade. Solutions were prepared with distilled-deionized water. The mercury was liberated with tin(II) chloride (20 % w/v) prepared in 5 M hydrochloric acid. This solution was aerated for 2 h before use to remove any traces of mercury present in the reagent and acid.

Mercury solutions. A 1000 p.p.m. stock solution of mercury as $HgCl_2$ (B.D.H.) was used for the preparation of standards by suitable dilutions. For the recovery studies, mercury(II) chloride and phenylmercury acetate were used.

Procedure. Use up to 25 mg of nail or hair sample. Wrap nail samples in Whatman No. 541 filter paper, or insert hair samples in gelatin capsules. Introduce 6 ml of 50 % (v/v) nitric acid into a dry 250-ml Quickfit conical flask, flush with a rapid flow of oxygen for a few seconds, ignite the fuse and burn the sample in the usual way. When combustion is complete, shake the flask for 1 min and allow to stand for 5 min.

Wash the stopper and gauze with 2 ml of 50 % (v/v) nitric acid followed by 10 ml of deionized water, and dilute to 140 ml with deionized water. Stir the solution with a magnetic stirrer for 5 min to remove any nitrous oxide fumes. Add 20 ml of tin(II) chloride solution, quickly connect to the Drechsel head of the aeration apparatus and mix well. Aerate the sample solution and conduct the air—mercury vapour through the gas cell until a steady equilibrium is achieved on the recorder. Record the maximum peak deflection. Use the 3-way valve to conduct the air—mercury vapour through the scrubber until the recorder pen returns to zero deflection.

Calibration. To 8-ml portions of 50 % (v/v) nitric acid in 250-ml Quickfit conical flasks add 0.1, 0.2, 0.3 or 0.4 ml of a freshly prepared mercury standard solution (1 $\mu g\ ml^{-1}$) and dilute to 140 ml with deionized water. Repeat the relevant stages of the procedure described above. The filter paper and gelatin capsule did not give an absorption reading for mercury.

Analytica Chimica Acta, 82 (1976) 431—434
© Elsevier Scientific Publishing Company, Amsterdam — Printed in The Netherlands

Short Communication

EXTRACTION SPECTROPHOTOMETRIC DETERMINATION OF NICKEL IN CRUDE OIL WITH 4-(2-PYRIDYLAZO)-RESORCINOL

TAKAO YOTSUYANAGI, RYUJI YAMASHITA, HITOSHI HOSHINO and KAZUO AOMURA

Laboratory of Analytical Chemistry, Faculty of Engineering, Hokkaido University, Sapporo, 060 (Japan)

HIDEO SATO and NOBUSUKE MASUDA

Tomakomai Technical College, Tomakomai, 059-12 (Japan)

(Received 27th June 1975)

The dimethyglyoxime—bromine (DMG—Br_2) method [1] has been used extensively for the colorimetric determination of nickel. To determine nickel in crude oil, 50—100 g of oil is usually treated with sulfuric acid (wet oxidation method) [2]. Since the digestion of such a large amount of oil is time-consuming and tedious, a more sensitive method has been developed.

4-(2-Pyridylazo)-resorcinol (PAR) has been applied to the determination of many metals [3], but it shows little selectivity, though EDTA can be used as a masking agent especially for d^3 ions (Cr^{3+}) [4], d^6 ions (Co^{3+}, Fe^{2+}) [5] and d^8 ions (Pd^{2+}) [6]. Iron and cobalt interfere seriously with the determination of nickel even in the presence of EDTA [7], however.

In the present work, a simple masking method for cobalt with 3-methylglyoxime and the extraction of the nickel—PAR chelate with tetradecyldimethylbenzylammonium chloride ($TDBA^+ Cl^-$) has been studied. A selective method for nickel is proposed; the sensitivity is much greater than that of the DMG—Br_2 method.

Experimental

Apparatus and reagents. A Hitachi model 124 double-beam recording spectrophotometer and Perkin-Elmer model 139 spectrophotometer were used with 10-mm optical cells.

For 0.1 % PAR solution, dissolve 0.100 g of PAR (Dojindo Co. Ltd., Japan) in 10 ml of 0.1 M sodium hydroxide solution and dilute to 100 ml with water. Prepare aqueous solutions containing 0.05 M tetradecyldimethylbenzylammonium chloride (Dojindo Co. Ltd.) and 0.1 % (w/v) 3-methylglyoxime (Tokyo Kasei Kogyo Co. Ltd.).

Procedure. Transfer an aliquot (not more than 40 ml), containing 0.2—5 μg

of nickel, to a 100-ml separatory funnel, and dilute to 30—40 ml. Add 1.0 ml of 0.1 % cupferron solution and adjust to pH 0.5—1 with 3 M hydrochloric acid solution. Extract twice with 10 ml of chloroform, shaking for 5 min each time. Transfer the aqueous layer to a 50-ml beaker, and add 2 ml of 0.1 % 3- methylglyoxime solution and 2 ml of 0.05 M borax solution. Adjust the pH to 8.5—8.8 with 0.2 M and 3 M sodium hydroxide solutions. After 10 min, add 0.5 ml of 0.1 % PAR solution and allow the mixture to stand for 30 min. Add in order (mixing after each addition) 2 ml of 0.2 M sodium hydroxide solution (adjust the pH to 9.3—9.5), 2 ml of 0.05 M EDTA (pH 9.3—9.5) and 1.5 ml of 0.05 M $TDBA^+ \cdot Cl^-$ solution. Transfer the solution to a 100-ml separatory funnel, and extract with 10 ml of chloroform, shaking for 10 min. Remove droplets of water in the chloroform solution with filter paper, and measure the absorbance at 500 nm against a reagent blank.

Results and discussion

The orange—red, water-soluble nickel—PAR complex can be extracted quantitatively into chloroform with $TDBA^+$ ($[TDBA^+] = 1—3 \cdot 10^{-3}$ M in aqueous solution). EDTA at similar concentrations acts not only as a masking agent for interfering metals but also as an emulsion breaker, which favors phase separation. A maximal and constant absorbance is obtained in chloroform over the pH range 8.5—9.5 and the color is stable for at least 3 h. The extracted complex has an absorption maximum at 500 nm; Beer's law applies in the range 0.2—12 μg of nickel in 10 ml of chloroform. The apparent molar absorptivity is $7 \cdot 10^4$; the sensitivity (Sandell index) is $8.5 \cdot 10^{-4}$ μg Ni cm^{-2}, which is about five times more sensitive than the dimethylglyoxime—bromine method ($4.2 \cdot 10^{-3}$ μg Ni cm^{-2})[1].

The composition of the nickel—PAR—$TDBA^+$ ternary complex was determined by Job's method to be $[Ni(R)_2^{2-}]$ $[TDBA^+]_2$, which corresponds well with the predominant nickel—PAR species, $[Ni(R)_2]^{2-}$, in alkaline solution [8].

Details of the equilibrium studies made on the extraction system will be published elsewhere.

Selective masking. The PAR chelates of metal ions, other than Ni^{2+}, Fe^{2+}, Co^{3+}, Cr^{3+} and Pd^{2+}, are decomposed by EDTA at room temperature. Therefore, interferences from ions such as Al^{3+}, Cd^{2+}, Cu^{2+}, Hg^{2+}, Mg^{2+}, Mn^{2+}, Pb^{2+}, Sn^{2+} and Zn^{2+} (all 500 μg) and 100 μg of Ag^+ and V(V) can be screened with EDTA.

Interference from Pd(II) and Cr(III) is negligible, because the abundance of Pd(II) in crude oil is very small compared with that of nickel, and the very slow color reaction of Cr(III) with PAR at room temperature can be neglected. Fe(III) can be removed by cupferrate extraction [9] at pH 1; this also removes V(V), Mo(VI), Ti(IV), Zr(IV) and Sb(III). Thus only cobalt interferes seriously with the determination of nickel.

3-Methylglyoxime is suitable for the selective masking of cobalt. It forms [10] stable colorless complexes with nickel (λ_{max} = 259 nm, $\epsilon = 1.53 \cdot 10^4$) and cobalt ($\lambda_{max}$ = 260 nm, $\epsilon = 1.67 \cdot 10^4$) at pH 8—9.3. The cobalt complex does not react with PAR, whereas the nickel complex reacts to form the PAR complex quantitatively within 30 min at pH 8.5—8.8 (Fig. 1). For a mixture of 50 μg Co(II) and 20 μg Ni(II), analysis gave a recovery of 20.0 μg Ni (with masking) and 65.6 μg Ni (without masking).

Determination of nickel in crude oils. Treat a sample, estimated to contain a minimum of 1 μg of nickel, with concentrated sulfuric acid [2] to obtain the inorganic salt solution, and then determine nickel as described above. The results are summarized in Table 1, together with the results determined by atomic absorption spectrometry for ten different crude oil samples.

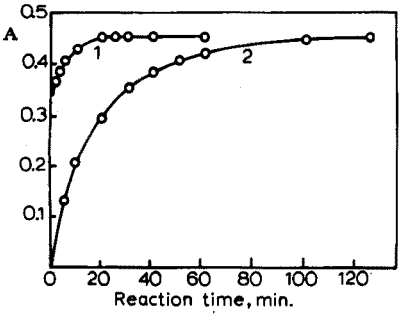

Fig. 1. Absorbance—reaction time curve. 1, at pH 8.8. 2, at pH 9.3. [Ni] = 20 μg/50 ml of water, without extraction. 500 nm.

TABLE 1

Determination of nickel in crude oil samples from Japanese petroleum refineries

Sample	Ni found (μg g^{-1} of crude oil)		Sample	Ni found (μg g^{-1} of crude oil	
	Present method	A.a.s.		Present method	A.a.s.
Arabian medium	2.8	2.7	Iranian heavy	31.9	31.6
Arabian heavy	15.2	15.1	Zubair	4.9	4.8
Kuwait	8.4	8.3	Sumatra light	8.8	7.6
Kahfji	15.4	16.6	Monagas	76.0	77.2
Hout	6.0	5.5	Tiajuana	38.0	37.4

REFERENCES

1 E. B. Sandell, Colorimetric Determination of Traces of Metals, Interscience, New York, 3rd edn., 1959, p. 668.
2 O. I. Milner, Analysis of Petroleum for Trace Elements, Pergamon, New York, 1953, p. 58.
3 S. Shibata, in A. J. Barnard and H. Flaschka (Eds.), Chelates in Analytical Chemistry, Vol. III, Dekker, New York, 1972.
4 T. Yotsuyanagi, Y. Takeda, R. Yamashita and K. Aomura, Anal. Chim. Acta, 67 (1973) 297.
5 T. Yotsuyanagi, R. Yamashita and K. Aomura, Anal Chem., 44 (1972) 1091.
6 T. Yotsuyanagi, H. Hoshino and K. Aomura, Anal. Chim. Acta, 71 (1974) 349.
7 Y. Shijo and T. Takeuchi, Jap. Anal., 14 (1965) 511.
8 D. Nonova and B. Evtimova, Anal. Chim. Acta, 62 (1972) 456.
9 J. Stary and J. Smizanska, Anal. Chim. Acta, 29 (1963) 546.
10 N. Masuda and M. Kajiwara, Jap. Anal., 19 (1970) 1613.

Analytica Chimica Acta, 82 (1976) 435—437
© Elsevier Scientific Publishing Company, Amsterdam — Printed in The Netherlands

Short Communication

RAPID EXTRACTION—SPECTROPHOTOMETRIC DETERMINATION OF GOLD(III) WITH 4-(2-THIAZOLYLAZO)-RESORCINOL

B. SUBRAHMANYAM and M. C. ESHWAR

Department of Chemistry, Indian Institute of Technology, Bombay-400 076 (India)

(Received 20th August 1975)

Various extractive spectrophotometric methods for the determination of gold(III) have been summarized recently [1]. 4-(2-Thiazolylazo)-resorcinol (TAR) has been used in acidic or slightly alkaline media for spectrophotometric determinations of various elements such as copper and bismuth [2], cobalt [3], nickel [4], niobium [5], tantalum [6], palladium [7], thorium [8] and uranium [9].

Gold(III) reacts with TAR in acidic solutions, and the resulting complex is extractable into xylene—n-butanol (4:1). The reaction of gold(III) with TAR is more sensitive than that with 4-(2-pyridylazo)-resorcinol (PAR) [1], the Sandell sensitivities being 0.013 and 0.051 $\mu g\ cm^{-2}$, respectively. The TAR method for gold proposed here is applicable for the determination of gold in the presence of silver, platinum metals, nickel and various fission products.

Experimental

Reagents and apparatus. A stock solution of gold was prepared from gold(III) chloride and standardized as described previously [1]. 4-(2-Thiazolylazo)-resorcinol (Fluka A.G., puriss) was used; other chemicals were of AnalaR grade (BDH).

Apparatus used included a Perkin-Elmer model 402 recording spectrophotometer, a Spektromom 204 spectrophotometer, and a Cambridge pH meter.

Procedure. Place an aliquot of gold solution containing less than 108 μg Au in a 50-ml beaker, add 20 ml of distilled water, and adjust the pH to 1.5 with 1 M nitric acid. Transfer the solution to a 100-ml separating funnel, add 1 ml of methanolic 0.1 % TAR solution, and leave for 5 min with intermittent shaking. Add 8 ml of xylene and 2 ml of n-butanol, shake thoroughly for about 1 min, allow the phases to separate, collect the organic layer in a 10-ml volumetric flask, and dilute to the mark with the mixed solvent. Add 1 g of sodium sulphate to remove water droplets and measure the absorbance of the complex at 520 nm in 10-mm cells against a reagent blank prepared under the same conditions.

Results and discussion

In nitric acid media at pH 1.5, gold(III) and TAR form a red complex which can be extracted into xylene—n-butanol (4:1). When the volume of TAR solution was varied from 0.1 to 4.0 ml for 72 μg Au/10 ml, the absorbance was constant with amounts greater than 0.3 ml; hence, 1 ml of reagent was used in further studies. When the pH of the reaction mixture was varied from 0.3 to 7.0, maximum absorbance was observed in the pH range 0.8—3.5, and a pH of 1.5 (adjusted with 1 M nitric acid) was chosen for the routine method.

In aqueous media, the gold(III)—TAR complex remained stable for only 10 min, but better stability was achieved by extraction into organic solvents. The complex was completely extracted into (4:1) xylene—n-butanol. The same absorbance was observed whether or not n-butanol was present, but a faint yellow color persisted in the aqueous phase — even in the blank — when xylene alone was used; possibly the excess of reagent was not completely extracted. The optimal ratio of xylene to n-butanol was found to be 8:2 or 7:3. The extracted complex was stable for at least 80 min. When the time of extraction was varied from 30 to 360 s, complete extraction was obtained within 45 s, hence a period of 60 s was adopted.

The absorption spectrum of the gold—TAR complex measured against a reagent blank over the range 470—710 nm, showed a single fairly broad peak with maximal absorbance at 520 nm. The spectrum of the reagent itself measured against the solvent showed negligible absorbance at this wavelength. The Job and mole ratio methods showed that the complex contained a 1:1 metal-to-ligand ratio.

Beer's law was obeyed in the concentration range 0.09—10.8 μg Au ml^{-1} at 520 nm. The molar absorptivity of the complex was $1.47 \cdot 10^4$ l mol^{-1} cm^{-1}, and the Sandell sensitivity index was 0.013 μg cm^{-2}. The relative standard deviation and relative error, calculated from 10 repeat determinations of solutions containing 3.6 μg Au ml^{-1}, were ± 1.02 % and ± 0.8 %, respectively.

Effect of diverse ions. In the study of interferences, the tolerance limit was set as the amount of diverse ion causing an error less than 2 % in the recovery of gold. The results are shown in Table 1. Among the important ions tolerated are silver, platinum, ruthenium, rhodium, iridium and nickel.

The authors express their sincere thanks to the Council of Scientific and Industrial Research, India, for the award of a Junior Research Fellowship to one of them (B.S.).

TABLE 1

Effect of diverse ions
(Amount of gold(III) taken, 36 μg/10 ml)

Tolerance limit (mg)	Ion added
5.0	Mg(II), Ca(II), Sr(II), Ba(II), Zn(II), Cd(II), Mn(II).
2.5	F^-, tartrate, citrate, acetate, malonate
2.0	Pb(II)
1.0	Ag(I), Ni(II), Cr(III), Rh(III), Ru(III), Ir(III), Th(IV), Se(IV) Te(IV), Re(VII).
0.5	V(V), U(VI), Tl(I), Be(II)
0.25	Al(III), Sb(III), Pt(IV), Ti(IV), Mo(VI), W(VI).
0.10	Hg(II)

REFERENCES

1 S. G. Nagarkar and M. C. Eshwar, Anal. Chim. Acta, 71 (1974) 461.
2 M. Hnilockova and L. Sommer, Talanta, 13 (1966) 667.
3 A. Kawase, Jap. Anal., 12 (1963) 817.
4 A. Kawase, Jap. Anal. 12 (1963) 810.
5 V. Patrovsky, Talanta, 12 (1965) 971.
6 G. Nickless, F. H. Pollard and T. J. Samuelson, Anal. Chim. Acta, 39 (1967) 37.
7 H.-K. Lin, K.-Y. Chen and F.-C. Cheng, Hua Hsueh Tung Pao, (1966) 365.
8 T. Sakai and K. Tonosaki, Bull. Chem. Soc. Japan, 42 (1969) 2718.
9 L. Sommer and V. M. Ivanov, Talanta, 14 (1967) 171.

Analytica Chimica Acta, 82 (1976) 439—442
© Elsevier Scientific Publishing Company, Amsterdam — Printed in The Netherlands

Short Communication

RAPID DETERMINATION OF LIME IN MAGNESIA, CHROME-CONTAINING MAGNESIA REFRACTORIES AND CHROME ORES BY EDTA TITRATION

SUBRATA BANERJEE and J. B. VIZZINI

General Refractories Research Center, P.O. Box 1673, Baltimore, Maryland 21203 (U.S.A.)

(Received 8th August 1975)

Lime plays a very important role in magnesia and chrome ore-containing magnesia refractory materials; CaO reacts with SiO_2 and MgO forming various compounds such as calcium silicates, merwinite, monticellite or forsterite depending on the temperature and the amounts and ratios of SiO_2 and CaO. The formation of eutectics from these compounds influences the properties of the refractory compositions to a great extent.

The existing ASTM methods for lime determination in magnesia [1] and chrome-containing refractories and chrome ores [2] are time-consuming and call for considerable technical skill in achieving accurate results; one set of six samples need 8—9 h for magnesia and about 25 h for chrome-containing refractory materials and chrome ores.

Moreover, the coprecipitation of calcium and magnesium ions by ammonium hydrogenphosphate may be unsatisfactory in the presence of a large amount of magnesium, resulting in slightly low values for calcium. A rapid and accurate method for lime determinations is therefore necessary. Fortunately all the calcium compounds formed in these materials are acid-soluble; this is the basis of the rapid method presented below.

EDTA, since its introduction in 1946 by Schwarzenbach for analytical application, has been investigated extensively for the determination of various elements, calcium and magnesium being the most studied ones. Various methods for the EDTA titration of CaO and MgO in cements, silicates, and related materials have been published; a comprehensive review has been given by Jugovic [3]. The R_2O_3 group can either be removed or complexed before addition of EDTA.

In the present investigation, the R_2O_3 group was masked with triethanolamine. Hydroxynaphthol blue was found to give the sharpest end-point; ca. 0.07 % CaO could be titrated. Polyvinyl alcohol [4] was added during the titration to reduce the adsorption of the dye on the large amount of $Mg(OH)_2$ precipitate. For chrome-containing refractory magnesia materials and chrome ores, the acid-insoluble portion (chromite spinel) was filtered off. The total times for lime determinations in sets of six samples in magnesia and chrome-containing magnesia refractory materials (and chrome ores) were 3 h and 7 h,

respectively, which is a time saving of 60—70 % over the corresponding ASTM procedures.

EXPERIMENTAL

Reagents. Distilled water was used throughout. All reagents were analytical grade unless otherwise mentioned. The 0.025 M EDTA, prepared in the usual way was stored in a polyethylene bottle.

For the 0.025 M $CaCl_2$ solution, reagent-grade $CaCO_3$ was dried at 105—110 °C for 2 h and cooled in a desiccator; 2.502 g of this $CaCO_3$ was dissolved in 5 ml of 12 M HCl and 25 ml of water by heating to boiling, and then the solution was evaporated nearly to dryness. Water (100 ml) was added and the solution was diluted to 250 ml in a volumetric flask.

For the 0.1 % polyvinyl alcohol solution, an aqueous 1 % (w/v) solution (100 ml) was prepared with boiling water; after cooling, 1.0 g of $MgCl_2 \cdot 6H_2O$ was added and the solution was diluted to 1 l.

Procedure. Boil 0.5 g of finely powdered (-325 mesh) sample with 20 ml of (1 + 2) HCl for 5—10 min in a 250-ml beaker. Magnesia samples go into solution completely. For chrome-containing magnesia materials and chrome ores, filter the solution through two No. 40 Whatman filter papers, and wash the residue several times with hot water. Add 3 drops of 0.1 % (w/v) methyl red indicator followed by 5 ml of 0.1 % polyvinyl alcohol solution and 5 ml (10 ml in case of materials with high R_2O_3) of aqueous 40 % (v/v) triethanolamine. Stir and allow to stand for 10 min. Add an appropriate amount (depending on the range of CaO content in the sample) of 0.025 M EDTA solution, and allow to stand for 15 min. Neutralize the solution with 20 % KOH solution, adding 20 ml in excess. Stir vigorously, add about 1 g of hydroxynaphthol blue indicator preparation (1 g of indicator ground with 50 g of KCl) stir again. Titrate the excess of EDTA with 0.025 M $CaCl_2$ solution to the color change from blue to the first permanent tint of purple. (% CaO = ml EDTA consumed × molarity of EDTA × 0.05608 × 100/sample wt.)

Results and discussion

Twelve magnesia samples normally used in the industry, thirteen chrome-containing magnesia materials (including NBS Standard Sample 104) and four chrome ores (including NBS Standard Sample 103a) were analysed in duplicate by this method and compared with the values obtained from ASTM methods (Table 1). The average percentage relative deviations from the ASTM results were 2.5 % and 3.5 % for the magnesias and chrome-containing magnesias, respectively; the latter value was obtained when results 11—13 were omitted. The correlation between the proposed method and ASTM method for CaO values was extremely good for magnesia materials, and for the chrome-containing magnesias, except for samples 11—13.

TABLE 1

Lime determination in standards and other samples

Sample	% CaO		Deviation (%)	% Relative deviation
	ASTM method	Rapid EDTA[a]		
Magnesia materials				
SL-96	2.46	2.41	−0.05	2.0
SL-98	0.72	0.70	−0.02	2.8
G-90	2.10	2.07	−0.03	1.4
SL-96	2.14	2.05	−0.08	3.7
DB-87	4.18	4.24	+0.06	1.4
SL-98	0.61	0.56	−0.05	8.2
CM-94	0.95	0.92	−0.03	3.1
SL-98	0.81	0.82	+0.01	1.2
SL-96	2.95	2.89	−0.06	2.0
SL-88	3.83	3.88	+0.05	1.3
SL-88	4.63	4.61	−0.02	0.4
HBG	2.70	2.62	−0.08	2.9
Chrome—magnesia refractory materials				
1	3.17	3.03	−0.14	4.7
2	3.10	3.09	−0.01	0.3
3	1.35	1.28	−0.07	5.5
4	0.67	0.65	−0.02	3.1
5	0.72	0.73	+0.01	1.4
6	1.01	0.97	−0.04	5.0
7	0.88	0.91	+0.03	4.0
8	0.67	0.70	+0.03	5.0
9 (NBS 104)	3.35[b]	3.30	−0.05	1.5
10	1.95	1.99	+0.04	1.5
11	2.55	3.25	+0.70	27.5
12	1.42	1.81	+0.19	11.8
12	2.13	2.38	+0.25	10.5
Chrome ores				
NBS 103a	0.69[b]	0.68	−0.01	1.4
Philippine	0.75	0.68	−0.07	10.4
Transvaal	0.12	0.16	+0.04	33.3
Russian	0.56	0.63	+0.07	12.5

[a] Average of duplicate results.
[b] From NBS Analysis Certificate.

It was noted that after the addition of triethanolamine at least 10 min was needed for complete reaction; at shorter times, CaO values were low. Also, a minimum of 10 min was needed after the EDTA addition to obtain reproducible results.

It can be seen from Table 1 that the results for the NBS Standard 104 for chrome refractory and 103a Chrome Ore agree satisfactorily; but for Samples

11, 12 and 13, and for the Transvaal and Russian chrome ores, the CaO values are considerably higher by the EDTA method than the ASTM method, possibly because of errors arising during coprecipitation as phosphates in the ASTM procedure. The EDTA method seems to be highly reproducible, rapid and convenient for these types of refractory materials.

The authors acknowledge constant inspiration by W. S. Treffner and gratitude to General Refractories Company management for permitting the publication of this work.

REFERENCES

1 Annual Book of ASTM Standards, April 1974, Part 17, C 574—71, p. 505—514.
2 Annual Book of ASTM Standards, April 1974, Part 17, C 572—70, p. 484—491.
3 Z. T. Jugovic, Analytical Techniques for Hydraulic Cement and Concrete, Special Technical Publication No. 395, ASTM, 1965 p. 65—93.
4 A. I. Vogel, A Textbook of Quantitative Inorganic Analysis, Longman, 1971, p. 439.

ANALYTICA CHIMICA ACTA, VOL. 82 (1976)

AUTHOR INDEX

ANALYTICA CHIMICA ACTA, VOL. 82 (1976)

SUBJECT INDEX

Amino Acids, Peptides and Proteins

Biochemical and Immunochemical Techniques in Protein Chemistry

by T. DÉVÉNYI, Enzymology Department, Institute of Biochemistry, Hungarian Academy of Sciences, Budapast, and J. GERGELY, Department of Immunochemistry, National Institute of Haematology and Blood Transfusion, Budapest.

1974. 344 pages. Dfl. 80.00 (about US$30.80) ISBN 0-444-41127-5

This practical textbook is a summary of the most important methods used in protein biochemistry and immunochemistry. These methods are finding steadily widening applications in biochemical and clinical laboratories, and their uses are increasingly interwoven. The book gives detailed, practical descriptions of the general methods, procedures and equipment of protein analysis; gel chromatography, ion-exchange chromatography and thin-layer chromatography of these substances are also discussed. A treatment is given of the most modern techniques of determining the amino acid sequence, of amino acid analysis on automatic basis. This is completed with the indication of the possible sources of error and their elimination.
Practical problems in the immunochemical and electrophoretic investigation of proteins and recent results concerning proteins of biological importance are also included.

CONTENTS:

Elsevier
P.O. BOX 211
AMSTERDAM, THE NETHERLANDS

1363 E

Molecular Spectroscopy of Dense Phases

Proceedings of the XIIth European Congress on Molecular Spectroscopy, Strasbourg, July 1-4, 1975.

edited by **M. GROSMANN, S.G. ELKOMOSS** *and* **J. RINGEISSEN**

1976. 848 pages. US $59.95/Dfl. 150.00. ISBN 0-444-41409-6

The European Congress on Molecular Spectroscopy is recognized as being one of the most important events on the calendar of spectroscopists. The proceedings of the twelfth Congress recorded in this book consist of twenty invited papers and one hundred and twenty shorter communications. The spectral properties of isolated molecules are nowadays fairly well understood. Increasingly, interest is becoming focused on the interactions which occur between nearby molecules in dense phases. These interactions are analysed by studying their evolution with time as well as their dependence on intermolecular distance. Seven separate topics were discussed at the Congress. Each provides a different view of the whole subject of molecular interaction in dense media. Taken together, the proceedings describe the current experimental and theoretical work in this field. It is to be hoped that they will provide a source of ideas for further studies.

CONTENTS: I. Exciton Physico Chemistry (Exciton Interactions, Bi-and Polyexcitons, Exciton Condensation, Stimulated Emission). II. Spectrometric Studies of Phase Changes in Crystals (Electromagnetic and Neutron Spectroscopy). III. Matrix Spectroscopy (Molecules, Radicals, Ions). IV. Induced Spectra in Dense Fluids. V. Short Range Order in Liquids: Solvation. VI. Vibrational and Rational Relaxation in Dense Phases. VII. Methodological and Instrumental Innovations. Author Index.

ELSEVIER SCIENTIFIC PUBLISHING COMPANY

P.O. Box 211, Amsterdam, The Netherlands

Distributed in the U.S.A. and Canada by:
AMERICAN ELSEVIER PUBLISHING COMPANY, INC.,
52 Vanderbilt Ave., New York, N.Y. 10017

The Dutch guilder price is definitive. US $ prices are subject to exchange rate fluctuations.

NEW IN CATALYSIS

CATALYSIS: HETEROGENEOUS AND HOMOGENEOUS

edited by B. DELMON and G. JANNES

1975. 584 pages. US $ 45.95/Dfl. 110.00. ISBN 0-444-41346-4

This book constitutes the Proceedings of the International Symposium on the relations between heterogeneous and homogeneous catalytic phenomena, held in Brussels on October 23-25, 1974.

The following topics were discussed in 28 contributed papers:
- Heterogeneous catalytic phenomena which exhibit some fundamental aspects of homogeneous catalysis; effects of modifying substances and selectivity promoters in heterogeneous catalysis; effects of carriers, when interpreted by fundamental concepts of homogeneous catalysis.
- Catalytic systems in which an attempt has been made to heterogenize coordination complexes. The corresponding papers give information on the progressive modification of the coordination and activity of the complexes.
- Similitude of mechanisms and precursors in homogeneous and heterogeneous catalysis.

In addition to the contributed papers 10 invited lectures or reviews are presented.

REACTION KINETICS AND CATALYSIS LETTERS

Editors: G.K. BORESKOV and F. NAGY
Associate Editor: L.I. SAMÁNDI
1975. 2 volumes in 8 issues. Subscription price: US $ 110.75/Dfl. 260.00 including postage.

This journal was established by the USSR and Hungarian Academies of Science on the realisation that a medium was urgently needed for the rapid publication of new results in the fields of Kinetics and Catalysis. The profusion of scientific papers originating from researchers in various parts of the world makes literature searches a formidable task. Specialised journals serve the purpose of concentrating information concerned with a specific group of subjects, whereas media for rapid communication efficiently reduce the time for the flow of information between research workers. REACTION KINETICS AND CATALYSIS LETTERS aims at assisting scientists of all countries in both respects, by ensuring rapid publication of original work in a specialised journal. Papers are, of course, accepted from all over the world, but a point of special interest is the inclusion of much new work from the USSR which hitherto became accessible only after great delay. Some of these papers will appear in Russian, but will be accompanied by an English summary.

ELSEVIER SCIENTIFIC PUBLISHING COMPANY
Amsterdam and New York

1675E

MARINE CHEMISTRY

An International Journal for Studies of all Chemical Aspects of the Marine Environment

EDITOR-IN-CHIEF:

P. J. WANGERSKY,
Institute of Oceanography,
Dalhousie University,
Halifax, Nova Scotia, Canada

During the last decade there has been a remarkable increase in research in the field of marine chemistry, concurrent with increases in studies of the ocean as a whole. The direction of this research has gradually shifted from descriptive studies of a static ocean to analytical studies of a dynamic ocean. The contents of MARINE CHEMISTRY reflect this dynamic approach to chemical processes in the ocean.

Manuscripts should be sent to the Editorial Office, MARINE CHEMISTRY, P.O. Box 1345, Amsterdam, The Netherlands.

Publication is in quarterly issues.

The **subscription price** for 1976 (Volume 4) is US$46.95 / Dfl. 117.00 postage included.

Private subscribers can obtain a subscription at the reduced rate of US$22.50 / Dfl. 56.00, postage included.

Subscription orders and requests for further details or examination copies may be sent to your usual supplier or to the Journal Division of Elsevier Scientific Publishing Company.

Journals are automatically sent by air to the U.S.A. and Canada at no extra cost and to Japan, Australia and New Zealand with a small additional postal charge.

Contents of Volume 3 No. 3:

Photochemical degradation of petroleum hydrocarbon surface films on seawater (H. P. Hansen). An improved specific interaction model for seawater at 25°C and 1 atmosphere total pressure (M. Whitfield). Stability of ion pairs from gypsum solubility (B. Elgquist and M. Wedborg). Reactions which remove dissolved alumina from seawater (J. D. Willey). Silica-alumina interactions in seawater (J. D. Willey). High molecular-weight material in Baltic seawater (M. Brown).

Contents of Volume 3 No. 4:

Thermodynamics of the system H_2O-NaCl-$MgCl_2$-Na_2SO_4-$MgSO_4$ at 25°C (R. F. Platford). Isotopic fractionation of dissolved nitrate during denitrification in the eastern tropical North Pacific Ocean (J. D. Cline and I. R. Kaplan). Solubility of calcite in the ocean (S. E. Ingle). Matière en suspension et phosphore en particules dans l'Atlantique tropical sud le long de 4°W en Novembre 1971 (L. Lemasson). Chlorinated hydrocarbons in seawater: analytical method and levels in the north-eastern Pacific (E. D. Scura and V. E. McClure). The non-biological oxidative degradation of dissolved xanthopterin and 2, 4, 6-trihydroxypteridine by the pH or salt concentration of seawater (N. J. Antia and A. F. Landymore). Theoretical model for the formation of ion-pairs in seawater (D. R. Kester and R.M. Pytkowicz).

Elsevier Scientific Publishing Company

P.O. Box 211
Amsterdam, The Netherlands

The Dutch guilder price is definitive. US $ prices are subject to exchange rate fluctuations.

5207E

(Continued from page 4 of cover)

Short Communications

© ELSEVIER SCIENTIFIC PUBLISHING COMPANY, 1976

All rights reserved. No part of this publication may be reproduced, stored in a retrieval system, or transmitted, in any form or by any means, electronic, mechanical, photocopying, recording, or otherwise, without permission in writing from the publisher.

Printed in The Netherlands

VOL. 82 NO. 2 ANALYTICA CHIMICA ACTA APRIL 1976

CONTENTS

(Continued on inside page of cover)

29.8.8.